

Spring 5-15-2019

Defining Gastric Epithelial Cell Population Dynamics At Homeostasis And Following Injury

Joseph Ronald Burclaff
Washington University in St. Louis

Follow this and additional works at: https://openscholarship.wustl.edu/art_sci_etds

 Part of the [Biology Commons](#)

Recommended Citation

Burclaff, Joseph Ronald, "Defining Gastric Epithelial Cell Population Dynamics At Homeostasis And Following Injury" (2019). *Arts & Sciences Electronic Theses and Dissertations*. 1778.
https://openscholarship.wustl.edu/art_sci_etds/1778

This Dissertation is brought to you for free and open access by the Arts & Sciences at Washington University Open Scholarship. It has been accepted for inclusion in Arts & Sciences Electronic Theses and Dissertations by an authorized administrator of Washington University Open Scholarship. For more information, please contact digital@wumail.wustl.edu.

WASHINGTON UNIVERSITY IN ST. LOUIS

Division of Biology and Biomedical Sciences
Developmental, Regenerative, and Stem Cell Biology

Dissertation Examination Committee:

Jason Mills, Chair

William Stenson, Co-Chair

Matthew Ciorba

Richard DiPaolo

Gwendolyn Randolph

Defining Gastric Epithelial Cell Population Dynamics At Homeostasis And Following Injury

by

Joseph Burclaff

A dissertation presented to
The Graduate School
of Washington University in
partial fulfillment of the
requirements for the degree
of Doctor of Philosophy

May 2019

St. Louis, Missouri

© 2019, Joseph Burclaff

Table of Contents

Acknowledgments.....	viii
Abstract of the Dissertation	x
Chapter 1: Introduction.....	1
1.1 Introduction to plasticity	2
1.2 Introduction to the stomach.....	5
1.3 Gastric Plasticity	7
1.4 Gastric Tumorigenesis	9
1.5 Conclusion	10
Chapter 2: Targeted Parietal Cell Apoptosis Is Insufficient To Induce Metaplasia In The Stomach	13
2.1 Abstract.....	14
2.2 Parietal Cell Death and Metaplasia.....	14
2.3 Methods and Materials.....	26
3.1 Abstract.....	31
3.2 Introduction.....	32
3.3 Methods and Materials.....	34
3.4 Chief cells take up little BrdU upon extended continuous pulsing.....	36
3.5 BrdU administered throughout acute injury marks nearly all epithelial cells.....	39
3.6 Chief cells are not the predominate terminal maturation state for neck cells	43
3.7 Chief cells give rise to SPEM cells following gastric injury	45
3.8 Metaplastic cells can redifferentiate into chief cells following recovery from injury	51
3.9 Discussion	52
Chapter 4: Chief cells can differentiate in the absence of parietal cells	61
4.1 Introduction.....	61
4.2 Results.....	62
4.3 Discussion	66
4.4 Methods and materials	67
Chapter 5: MNU can be used to initiate gastric tumorigenesis	70
5.1 Introduction.....	70
5.2 Results.....	71

5.3 Discussion.....	76
5.4 Methods and Materials.....	77
Chapter 6: Nitric Oxide may act as a damage signal between dying parietal cells and the gastric epithelium	80
6.1 Introduction.....	80
6.2 Results.....	82
6.3 Discussion.....	87
6.4 Methods and Materials.....	88
Chapter 7: Neck cells undergo many of the defined steps of Paligenosis when re-entering the cell cycle following injury	92
7.1 Introduction.....	92
7.2 Results.....	93
7.3 Discussion.....	99
7.4 Methods and Materials.....	100
Chapter 8: Conclusions and Future Directions	103
8.1 Overall summary.....	103
8.2 Future directions	107
Appendix 1: Modeling murine gastric metaplasia through tamoxifen-induced acute parietal cell loss	114
A1.1 Summary	115
A1.2 Introduction.....	115
A1.3 Materials.....	116
A1.4 Methods.....	117
A1.5 Notes	121
A1.6 References.....	125
Appendix 2: Unintended targeting of Dmp1-Cre reveals a critical role for Bmpr1a signaling in the gastrointestinal mesenchyme of adult mice	128
A2.1 Abstract.....	129
A2.2 Introduction.....	129
A2.3 Materials and Methods.....	131
A2.4 Results.....	133
A2.5 Discussion.....	142
A2.6 References.....	144

Appendix 3: Metaplastic cells in the stomach arise, independently of stem cells, via dedifferentiation or transdifferentiation of chief cells	147
A3.1 Abstract	148
A3.2 Stem Cell Independent Gastric Metaplasia	148
A3.3 Methods and Materials	161
Appendix 4: Regenerative proliferation of differentiated cells by mTORC1-dependent paligenosis.....	166
A4.1 Abstract	167
A4.2 Introduction.....	167
A4.3 Diverse organs show similar changes in metabolic activity during acute injury	170
A4.4 mTORC1 is required for injury-induced proliferation.....	179
A4.5 Changes in mTORC1 also characterize human metaplasia.....	185
A4.6 Loss of mTORC1 inhibits cell cycle progression at S-phase.....	191
A4.7 Autodegradative machinery is massively upregulated early following injury	196
A4.8 Autodegradative machinery is required for normal progression to later stages	198
A4.9 Discussion	206
A4.10 Materials and Methods.....	213
A4.11 Author contributions	218
A4.12 References.....	218
Works Cited	226

List of Figures

Figure 1.1: Proposed models of mature cells acting as cancer cells of origin.	4
Figure 1.1: The gastric unit and its response to injury.	6
Figure 2.1: Atp4b-Cre;LSL-DTR drives iDTR specifically in parietal cells.	16
Figure 2.2: DT specifically kills parietal cells.	17
Figure 2.3: Diphtheria toxin-mediated parietal cell ablation does not cause metaplasia	19
Figure 2.4: Changes in protein localization for markers of SPEM and chief cell differentiation following TAM and DT.	20
Figure 2.5: Quantitative Real-Time PCR of selected transcripts implicated in SPEM.	22
Figure 2.6: SPEM can be induced in the absence of parietal cells	24
Figure 2.7: DMP-777 control showing deletion of parietal cells.	25
Figure 3.1: Continuous BrdU marks few chief cells in the healthy stomach	38
Figure 3.2: BrdU+TAM pulse chases indicate that chief cells are a self-maintaining population	41
Figure 3.3: BrdU retention in parietal cells and other epithelial lineages	42
Figure 3.4: Chief cells are not the final fate for neck cells	44
Figure 3.5: Metaplastic cells arise from chief cells following chronic and acute injury	46
Figure 3.6 Additional <i>Helicobacter pylori</i> data	48
Figure 3.7 Additional SPEM data	49
Figure 3.8 EdU ⁺ progenitors do not give rise to EdU ⁺ SPEM cells	51
Figure 3.9: Metaplastic cells can redifferentiate into chief cells following recovery from injury	52
Figure 3.10: Chief cells appear to maintain an independent population at homeostasis	53
Figure 3.11: Models for BrdU pulse-chase experiments comparing the canonical isthmal stem cell model with our independent base model.	55
Figure 4.1: Chief cells recover from tamoxifen even in the absence of PCs.	64
Figure 4.2: Chief cells develop in the young stomach even in absence of PCs	65
Figure 5.1: MNU timecourse and in vivo fluorescence imaging.	73
Figure 5.2: PET/CT Scanning on MNU treated mice.	74
Figure 5.3: MNU induced tumors	75
Figure 6.1: iNOS expresses in individual PCs following injury.	83
Figure 6.2: The NO donor SNAP has a limited effect on gastric proliferation.	84
Figure 6.3: Inhibition of iNOS activity has no significant effect on proliferation.	85
Figure 6.4: sGC in chief and neck cells is unchanged following floxing.	86
Figure 6.5: Sporadic iNOS is driven from Tet-On iNOS overexpression mice.	87
Figure 7.1: Sox9 expression in healthy and injured stomachs.	94
Figure 7.2: Neck cells have dynamic mTorc1 activity following injury.	95

Figure 7.3: Neck cells activate autophagy following injury.	97
Figure 7.4: IFRD1 status has no effect on neck cell proliferation following injury.	98
Figure 8.1: Transgenic construct for HKDTR mouse engineering.	109
Figure 8.2: Checking for proper HKDTR mouse development.	110
Figure A1.1: Tamoxifen treatment results in acute parietal cell loss.	119
Figure A1.2: Tamoxifen treatment causes acute parietal cell loss and alters the GSII expression pattern in gastric units.	120
Figure A2.1: Dmp1-Cre targets osteoblast lineage cells, skeletal muscle, and bone marrow cells in 2-month-old mice.	135
Figure A2.2: Dmp1-Cre targets bone marrow cells near blood vessels.	136
Figure A2.3: Dmp1-Cre does not target bone marrow adipocytes.	136
Figure A2.4: Dmp1-Cre targets cells in the cerebellum and the hindbrain.	138
Figure A2.5: Dmp1-Cre targets lamina propria of the stomach and the small intestine.	139
Figure A2.6: Dmp1-Cre targets Pdgfra-positive mesenchymal cells in the small intestine.	140
Figure A2.7: Dmp1-Cre Bmpr1af/f mice develop gastric hyperplasia and polyps.	141
Figure A2.8: Dmp1-Cre Bmpr1af/f mice develop intestinal polyps.	142
Figure A3.1: SPEM can occur without proliferation.	150
Figure A3.2: No SPEM occurs 24h after HDT treatment.	152
Figure A3.3: qRT-PCR for SPEM-associated genes.	153
Figure A3.4: Metaplastic cells arise below the isthmus	155
Figure A3.5: Proliferation is sufficiently blocked over the course of injury in 5FU+HDT mice.	156
Figure A3.6: Proliferating pre-parietal cells begin to appear 96h after HDT treatment.	157
Figure A3.7: Proliferation after SPEM induction.	158
Figure A3.8: Human SPEM in gastric cancer patients	160
Figure A3.9: Primers used for quantitative RT-PCR	165
Figure A4.1: pS6 is an accurate proxy for rapamycin-sensitive mTORC1 activity and shows that loss of mTORC1 does not affect parietal cell death or induction of metaplastic gene expression in reprogramming chief cells.	172
Figure A4.2: mTORC1 activity undergoes dramatic changes during stomach and pancreas metaplastic injury response.	174
Figure A4.3: Acute kidney injury and partial hepatectomy both cause upregulation of mTORC1 activity during proliferative phases.	178
Figure A4.4: Histological changes in the injured stomach and pancreas with and with rapamycin treatment.	180
Figure A4.5: Recruitment of proliferating cells during stomach and pancreas metaplastic injury depends on mTORC1.	182
Figure A4.6: mTORC1 is not required for increased SOX9 during metaplasia.	184
Figure A4.7: Patient Demographics.	187

Figure A4.8: mTORC1 activity correlates with stages of metaplasia during human gastric tumorigenesis.	188
Figure A4.9: Representative IHC images from human tissue microarray.	189
Figure A4.10: Gene Set Enrichment Analyses for Rapamycin + Tamoxifen experiments.	192
Figure A4.11: mTORC1 activity is required predominately for progression through S-, G2-, and M-phases during metaplastic induction of proliferation.	194
Figure A4.12: Lysosomal and autophagic pathways are upregulated acutely following stomach and pancreas injury.	197
Figure A4.13: Lysosomal activity is raised in the pancreas in early injury.	198
Figure A4.14: Histological appearance of <i>Gnptab</i> ^{-/-} stomach and pancreas tissue at injury time point.	200
Figure A4.15: Lysosomal function is required for metaplasia-associated gene expression and increased proliferation.	202
Figure A4.16: Lysosomal activity is required to re-activate mTORC1 following HD tamoxifen injury.	204
Figure A4.17: <i>Gnptab</i> ^{-/-} acinar cells maintain mature markers following injury.	205
Figure A4.18: Loss of GNPTAB increases apoptosis of chief cells following injury.	206
Figure A4.19: Schematic model of shared program: paligenosis.	208

Acknowledgments

The path towards earning a PhD is neither quick nor easy, yet many people along the way helped make it the best possible experience for me. First and foremost, I would like to thank my mentor, Jason Mills. Jason was one of the first people I met at Washington University, as one of my interviewing professors during recruiting weekend. His passion for his work and excitement about science in general was evident from that first meeting and never faded, making it easy to stay motivated and excited while working with him. The Mills Lab provided an amazing environment for learning the foundations of biological research, and I feel well prepared to move to my next career step largely thanks to Jason and his mentorship.

A lab does not consist solely of its PI, and the Mills Lab has seen its fair share of great members throughout my time here. While there are too many to name each individually, I want to especially thank Greg Sibbel, who I connected with during recruiting weekend and worked with during my rotation, but who passed away from Ewing's sarcoma before I joined the lab as a full member. I would also like to thank Shradha Khurana and Ben Moore for welcoming me to the lab and starting me off on the right path, Luciana Osaki and Grant Lo for keeping lab fun during the always-difficult third and fourth years, Megan Radyk for helping keep me sane during the latter years, and everyone else for their help, training, and support throughout my entire time here. Connie Marshall deserves a special shout out for being an amazing lab manager who keeps the lab running both physically and emotionally. The people of the Mills Lab were a huge component of my success throughout my time at Washington University, and I hope our careers stay aligned so we need to stay in touch!

Funding is an important part of scientific life, and I have multiple funding sources that made my work possible. I would like to thank the professors who decided to include me on the

incoming T32 CMB Training Grant, the DeNardo Education and Research Foundation for funding my projects, and especially Philip and Sima Needleman, whose fellowship directly funded my work and travel for multiple years.

The greater community of Developmental, Regenerative, and Stem Cell Biology at Washington University also presented an optimal learning environment for me, and I would like to thank all the DRSCB professors for their teaching, collaborating, and community. A very special ‘Thank You’ is warranted for Dr. Jim Skeath, who spends countless hours and immeasurable effort helping DRSCB students succeed, as well as our Program Coordinator Sally Vogt, who was always open to discuss the program, my work, or life in general. As I am leaving, I hope that they know how instrumental they were for my success these past years.

Science is not all always fun, so a strong group of friends is invaluable. I want to thank everyone who made my adventure here more enjoyable, from my first year Ultimate Frisbee group to my DRSCB classmates who came to my Semi-Annual Dev Bio Dinners throughout the years. I hope I helped others along on their graduate journeys as much as they all helped me.

Finally, I want to offer my warmest thanks to my family and my girlfriend. My brothers all came to visit, my parents listened to countless hours of excitement, doubts, and strategizing from my end, and Cynthia supported me in every step I made in the past three years. Thank you all so much. You truly made my PhD more attainable and the path toward it more enjoyable.

Joseph Burclaff

Washington University in St. Louis

May 2019

Abstract of the Dissertation

Defining Gastric Epithelial Cell Population Dynamics at Homeostasis and Following Injury

by

Joseph Burclaff

Doctor of Philosophy in Biology and Biomedical Sciences

Developmental, Regenerative, and Stem Cell Biology

Washington University in St. Louis, 2019

Professor Jason C Mills, Chair

Gastric diseases affect many people around the world, yet surprisingly little is known about the basic dynamics of gastric epithelial cells. Loss of acid-secreting parietal cells has long been observed to precede pre-cancerous gastric metaplasias like Spasmolytic Polypeptide-Expressing Metaplasia (SPEM), yet no signaling component from dying parietal cells has yet been implicated in initiating the metaplastic responses. Also, experiments pulsing ^3H -thymidine and or examining intracellular components suggest that gastric mucous neck cells are short-lived transient intermediates between the gastric stem cell and mature zymogenic “chief” cells, yet specifics about this transition remain elusive. Here, we develop a novel mouse line and new techniques for tracing gastric cell lines to further probe these interactions.

To identify the changes in parietal cell signaling upon injury which lead to chief cell dedifferentiation and the appearance of SPEM, we bred mice expressing the human diphtheria toxin receptor solely in parietal cells. Injection of diphtheria toxin specifically kills parietal cells through apoptosis. Surprisingly, while the parietal cells died in similar numbers to those in mice

treated with tamoxifen, no SPEM or chief cell dedifferentiation was observed, and proliferation only increased through the neck, with minimal proliferation in the base. We also showed that SPEM can still arise if we inject tamoxifen or DMP-777 after the parietal cells are already killed via diphtheria toxin. These experiments indicate that chief cell dedifferentiation is not simply triggered by the loss of parietal cells, nor are dying parietal cells necessary for acute drugs to initiate metaplasia. However, the signal which initiates the metaplasia remains unknown.

Furthermore, we studied the dynamics of long-lived cells in the mouse stomach using a modified BrdU pulse-chase protocol. Published reports describing gastric epithelial cell population dynamics have relied on continuous infusion or relatively short pulse-chases of DNA markers such as ^3H -thymidine. Here, we pioneer a new technique, pulsing BrdU throughout our normal tamoxifen injury regimen to label nearly all cells in the unit, allowing us to chase for months and track long-lived label-retaining cells. Following our pulse of tamoxifen and BrdU, we find that nearly two thirds of chief cells retain label even through a 9-month chase, indicating that they are either longer-lived than expected or that chief cells slowly divide to maintain their own population without being replaced by newer cells from higher in the unit. We also find subpopulations of label-retaining neck cells and parietal cells exist after a 9-month chase, shedding more light on their population dynamics. To further test whether neck cells give rise to chief cells, as others have reported, we administered a short BrdU pulse followed by various chase lengths and found that most neck cells do not directly give rise to chief cells, indicating that neck cells likely have a functional, as yet unidentified purpose, other than acting as a precursor to chief cells. Finally, we show through additional tamoxifen and *Helicobacter pylori* injury that long-lived chief cells give rise to acute and chronic SPEM cells and find that SPEM cells can directly redifferentiate back into chief cells upon recovery from injury. Altogether, we

suggest for the first time that chief cells may be a stable population in the gastric unit, largely maintaining their own census at homeostasis and in injury independently of neck cell transitions or parietal cell status.

Chapter 1: Introduction

The following section is modified from a review published in Disease Models & Mechanisms
Burclaff, Joseph, and Jason C. Mills. "Plasticity of differentiated cells in wound repair and
tumorigenesis, part I: stomach and pancreas." Disease models & mechanisms 11, no. 7 (2018):
dmm033373.

1.1 Introduction to plasticity

The series of sequential cell fate choices governing how normal, adult differentiated cells arise from their precursors has been well delineated over the last decades. The opposite process, in which cells dedifferentiate to reacquire progenitor properties, though noted by pathologists over a century ago (Adami, 1900) and demonstrated by occasional, pioneering studies only reentered the scientific mainstream with the demonstration a decade ago by Yamanaka and others that multiple adult cell types can be induced to return to pluripotency (Takahashi and Yamanaka, 2006). Since then, research has expanded to also examine the native capacity of mature cells *in vivo* to reverse their differentiated state in nearly all tissues (Mills and Sansom, 2015; Tata and Rajagopal, 2016). The plasticity of cells in a tissue manifests in multiple ways: stem cells (SCs) can interconvert to other SC populations, mature cells can dedifferentiate to recapitulate the earlier stages of their ontogeny, and mature cells can transdifferentiate to mature cell types of different lineages (Jopling et al., 2011).

Cellular plasticity may be key to regeneration following large-scale injury, yet a tissue's capacity for plasticity may also carry an inherent potential for adverse consequences like cancer. Here, we will discuss how plasticity may help refine a long-standing model for how cancer begins. The well-established 'multi-hit model' postulates that tumors arise as long-lived SCs accrue mutations necessary for tumorigenesis (Fearon and Vogelstein, 1990). Recently, though, it has become clear that individual stem cells in mice may not be as long-lived as traditionally believed (Lopez-Garcia et al., 2010; Snippert et al., 2010; Baker et al., 2014), raising the question of how a single SC could accumulate multiple mutations over the course of years (Mills and Sansom, 2015). Even if the SC population remains stable over time, intestinal SCs are relatively short-lived, as SCs divide frequently and stochastically, commonly jostling each other out of the niche

in mice (Lopez-Garcia et al., 2010; Snippert et al., 2010) and in humans (Baker et al., 2014). Although some intestinal SCs tend to be longer-lived (Ritsma et al., 2014) and SCs with oncogenic mutations hold a competitive advantage over wild-type SCs in the intestinal crypt (Snippert et al., 2014), the question remains whether SCs are the sole population that accumulates tumor-inducing mutations over the lifetime of an organism. Moreover, in organs such as the pancreas that lack a constitutive SC, other cell types must accumulate such mutations.

Increasing evidence shows that plasticity can be involved in the origin of cancers in numerous epithelial tissues (Giroux and Rustgi, 2017) and even astrocytes (Friedmann-Morvinski and Verma, 2014). This dissertation examines the gastric chief cells, which undergo plasticity following injury and may accrue the ‘multiple hits’ defined by Kinzler and Vogelstein (Vogelstein and Kinzler, 1993) and initiate tumor formation. Similar events in the intestine, pancreas, and skin are further reviewed in the following works (Burclaff and Mills, 2018a; Burclaff and Mills, 2018b). A more complete understanding of the process of mutation accumulation may further our understanding of how every organ produces tumors with a multitude of phenotypes that vary not only from person to person but even within a single person: tumors initiated by cells stem cells or cells at various stage of differentiation or dedifferentiation may contribute to this diversity (Visvader, 2011; Song and Balmain, 2015).

Plasticity can allow post-mitotic cells to re-enter the cell cycle, and we have proposed that cycles of proliferation and quiescence can favor tumorigenesis as accumulated mutations can become fixed in long-lived differentiated cell populations. We have termed this the ‘cyclical hit’ model in which cell lineages cycle through phases of dedifferentiation and redifferentiation, allowing

for the accumulation and unmasking of mutations in long-lived cells (Figure 1) (Mills and Sansom, 2015; Saenz and Mills, 2018b).

Before discussing the work done for this dissertation, we survey the current state of plasticity research in the stomach which experiences the recruitment of long-lived, mature secretory cells back into the cell cycle upon certain types of physiological injury. We discuss how recent advances in our knowledge of these events and their governing mechanisms address how mature cells might initiate or be involved in tumorigenesis, challenging the idea that adult SCs are the sole cell type responsible for both accumulating mutations and spawning cancers (White and Lowry, 2015). We end by postulating how the changes undergone in gastric plasticity might be governed by conserved cellular programs, which hold important implications for cancer initiation.

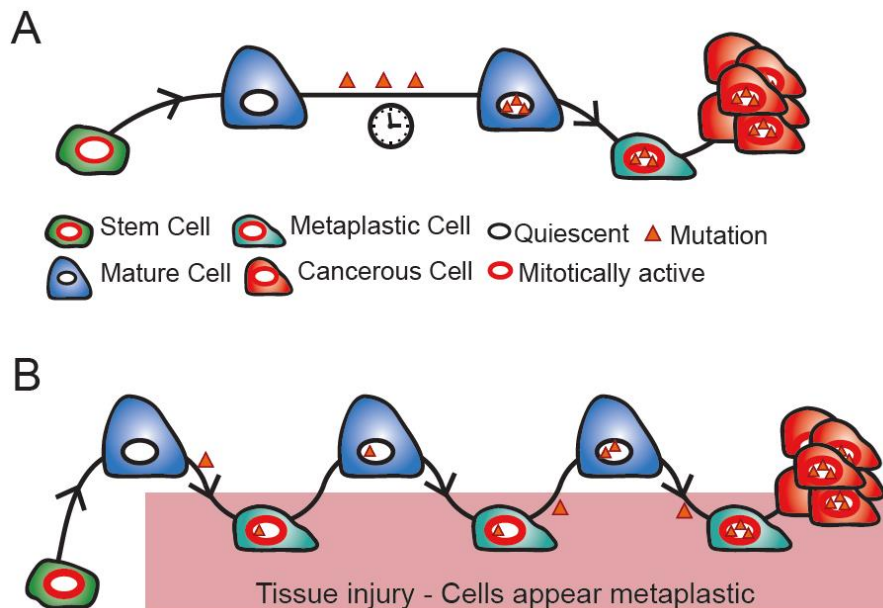


Figure 1.1 Proposed models of mature cells acting as cancer cells of origin.

We propose that long-lived mature cells may accumulate and store mutations, eventually acting as – or giving rise to cells that can act as – cells of origin for tumors in diverse tissues. This

mutational accumulation may occur in two main ways: A) Mature cells (dark blue) may accumulate mutations (orange triangles) as they maintain their mature functioning cell fate over time. The mutations themselves or outside stressors may cause dedifferentiation (teal cell). If the acquired mutations are sufficiently carcinogenic, they may then block the cell in the dedifferentiated state, causing it to expand as a clone that can give rise to cancer (red). B) The ‘cyclical hit’ model describes mature cells which dedifferentiate and redifferentiate multiple times in response to injury/inflammation. Each time cells are called back into the cell cycle, replicative stress can promote mutation accumulation. Differentiated cells can store such mutations indefinitely. Eventually, a mutation or combination of mutations is sufficient to block the cell in one of its replicative phases and lead to clonal expansion and potential tumorigenesis.

1.2 Introduction to the stomach

The stomach body (corpus) is lined by an epithelium that is flat on the luminal surface but invaginates into glands descending towards the musculature. The gland and its surface epithelial cells form the gastric unit, containing mucus-secreting surface pit foveolar cells at the surface, mucous neck cells interspersed between acid secreting parietal cells in the neck region (Bredemeyer et al., 2009), and zymogenic chief cells at the base (Karam, 1993; Karam and Leblond, 1993b; Karam and Leblond, 1993a; Karam and Leblond, 1993c) (Figure 2A). Proliferation in the healthy gastric epithelium is overwhelmingly confined to morphologically undifferentiated cells located above the neck cells at the isthmus of the unit. Based on their ultrastructure and on nucleotide tracing studies (Hattori and Fujita, 1976b; Mills and Shivdasani, 2011), these isthmal cells have long been assumed to be multipotent SCs that fuel replacement of all mature cells in the gastric unit, though the extant data do not rule out other self-renewal mechanisms (Bjerknes and Cheng, 2002; Quante et al., 2010; Willet and Mills, 2016; Wright, 2016).

Although several candidate markers have been identified in cells that populate the gastric unit (Pesse and Sansom, 2017), none of these have been shown to be enriched exclusively in the

isthmal cells. This means that a verified marker of gastric epithelial SCs in the body of the stomach remains to be identified.

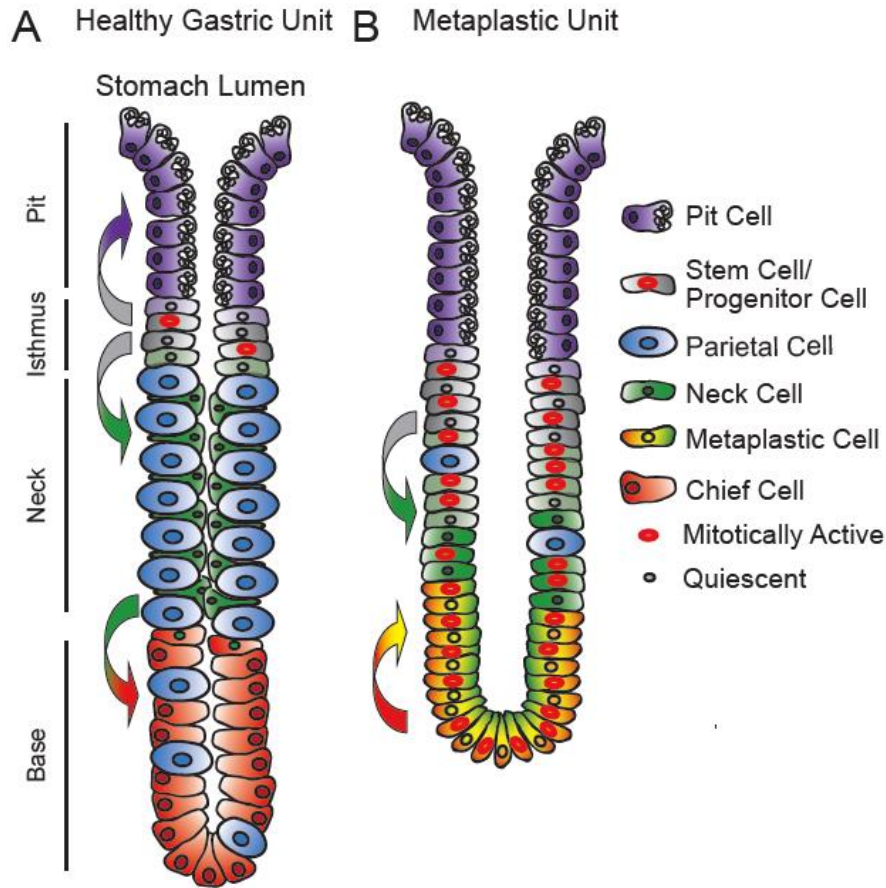


Figure 1.2: The gastric unit and its response to injury.

A) The healthy gastric unit, with pit cells at the opening to the gastric lumen, stem cells at the isthmus, parietal cells and neck cells in the middle of the unit, and chief cells at the base. Not pictured: endocrine and tuft cells. Proliferation (red nuclei) is confined to the isthmus, with new pit cells migrating up and parietal and mucous neck cells migrating down. Neck cells transition to chief cells at the zone between neck and base. Colored arrows mark the direction of cell changes. B) A metaplastic gastric unit following injury such as *Helicobacter pylori* infection or acute pharmacological agents. Parietal cells quickly die and mature chief cells become metaplastic cells co-expressing chief and neck cell markers. Proliferation occurs from the isthmus through the base, with paligenotic chief cells re-entering the cell cycle.

1.3 Gastric Plasticity

Chief cells are large, long-lived, and non-proliferating cells that devote their energies to producing digestive enzymes. However, surprisingly, chief cells in both mice and humans are plastic; they can disassemble their complex secretory apparatus (Capoccia et al., 2013; Lo et al., 2017) to re-enter the cell cycle and, potentially in some cases, act as reserve SCs upon injury (Stange et al., 2013b). In humans, *Helicobacter pylori* infection can cause chronic atrophic gastritis. In this condition, parietal cells die (atrophy), and increased proliferation is observed among the remaining cells in the gastric unit. In mouse models, both *H. pylori* and various drugs can be used to kill the parietal cells and force the recruitment of other cells as additional reserve SCs (Sigal et al., 2015; Petersen et al., 2017b). Drugs that mimic the *H. pylori*-induced cellular changes include high doses of the selective estrogen receptor modulator tamoxifen (Huh et al., 2012b; Saenz et al., 2016), the neutrophil elastase inhibitor DMP-777 (Goldenring et al., 2000; Nomura et al., 2005), and its ortholog L635 (Weis et al., 2013). In all cases, the observed changes include loss of parietal cells, loss of mature chief cells, and the emergence of metaplastic cells. In the stomach, the metaplastic cells that emerge upon parietal cell death express large amounts of trefoil factor 2 (TFF2, also Spasmolytic Polypeptide), so the cell lineage shifts in chronic atrophic gastritis have been called Spasmolytic Polypeptide Expressing Metaplasia (SPEM).

SPEM cells were originally thought to arise via proliferation from the isthmal SCs undergoing an alternate differentiation path, and some continue to believe that to be the case (Hayakawa et al., 2015; Hayakawa et al., 2017; Kinoshita et al., 2018a), yet lineage tracing studies with multiple genetic drivers from the base and isthmus of the gastric unit in mice, with corroboration in human tissues, indicate that the majority of SPEM cells, at least in the acute setting, likely arise

from chief cells that reprogram to express TFF2 and re-enter the cell cycle (Lennerz et al., 2010; Nam et al., 2010; Goldenring et al., 2011a; Capoccia et al., 2013; Leushacke et al., 2017; Matsuo et al., 2017; Mills and Goldenring, 2017) (Figure 2B). Gene promoters that have been used to lineage trace chief cell reprogramming into progenitor cells include: Tumor necrosis factor receptor superfamily, member 19, (*Tnfrsf19*, known as *Troy*), which is mostly expressed in mature chief cells; basic helix loop helix family member A15 (*Bhlha15*, known as *Mist1*), which is almost exclusively expressed in chief cells; and Leucine Rich Repeat Containing G Protein-Coupled Receptor 5 (*Lgr5*) mRNA, which is likewise almost exclusively expressed in chief cells. Recent work further supports the interpretation that mature chief cells are the predominant source of acute SPEM cells, showing that SPEM can arise even when any potential proliferative contribution from the SC or progenitor cells is abrogated (Radyk et al., 2018). Interestingly, SPEM cells recapitulate many aspects of immature cells in the early developing stomach where there are abundant proliferating cells that co-express TFF2 and markers of chief cell differentiation (Keeley and Samuelson, 2010). The SPEM cells are not characteristic of the adult isthmal SCs, which lack granules or other ultrastructural characteristics of any specific differentiated cell lineage (Karam and Leblond, 1993a).

While parietal cell loss is nearly always correlated with SPEM, a recent study demonstrated that highly targeted parietal cell apoptosis alone is insufficient to induce metaplasia (Burclaff et al., 2017). The cause and mechanism of SPEM initiation remain enigmatic, though several players have been implicated, such as requirement for a signaling cascade including Extracellular Signal-regulated Kinase (ERK), Cluster of Differentiation 44 (CD44), and Signal transducer and activator of transcription 3 (STAT3) (Khurana et al., 2013), macrophages, and interactions between interleukins (IL) IL-33 and IL-13 (Petersen et al., 2014; Petersen et al., 2017a). Our

recent work also showed that a sequential, stepwise process of 1) autodegradation, 2) induction of metaplastic gene expression like SRY-box 9 (SOX9) and TFF2, and 3) cell cycle re-entry characterized the process chief cells used to reprogram (Willet et al., 2018a). Each step has checkpoints that cells must traverse to complete proper tissue regeneration. For example, blocking lysosomal functioning stopped cells from inducing SOX9/TFF2, and inhibiting mTORC1 stopped cell cycle re-entry. The stages and checkpoints were preserved in pancreatic regeneration, and additional experiments as well as other literature indicated that kidney and liver regeneration follow the same sequence. Thus, there is support for a conserved cellular regenerative/dedifferentiation program that has been called ‘paligenosis’, suggesting that cells, in addition, to programs for cell death (apoptosis) have programs to regain regenerative ability (Messal et al., 2018).

1.4 Gastric Tumorigenesis

Since Pelayo Correa’s early work mapping the histological stages of gastric cancer progression (Correa, 1988), it has been known that patients with metaplasia/chronic atrophic gastritis have an increased risk for gastric cancer (Hattori, 1986; Kakinoki et al., 2009; Goldenring et al., 2010) and that gastric cancer seems to arise in a stepwise fashion. The stages of gastric tumorigenesis cannot be fully studied in mice, as no mouse models of gastric cancer faithfully replicate late-stage human disease (Petersen et al., 2017b). Humans with extensive metaplasia and SPEM nearly invariably also get intestinal metaplasia, but intestinal metaplasia does not seem to be a common feature of injury response in mice. In some mouse models, however, SPEM can progress to proliferative lesions with histological abnormalities resembling human dysplasia (Nomura et al., 2004; Petersen et al., 2017b). The architecture of the gastric unit is useful to consider, as the spatial separation between the normal isthmal and basal proliferation zones via

chief cell dedifferentiation allows for inferences to be made about the cells of origin for metaplasias and dysplasias (Radyk and Mills, 2017). Multiple recent studies have shown how proliferative dysplasia can be induced solely by expressing activated Kirsten Rat Sarcoma (KRAS) using multiple promoters found in chief cells (Choi et al., 2016; Leushacke et al., 2017; Matsuo et al., 2017). Such studies show that chief cells are able to act as cells of origin for tumorigenesis. As there is no known promoter reliably specific to the isthmal SC in the stomach, similar direct evidence does not exist for the SC acting as another potential cell of origin, though of course this is certainly a possibility awaiting better genetic tools in future work. The ability of the chief cells to act as cells of origin for gastric cancer is consistent with the ‘cyclical hit’ model of tumorigenesis, whereby long-lived chief cells may accumulate and store mutations in rounds of dedifferentiation and redifferentiation in chronic inflammation or metaplasia, possibly leading to tumorigenesis (Figure 1) (Mills and Sansom, 2015; Saenz and Mills, 2018b).

1.5 Conclusion

In the search for the cell of origin for epithelial cancers, investigators have long favored stem and progenitor cells as the likely culprits owing to their constitutive proliferative capacity and supposed longevity (Fearon and Vogelstein, 1990; Vogelstein and Kinzler, 1993). However, interestingly, before the rise of the specific field of Developmental Biology, pathologists had considered three possible cancer cells of origin with relatively equal potential: 1) stem cells (or ‘mother cells’, as they were known over a century ago) (Adami, 1900); 2) ‘rests’ or cryptic embryonic cells that never really differentiated in the adult; and 3) differentiated cells that can become proliferative again after potentially accumulating deleterious phenotypes. We are in the process of shifting our understanding of how tissues renew towards accepting that the more fluid/plastic notions of a century ago might describe reality more comprehensively than the rigid

stem-cell-based, unidirectional differentiation theories that predominated the latter half of the Twentieth Century. A more nuanced understanding of stem and differentiated cells and tissue repair, now with molecular underpinnings of the underlying cellular processes, may help refine models of tumorigenesis. For example, intestinal SCs live shorter than had been expected (Lopez-Garcia et al., 2010; Snippert et al., 2010). Thus, the longest-lived cells in many adult solid organs may actually be the differentiated populations. Thus, while many types of tumors may still arise ultimately from SCs (Visvader, 2011), the studies presented in this review give cause to re-imagine the multi-hit model to include the potential contribution of fully differentiated post-mitotic cells such as gastric chief cells (Choi et al., 2016; Leushacke et al., 2017) either as direct cells of origin for tumors or as sources for the stem/progenitor cells that go on to spawn cancer.

Opportunities to inhibit tumor initiation at the cell of origin may arise in multiple tissues if common pathways can be identified and manipulated to block their dedifferentiation. As a start, we can look at the many similarities between the stomach and the pancreas, in which mature secretory acinar cells undergo a similar plastic event following injury (Burclaff and Mills, 2018a). Both systems begin with large, long-lived secretory cells that undergo paligenosis to give rise to smaller, simpler cells reminiscent of embryonic cell types. Both systems also lose similar maturity markers and share many signal-transducing and metaplastic genes, and both involve a role for inflammation. Recent evidence indicates that paligenosis may be the process used during dedifferentiation of mature non-secretory cells in other organs as well, including liver and kidney (Willet et al., 2018a), and evidence for proliferative dedifferentiation is also being delineated in diverse tissues such as glia, warranting investigation into further mechanistic conservation (Friedmann-Morvinski and Verma, 2014). Our scope is expanded to describe

plasticity in the skin and intestine in published work (Burclaff and Mills, 2018b) to continue to discuss its implications for tumorigenesis and further highlight the conservation of plasticity-related genes and processes across tissues.

Data from the stomach and pancreas support a model wherein mutations are acquired and stored through cycles of differentiation and dedifferentiation until a neoplastic mutation such as *Kras* activation inhibits a paligenotic cell's ability to redifferentiate, which we describe as the cyclical hit model (Figure 1). This model also might help answer longstanding questions about tumor development. So-called 'oncofetal' gene expression in adult tumors has long puzzled oncologists (Uriel, 1979), with genes that are normally expressed only in early development becoming re-expressed in many tumors (Ahrlund-Richter and Hendrix, 2014). Metaplastic gene re-expression is the second stage of paligenosis (Willet et al., 2018a), consistent with the expression of embryonic genes being observed in ADM (Jensen et al., 2005), and the metaplastic stomach establishes morphology and cell types similar to the developing fetal gastric epithelium (Keeley and Samuelson, 2010; Osaki et al., 2010). It is thus likely that tumor cells express these embryonic genes because the genes were reintroduced via a paligenosis event that occurred at some point in one of their cellular ancestors.

Clearly, we are at only the beginning of the beginning of understanding how cell plasticity plays a role in tumorigenesis and even in how tumors can adapt to chemotherapy and radiation therapy. The following dissertation presents many projects describing the dynamics of this plasticity, and all indications are that there may be an explosion of new ideas and potential therapeutic approaches as the concepts of cell plasticity and dedifferentiation, and the underlying conserved mechanisms and cellular processes, begin to be more deeply explored.

Chapter 2: Targeted Parietal Cell Apoptosis Is Insufficient To Induce Metaplasia In The Stomach

The following chapter was published in Gastroenterology

Burclaff, Joseph, Luciana H. Osaki, Dengqun Liu, James R. Goldenring, and Jason C. Mills.

"Targeted apoptosis of parietal cells is insufficient to induce metaplasia in stomach."

Gastroenterology 152, no. 4 (2017): 762-766.

2.1 Abstract

Parietal cell (PC) atrophy is widely considered to cause metaplasia in the stomach. We bred mice with PC-specific diphtheria toxin receptor expression and found that targeted PC death increased proliferation in the normal stem cell zone but did not cause metaplastic reprogramming of chief cells. Furthermore, the metaplasia-inducing agents tamoxifen or DMP-777 still induced metaplasia even following previous ablation of PCs via diphtheria toxin. Thus, we demonstrate the surprising finding that PC atrophy alone is not sufficient to induce metaplasia and that completion of metaplastic reprogramming of chief cells requires further mechanisms beyond PC injury/death.

2.2 Parietal Cell Death and Metaplasia

Metaplasia in the stomach consistently occurs in the setting of parietal cell (PC) atrophy: in autoimmune gastritis patients(Adams et al., 1964), in *Helicobacter pylori* induced atrophic gastritis(Yoshizawa et al., 2007), and in animal models of acute injury(Nomura et al., 2005; Huh et al., 2012a). Thus, we and others have proposed that PC death *causes* metaplasia. For example, PCs might constitutively elaborate gastric-differentiation-promoting factors whose loss during PC atrophy might lead to aberrant (metaplastic) differentiation of remaining cells(Mills et al., 2001). Alternatively, the immune response to PC death could cause metaplasia, or dying PCs might elaborate specific injury-induced factors or by-products that trigger metaplasia.

Here, to better determine the specific role of PCs, we employed a method to precisely induce PC apoptosis. We bred PC-specific, Cre-inducible simian Diphtheria Toxin Receptor(Buch et al., 2005; Zhao et al., 2010) (*Atp4b-Cre;LSL-DTR*) mice [hereafter called “DTR mice” (Figure 2.1)]. In these mice, PCs are the only cells that can respond to apoptosis-inducing diphtheria toxin. As a positive control for PC atrophy and Spasmolytic Polypeptide-Expressing Metaplasia (SPEM),

the metaplasia seen in direct temporal and spatial correlation with human and mouse PC atrophy (Lennerz et al., 2010), we used a system previously described by us and others (Huh et al., 2012a; Sigal et al., 2015; Saenz et al., 2016) involving injections of high-dose (5 mg/20 g mouse body mass) tamoxifen (“TAM”). Consistent with previous results, TAM caused atrophy of >90% of PCs and increased cell proliferation throughout the gastric unit. In >75% of gastric units, the pathognomonic pattern of SPEM was identified: GIF⁺ chief cells (ZCs) at the base of the units co-expressing the epitope for the lectin GSII. As previously shown, many SPEM cells were also proliferative (yellow arrowheads, Figure 2.3A,B). Three daily injections with 225 ng DT also killed >90% PCs and increased mucosal cell proliferation in the isthmal region deep to the foveolar cells (Figure 2.3A-C). Both atrophy and proliferation were maintained by daily DT injection up to 14 days, while cessation of injection at D3 allowed for complete recovery within the same timeframe (Figure 2.3C).

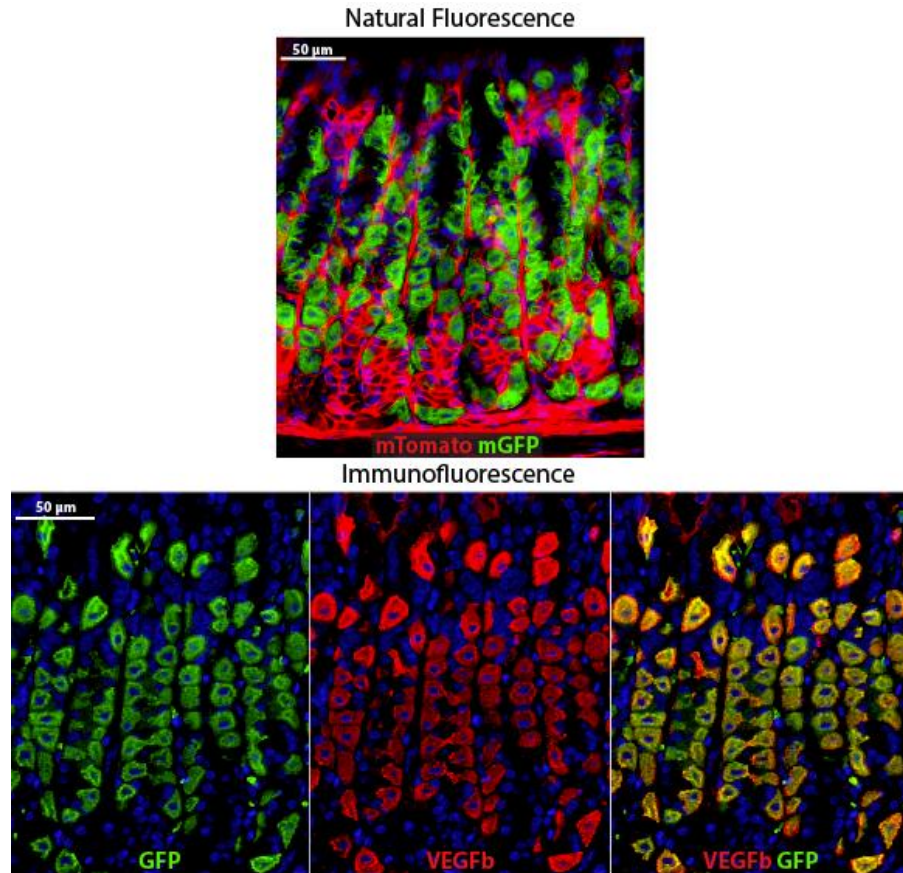


Figure 2.1: Atp4b-Cre;LSL-DTR drives iDTR specifically in parietal cells.

Top) Natural fluorescence in Atp4b-Cre;LSL-DTR;ROSAmTmG mice. Cells with Cre driver express GFP (green), and all cells without Cre driver express mTomato (red). Bottom) IF staining for GFP (green), driven by Cre driver, and the parietal cell marker VEGFB (red).

To confirm that DT was directly targeting PCs, we grew gastroids from DTR mice crossed with mTmG reporter mice (Muzumdar et al., 2007). In these mice, PCs express membrane-associated eGFP (as in Figure 2.1). We cultured these gastroids with vehicle or DT for three days (Figure 2.2) in the absence of Wnt3a, R-Spondin 1 and Noggin. Control gastroids had negligible death. DT treatment of DTR-derived organoids resulted only in specific extrusion of eGFP⁺ cells

without change in overall gastroid size or number. Thus, DT causes specific killing of parietal cells.

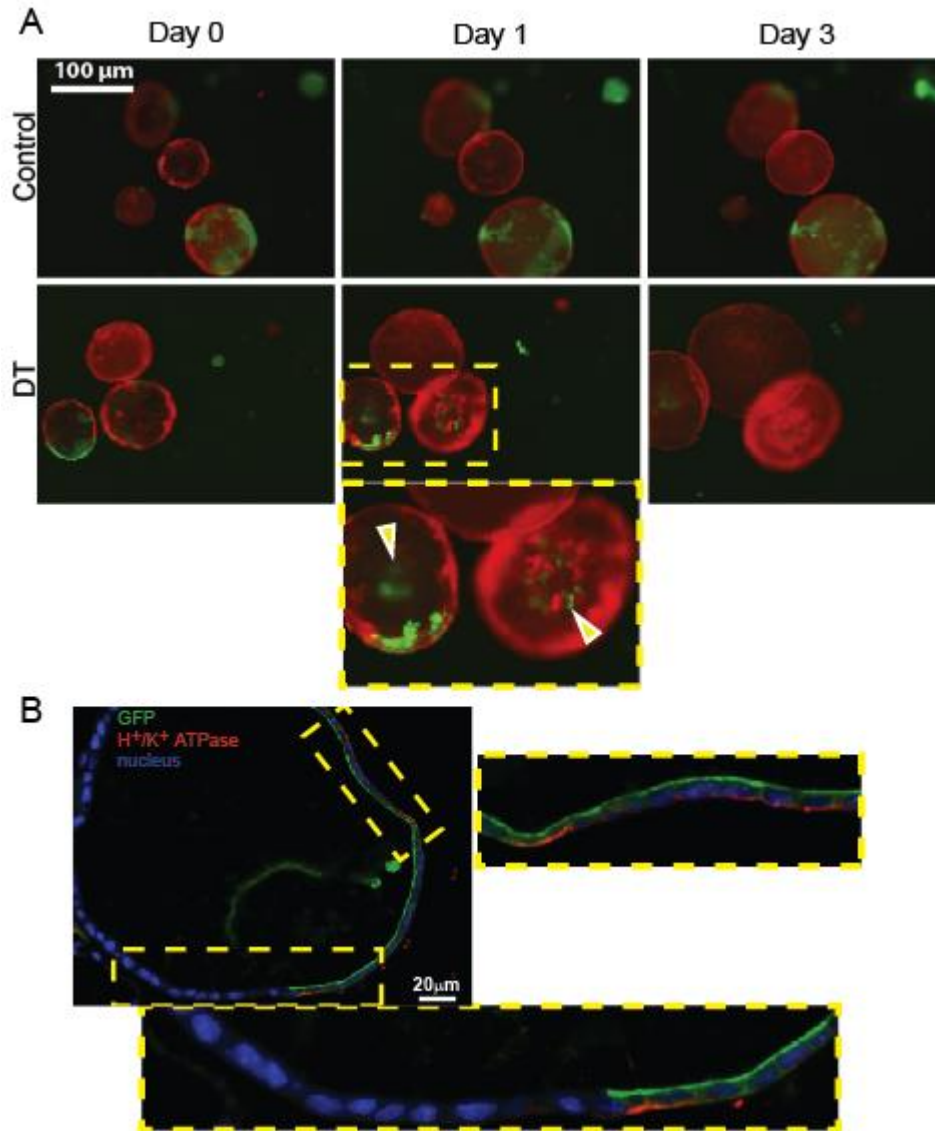


Figure 2.2: DT specifically kills parietal cells.

Top) Gastroids from DTR mice with the Atp4b⁺ parietal cell lineage fluorescing green (Atp4b-Cre;LSL-DTR;ROSA^{mTmG} mice) and all other lineages in red. The same gastroids were monitored over 3 days of control or DT treatment. Note DT treatment does not affect gastroid survival, but PCs are specifically extruded into lumen of gastroids by Day 1 (arrowheads in inset) and then are largely gone by Day 3. PC extrusion – which is consistent with cell death in these cultures – does not occur in controls. Bottom) Immunofluorescence co-staining with anti-

GFP (green) and anti-PC-marker H⁺/K⁺ATPase (red) antibodies.

In marked contrast to the TAM atrophy model, the DT treatment never caused substantial SPEM at any timepoint (n>40 total mice examined to date), and proliferation was almost entirely excluded from the base of the unit, localizing instead to the upper isthmus and neck regions (Figure 2.3A, B). SPEM is thought to arise from reprogramming of ZCs and reentry into the cell cycle (Goldenring et al., 2011b; Mills and Sansom, 2015), so we examined the morphology of the basal cells carefully. Whereas ZCs after TAM treatment had the expected simple columnar morphology with scant GIF that occurs in SPEM cells, the ZCs in DT-treated DTR mice maintained largely normal morphology with apical GIF granules still apparent (Figure 2.3D). CD44v9, a marker upregulated during proliferative metaplasia, was increased only in the proliferating neck of DT treated mice, but not in the base, contrasting with TAM treatment, which caused CD44v9 expression in neck and base (Figure 2.4). Clusterin, a secreted protein increased in SPEM (Weis et al., 2013), also labeled cells in the base of the gastric unit in TAM mice, while in DT mice, it marked only rare basal cells (Figure 2.4). Thus, apoptosis of PCs alone, even for as long as two weeks, was not sufficient to cause metaplasia.

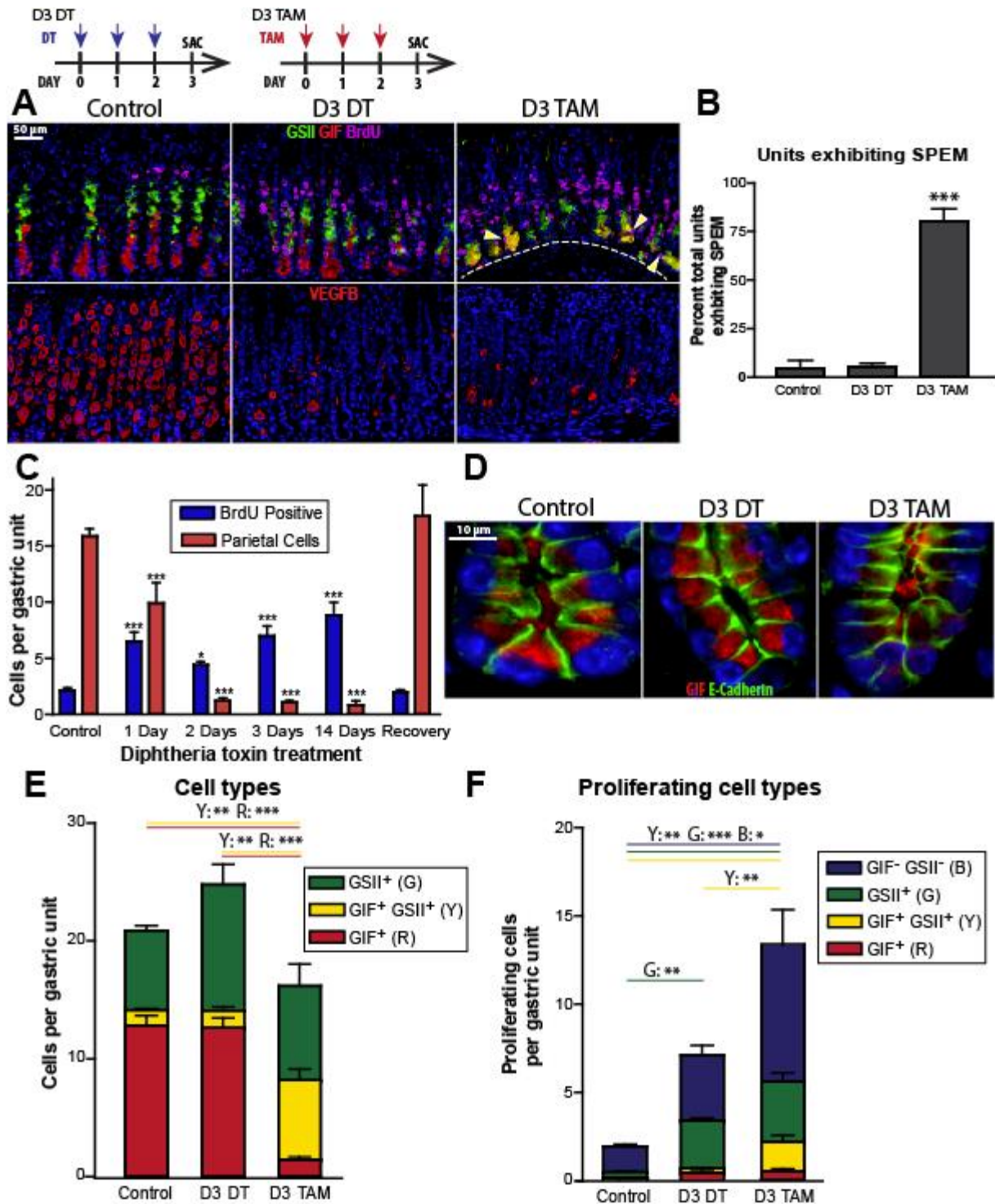


Figure 2.3: Diphtheria toxin-mediated parietal cell ablation does not cause metaplasia

A) Stomachs following three days of vehicle, DT, or TAM injections (*top*: green: GSII, red: anti-GIF, magenta: anti-BrdU); arrowheads = representative proliferating SPEM cells (yellow

cytoplasm+magenta nucleus). *Bottom*: red:anti-VEGFB (parietal cells). **B,C**) Quantification of immunofluorescence staining. **D**) Bases of units with anti-E-Cadherin (green) and anti-GIF (red). **E**) Stomachs as for panel A (red: anti-CD44v9, green: GSII, magenta: anti-BrdU; bottoms of units traced in white). **F**) qRT-PCR from whole corpus at D3. For all data: “*”, “**”, “****” = $p < 0.05, 0.01, 0.001; n \geq 3$ mice per group.

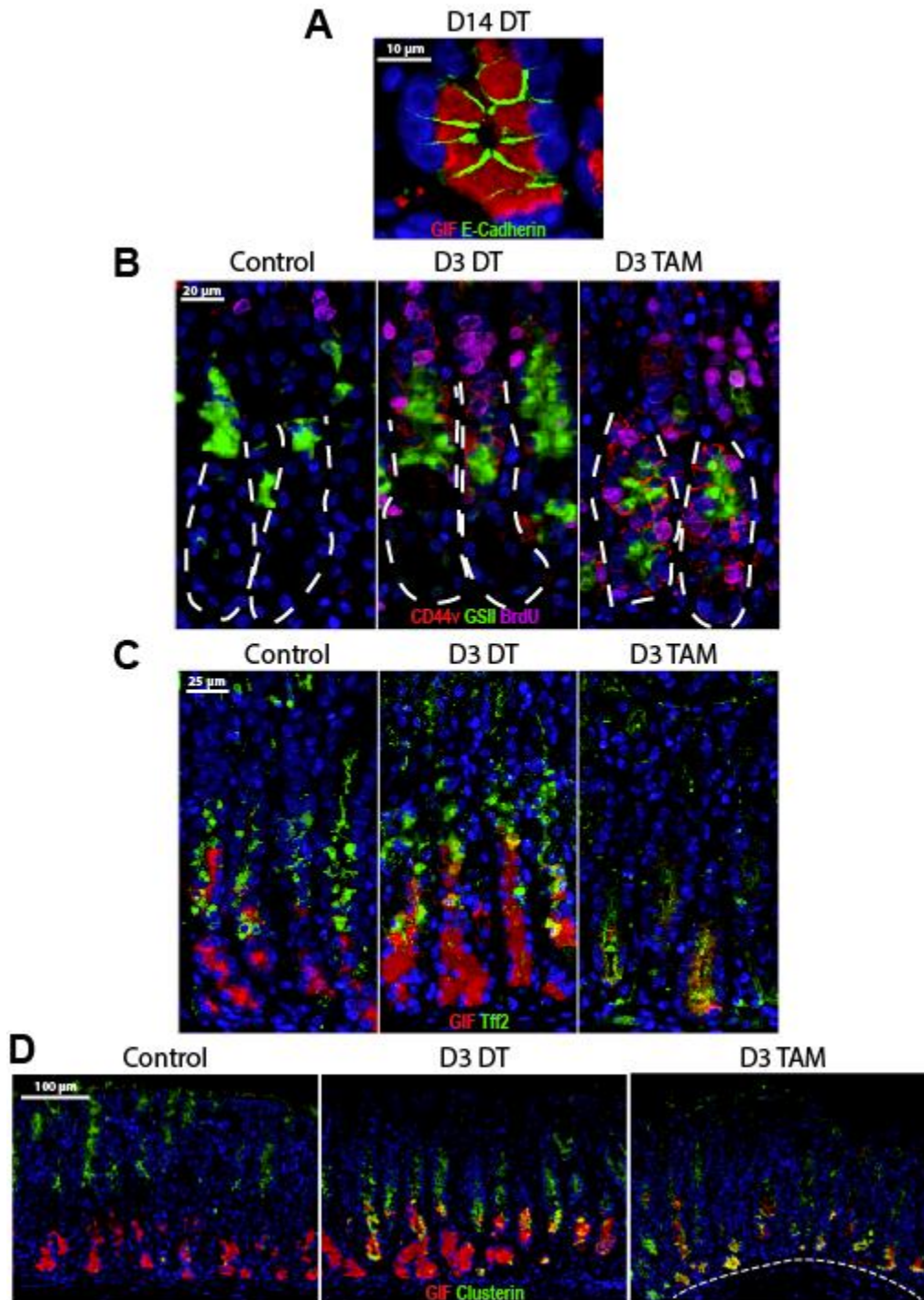


Figure 2.4: Changes in protein localization for markers of SPEM and chief cell differentiation following TAM and DT.

A) Base of D14 DT treated unit with anti-E-Cadherin (green) and anti-GIF (red). (B-D) Immunofluorescence of stomachs following three days of vehicle, DT, or TAM injections. B) Red CD44v, Green: GSII, magenta: BrdU. C) Red: GIF, Green: Tff2. D) Red: GIF, Green: Clusterin.

We next examined expression of transcripts associated with normal gastric differentiation and metaplasia (Weis et al., 2013). We observed a significant decrease in GIF mRNA expression across the whole corpus of the stomach in DT mice and a trend towards a decrease in the critical chief cell differentiation factor MIST1 (BHLHA15); however, both markers were far more substantially reduced in TAM mice (Figure 2.3F). Further corroborating histological findings, Clusterin and another commonly used SPEM marker HE4 (*Wfdc2*) (Nozaki et al., 2008) were significantly increased following TAM, but were unaffected by DT treatment (Figure 2.3F). Of eight other transcripts that showed statistically significant changes, TAM – but not DT – treatment caused significantly increased expression of genes involved in metaplasia and the immune response (*Cd14*, *Ceacam10*, *Cftr*, *Ctss*, *Dmbt1*, *Vill1*). Consistent with the histology, both TAM and DT increased proliferation-related transcripts (*Ccnb2*, *Chek2*) (Figure 2.5).

No significant change

Arhgap9
Casp1
Ceacam1
Cenpk
Cxcl17
ETV5
Figl1
Glipr1
Gpx2
Ly6a
Lyz2
Mad2l1
Mal2
Mmp12
Ms4a6b
Ms4a6c
Muc4
Pigr
Prom1
Sfn9
Tff2
Tmem48
Top2a
Traf4
Tyropb
Ube2c

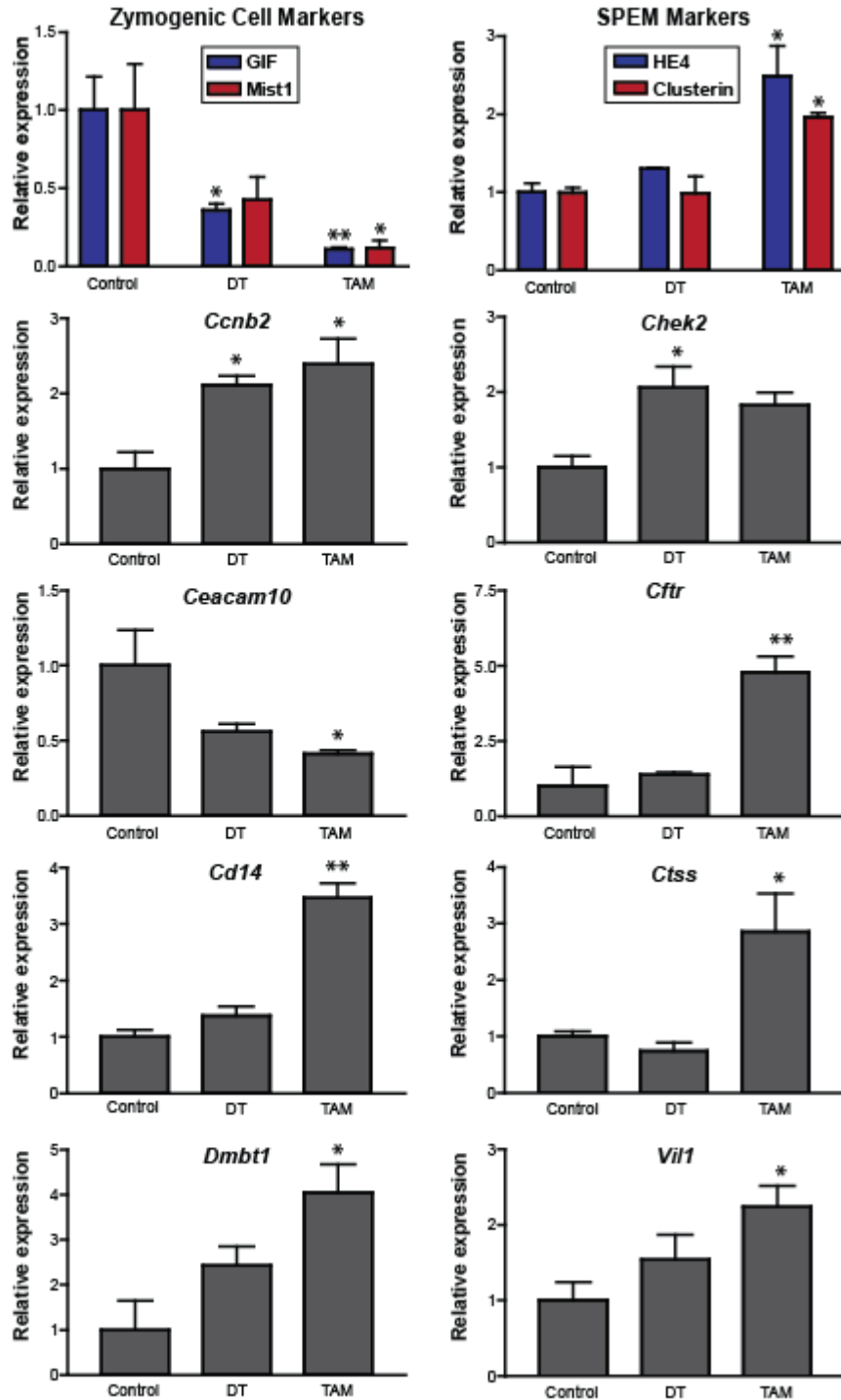


Figure 2.5: Quantitative Real-Time PCR of selected transcripts implicated in SPEM.

Transcripts were analyzed from RNA isolated from the whole gastric corpus of mice treated with vehicle, DT or TAM for three days. 12 transcripts with significant changes in experimental groups compared to control (* indicates $p \leq 0.05$, ** indicates $p \leq 0.01$) are shown.

The results described thus far argued against the model wherein PCs constitutively elaborate factors that promote differentiation, as non-metaplastic ZCs can clearly be maintained in the absence of PCs. However, it was still possible PC atrophy caused metaplasia, but the manner of death was critical. Perhaps PCs dying in *H pylori* infection or TAM – but not DT – treatment release metaplasia-inducing signals when they are injured. If true, metaplasia should not occur in DTR mice once PCs were already dead. Thus, we injected DTR mice with DT to kill PCs first and then co-injected DT and TAM for three days (DT+TAM). Mice injected with DT for 5 days showed increased isthmal/neck proliferation without SPEM, as expected; however, mice that received DT then TAM exhibited proliferative SPEM similar to what occurred with TAM alone (Figure 2.6A-C). Therefore, SPEM can occur even without substances released from injured PCs. Similar results were obtained with another atrophy/SPEM-inducing agent, DMP-777(Nomura et al., 2005), with DMP-777 treatment causing SPEM just as effectively even if PCs were already pre-killed by DT (Figure 2.6D-F; Figure 2.7).

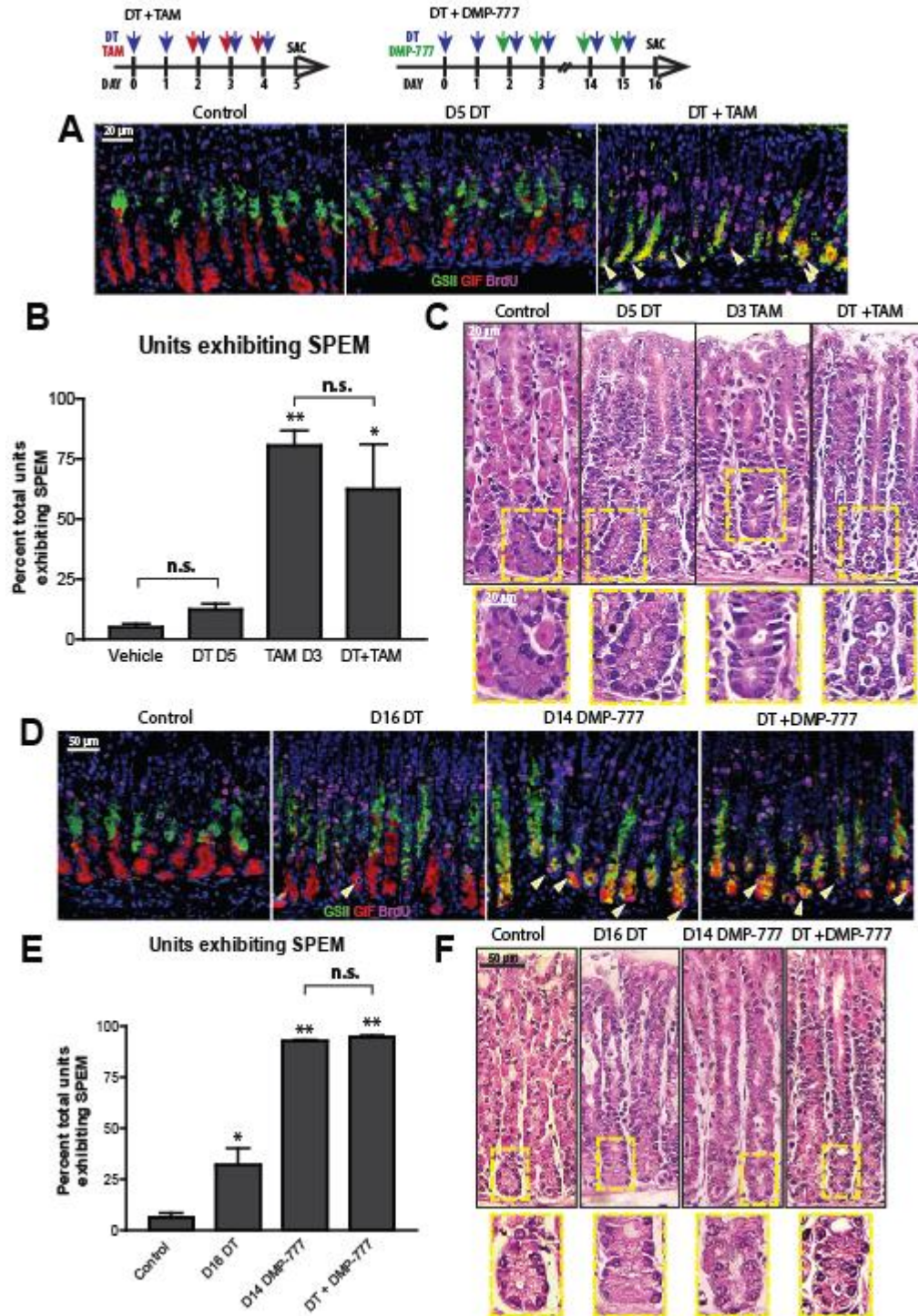


Figure 2.6: SPEM can be induced in the absence of parietal cells

A Stomachs following five days control, DT, or DT then TAM injections (green: GSII, red: anti-GIF, magenta: anti-BrdU; arrowheads = representative proliferating SPEM cells (yellow cytoplasm+magenta nucleus). **B**) Immunofluorescence data quantified. **C**) H&E. **D**) Stomachs

following 16 days control, DT, or DT then DMP-777, stained as for panel A. **E)** Immunofluorescence data quantified. **F)** H&E. For all data: “*”, “**”, “***” = $p < 0.05$, 0.01, 0.001 vs. Control in ANOVA with Dunnett; $n \geq 3$ mice per group

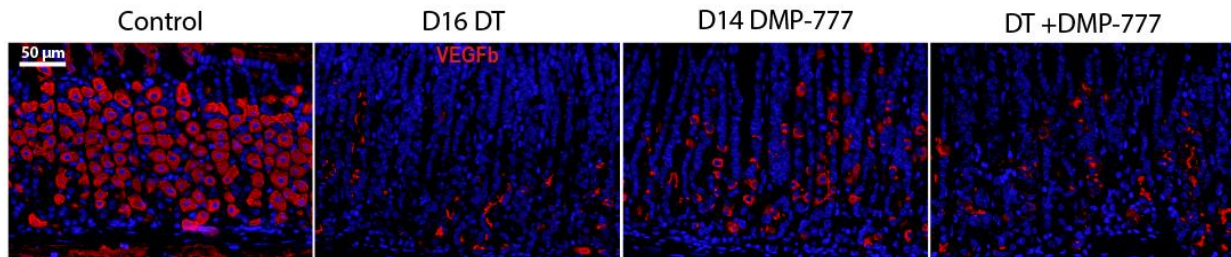


Figure 2.7: DMP-777 control showing deletion of parietal cells.

IF of stomachs following 16 days control, DT, or DT then DMP-777 for the PC marker VEGFB (red).

Overall, our results show that PC atrophy may be required but is not sufficient for metaplasia. Furthermore, signals from injured/dying PCs do not seem to be required for metaplasia induction. Additionally, we observe that the DTR mice had increased proliferation only in the normal isthmal progenitor zone, whereas TAM/DMP777 treatment showed both isthmal proliferation and proliferation of metaplastic cells in the base. Thus, the results are also consistent with previous findings that the stomach has two distinct cellular sources for progenitors: 1) constitutive stem cells in the isthmus and 2) ZCs in the base which can be induced to undergo metaplastic cell cycle reentry. If, as we have shown here, atrophy alone is not sufficient to induce cell cycle reentry, then ZCs undergoing metaplasia must require additional, as yet unidentified factors (e.g. cytokines/specific immune cell activation) to undertake this cellular reprogramming

2.3 Methods and Materials

Animals and injections

All experiments involving animals were performed according to protocols approved by the Washington University School of Medicine Animal Studies Committee. Mice were maintained in a specified-pathogen-free barrier facility under a 12 hour light cycle. Wild type *C57BL/6*, *Gt(ROSA)26Sor^{tm1(HBEGF)Awai}* (iDTR)(Buch et al., 2005), and B6.129(Cg)-*Gt(ROSA)26Sortm4(ACTB-tdTomato,-EGFP)Luo/J* (mT/mG)(Muzumdar et al., 2007) mice were all purchased from Jackson Laboratories. *ATP4b-Cre* mice(Syder et al., 2004) were crossed with iDTR mice, which express the inducible simian diphtheria toxin receptor under the control of the Rosa26 promoter. Littermate controls were housed together when possible to minimize differences in gastric microflora. To selectively kill parietal cells, Diphtheria Toxin (225 ng/mouse, Sigma) was injected intraperitoneally one or three times per day. Since parietal cells (PCs) die at a comparable rate to those previously published with D3 TAM, most analysis was done at D3 DT. Diphtheria Toxin was dissolved in sterile 0.9% sodium chloride saline. To induce SPEM, Tamoxifen (5 mg/20 g body weight, Toronto Research Chemicals Inc.) was injected intraperitoneally daily for three days or DMP-777 (7 mg/20 g body weight, gift of DuPont-Merck Corporation) was gavaged daily for 14 days. Tamoxifen was dissolved in a vehicle of 10% ethanol and 90% sunflower oil (Sigma), and DMP-777 was suspended in 1% methylcellulose (Sigma) in distilled H₂O.

Immunofluorescence

Mice were given an intraperitoneal injection containing 5-bromo-2'-deoxyuridine (BrdU, 120 mg/kg) and 5-fluoro-2'-deoxyuridine (12 mg/kg) in sterile water 90 min before sacrifice.

Following sacrifice, stomachs were immediately excised and flushed with PBS, then pinned out and fixed in freshly prepared methacarn (60% methanol, 30% chloroform, 10% glacial acetic acid) for 20 minutes and stored overnight in 70% ethanol. Tissues were arranged in 3% agar in a tissue cassette, underwent routine paraffin processing, and 5µm sections were cut and mounted on glass slides. Sections underwent a standard deparaffinization and rehydration protocol, were blocked in 1% BSA, 0.3% Triton-X100, in PBS, left overnight with primary antibodies, washed in PBS and incubated for one hour with secondary antibodies, washed, incubated 5 minutes in 1 g/ml bisbenzimidazole (Molecular Probes), washed, then mounted using glycerol:PBS.

Primary Antibodies used in this study: rabbit anti-human gastric intrinsic factor (1:10,000, gift of Dr. David Alpers, Washington University), goat anti-BrdU (1:20,000, gift of Dr. Jeff Gordon, Washington University), goat anti-VEGFb (1:100, Santa Cruz), goat anti-Clusterin (1:100, Santa Cruz), mouse anti-E-Cadherin (1:200, BD Biosciences), rabbit anti-GFP (1:100 Santa Cruz), mouse anti-TFF2 (1:500, Abcam), rat anti-CD44 v10-e16, ortholog of human v9 (1:200, Cosmo Bio), or 1 g/ml fluorescently labeled GSII lectin (Alexafluor488, 594, Molecular Probes).

Secondary Antibodies included AlexaFluor (488, 594 or 647) conjugated donkey anti-goat, anti-rabbit, or anti-mouse (1:500, Molecular Probes).

Immunofluorescence quantification

All timepoints were quantified with at least three mice, with representatives from both genders. Stomachs were fluorescently stained with bisbenzimidazole and either anti-BrdU or anti-VEGFb markers along with the neck cell marker GSII lectin and zymogenic cell marker anti-GIF. Images

were captured as TIFF files from a Zeiss Axiovert 200 microscope with Axiocam MRM camera and with Apotome optical sectioning filter. Each stomach had at least 5 images taken containing 10+ well-oriented gastric units each. Units were counted using the neck staining, and total quantifications of proliferating cells (BrdU⁺) or PCs (VEGFb⁺) (Mills et al., 2003) were averaged over total unit numbers per mouse.

For quantifying units exhibiting SPEM, SPEM was defined exclusively in corpus gastric units as either 5+ cells per unit co-expressing GSII and GIF or GSII-expressing cells extending to the base of the unit.

Genotyping

Tissue was lysed with DirectPCR reagent (Viagen Biotech Inc) with added Proteinase K (New England BioLabs) at 55 °C for 11 hours, then 85 °C for 15 minutes. Genotyping PCR was run with Redtaq (Sigma). Primers: *H⁺/K⁺ATPase-Cre* Forward: AGGGATCGCCAGGCGTTTTTC, Reverse: GTTTTCTTTTCGGATCCGCC.

Corpus gastroid culture

Gastric glands from the corpus of the stomach were isolated from *Atp4b-Cre;LSL-DTR*; ROSA^{mT/mG} mice (Muzumdar et al., 2007) according to (Barker et al., 2010) and (Stange et al., 2013a). Whole gastric glands were mixed with Matrigel, distributed in 48-well plates and grown in Advanced DMEM/F12 medium (Invitrogen), 50% Wnt3a conditioned medium, 10% R-Spondin1 and Noggin conditioned medium supplemented with 10mM HEPES, 1X N-2, 1X B27, 1X glutamax (Invitrogen), 2.5 mM *N*-Acetylcysteine (Sigma-Aldrich), 50 ng/mL EGF, 100 ng/mL FGF10 (Peprotech) and 10 nM gastrin (Sigma-Aldrich). 10 μM ROCK inhibitor (Y-

27632, Sigma-Aldrich) was provided for the first 3 days. Three days after initial culturing, gastroids were treated with 10 ng/mL of diphtheria toxin in the absence of Wnt3a, R-Spondin 1 and Noggin. Fresh medium containing DT was added the following day. Using Cytation 3 (Biotek), all wells were microscopically scanned every 24 hours throughout the whole experiment, and the number of dead gastroids was scored.

Quantitative RT-PCR

Total RNA was extracted from corpus stomach tissue using the RNeasy Mini Kit (Qiagen). RNA was treated with DNase I then cDNA was synthesized with Superscript III (Invitrogen) and random primers. qRT-PCR was performed using PowerUp SYBR Green Master Mix (ThermoFisher) and gene specific primers (Figure 2.8) on a QuantStudio 3 PCR System (ThermoFisher) and data analyzed using QuantStudio Design & Analysis Software. Every run was standardized to TATA Box Binding Protein (TBP) primers. All primers were exon-spanning when possible, (i.e. for genes having multiple exons of sufficient length). For full list of primers, see Supplemental Table. All graphs and statistics were completed in GraphPad Prism, using one-way ANOVA with either Dunnett's or Tukey's post-hoc multiple comparison tests to determine significance.

Gene	Forward Primer 5'→3'	Reverse Primer 3'→5'
TBP	CAAACCCAGAATTGTTCTCCTT	ATGTGGTCTTCCTGAATCCCT
GIF	GAAAAGTGGATCTGTGCTACTTGCT	AGACAATAAGGCCCCAGGATG
Mist1	GAGCGAGAGAGGCAGCGGATG	AGTAAGTATGGTGGCGGTCAG
TFF2	TGCTTTGATCTTGGATGCTG	GGAAAAGCAGCAGTTTCGAC
Clusterin	CCAGCCTTTCTTTGAGATGA	CTCCTGGCACTTTTCACACT
Wfdc2/HE4	TGCCTGCCTGTCGCCTCTG	TGTCCGCACAGTCCTTGTCCA
Mal2	GCTTTCGTCTGTCTGGAGATTG	ACACAAACATGACCCATCCTTG
Arhgap9	TGCTGCCTGACTTTCGTGATG	GCGGTCATTCGGTTCCTATCC
Casp1	GAAAGACAAGCCCAAGGTGAT	GGTGTGAAGAGCAGAAAGCA

Ccnb2	TGAAGTCCTGGAAGTCATGC	GAGGCCAGGTCTTTGATGAT
CD14	CTCTGTCCTTAAAGCGGCTTAC	GTTGCGGAGGTTCAAGATGTT
Ceacam1	CCTCAGCACATCTCCACAAAG	TATAGCCGTAGTGTTCCTTG
Ceacam10	CTCCGATTTCTGTGCGATTTTC	GTCCGTGGCAGATTGTGAAC
Cenpk	AATACTGGACACTCTTAACG	GGATCTTAGTTGTCAGTTCAT
CFTR	CTGGACCACACCAATTTTGAGG	GCGTGGATAAGCTGGGGAT
Chek2	TCGGCTATGGGCTCTTCA	CGTCCTTCTCAACAGTGGTC
Ctss	TCTATGACGACCCCTCCTG	TTGCCATCCGAATGTATCCTT
Cxcl17	AGGTGGCTCTTGAAGGTG	CTCTGGAGGGTCTTTGCGA
Dmbt1	ACCTCCTCACGGTGCTACAG	GCTTCTTCACATCCTCCACTG
ETV5	GCTCTTGGTGCTAAGTAGGA	TCTGATGGGTGGGTGACA
Figl1	TTATATTCCCCTCCCAGAAGC	GCCAGAAAACCCATCAGACT
Glipr1	CCAGCTTCGGTCAAAAGTGAG	TGGGTGTATCCGTGAATGCAG
Gpx2	CAGGGCTGTGCTGATTGAG	CGGACATACTTGAGGCTGTTC
Ly6a	GACTTCTTGCCCATCAATTACC	TTAGTACCCAGGATCTCCATAC
Lyz2	GCCAGAACTCTGAAAAGGAATG	CTTTGGTCTCCACGGTTGTAG
Mad2l1	TGCTTACAACACTGACCCCG	ACTGCCATCTTTCAAGGACTTC
Mmp12	CATGAAGCGTGAGGATGTAGAC	CTAGTGTACCACCTTTGCCA
Ms4a6b	TCCCTCCAATCTACACTTTACC	GACTTTGTCTCCGTGACGATG
Ms4a6c	AAAAGACGAGTCCCAGCCTAC	ATGGGACAGGAGGAACAGATG
Muc4	GCTGCCTGTATTCTTGCCT	ATGTTCTGGTGCTGCTGGA
Pigr	GATTTGGGAGGCAATGACAAC	GCTTTCTTGGATTCTTCTGGC
Prom1	TGGATAACACAGGAAGGAAGAG	CAGGGTAGAGGCAAATGTCAG
Slfn9	TCCTTAGTGGTCAAACGGTCT	TCAGGTTGCTCACTCTGGTTG
Tmem48	GCTGCTACAAATGGGAGGAT	CACGGAAGGCGTCTGACTA
Top2a	CGAAATGGCTATGGAGCTAA	TATCTTTGTCCAGGCTTTGC
Traf4	CAGGTGTTAGGCTTGGCTATC	CGATTAGGGCAGGGGACTA
Tyrobp	GGTGTGACTCTGCTGATTGC	AAGCTCCTGATAAGGCGACTC
Ube2c	CAACATCTGCCTGGACATC	CCTGCTTTGAATAGTTTCTTGC
Vil1	TCAAAGGCTCTCTCAACATCAC	GGTGCTGGAAGGAACAGG

Figure 2.8: Primers used for quantitative RT-PCR

Chapter 3: Gastric chief cells self-maintain, independent of isthmal stem cells, in homeostasis and injury

3.1 Abstract

Background & Aims

Chief cells are thought to arise from mucous neck cells in the adult mammalian stomach during homeostasis. The cellular source of injury-induced Spasmolytic Polypeptide-Expressing Metaplasia (SPEM) is debated and there is no evidence yet of how SPEM resolves upon recovery from injury. We investigated the dynamics of the chief cell lineage in homeostasis and following injury to further investigate these topics.

Methods

We used pulse-chase experiments of varying lengths with two nucleotide analogues during homeostasis and throughout acute tamoxifen injury to track long-lived label-retaining cells.

Results

BrdU-labeling was seen to enter chief cells very slowly with continual pulsing, and the majority of the labeled chief cells were nonadjacent to the transitional zone. Varying pulse and chase windows of BrdU showed that BrdU exited the neck but did not enter the chief cell population. Our label-retention assays showed that the majority of chief cells retain label for over 9 months at homeostasis. When labeled chief cells are challenged with acute or chronic injury, label is

retained in metaplastic cells, and this can be following back into healthy chief cells upon recovery from acute injury.

Conclusions

Our data is consistent with a model wherein chief cells are a self-sufficient cell population at homeostasis maintained through infrequent self-replication, with neck cells shown not to give rise to chief cells, as had previously been believed. Chief cells are also able to maintain their own population following injury through dedifferentiating into metaplastic cells which can then redifferentiate upon resolution of the insult.

3.2 Introduction

The lineage relationships between the stem cells, progenitors, and differentiated cells of the adult mammalian stomach have been poorly defined, largely due to the lack of specific markers and genetic tools to investigate the gastric stem cell. All cells in the healthy stomach are posited to arise from a multipotent stem cell at the isthmus of the gastric unit (Karam and Leblond, 1993a). In this model, stem cells give rise to immature progenitors of most mature gastric lineages that mature as they migrate to their functional location within the gastric unit. This model also posits a special relationship between mucous neck cells and gastric chief cells. Immature mucous neck are borne from the isthmal stem cell then migrate down the unit and differentiate into mature mucous neck cells, a process that takes about two weeks. When mucous neck cells reach top of the base, they transdifferentiate into zymogenic ‘chief’ cells w are estimated to live for around half a year (Karam and Leblond, 1993c; Quante et al., 2010; Goldenring et al., 2011a). The conversion of neck cells to chief cells is supported by the existence of ‘transitional’ cells between neck and chief cells which express markers of both populations (Suzuki et al., 1983), experiments showing that labels such as ^3H -Thymidine slowly fill into the base after the neck

cells are labeled in long pulses (Karam and Leblond, 1993c), and experiments showing increased transitional cells when chief cell maturation is blocked (Ramsey et al., 2007).

Gastric injury induces the loss of mature chief characteristics and the appearance of metaplastic cells co-expressing chief and neck cell markers termed Spasmolytic Polypeptide-Expressing Metaplasia (SPEM) (Schmidt et al., 1999). Lineage tracing from the chief cell-marking *Mist1* locus indicates that these metaplastic cells arise via dedifferentiation of chief cells (Nam et al., 2010). However, *Mist1* expression has also been shown in rare isthmal cells (Hayakawa et al., 2015; Kinoshita et al., 2018b), questioning the specificity of the lineage marker, and nearly all other genetic drivers which mark chief cells have also been shown to have some isthmal activity as well (Pheesse and Sansom, 2017), making further genetic lineage tracing approaches currently unfeasible. SPEM can arise from pre-existing cells without the need for cellular division (Radyk et al., 2018), supporting the chief cell origin. SPEM resolves within weeks following acute injury (Huh et al., 2012b), yet it is not yet known on a cellular level what becomes of the metaplastic cells.

In this study, we use multiple pulse-chase experiments with 5-bromo-2'-deoxyuridine (BrdU), including experiments pulsing BrdU during injury, to mark long-lived label-retaining cells allowing us to track the dynamics of the chief cell population at homeostasis and following SPEM-inducing injury independently of genetic lineage tracing. We find that chief cells appear to self-replicate at homeostasis and that the majority of neck cells are not fated to becoming chief cells, contrary to current belief. We then illustrate the conversion of chief cells to SPEM cells following acute and chronic injury, and further indicate that metaplastic cells can re-differentiate back into chief cells. Following our results, we suggest a model wherein chief cells are a largely self-maintaining population at homeostasis and following injury.

3.3 Methods and Materials

Animals and Injections

All experiments involving animals were performed following protocols approved by the Washington University School of Medicine Animal Studies Committee. Mice were maintained in a specified pathogen-free barrier facility under a 12-hour light cycle. Wild type *C57BL/6* mice were purchased from Jackson Laboratories (Bar Harbor, ME). Littermate controls were housed together when possible. To induce SPEM, tamoxifen (5 mg/20 g body weight; Toronto Research Chemicals, Inc, Toronto, Canada) was injected intraperitoneally daily for 3 days. Tamoxifen was dissolved in 10% ethanol and 90% sunflower oil (Millipore Sigma, MO). 5-bromo-2'-deoxyuridine (BrdU; MilliporeSigma) was administered via drinking water (800 mg/L) for up to 8 weeks, changed on the third day. 5-ethynyl-2'-deoxyuridine (EdU; Baseclick, Bavaria, Germany) was injected intraperitoneally daily for 4 days (30 mg / kg mouse mass, dissolved in PBS).

Immunofluorescence

Upon sacrifice, stomachs were immediately excised, flushed with phosphate buffered saline (PBS), inflated, and fixed overnight in cold formalin (3.4% formaldehyde in PBS; Millipore Sigma, MO). The following day, stomachs were transferred to 70% ethanol then cut into rings, embedded in 3% agar, and underwent routine paraffin processing. 5 μ m sections were mounted on glass slides. Slides were deparaffinized and rehydrated with xylenes and isopropanol, and antigen retrieval was done via pressure cooking in a Tris solution. Slides were blocked with 1% bovine serum albumin and 0.3% Triton X-100 in phosphate-buffered saline for 1 hour, then primary antibodies were incubated overnight at 4 °C. The following day, secondary antibodies

were applied for 1 hour then slides were mounted using ProLong Gold antifade reagent with DAPI (Invitrogen, CA).

Primary antibodies used in this project include: rabbit anti-human gastric intrinsic factor (1:10,000; a gift from Dr. David Alpers, Washington University, St Louis, MO), goat anti-5-bromo-2'-deoxyuridine (1:20,000; a gift from Dr. Jeff Gordon, Washington University, St Louis, MO), Rabbit anti-Ki67 (1:100; Abcam, Cambridge, UK), Sheep anti-pepsinogen II (1:1000, Abcam), Rabbit anti- α SMA (1:200, Abcam), goat anti-clusterin (1:200, Santa Cruz), rat anti-BrdU (1:200, Abcam), rat anti-CD44 v10-e16, ortholog of human v9 (1:200, Cosmo Bio), AAA Lectin (1:500, EY Labs), and 1 g/mL fluorescently labeled GSII lectin (Alexa Fluor 488, 594, and 647; Molecular Probes). Secondary antibodies included AlexaFluor (488, 594, or 647) conjugated donkey anti-goat, anti-rabbit, anti-sheep, anti-rat, or anti-mouse antibodies (1:500; Molecular Probes). EdU was imaged using the BCK-EdU488 kit following the manufacturer's instructions.

Helicobacter pylori infection

The mouse-adapted, wild-type pre-mouse Sydney strain of *Helicobacter pylori*, PMSS1, was kindly provided by Dr. Rick Peek (Vanderbilt University). Growth of the PMSS1 strain prior to inoculation of mice has been previously described (Saenz et al., In press.). Mice were fasted for 4-6 hours prior to oral gavage with 200 μ L of an overnight H pylori culture ($\sim 1 \times 10^8$ cfu/mouse), then fasted for an additional 1-2 hours after infection. Mice were then allowed to feed ad libitum and were sacrificed 8-12 weeks after infection. Mouse stomachs were excised and opened along the lesser curvature. Food was gently scraped away, and the forestomach

removed. Stomachs were pinned out in cold formalin and fixed overnight at 4°C. The next day, stomachs were cut in longitudinal sections and underwent routine paraffin processing.

Immunofluorescence Quantification

All quantifications were from at least three mice, with both sexes used. Quantifications were done on stomachs stained fluorescently for anti-5-bromo-2'-deoxyuridine, neck cell marker GSII lectin and chief cell marker anti-GIF. Single GIF⁺ cells were scored as mature chief cells; Single GSII⁺ cells as mucous neck cells, and GIF⁺/GSII⁺ cells were considered metaplastic. Slides were imaged on a Zeiss Axiovert 200 microscope with an AxioCam MRM camera. For BrdU-retention assays, only fully imaged units with >3 label-retaining chief, SPEM, or neck cells were quantified, and at least 20 label-retaining units were quantified per stomach when possible.

Counts were done using Axiovision LE64 software to selectively overlay color channels to count label-retaining cells co-staining with GIF and/or GSII, as previously described (Radyk et al., 2018). Counts were averaged over the total number of units quantified per mouse, then all mice for a condition were averaged for the final value. Graphs were completed in GraphPad Prism (La Jolla, CA), using one-tailed student t-tests to determine significance, *P<0.05, **P<0.01, and ***P<0.001.

3.4 Chief cells take up little BrdU upon extended continuous pulsing

To track the cellular dynamics of the corpus unit independent of genetic lineage tracing, we performed continuous BrdU labeling experiments. We administered BrdU in drinking water continuously for up to eight weeks, harvested stomachs, then immunostained and quantified the proportion of each cell lineage labeled with BrdU. All cells that performed DNA-replication during our labeling window will be BrdU⁺. Due to the continuous labeling paradigm, once a cell

is labeled it will remain labeled during the entire pulse window, allowing us to interpret the entire proliferative history of the gastric corpus unit during our labeling window. As shown in Figure 3.1, neck cells readily labeled with BrdU, with 70% labeled at two weeks, 77% at four weeks, and 88% at eight weeks, with neck cells near the isthmus incorporating label before those lower in the unit, consistent with data published by Karam for a similar experiment giving continuous ^3H -Thymidine (Karam and Leblond, 1993c). Parietal cells incorporated BrdU at a lower rate than neck cells, as expected, with 24% labeling at two weeks, 37% by four weeks, and 50% at eight weeks, slightly below the rate reported by Karam yet following a similar trend (Karam, 1993). However, chief cells remained largely BrdU-negative, with less than 10% BrdU⁺ at all timepoints (Figure 3.1A-B). Surprisingly, we noticed that the chief cells that did take up BrdU were often nonadjacent to the transitional zone between the unit neck and base, contrary to what would be expected if chief cells derive from BrdU⁺ transitional cells. Less than one quarter of BrdU⁺ chief cells were adjacent to the transitional zone, with the rest distributed throughout the base (Figure 3.1C). BrdU⁺ chief cells were also often found in pairs regardless of position (Figure 3.1D), suggesting that chief cells may infrequently divide into additional chief cells at homeostasis, consistent with other works describing a low level of proliferation at the unit base (Suzuki et al., 1983; Karam and Leblond, 1993c).

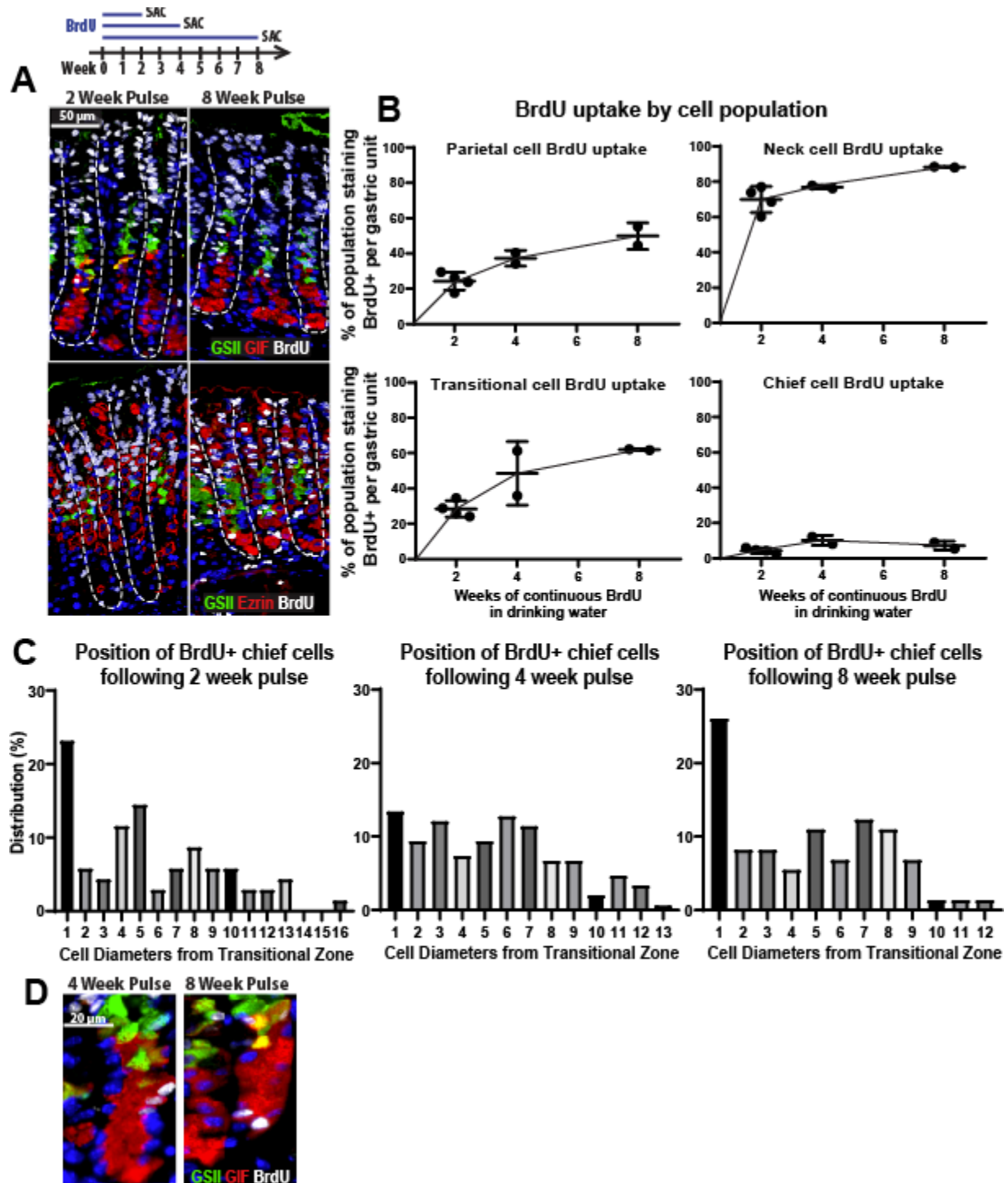


Figure 3.1: Continuous BrdU marks few chief cells in the healthy stomach

A) Stomachs of mice administered BrdU via drinking water for two or eight weeks. BrdU (white nuclei) incorporation into the main gastric epithelial cell types was tracked (Top panels: GSII⁺ neck cells in green, GIF⁺ chief cells in red, GSII⁺GIF⁺ transitional cells seen as yellow. Bottom

panels: Ezrin-expressing parietal cells in red). **B)** BrdU uptake quantified from images such as in panel A for each cell population, counted as percentage of the population per unit positive for BrdU. **C)** The location within the base of each BrdU⁺ chief cell was noted, counted as numbers of cells below the lowest GSII⁺ (or GSII⁺CIF⁺) cell. **D)** Representative images of BrdU⁺ chief cell pairs, stained as for panel A.

3.5 BrdU administered throughout acute injury marks nearly all epithelial cells

With less than 10% of chief cells incorporating BrdU within an 8-week pulse, pulsing long enough to mark all chief cells then still chasing multiple months to deplete label from all non-chief cells would be impractical. To label chief cells in a more feasible time window, we tried continuous labeling with BrdU throughout acute gastric injury using high doses of the selective estrogen receptor modulator, tamoxifen (TAM). Three daily injections of TAM causes ablation of nearly all parietal cells and initiates a proliferative and metaplastic response from the remaining epithelial cells (Huh et al., 2012b; Saenz et al., 2016). To test whether there is enough proliferation for BrdU to mark nearly all cells, we continuously labeled with BrdU in the drinking water one day prior to treating with TAM through two days following TAM treatment. At the end of the BrdU+TAM labeling period, BrdU marked $98.3 \pm 0.2\%$ of neck cells, $96.3 \pm 0.7\%$ of SPEM cells, and $77.9 \pm 3.5\%$ of chief cells (Figure 3.2A-B). TAM-induced SPEM resolves within two weeks (Huh et al., 2012b), so we performed the same experiment followed by a chase with normal drinking water for up to nine months. Over 80% of chief cells were BrdU⁺ following one month chase, along with 80% of parietal cells and 65% of neck cells (Figure 3.2C-D). Parietal and neck cells regularly lost label for the first six months before leveling out with around 20% of parietal cells (Figure 3.3A) and 8% of neck cells retaining label from months six through nine. Chief cells maintained label throughout the full chase, with

65.9±4.7% BrdU⁺ even after nine months, notably longer than their calculated half-year survival rate (Karam and Leblond, 1993c; Quante et al., 2010). BrdU was diluted from nearly all isthmal cells within the first months and nearly all neck cells by five months, indicating that the chief cell population maintains BrdU with no contributions from the upper unit, either through living much longer than previously recognized or through infrequent self-replication.

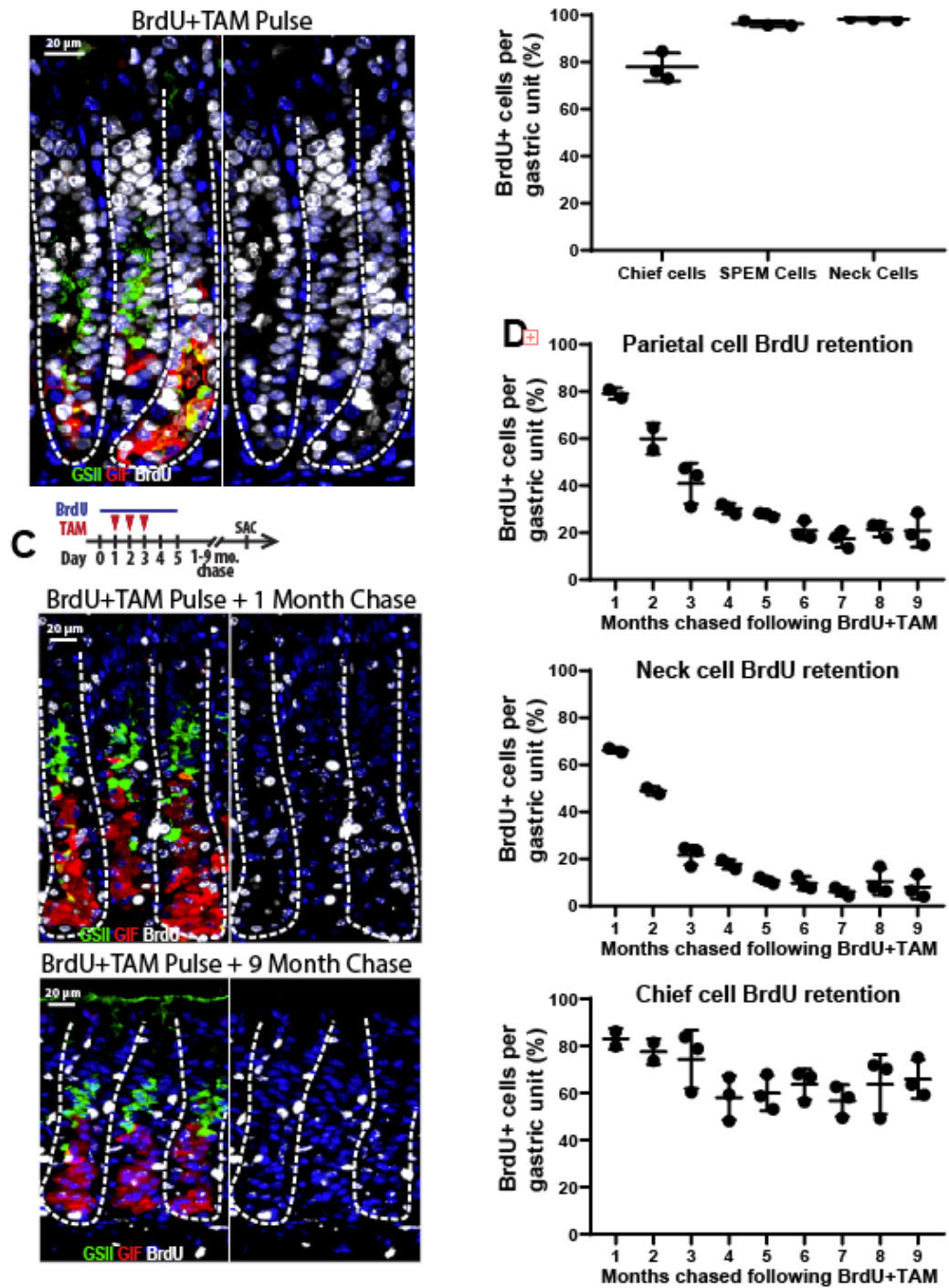


Figure 3.2: BrdU+TAM pulse chases indicate that chief cells are a self-maintaining population

A) Stomach of a mouse administered BrdU alongside three daily injection with TAM. BrdU (white nuclei) incorporated into all main cell types of the damaged gastric epithelium (GSII⁺ neck cells in green, GIF⁺ chief cells in red, GSII⁺GIF⁺ SPEM cells seen as yellow). Right panel

shows same gastric units with only DAPI and BrdU for better visualization of BrdU uptake. **B)** BrdU uptake for each cell population quantified from images such as in panel A, counted as percentage of the population per unit positive for BrdU. **C)** Stomachs of mice given the BrdU+TAM pulse as in panel A then chased for 1-9 months with normal drinking water. Stained as for panel A. **D)** BrdU uptake for each cell population quantified from images of 1-9 months chased, such as in panel C, counted as percentage of the population per unit positive for BrdU.

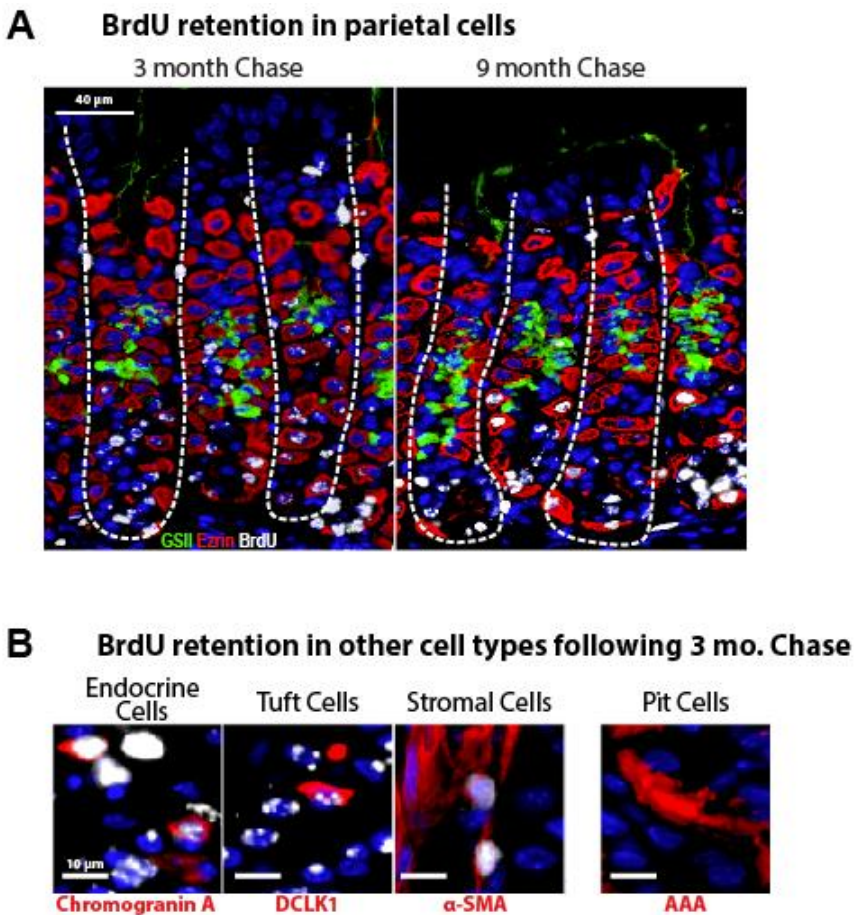


Figure 3.3: BrdU retention in parietal cells and other epithelial lineages

A) BrdU (white nuclei) is retained in parietal cells (red, Ezrin) through 9 months of chasing, with long held label generally seen in the lower-most parietal cells. **B)** Label is seen in endocrine cells, tuft cells, and stromal cells following three a month chase, but not in pit cells.

3.6 Chief cells are not the predominate terminal maturation state for neck cells

Both continuous labeling with BrdU and the BrdU+TAM pulse-chase experiments suggested that chief cells maintain their own census in the adult stomach, so we next tested the dynamics of neck cells, as they have been considered transient intermediate precursors to chief cells. We administered BrdU for two weeks, by which point six neck cells ($69.9 \pm 4.2\%$ of total), but less than one chief cell ($4.3 \pm 0.9\%$ of total) per unit incorporated label. After the continuous 2 weeks of BrdU labeling, we then chased with normal water for up to eight weeks to see if chief cells would gain label as neck cells lost it, as would occur if neck cells transitioned into chief cells. After the eight-week chase, only two neck cells per unit retained label (net loss of 4) while still only one chief cell per unit had BrdU (no net gain) (Figure 3.4A-B). To find other mechanisms by which the neck cells could be losing their label, we stained for cleaved caspase 3 and Ki67 in uninjured stomachs. As expected, no apoptosis was observed in the neck region, and Ki67 was generally only expressed in the uppermost neck cells (Figure 3.4C), making it unlikely that BrdU was lost through programmed cell death or diluted by proliferation. We did notice BrdU⁺ pit cells fairly regularly at 4 weeks chase (Figure 3.4D), beyond what would be expected for cells with a published lifespan of 3-4 days (Karam and Leblond, 1993b), otherwise we observed no process other than dilution in proliferative isthmal cells for any gastric cells to lose BrdU label. Regardless of how neck cells lose their BrdU, our experiments indicate that neck cells are not predominately fated to become chief cells, again consistent with chief cells maintaining their own population.

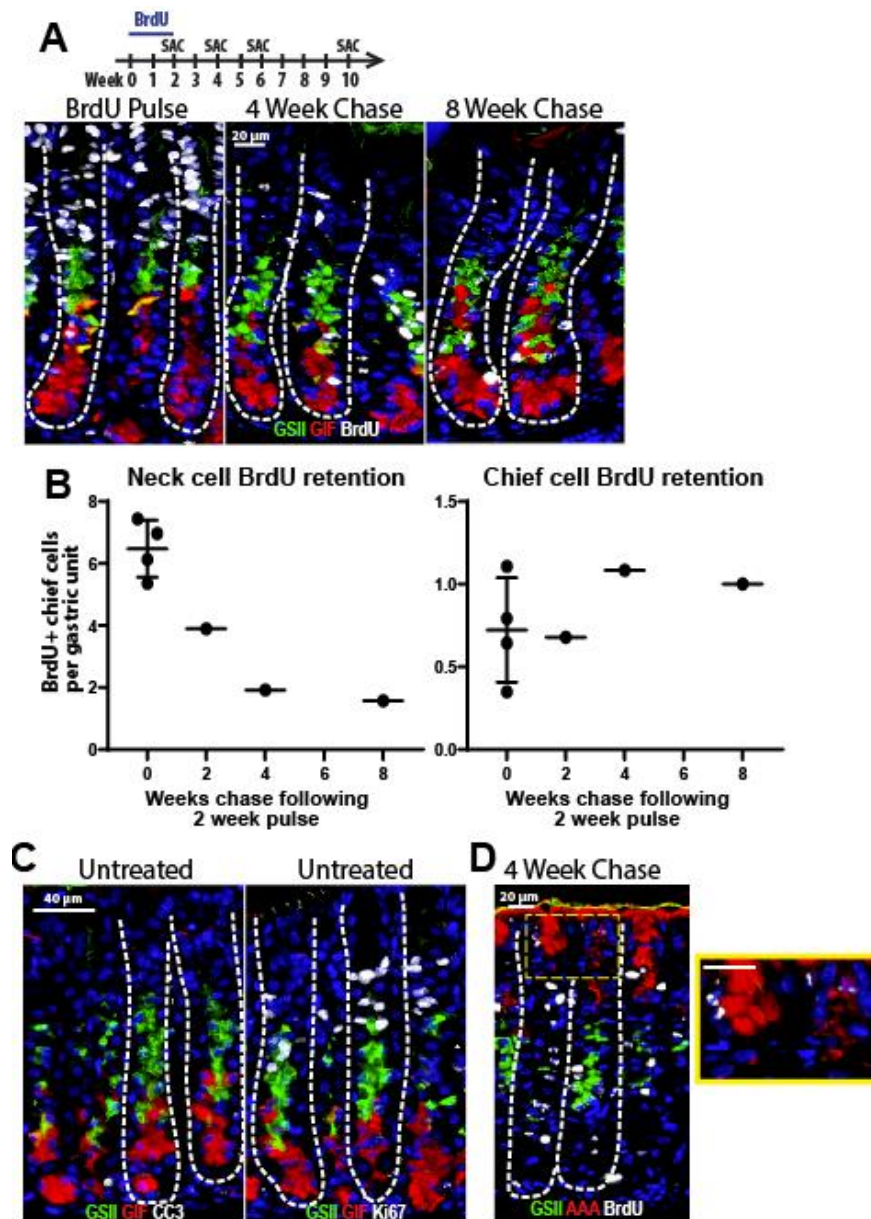


Figure 3.4: Chief cells are not the final fate for neck cells

A) Stomachs of mice administered BrdU for two weeks then chased for 4-8 weeks. BrdU (white nuclei) retained in all main cell types of the damaged gastric epithelium was tracked (GSII⁺ neck cells in green, GIF⁺ chief cells in red, GSII⁺GIF⁺ transitional cells seen as yellow). **B)** BrdU retention for neck and chief cells quantified from images such as in panel A for the pulse and for 2, 4, and 8 week chases. **C)** Healthy stomachs stained with GSII (green), GIF (red), and either cleaved caspase 3 (white, left panel) or Ki67 (white, right panel) to check for cells undergoing apoptosis or entering the cell cycle. **D)** Stomach of mice administered BrdU for two weeks then chased for 4 weeks often had BrdU⁺ pit cells (AAA, red).

3.7 Chief cells give rise to SPEM cells following gastric injury

All of our experiments thus far support a model wherein chief cells self-maintain their population at homeostasis from self-duplication. We next probed whether the same is true following injury. We performed previously mentioned experiments with BrdU+TAM injury to drive high labeling throughout the chief cell population and then chased for 3 months. As noted above, at the end of the 3 month chase $75\pm 7\%$ of chief cells retain label (Figure 3.5A), while the pit, isthmus, and upper mucous neck cells are unlabeled. In fact at the 3 month chase stage, we only observe an average of 0.8 BrdU⁺ epithelial cells in the pit-isthmus-upper neck region that were not obviously mature parietal cells based on morphology. Separate staining showed that rare gastric cell populations like endocrine cells, tuft cells, and stromal cells retained label at 3 months. Pit cells were never seen retaining label after 3 months chase (Figure 3.3B).

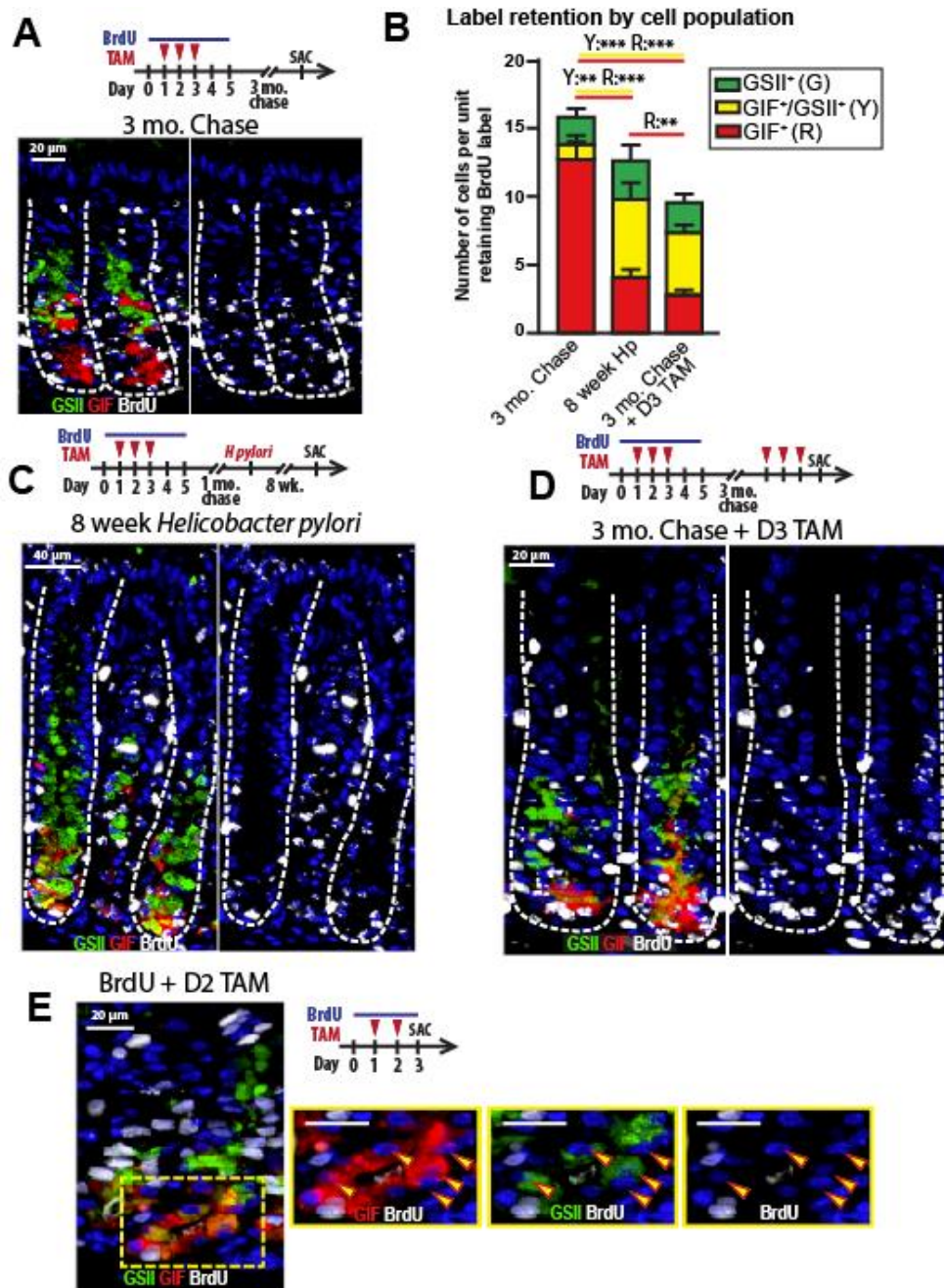


Figure 3.5: Metaplastic cells arise from chief cells following chronic and acute injury

A) Stomach of mouse given BrdU+TAM pulse then a 3 month chase (BrdU, white; GIF, red; GSII, green). **B)** Stomach of mouse given BrdU+TAM pulse, 1 month chase, then infected with *Helicobacter pylori*, stained as for panel A. **C)** Stomach of mouse given BrdU+TAM pulse, 3 month chase, then 3 days TAM, stained as for panel A. **D)** BrdU retention for neck (green), chief (red), and SPEM (yellow) cells quantified for panels A-C. **E)** Stomach of mouse given BrdU over only two days of TAM (BrdU, white; GIF, red; GSII, green). Right panels: split colors

showing GIF, GSII, and BrdU separately, arrowheads denote SPEM cells that have not yet proliferated (GIF⁺, GSII⁺, BrdU⁻). *P<0.05, **P<0.01, and ***P<0.001 in one-tailed Student's t tests.

To address whether chief cells sourced SPEM, we combined our TAM+BrdU experiments with *Helicobacter pylori* (HP) infection. HP infection causes the appearance of small, focal regions of SPEM beginning around 6 weeks after initiation of infection (Saenz et al., 2018). We generated TAM+BrdU mice and allowed them to rest for 1 month and initiated HP infection. We then waited an additional 2 months to allow HP infection to cause metaplasia in the corpus. After 2 months of HP infection, TAM+BrdU mice had small numbers of corpus units with SPEM, while the rest of the corpus was unaffected and closely mimicked TAM+BrdU mice without HP infection chased for 3 months (Figure 3.6A). Within the metaplastic units, 67±4% of metaplastic cells retained BrdU. Additionally, 22±5% of neck cells (GSII only) retained label in metaplastic units after HP infection, same as the 22±2% seen in TAM+BrdU mice chased for 3 months without HP infection (Figure 3.5B,D). Given that neck cell label-retention within metaplastic units of HP infected mice was similar to TAM+BrdU mice chased for 3 months without HP infection, this indicated that neck cells did not transdifferentiate into the metaplastic cells. If SPEM cells had arisen from a small number of stem or progenitor cells, we would expect the multiple rounds of proliferation to dilute the BrdU. Instead, the BrdU⁺ metaplastic cells appeared to principally arise at the expense of the preexisting labeled chief cell population with minimal proliferation. On average, metaplastic units had 6 BrdU⁺ 'yellow' SPEM cells following HP infection, while the 'red' chief cell population lost 8 labeled cells, with no change in 'green' neck cells. Similar results were seen in 15 mice over 8-12 weeks' infection (Figure 3.6B).

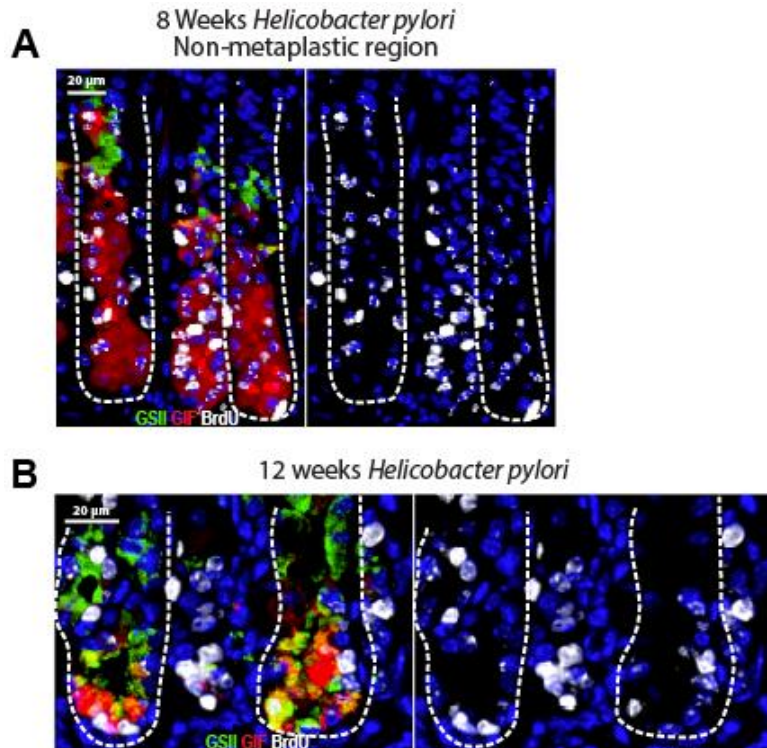


Figure 3.6 Additional *Helicobacter pylori* data

A) Non-metaplastic regions of mice given BrdU+TAM, rested one month, then infected with HP for two months closely resemble units in mice given BrdU+TAM followed by a three month chase. **B)** Metaplastic units following 12 weeks HP infection resemble those at 8 weeks.

To test whether acute drug-induced SPEM arises in the same manner as HP-induced SPEM, we generated TAM+BrdU mice and chased them for three month and subsequently injected them with an additional three days of TAM to induce metaplasia. Re-injury with TAM induced a population of BrdU⁺ SPEM cells to arise while BrdU⁺ chief cells decreased and BrdU⁺ neck cells remained their label (Figure 3.5C-D). To ascertain that the expanded label-retaining GIF⁺GSII⁺ cells were truly metaplastic, we co-stained for additional SPEM markers Clusterin and CD44v (Wada et al., 2013; Weis et al., 2013) and found both markers to overlap with the label-retaining cells (Figure 3.7A). These findings are consistent with HP-induced injury and strongly support the idea that SPEM arises from pre-existing chief cells following injury. We noticed a lesser

amount of label retention following TAM than in HP infection, likely due to label dilution because TAM-induced SPEM is much more proliferative than *Hp*-induced SPEM (Figure 3.7B).

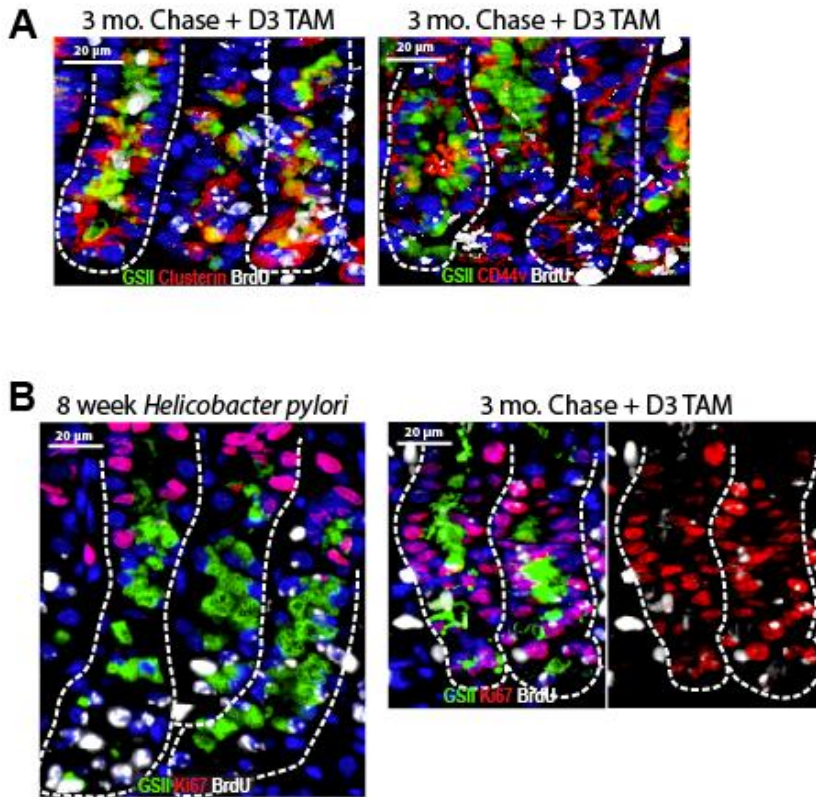


Figure 3.7 Additional SPEM data

A) BrdU-retaining SPEM cells (BrdU⁺ and GSII to the base of the unit) following re-injury with TAM express clusterin (left) and CD44v (right), indicating that they are fully metaplastic. **B)** Label-retaining SPEM cells following HP infection (left) are largely quiescent (Ki67, red, marks nuclei of cells in the cell cycle), whereas SPEM cells following TAM (right) are proliferative

An alternate model for how SPEM forms posits that progenitors in the isthmus or neck give rise to metaplastic cells upon injury (Hayakawa et al., 2015; Kinoshita et al., 2018b). Previous data from our group showed that SPEM can arise from pre-existing cells when all proliferation is blocked with fluorouracil (Radyk et al., 2018). To confirm that metaplastic cells arise via plasticity of pre-existing cells when proliferation is not constrained, we gave continuous BrdU one day prior to injury and then through two days of TAM. We harvested stomachs following

two days of TAM instead of the normal peak-SPEM timepoint of 3 days TAM to view the gastric units as SPEM was actively forming. The presence of cells positive for both GIF and GSII but not yet BrdU⁺ (Figure 3.5E) confirmed that SPEM cells arise from existing cells at the base of the unit, as all SPEM cells would be BrdU⁺ if they arose from a progenitor population.

To further address potential contributions of isthmal progenitors to metaplasia, we injected mice that had undergone the BrdU+TAM pulse and three-month chase with EdU for 4 days. After this 4 day label period, we observed EdU incorporated into isthmal cells, lower pit cells, and upper neck cells, as expected. Negligible overlap was seen with BrdU⁺ cells at the base (Figure 3.8A). We then injured mice that had undergone the BrdU+TAM pulse, a three-month chase, and a 4 day EdU label with TAM and sacrificed the mice the next day. EdU was diluted from the isthmal and neck cells due to the high proliferation induced by TAM, and negligible EdU incorporation was seen in BrdU⁺ SPEM cells at the base (Figure 3.8B). Thus, while a minority of SPEM cells that no longer retain label may possibly arise from non-chief cells, our observations indicate that the principle source of metaplastic cells following injury are pre-existing chief cells.

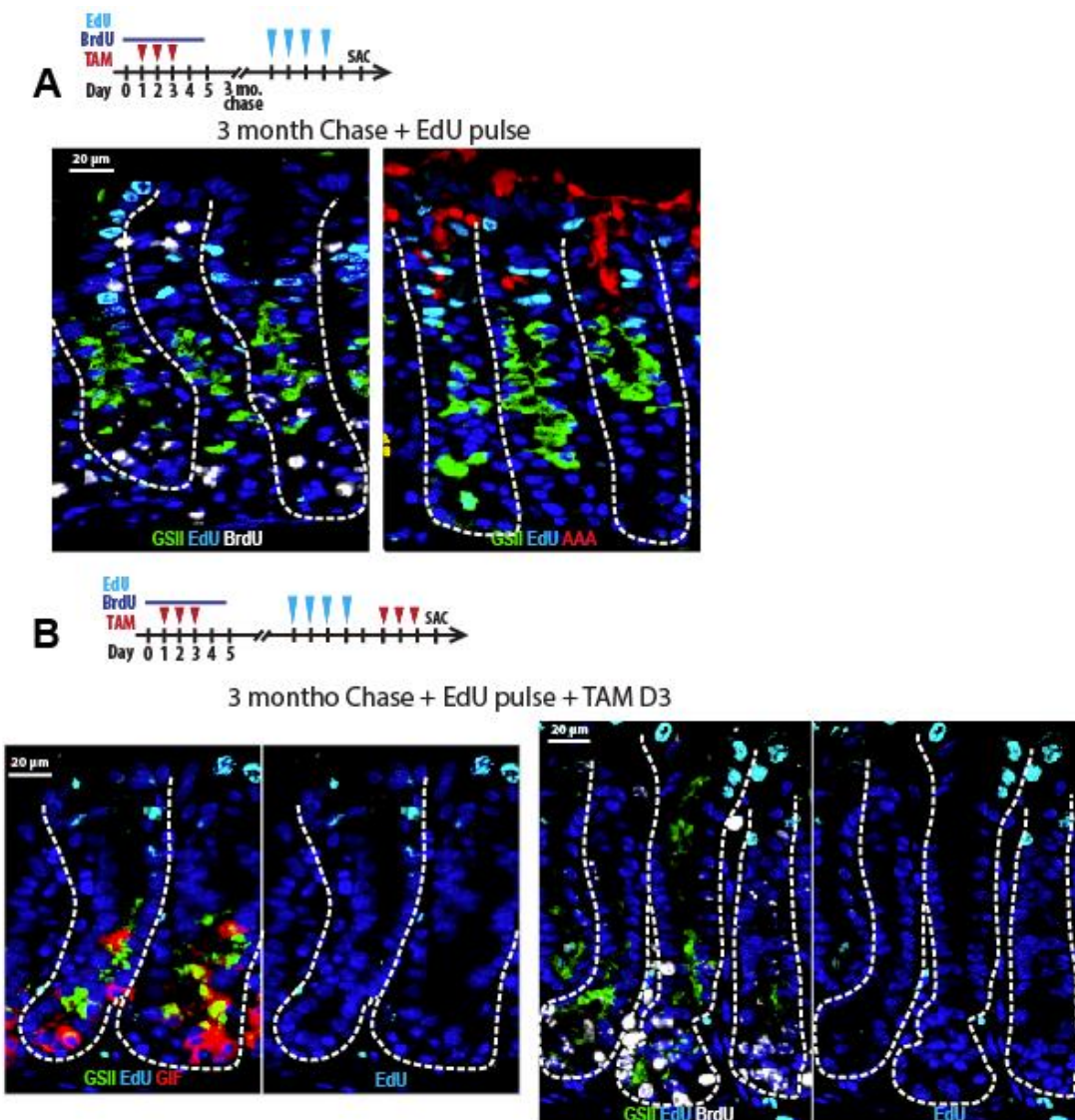


Figure 3.8 EdU⁺ progenitors do not give rise to EdU⁺ SPEM cells

A) EdU (cyan) injected for four days labels isthmal, pit (red), and upper neck (green) cells with no overlap with BrdU⁺ chief cells (white) **B)** Label-retaining SPEM cells following HP infection (left). **B)** Mice as in panel (A) injected with TAM three days. No EdU staining is seen in SPEM cells.

3.8 Metaplastic cells can redifferentiate into chief cells following recovery from injury

To track SPEM cell fate upon recovery, we treated mice with the TAM+BrdU pulse, a three-month chase, a second round of TAM, then allowed them to recover for two weeks. While many units completely diluted their label (<4 BrdU⁺ GIF and/or GSI positive cells) due to the high

proliferation, units that were not washed out retained BrdU in $47 \pm 7\%$ of chief cells (Figure 3.9A-B). Upon recovery, an average of 7.3 ± 0.3 chief cells per unit retained label, equal to the sum of the 2.8 ± 0.1 chief cells and 4.6 ± 0.3 SPEM cells retaining label following the TAM injury. This indicates that SPEM cells re-differentiate into chief cells with minimal additional proliferation or death.

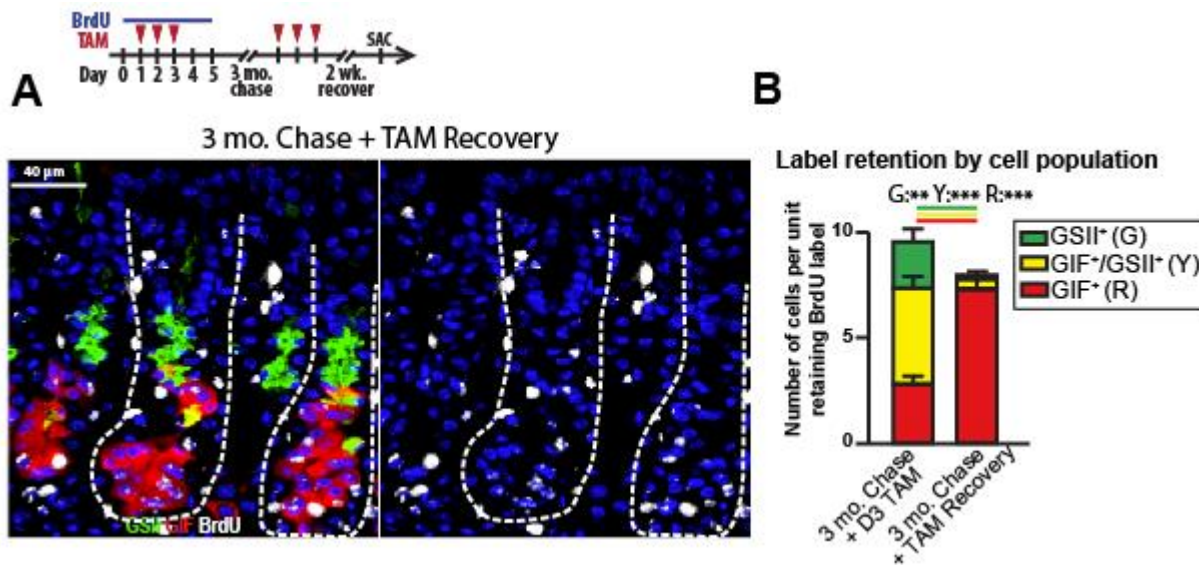


Figure 3.9: Metaplastic cells can redifferentiate into chief cells following recovery from injury

A) Stomach of mouse given BrdU+TAM pulse, 3 month chase, 3 days TAM, then allowed to recover for 2 weeks (BrdU, white; GIF, red; GSII, green). **B)** BrdU retention for neck (green), chief (red), and SPEM/transitional (yellow) cells quantified for panel A. * $P < 0.05$, ** $P < 0.01$, and *** $P < 0.001$ in one-tailed Student's *t* tests.

3.9 Discussion

In this study, we combined nucleotide analog labeling techniques with acute and chronic gastric injury models to test the dynamics of gastric cells at homeostasis and following injury. Our pulse-chasing strategies, including pulsing BrdU throughout TAM injury then tracking label-retaining cells, expanded upon previous reports which mostly relied on long pulses or simple pulse-chase set-ups. Our combined results indicate that chief cells largely maintain their own

census at the unit base independently from other lineages at homeostasis, and they retain the capability to replace themselves upon injury (Figure 3.10, Figure 3.11).

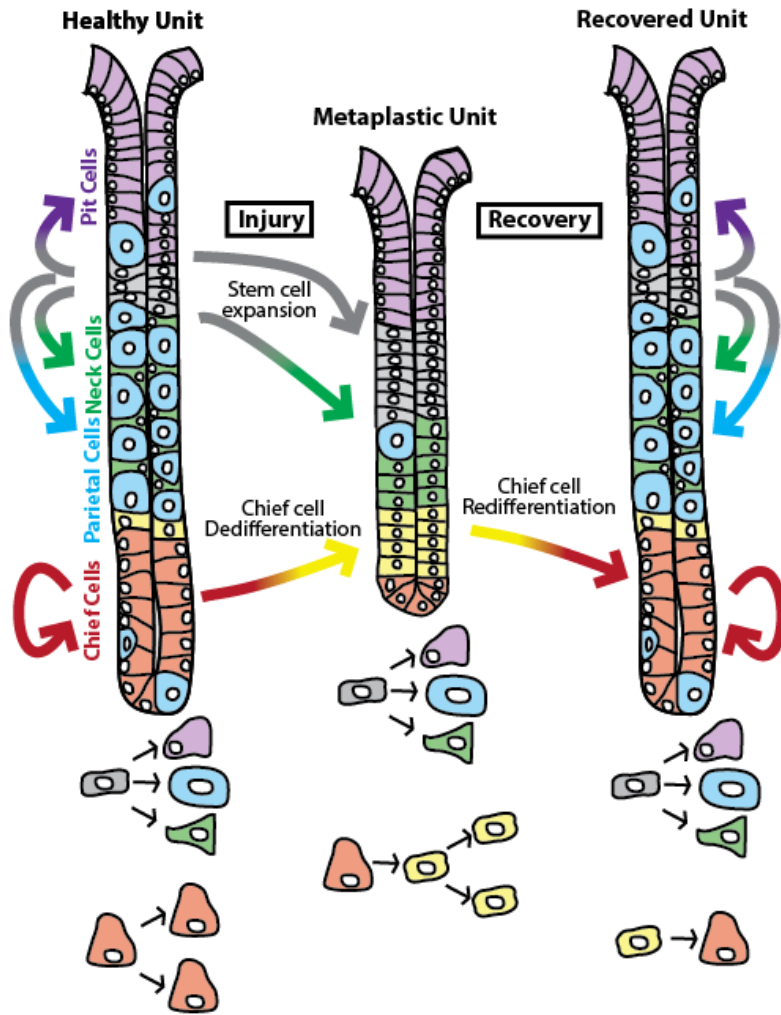


Figure 3.10: Chief cells appear to maintain an independent population at homeostasis

(Left) Our proposed model for how each major gastric cell population is maintained in homeostasis. Stem cells (grey) give rise to pit cells (purple) neck cells (green) and parietal cells (blue). Chief cells form a self-maintaining population at the base largely independent of input from upper cell populations. Colors on arrows denote cell conversions. (Middle) Upon metaplasia inducing injury such as infection with *Helicobacter* species or acute drugs, units lose their parietal cells and see proliferative expansion of the isthmus and neck cells. Chief cells

dedifferentiate to metaplastic cells (yellow) and re-enter the cell cycle as well. (Right) As the injury resolves, SPEM cells can redifferentiate into chief cells, then the unit reverts to its normal homeostatic maintenance.

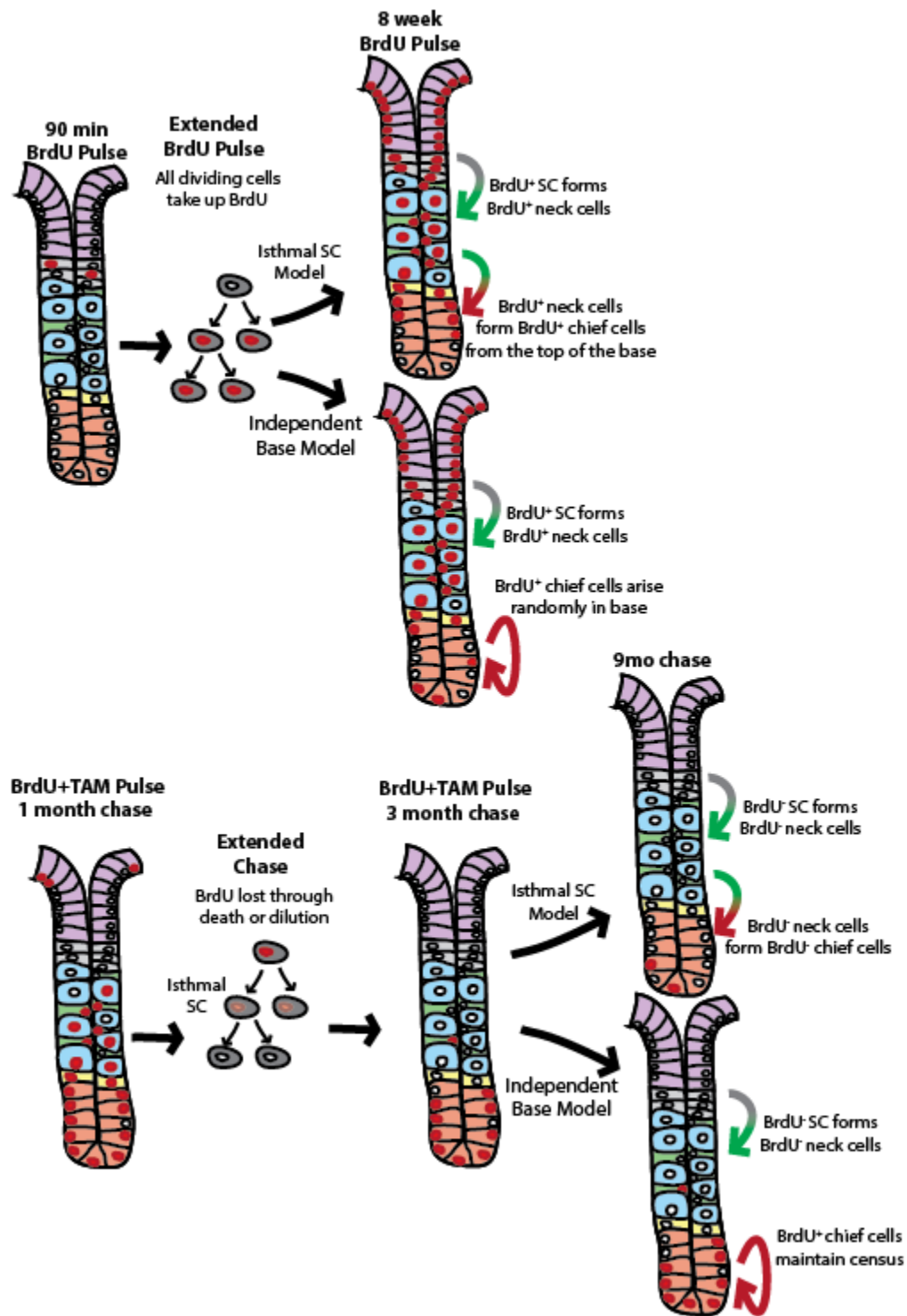


Figure 3.11: Models for BrdU pulse-chase experiments comparing the canonical isthmal stem cell model with our independent base model.

Multiple experiments suggest that chief cells form a largely self-maintaining population. Our TAM+BrdU pulse chase strategy allows us to monitor label retention in chief cells, and we see 2/3 of chief cells maintaining label after nine months (Figure 3.2). This longer-than-expected label retention has three possible explanations: 1) the population could be replenished from other label-retaining cells, 2) individual chief cells may live longer than nine months, or 3) BrdU⁺ chief cells may infrequently self-replicate, spreading their label between progeny. Option 1 is unlikely since neck and parietal cells reach their minimal retention levels by five months. Individual chief cells were calculated to live around 160 days by two independent studies (Karam and Leblond, 1993c; Quante et al., 2010), making option 2 unlikely as well. Option 3 seems correct, as chief cells are known to proliferate and die at low levels (Suzuki et al., 1983; Karam and Leblond, 1993c), and we likewise show low levels of BrdU accumulate in chief cells over time. The majority chief cells that incorporate BrdU in our continuous BrdU experiments are nonadjacent to the transitional zone, with BrdU uptake scattered from the upper-most to the lower-most chief cell (Figure 3.1). This is only possible if chief cells are either dynamically migrating in the base or, consistent with our model, if they are self-propagating.

Our conclusion that chief cells predominately maintain their own census is also supported by our two-week BrdU pulse-chase experiments (Figure 3.4). A two-week pulse is sufficient for 68% of neck cells to incorporate label. Following an eight-week chase, all but 16% of necks cell lose label, yet there is no increase in BrdU⁺ chief cells, indicating that neck cells predominately have a fate other than transitioning into gastric chief cells. This is supported by a paper showing that neck cells have a distinct function, with protective proteins expressed by neck cells seen coating the canaliculi of neighboring parietal cells (Hanby et al., 1999). The authors point out that having a cell with one secretory function converting to a cell with a distinct secretory function would be

unique throughout the GI tract and unlikely to occur. However, as no apoptotic death is observed in neck cells and lower neck cells are not proliferative (Figure 3.4), it is unclear from our experiments what the final fate of these cells might be.

While our experiments suggest a new model for cellular dynamics in the homeostatic stomach, our data does not conflict with the body of gastric literature. Published continual labeling experiments show label incorporation into neck cells significantly earlier than in chief cells, helping lead to the model wherein neck cells transition into chief cells (Karam and Leblond, 1993c; Ramsey et al., 2007). Our results agree with this, as neck cells label long before chief cells, yet chief cells will eventually label with continuous pulsing based on their low intrinsic proliferation. Even our data that label is retained by a small proportion of neck cells, transitional cells, and parietal cells for several months is consistent with the expansive works published by Dr. Karam in 1993, as he is never able to fully label any of these populations with ^3H -thymidine infusion (Karam, 1993; Karam and Leblond, 1993c). Our model also does not conflict with papers showing non-expanding subpopulations within the chief cell zone at homeostasis, such as Lgr5^+ chief cells or the minority of chief cells labeled by $\text{Mist1CreERT2};\text{Rosa}^{\text{YFP}}$ (Leushacke et al., 2017; Weis et al., 2017), or with those showing expanding chief cell subpopulations, such as Troy^+ chief cells, which are shown to slowly expand to fill the base even at homeostasis (Stange et al., 2013b). Our BrdU+TAM strategy labels nearly all chief cells (>80%) regardless of subpopulation. A more-proliferative subset of chief cells could slowly replace less-proliferative subsets at homeostasis while still retaining label as full population.

The transitional zone between the neck and chief cells remains enigmatic. Our data shows that neck cells do not predominately mature into chief cells, questioning whether the transitional zone is used for neck-to-chief cell transitioning, as has long been believed (Suzuki et al., 1983; Karam

and Leblond, 1993c). It is intriguing to speculate that the transitional zone may allow small numbers of cells to move down from neck to base *and* up from base to neck, though our experimental design cannot sufficiently test this. A two-way model would be consistent with ours and published data. Multiple papers show that a small number of chief cells can eventually obtain label that was only pulsed into neck cells, with <5 chief cells per unit eventually gaining label following a TFF2-CreERT2 pulse (Quante et al., 2010) and 10% of chief cells taking up ³H-Thymidine following a short pulse and longchase (Hattori and Fujita, 1976a). Yet another report indicates that chief cell progeny can occasionally escape the base and populate full gastric units at homeostasis (Stange et al., 2013b). Our data do not conflict with either of these phenomena. We never stain 100% of the chief cells, and 20% of the labeled population is lost within the nine month chase. This could result from chief cell proliferation diluting the label or from a small contribution from the necks to the base. Surprisingly, we observed that nearly one transitional cell and nearly one neck cell per unit retain label even following nine months chasing. This can either indicate that a subset of both populations live an order of magnitude longer than expected, or it could be marking a small number of chief cell-derived cells able to cross up through the transitional zone into the neck of the unit. Further work is needed to clarify these transitional zone dynamics.

We also show that chief cells can directly become SPEM cells following chronic *Hp* infection or acute injury with TAM and that these SPEM cells can redifferentiate into chief cells upon recovery. One major limitation of using label-retention to track cells throughout an injury response is that it is impossible to determine the origin of a BrdU-negative cell. In mice given BrdU-TAM, a three month chase, and then re-injury with TAM, a BrdU-negative SPEM cell could result from many things: 1) a chief cell which was already BrdU-negative

dedifferentiating, 2) a BrdU⁺ chief cell dedifferentiating but diluting its label through proliferation, or 3) a cell from higher in the unit becoming a SPEM cell. Thus, all we can conclude is that BrdU⁺ SPEM cells must derive from pre-existing BrdU⁺ cells. BrdU⁺ SPEM cells likely arise via chief cell dedifferentiation since the two BrdU⁺ neck cells per unit found following BrdU+TAM and a three month chase would need to divide several times to give rise to the 6 BrdU⁺ SPEM per unit, yet the neck cells retain their label in both injury models. Similarly, it is extremely unlikely that BrdU⁺ SPEM cells could result from isthmal progenitors, as less than 1 label-retaining cell is seen near the isthmus in each unit prior to injury, necessitating numerous rounds of proliferation to form 6 SPEM cells. This was further confirmed by showing that SPEM cells arise before proliferation occurs in early TAM treatment and by injecting three-month chased mice with EdU for 4 days before causing TAM-induced SPEM. EdU was retained in upper isthmal and pit cells, but negligible EdU is seen near the metaplastic bases. This indicates either that if SPEM cells were to arise from the isthmus, they would proliferate enough to lose label before becoming SPEM cells. Similar limitations remain for analyzing BrdU-negative chief cells following recovery from the TAM insult. Thus, while we cannot say that all SPEM cells arise from or redifferentiate to chief cells, we can say that the BrdU⁺ portion likely do, showing that chief cells have the ability to maintain at least a portion of their population following injury.

Growing published evidence supports that chief cells are more independent than previously assumed. While it was long believed that parietal cell loss triggers SPEM, our lab demonstrated that parietal cell loss alone is not sufficient to induce chief cell dedifferentiation and highlighted that neck cells can undergo regenerative proliferation with no change in the base (Burclaff et al., 2017). Another study revealed that chief cells can dedifferentiate with parietal cells present (Busada et al., 2019). These reports are consistent with chief cells functioning largely

independently from all other gastric lineages, which has been obscured by the temporal intertwining of parietal cell death, neck cell proliferation, and chief cell dedifferentiation following physiological insults.

Our data is consistent with a new model wherein chief cells largely maintain their own population at homeostasis and through injury recovery (Figure 3.10). As a population, we see that chief cells can undergo two rounds of dedifferentiation and redifferentiation without dying. In the initial BrdU+TAM pulse, chief cells dedifferentiate and proliferate minimally to acquire label then redifferentiate into BrdU⁺ chief cells. The second TAM injury repeats this process, though it dilutes some of the label. This holds implications for gastric health. Our lab has proposed a Cyclical Hit Model of Tumorigenesis by which long-lived cells able to re-enter the cell cycle following injury such as the gastric chief cells, pancreatic acinar cells, and intestinal Paneth cells may initiate tumors independently of stem cell contribution (Mills and Sansom, 2015; Burclaff and Mills, 2018b; Burclaff and Mills, 2018a; Saenz and Mills, 2018a). Cycles of dedifferentiation, proliferation, and redifferentiation in chief cells could cause mutations which are then maintained within the long-lived chief cell population until a neoplastic mutation locks the cells in a proliferative, cancerous state. Thus, it is important to search for conserved mechanisms for dedifferentiation between organs - such as the conserved Paligenosis pathway that was recently identified between SPEM and pancreatic acinar cells dedifferentiating in acinar-to-ductal metaplasia (Willet et al., 2018b) - to find potential therapies for blocking or reversing this plasticity to prevent or treat early cancers.

Chapter 4: Chief cells can differentiate in the absence of parietal cells

4.1 Introduction

Parietal cells (PCs) have long been regarded as important for proper zymogenic chief cell maintenance and function. Mature chief cells are lost, many to dedifferentiation, following parietal cell injury in autoimmune gastritis (Adams et al., 1964) or chronic *Helicobacter pylori* infection (Lennerz et al., 2010). The relationship between PC loss and metaplasia has been known for decades, with researchers commenting on the “intimate association among the parietal cell loss in the fundic gland, a rise in pH value and the development of intestinal metaplasia” (Watanabe et al., 1980) 40 years ago. Multiple acute drugs recapitulate this relationship in mouse models, including DMP-777 (Nomura et al., 2005), L-635 (Weis et al., 2013), and tamoxifen (TAM) (Huh et al., 2012b; Saenz et al., 2016), all of which cause PC loss and result in loss of chief cells to dedifferentiation within 2-14 days. This dependence of s on PCs is further published upon in gastric development, where several models have shown that PCs, or their secreted components, are necessary for the development of mature chief cells. Models for the constitutive killing of PCs have used the driver for *Atp4b*, a component of the H⁺/K⁺-ATPase proton pump, to express diphtheria toxin (DT) (Li et al., 1996; Bredemeyer et al., 2009), Simian Virus 40 (Li et al., 1995), or herpes herpes simplex virus (Canfield et al., 1996). All of these models cause chronic loss of PCs from birth and result in a severe or complete depletion of chief cells in adult mice. Similar loss of formation can be seen even without killing the PCs, such as when acid secretion is blocked through constitutive knockout of ATP4b (Xiao et al., 2010) or with loss of Sonic Hedgehog expression from PCs (Franic et al., 2001). Intriguingly, constitutive

knockout of ATP4a, which is also necessary for acid secretion, did not result in depletion (Spicer et al., 2000). From these experiments and pathological observations of the absence of mature chief cells in areas of atrophic gastritis in human patients, gastroenterologists have long considered the chief cell population to be dependent on PCs.

Recent work from our lab has questioned this conclusion. When mice with an *Atp4b*-driven inducible DT receptor (HKiDTR) were injected with DT, nearly all PCs were killed, yet there were surprisingly minimal effects on the chief cells, with most remaining mature (GSII⁺) and non-proliferative. This was seen even when DT injections were administered for 16 days (Burclaff et al., 2017). This clearly indicated that chief cells do not need PCs present to maintain survival and maturity and that the loss of PCs in a gastric unit does not actively drive chief cell loss or dedifferentiation. This acute model as used in its introductory publication could not show whether chief cells could develop in the absence of PCs, though, as chief cells are calculated to live nearly half of a year, so minimal turnover would be expected in 16 days (Karam and Leblond, 1993c; Quante et al., 2010).

4.2 Results

To test whether chief cells can develop in the absence of PCs, two approaches were used. In the first, we tested whether mature chief cells could redevelop following TAM-induced metaplasia in the absence of PCs. We injected HKiDTR mice with TAM for three days to kill PCs and cause chief cell dedifferentiation and metaplasia (Huh et al., 2012b). We then continued to inject daily with DT to keep PCs away for 14 days but without directly affecting the chief cells or their precursors. One mouse was sacrificed immediately following the 3 days of TAM, showing that the drug killed PCs and caused chief cell dedifferentiation as expected. Other control mice were

injected with TAM three days then allowed to recover for 14 days or with vehicle for three day then 14 days of diphtheria toxin. Following the full 17-day time course, the TAM-then-rest mice were seen to recover full chief cell and PC populations, with proliferation contained in the isthmus as would be expected at homeostasis. As in the HKiDTR paper, mice only injected with DT for 14 days had full PC loss and proliferation throughout the isthmus and neck, yet the chief cells remained largely unchanged at the base (Figure 4.1A). Interestingly, mice treated with TAM then DT appeared very similar to DT alone, with no sign of metaplasia at the base and a full contingent of $GIF^+/GSII^-$ mature chief cells, even though PCs were still absent (Figure 4.1A) TAM-then-rest mice were seen to ‘overshoot’ in their chief cell population, with 18.1 chief cells seen per unit following TAM recovery compared to 12.9 in a healthy unit. DT-alone or TAM + DT were both seen with chief cell counts nearer their homeostatic levels, with 12.9 ad 14.0, respectively (Figure 4.1B) Altogether, this shows that chief cells can recover following metaplastic injury in the absence of PCs, though it is unclear whether these were newly-formed chief cells or metaplastic cells which re-differentiated into chief cells.

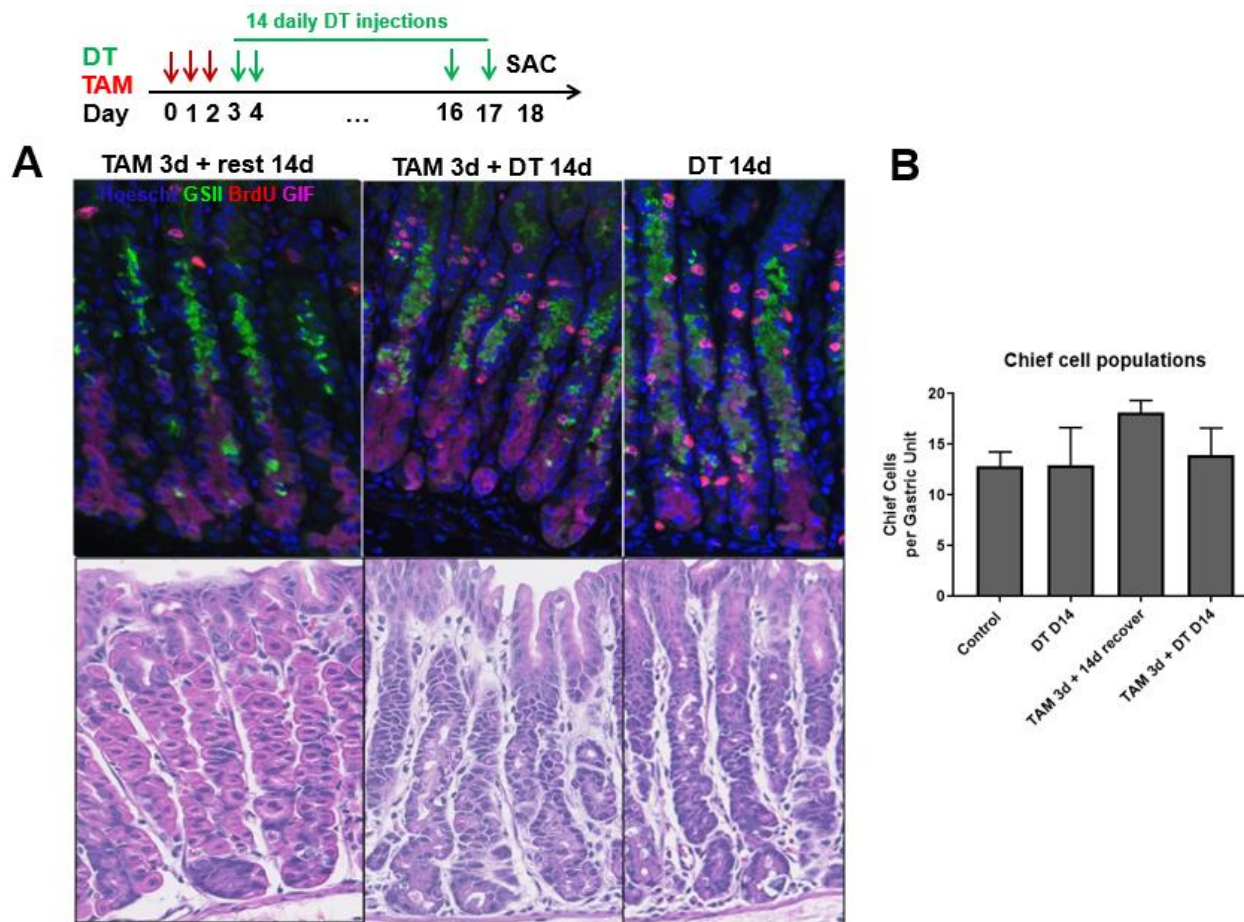


Figure 4.1: Chief cells recover from tamoxifen even in the absence of PCs.

A) Stomachs from adult mice following three days of TAM then 14 days of recovery (left), three days TAM then 14d DT (center), or just 14d DT injections (right) (*top*: green: GSII, red: anti-BrdU, magenta: anti-GIF). *Bottom*: Hematoxylin and eosin staining of the same stomachs as on *top* to visualize loss of PCs (large, round, bright pink cells). **B)** Quantification of GIF⁺/GSII⁺ chief cells per gastric unit via immunofluorescence staining.

Since it is unknown whether chief cells recovering from injury follow the same developmental pathways as those forming initially in newborn mice, we also tested if PCs were necessary for these first chief cells to form in developing pups. We analyzed the stomach of a P5 mouse and found that, consistent with the literature (Keeley and Samuelson, 2010), the epithelium of the developing stomach largely consists of GIF⁺/GSII⁺ precursors instead of mature chief or neck cells (Figure 4.2A) We thus picked P5 as the starting point and injected HKiDTR pups with DT

daily from P5-P21, when populations of all mature gastric cell types are known to exist. H&E staining on the P21 stomachs showed that PCs were efficiently killed at similar levels to adult HKiDTR mice, yet a full population of GIF⁺/GSII⁻ chief cells was still seen to develop at the base of the units. Proliferation was also seen throughout the necks of the DT-injected pups, again similar to adult mice, while proliferation is seen contained to the isthmus in control littermates by P21 (Figure 4B). Since PCs were effectively killed before and during chief cell development, this shows that mature PCs are not necessary for even primary chief cell development in a young mouse stomach.

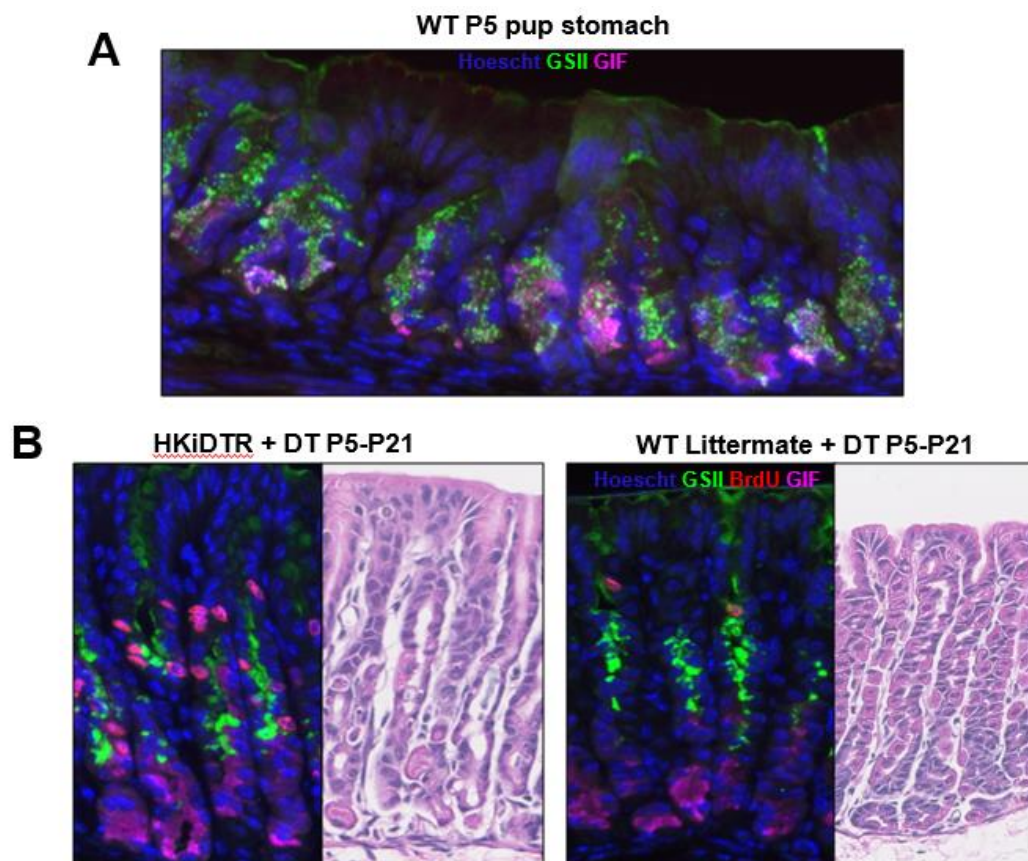


Figure 4.2: Chief cells develop in the young stomach even in absence of PCs.

A) Representative stomach from a P5 pup (green: GSII, magenta: anti-GIF). **B)** Stomachs of HKiDTR (left) or WT (right) pups following DT injections from P5-P21 (green: GSII, red: anti-BrdU, magenta: anti-GIF).

4.3 Discussion

Many papers have shown that PCs or their secreted acid are necessary for chief cell formation in mice. All of these were done with mechanisms for constitutively ablating PCs or knocking out their acid secretion. The HKiDTR mouse model allows us to cleanly and inducibly ablate PCs, which initially allowed us to demonstrate that PC loss does not necessarily initiate the full metaplastic regenerative response as seen after all other forms of PC injury (Burclaff et al., 2017). This mouse model allows us to take a further look at the question of chief cell development. Here, we show that chief cells can recover following injury in adult mice and develop for the first time in young mice all in the absence of mature PCs.

While our conclusion appears contradictory to the wealth of literature, there are several distinct reasons for why our experiments might be showing different results. DT and TAM models are very acute and fast acting damage models, allowing us to look at PC death and chief cell dedifferentiation and recovery in a couple of weeks instead of the months-long experiments done with constitutive mutations in most published work. We do not believe that the amount of time that PCs are gone directly affects chief cell form and function, as the bases appear very similar after two weeks DT as they do at three days DT. Instead, it is plausible that constitutive loss of PCs or their acid from birth to adulthood might have allowed for colonization of the stomachs with pathogenic bacteria which secondarily effected the metaplastic responses seen. Another possibility arises from the experimental set up for how PCs are killed between experiments. Our model expresses a toxin receptor on the PCs, only allowing a small amount of toxin into each cell upon injection. Other models drive toxin or viral factors directly into the parietal cells. As

neighboring cells are suspected to phagocytose dead cell debris of neighbors at the unit base (Karam and Leblond, 1993c), it is possible that developing chief cells ingest toxin-filled PC debris and are collaterally killed. Finally, it is also possible that other published PC-killing experiments are more effective in their PC ablation, possibly killing PCs at an earlier stage or even earlier in the development of the stomach in newborn mice. HKiDTR mice lose 95% of PCs following DT injections, yet it is possible that chief cell maturation may be supported by the remaining 5% of PCs, the not-yet-killed pre-PCs, or a small population of PCs which arose before P5. Our current model and data are insufficient to test which of these possibilities may be the cause of our conflicting data.

Even though we cannot say specifically how our model results in different chief cell dynamics than the body of published literature, our results still add important data and advance the field of stomach development. We show for the first time that chief cells can develop and recover from injury in the absence of PCs. This may be important for advancing our knowledge of human health, as precancerous metaplasias are known to begin with atrophic gastritis, or loss of PCs (Correa, 1988). Our results indicate that the progression to further damaged states might not result from the loss of any specific PC factor or the physical loss of the cells themselves. Instead, focus should be given to inflammation and colonizing pathogens to identify what specific factor may be driving the metaplastic changes in the bases of the gastric units.

4.4 Methods and materials

Animals and Injections

All experiments involving animals were performed following protocols approved by the Washington University School of Medicine Animal Studies Committee. Mice were maintained in a specified pathogen-free barrier facility under a 12-hour light cycle. Wild type *C57BL/6* mice were purchased from Jackson Laboratories (Bar Harbor, ME). Littermate controls were housed together when possible. HKiDTR mice were derived from ROSA26^{iDTR/iDTR} mice purchased from Jackson Laboratories bred to *Atp4b-Cre* mice from our in-house stock.

To ablate PCs, diphtheria toxin (225ng/mouse in 0.9% sodium chloride saline; Sigma) was injected intraperitoneally every day for up to 16 days. To induce SPEM, tamoxifen (5 mg/20 g body weight; Toronto Research Chemicals, Inc, Toronto, Canada) was injected intraperitoneally daily for 3 days. Tamoxifen was dissolved in 10% ethanol and 90% sunflower oil (Sigma), following the procedure outlined in (Saenz et al., 2016).

Immunofluorescence

Mice were given an intraperitoneal injection of 5-bromo-2'-deoxyuridine (BrdU, 120 mg/kg) and 5-fluoro-2'-deoxyuridine (12 mg/kg) in sterile water 90 min before sacrifice. Following sacrifice, stomachs were immediately excised and flushed with PBS, then inflated and fixed overnight in cold formalin (3.4% formaldehyde in phosphate buffered saline; Sigma). Tissues were arranged in 3% agar in a tissue cassette, underwent routine paraffin processing, and 5µm sections were cut and mounted on glass slides. Sections underwent a standard deparaffinization and rehydration protocol, were blocked in 1% BSA, 0.3% Triton-X100 in PBS, left with primary antibodies

overnight, washed then and incubated for one hour with secondary antibodies, washed, washed, then mounted using ProLong Gold antifade reagent with DAPI (Invitrogen, CA).

Primary Antibodies used in this study: rabbit anti-gastric intrinsic factor (gift of Dr. David Alpers, Washington University), goat anti-BrdU (gift of Dr. Jeff Gordon, Washington University), and 1 g/ml fluorescently labeled GSII lectin (Alexafluor488, 594, Molecular Probes). Secondary Antibodies included AlexaFluor (488, 594 or 647) conjugated donkey anti-goat or anti-rabbit (Molecular Probes).

Immunofluorescence quantification

Chief cell census was quantified with at least three mice for each condition. Stomachs were fluorescently stained with DAPI and anti-BrdU along with the neck cell marker GSII lectin and chief cell marker anti-GIF. Images were captured as TIFF files from a Zeiss Axiovert 200 microscope with AxioCam MRM camera and with Apotome optical sectioning filter. Each stomach had at least 5 images taken and only well-oriented gastric units were counted. Total chief cell counts were averaged over total number of units counted for each mouse.

Chapter 5: MNU can be used to initiate gastric tumorigenesis

5.1 Introduction

The risk of developing cancer increases as a person ages, but we still don't know why. The intersection of cellular dedifferentiation and response to inflammation may hold the key. In response to inflammation, one tissue can take on the characteristics of a different tissue in a process called metaplasia. Metaplasia almost always occurs following inflammation, and this is known to increase cancer risk, yet it remains unclear how. Mature cells can be recruited back into the cell cycle in adult organs, termed dedifferentiation. The ability of differentiated cells to be called back into a proliferative, more progenitor-like state may be a normal, evolutionarily conserved feature of many adult tissues. Organisms may use this process to reserve differentiated cells as potential stem cells during injury/inflammation (Mills and Sansom, 2015).

We believe that metaplasia arises when cells dedifferentiate and re-enter the cell cycle in response to injury (Mills and Sansom, 2015). As normally post-mitotic cells re-enter the cell cycle, they increase their risk of acquiring mutations. If the mutations do not cause death or cell cycle arrest, the cells redifferentiate to their mature state once the tissue recovers. Through cycles of dedifferentiation and redifferentiation, mutations accumulate in these long-lived cells until a tumor-inducing mutation occurs, locking the cells into a proliferative state. For example, pancreatic adenocarcinomas arise when mature acinar cells with constitutively active K-Ras undergo metaplastic dedifferentiation, but activating K-Ras does nothing until another signal causes the acinar cells to dedifferentiate and proliferate (von Figura et al., 2014). Likewise,

melanocytes with constitutively active BRAF only induce melanomas upon dedifferentiation (Kaufman et al., 2016). This could explain why tissue surrounding a tumor can harbor the same mutations without malignancy. The cancer-driving power of the mutations are only fully realized when the cell re-enters the cell cycle and can no longer redifferentiate.

Newly developed model systems from our lab should allow us to test this hypothesis in the mouse stomach. We previously discovered that injecting a high dose of tamoxifen causes death of the acid-secreting parietal cells, inflammation, and rapid and reversible gastric metaplasia, with mature enzyme-secreting cells at the base dedifferentiating to re-enter the cell cycle. This response occurs in a pattern recapitulating precancerous metaplasias caused by *Helicobacter pylori* in human patients (Huh et al., 2012b; Saenz et al., 2016). We also bred mice expressing the human diphtheria toxin receptor specifically on parietal cells. Treatment with diphtheria toxin kills all parietal cells and results in inflammation and increased proliferation of the constitutive stem cell, but not metaplasia (Burclaff et al., 2016). Both systems cause similar parietal cell death and stem cell proliferation; the only difference is the lack of dedifferentiation with metaplastic proliferation after diphtheria toxin. These systems will allow us to specifically test for the first time whether metaplastic dedifferentiation of mature, long-lived cells is critical for mutation accumulation and cancer initiation as opposed to increased stem cell proliferation and inflammation alone.

5.2 Results

Previous reports show that FVB mice form more tumors with less death than C57Bl6 mice when treated with the carcinogen N-methyl-N-nitrosourea (MNU) (Yamamoto et al., 2002). 25

FVB/NJ mice were ordered from Jackson Laboratories then treated with a published protocol for

MNU (Yamachika et al., 1998), wherein 240ppm MNU is given in the drinking water for a full week on alternating weeks for ten weeks. To test whether rounds of injury/metaplasia increase chances for tumor formation, mice were split into three groups: 10 mice were treated with MNU with rounds of tamoxifen administered on weeks 1, 3, and 5, 10 were treated with MNU and rounds of vehicle, and 10 were only given rounds of tamoxifen with no MNU (Figure 5.1A). Published literature shows that tumors should form by week 36.

Starting 10 weeks following the MNU cycles, mice were live-imaged to test for tumor formation using a FMT imager to track tumorigenesis. ProSense 680 (Perkin Elmer, enzymatically activated by Cathepsin B and other lysosomal enzymes) and MMPSense 750 FAST (Perkin Elmer, enzymatically activated by MMP-2, MMP-9 and others) have both been shown to be able to track gastric cancer in mice in vivo (Ding et al., 2012), even in a context of chronic inflammation (Zhang et al., 2008). Immunofluorescent signal was observed in the abdomen of HD-TAM treated mice, so we performed a bio-distribution assay to quantify the amount of fluorescence coming from each individual harvested organ. This indicated that the signal was originating in the spleen and liver, with minimal signal emanating from the gastric tissue (Figure 5.2B,C).

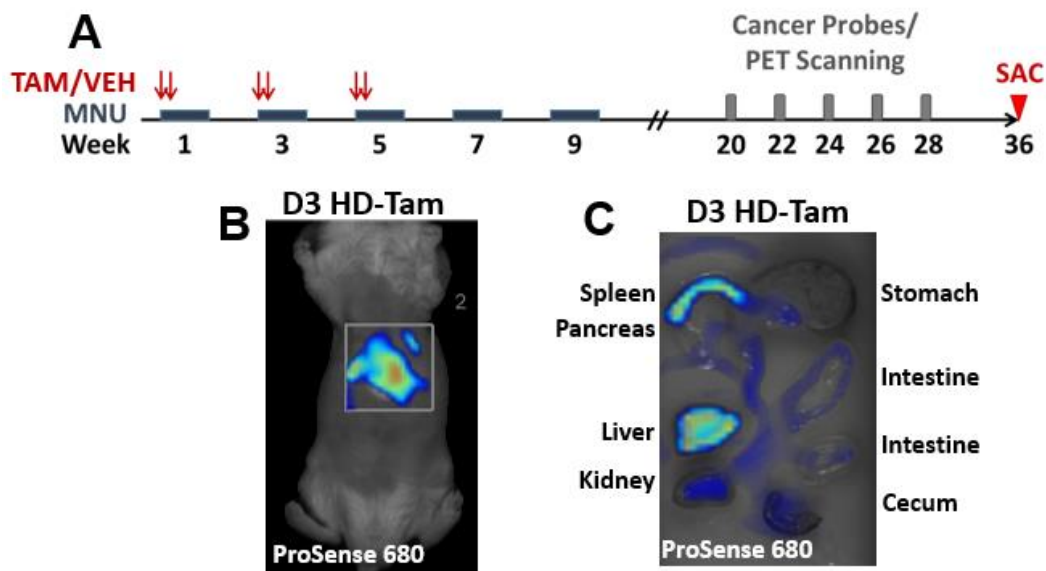


Figure 5.1: MNU timecourse and in vivo fluorescence imaging.

A) The timecourse for the pilot trial of MNU + rounds TAM or vehicles. Following published protocols, MNU was given via drinking water on alternating weeks for 10 weeks. TAM or VEH were injected on two consecutive days on weeks 1, 3, and 5. Living mice were to be imaged starting on week 20 for tumor formation. **B)** The stomach regions of mice were seen to fluoresce in the channel for ProSense680 at D3 TAM. **C)** The Bio-distribution of the ProSense 680 probe was checked in freshly harvested organs immediately following in vivo live imaging. Most signal was seen in the spleen and liver, with negligible fluorescence originating from the stomach (upper right).

Once we found that the in vivo immunofluorescence probes gave non-stomach-specific signal, we tried an alternate form of in vivo live imaging on the same mice: PET/CT scanning using Fludeoxyglucose (18-FDG) glucose analogue to highlight tissues with highly metabolic cells. Signal was seen around the expected area for the stomach in many mice (Figure 5.2A). To determine whether the signals originated from the stomachs themselves, the mice with the best PET/CT signaling were sacrificed by the Small Animal Radiology Core personnel. Stomachs showed signal, yet the upper duodenum and other nearby organs did as well, so it remains unclear whether the signal seen on the PET scanning was truly stomach specific. Since we were not allowed to be present during the sacrifice due to the radioactive injections, we were unable to

fix the stomachs ourselves, resulting in poor orientation for scanning for polyps on the full stomach or histological staining (Figure 5.2B).

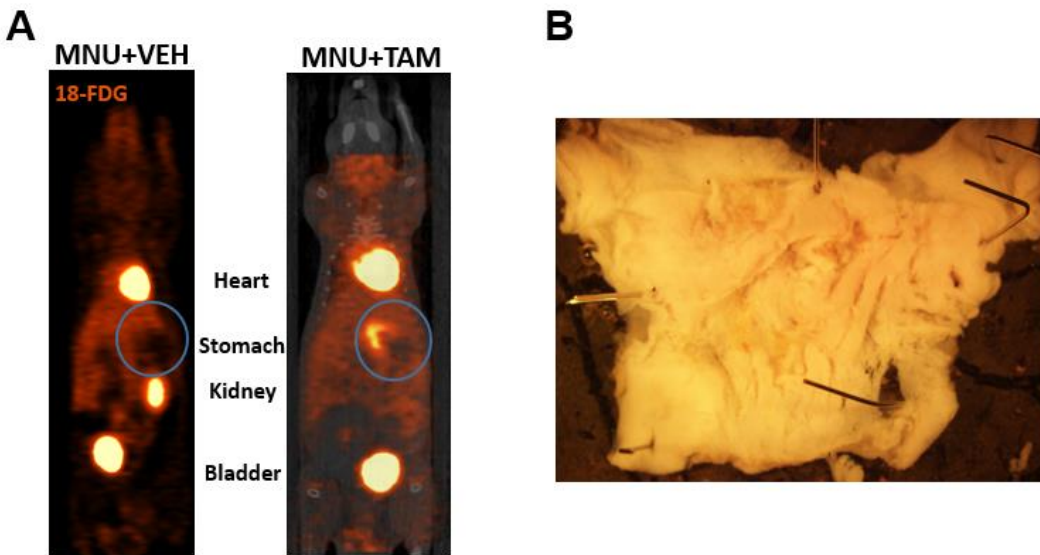


Figure 5.2: PET/CT Scanning on MNU treated mice.

A) Signal seen in live mice using PET/CT Scanning with 18-FDG. Hearts, kidneys, and bladders are expected to fluoresce due to their high metabolic activity. Stomach tissue was not always seen (blue circle, left image), yet some mice had high signal in what appeared to be the outline of the stomach epithelium (blue circle, right image). **B)** Stomach pinned out after fixing following harvesting at the Small Animal Cancer Imaging Core.

Throughout the experiment, many mice died from infection, fighting, isofluorane and imaging, or sacrifice for bio-distribution imaging, leaving only 7 TAM+MNU mice, 6 VEH+MNU mice, and 3 TAM-only mice living longer than 30 weeks. Of these, 5/7 TAM+MNU, 2/6 VEH+MNU, and 0/3 TAM-only mice showed evidence of gastric polyps/tumors, nearly all in the antral portion of the stomach (Figure 5.3 A,B) While not quantified, many mice showed polyps in their liver, kidneys, or other organs as well (Figure 5.3C).

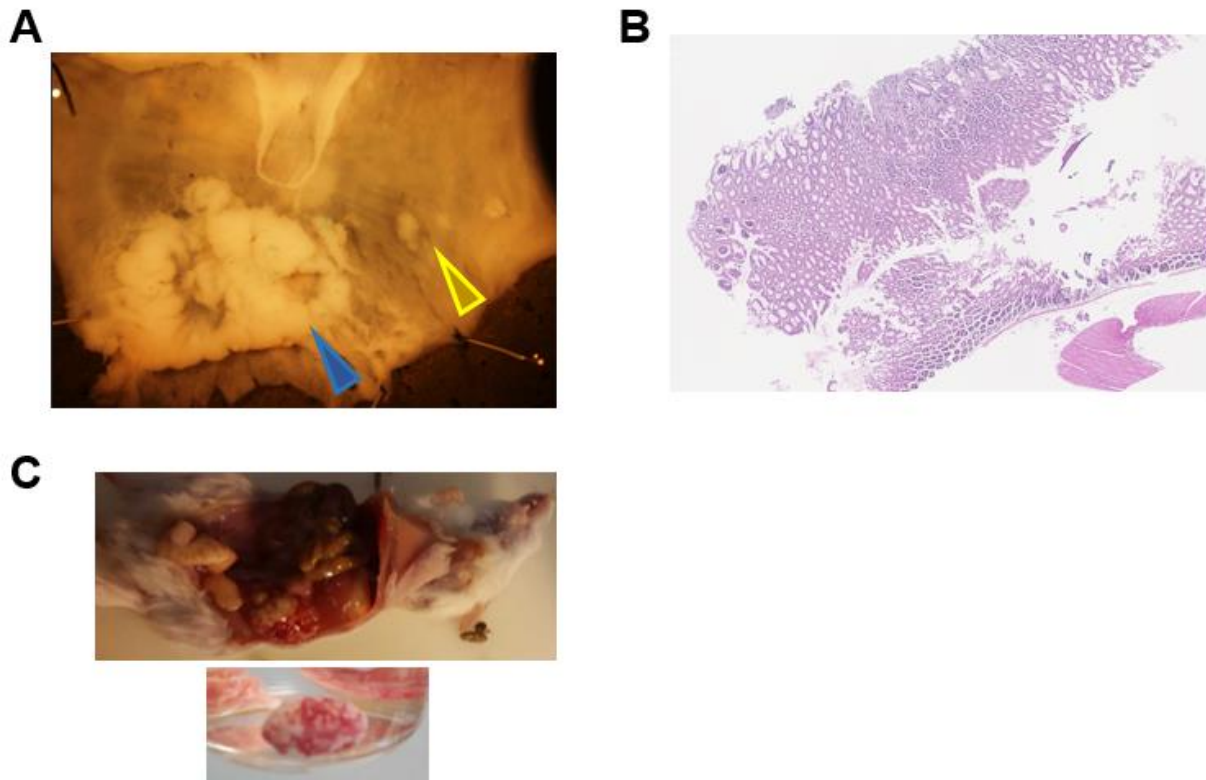


Figure 5.3: MNU induced tumors.

A) The most impressive tumors were seen in an MNU+TAM mouse which died at week 30. Most tumor formation was confined to the antral region (blue arrowhead) with some sparse polyps seen in the corpus region as well (yellow arrowhead). 2) Polyp formation on the badly-oriented stomachs following the bio-distribution assay for ^{18}F -FDG was monitored via hematoxylin and eosin staining did not allow for proper staging of the polyp severity. C) A large cancerous kidney found in a dead mouse at week 30, an example of MNU off-target effects.

A second trial was begun to increase N and to fix stomachs with better orientation. In this trial, the same 10 week MNU protocol was followed, but TAM or VEH was injected every 4 weeks throughout the entire experiment to test whether the rounds of metaplasia have more effect after the cells had undergone the MNU treatments. 15 MNU+TAM, 15 MNU+VEH, 5 TAM-only, and 5 VEH-only mice were tested. Mice died from all groups nearly weekly starting at week 17, with cause of death generally undetermined. So many mice died that the remaining mice were all

sacrificed at week 26 to have enough N to use the data, yet almost no polyps were seen at this early time point.

5.3 Discussion

These pilot trials were mainly used to test the techniques for long-term carcinogenesis studies, and they were successful in that manner. The 10-week published MNU protocol was seen to cause polyp formation in the stomachs of FVB/N mice when they lived for longer than 30 weeks from the beginning of the experiment. While there were rarely well-oriented fixed stomachs available to directly analyze polyp/tumor pathology, preliminary numbers indicate that TAM-treated mice are twice as likely to form polyps/tumors as VEH-treated mice within the MNU protocol. This is consistent with the Cyclical Hit Model of Tumorigenesis, wherein long-lived cells may undergo rounds of dedifferentiation and redifferentiation resulting from physiological injury over the lifetime of an animal. These rounds of entering and leaving the cell cycle may allow the long-lived cells to accumulate and store mutations, eventually leading to tumorigenesis in a stem cell-independent manner (Burclaff and Mills, 2018b; Burclaff and Mills, 2018a).

The pilot studies also showed us many ways to improve experimental design for future trials. It was demonstrated that TAM-treated mice have more fluorescence in their spleen and liver than in their stomachs when probed with ProSense 680 and MMPSense 750 FAST. Since these two organs reside near the stomach, it is difficult to ascertain if any signal is specific to the stomach when imaging live mice. PET/CT scanning with 18-FDG appears to mark the actual stomach, with the curve of the antrum likely visible in some images. However, bio-distribution imaging

indicated that the upper duodenum also had signal, so future work should verify that the signal is stomach-specific.

The issue of mice dying was also highlighted by both trials. While some death may be unavoidable in these experiments due to their length and number of injections, a large amount of early death seemed to result from the mice fighting. All FVB/N mice used were males ordered in bulk from Jackson Laboratories. Future studies should consider using female mice or males bred in-house and only housed with direct siblings to reduce fighting. If the mice can be kept alive throughout the experiment, it will be exciting to see further studies repeat these trials to properly determine whether rounds of injury and/or metaplasia increase tumor incidence and rate.

5.4 Methods and Materials

Animals and tumorigenesis

All experiments involving animals were performed following protocols approved by the Washington University School of Medicine Animal Studies Committee. Mice were maintained in a specified in-and-out facility under a 12-hour light cycle. Wild type FVB/N mice were purchased from Jackson Laboratories (Bar Harbor, ME). Mice were kept on a low-fluorescence chow prior to in vivo fluorescence imaging to minimize autofluorescence throughout the GI tract. To induce tumorigenesis, mice were given N- methyl-N-nitrosourea (MNU, 240ppm, Toronto Research Chemicals) in their drinking water on alternating weeks for 10 total weeks. Tamoxifen (5 mg/20 g body weight; Toronto Research Chemicals) or vehicle (10% ethanol, 90% sunflower oil, Sigma) were injected intraperitoneally for two days.

Live near-infrared fluorescence imaging

Mice were pre-imaged on a FMT Imager without probes injected to record the natural autofluorescence of the stomach region. Immediately following the pre-imaging, mice received ProSense 680 (2nmol/150 μ l, Perkin Elmer) via tail-vein injection. The following day, mice were injected with MMPSense 750 FAST probes (2nmol/100 μ l, Perkin Elmer) 6 hours before imaging.

To image, mice were knocked out using isoflurane then their full abdomen was shaved smooth with an electric razor and Nair hair remover. Mice were imaged for the manufacturer-installed channels for Prosense 680 and MMPSense 750 Fast on a fluorescence molecular tomography (FMT4000, Perkin Elmer) system with a Region of Interest drawn around the stomach area of their upper left abdominal quadrant.

PET/CT Scanning

All PET/CT scanning and relevant injections were done by the Small Animal Cancer Imaging core at Washington University. Mice were fasted overnight prior to imaging, then injected with ¹⁸F-FDG. Kinetic imaging was taken for 1 hour after probe injection. Images were viewed using Inveon Research Workplace software

Histology

When possible, stomachs were harvested, flushed in PBS, opened along the greater curvature, then pinned out in fresh 10% formalin overnight at 4 °C. Images of full stomachs were taken

using a dissecting microscope (Olympus SZX7). Stomachs were then cut into thin strips and embedded in agar for normal processing and mounting onto glass slides. Polyp pathology was imaged after staining for hematoxylin and eosin following the standard protocol.

Chapter 6: Nitric Oxide may act as a damage signal between dying parietal cells and the gastric epithelium

6.1 Introduction

The major physiological and morphological changes of SPEM are becoming better understood, yet work remains to characterize its molecular regulation, especially the mechanism by which it is initiated. SPEM consistently seems to occur in units with injured/dead parietal cells (PCs), suggesting that there are intercellular signals passed between PCs and the stem cells, neck cells, and chief cells which respond to their atrophy. Two possible mechanisms could explain how this signaling occurs. Healthy PCs may secrete signals that promote normal adult gastric differentiation and inhibit SPEM. In this idea, SPEM changes only begin after sufficient PC atrophy occurs such that there may be differentiation-promoting/SPEM-inhibiting products are lost from the PCs as they are killed. The other, not mutually exclusive, possibility is that injured/dying PCs may express an as-yet-uncharacterized damage signal which is received by the surrounding cells to actively induce SPEM (Mills and Shivdasani, 2011). To date, several paracrine-acting factors have been identified to originate from healthy PCs, supporting the first theory. Known PC-elaborated factors include amphiregulin, sonic hedgehog, VEGF-B, BMP4, and EGF family members (Goldenring et al., 1996; Mills et al., 2001; Nitsche et al., 2007; Nam et al., 2009; Huh et al., 2010; Xiao et al., 2010). To our knowledge, no one has published factors that PCs secrete specifically during injury that might affect neighboring epithelial cells.

Nitric oxide (NO) is a small, short-lived, soluble gaseous signaling molecule often used in intercellular and intracellular signaling. NO is a well-studied signaling molecule implicated in many systems throughout the body including neuronal, cardiovascular, renal, pulmonary, endocrine, and immune system signaling (Nathan, 1992). The mammalian body has three nitric oxide synthases (NOS): the constitutively expressed neuronal and endothelial synthases (nNOS and eNOS), which are activated by intracellular calcium and calmodulin, and the inducible nitric oxide synthase (iNOS), which is regulated at the transcriptional level by cytokines and other signals (Nathan, 1992)

There is only one known protein receptor for NO in the cell: soluble guanylyl cyclase (sGC), which converts GTP to cGMP when activated by NO binding (Pyriochou and Papapetropoulos, 2005). NO remains bound to sGC with a half-life of around 2 minutes, which decreases to 5 seconds with MgGMP present, indicating that sGC can have quick and dynamic response times (Kharitonov et al., 1997). NO levels are also extremely dynamic. Physiological levels of NO can range over six orders of magnitude, from picomolar to micromolar levels (Hetrick and Schoenfisch, 2013). These levels can also change quickly due to NO's low half-life (<10 seconds), and data shows that iNOS can inactivate within minutes (Palmer et al., 1987; Hetrick and Schoenfisch, 2013). Both of these characteristics make NO-sGC signaling extremely responsive to quick stimuli.

While sGC is the only known protein receptor for NO and it is considered the 'classical' signaling mechanism, NO can also have sGC independent effects within the cell (Martinez-Ruiz et al., 2011). NO has been shown to S-nitrosylate thiol-containing proteins, binding to cysteine residues (Stamler, 1994). NO is also able to form disulfide bridges and induce post-translational

modifications to various proteins (Burke et al., 2013). Several enzymes include cysteines at their active sites, so NO can have wide ranging effects outside of NO-sGC signaling.

Preliminary data from our lab indicate that inducible nitric oxide synthase expression is observed in PCs following injury. NO produced in these dying cells could explain why SPEM only occurs locally in units with dying PCs. Thus, NO may be one of the key activating signals inducing SPEM. Here, we study whether NO signaling propagates the gastric damage response following PC injury and attempt to determine whether it acts through sGC in the process.

6.2 Results

Previous unpublished data from our lab indicated that inducible nitric oxide synthase (iNOS) expression is observed in PCs 6-12 hours post HD-TAM and in tissue from human gastric cancer patients following *H pylori* infection, though no expression is seen in homeostatic PCs (Khurana, S.S. Dissertation, 2014). To continue this project, I began by confirming iNOS expression in PCs following HD-TAM as well as in tissue from mice injected with DMP-777 (gift of Dr James Goldenring, Vanderbilt University). While iNOS is seen in some PCs following damage, its expression is often light with only rare individual PCs expressing high iNOS (Figure 6.1). This may be a result of experimental technique or it could be indicative of an extremely short and controlled expression time for iNOS within dying cells. Regardless, it makes quantifying iNOS⁺ PCs impractical.

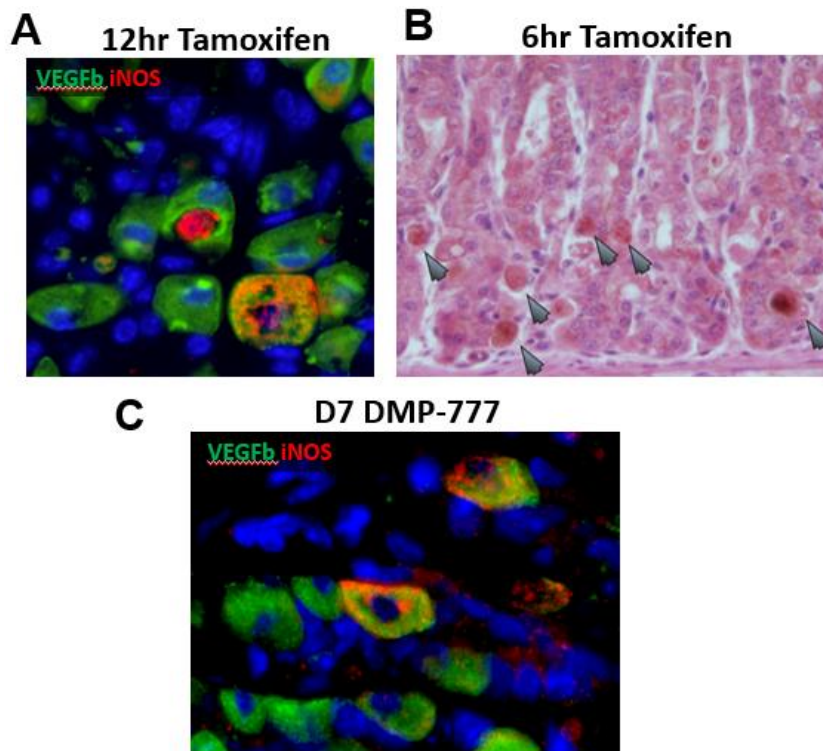


Figure 6.1: iNOS expresses in individual PCs following injury.

A) Immunofluorescence staining of parietal cells after 12h TAM (Blue: hoescht, green: VEGFb (PCs), red: iNOS). **B)** Immunohistochemical staining for iNOS following 6hr TAM. Grey arrowheads show PCs lightly expressing for iNOS. **C)** Immunofluorescence staining of parietal cells after 7 days of DMP-777, stained as in A.

To test whether NO introduced to the full mouse body is sufficient to increase gastric proliferation, the NO donor S-nitroso-N-acetyl penicillamine (SNAP) was injected intraperitoneally into uninjured mice (Singh et al., 1996). When injected at 3mg/kg mouse weight for 3 days, SNAP caused significantly increased gastric proliferation, though it only effected a subset of mice (Figure 6.2A,B). Also, the proliferation increase was still confined to the isthmus of the gastric units, and no SPEM or other damage response signatures were seen. The biphasic proliferative response and lack of metaplasia may result from the method of introduction, as physiological NO is a short-lived and locally-acting signal. Therefore, a diffuse

injection of an NO donor having any effect on gastric proliferation was considered as a positive indication that local NO may have important effects.

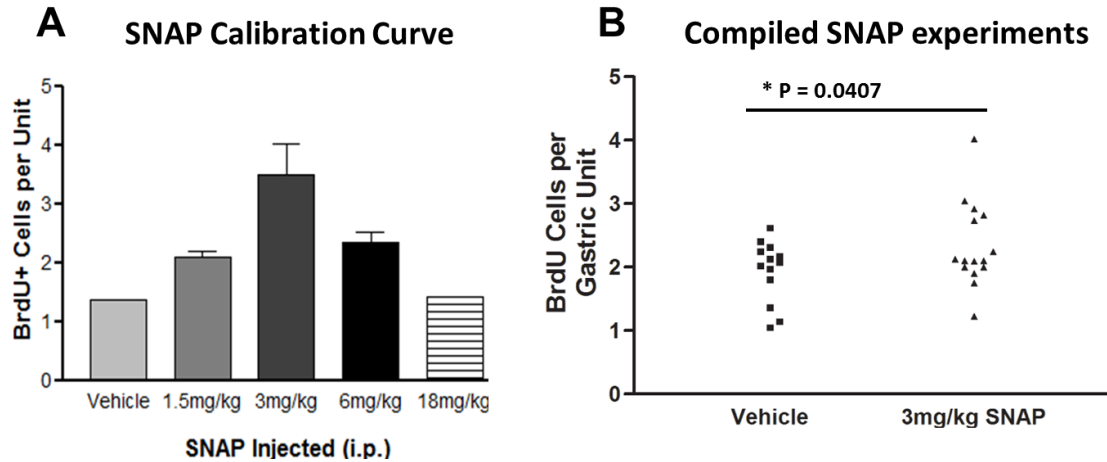


Figure 6.2: The NO donor SNAP has a limited effect on gastric proliferation.

A) Quantification of proliferating cells per unit in mice injected with varying concentrations of SNAP for three days. **B)** Compiled proliferation data from all experiments where mice were injected with vehicle or 3mg/kg SNAP for 2 or 3 days. SNAP is seen to significantly increase proliferation, though the effect is mainly seen in a subset of the mice.

We next wanted to see whether NO production via iNOS expression is necessary for the full damage response to occur. Aminoguanidine hemisulfate (AG) inhibits iNOS activity without affecting basal NO production from eNOS or nNOS (Corbett and McDaniel, 1996). If NO is active as PCs are injured yet still alive, we would expect the effect to be seen early in the damage response. Therefore, we injected AG before and alongside 24 hours HD-TAM and monitored proliferation. We saw no difference in BrdU⁺ cells per unit at 24h TAM with or without AG co-injected (Figure 6.3)

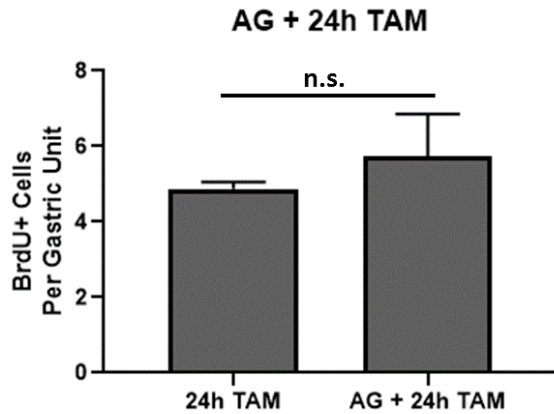


Figure 6.3: Inhibition of iNOS activity has no significant effect on proliferation.

Seeing that NO levels appear to effect gastric proliferation following SNAP injections, we wanted to test whether NO acted through its sole known protein receptor, sGC. Staining for sGC indicated expression in the cytoplasm of chief cells and, to a lesser extent, neck cells (Figure 6.4A), consistent with the cellular populations shown to respond to PC injury. To test the necessity of sGC for the proper damage response, sGC^{flox/flox} mice were purchased from Jackson Laboratories and bred to Mist1-CreERT mice. Interestingly, Mist1-CreERT; sGC^{flox/flox} mice did not appear to lose sGC expression following low dose tamoxifen administration, and sGC-floxed mice showed no difference in their response to HD-TAM (Figure 6.4B,C).

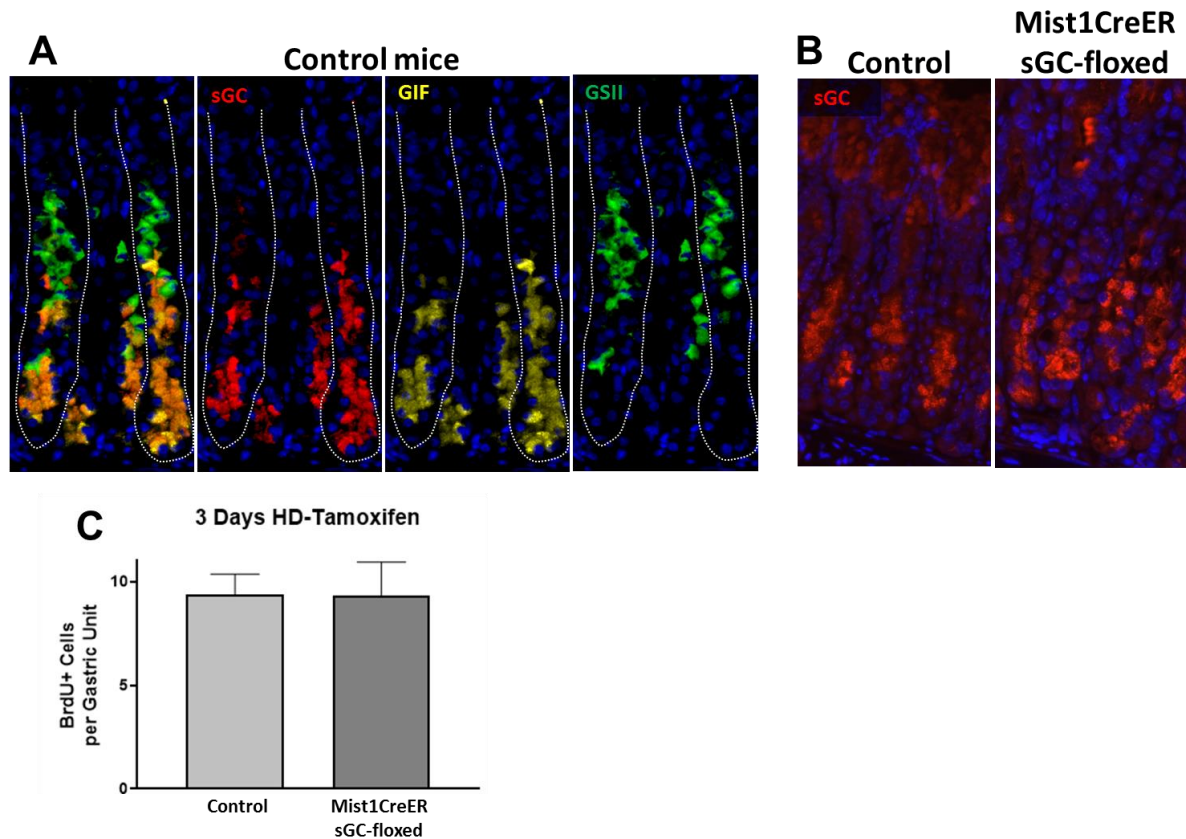


Figure 6.4: sGC in chief and neck cells is unchanged following floxing.

A) Immunofluorescence staining for sGC in a wild type stomach (blue: hoescht, red: sGC, yellow: GIF, green: GSII). sGC is seen to strongly overlap with GIF expression and is also expressed, to a lesser extent, in GSII⁺ neck cells. **B)** Immunofluorescence staining for sGC in control mice and in Mist1CreER;sGC^{flox/flox} mice after a week of low-dose tamoxifen to induce the Cre recombinase. **C)** Quantification of proliferating cells per gastric unit show no change between control mice and mice with sGC floxed.

All of the experiments done so far modulated NO levels or reception on a systemic level, but NO is known to be a highly localized signaling agent. To model more physiological NO expression from PCs, TetO-iNOS-lacZ mice (Mungrue et al., 2002) were crossed with a constitutively active PC-specific Cre driver line (ATP4b-Cre) and a ROSA26-LSL-rtTA.IRES.EGFP line, which will only express the rtTA “Tet-On” system in the presence of a Cre driver. These crosses should result in mice that express iNOS specifically in PCs, and only following induction via doxycycline injection. They have the added benefit of driving LacZ reporter expression in any

cell that expresses iNOS. Unfortunately, the LacZ reporter was only seen in rare clumps of non-PC cells following induction (Figure 6.5). Since NO was not being produced in PCs or efficiently across the stomachs, it was impossible to draw conclusions from these mice.

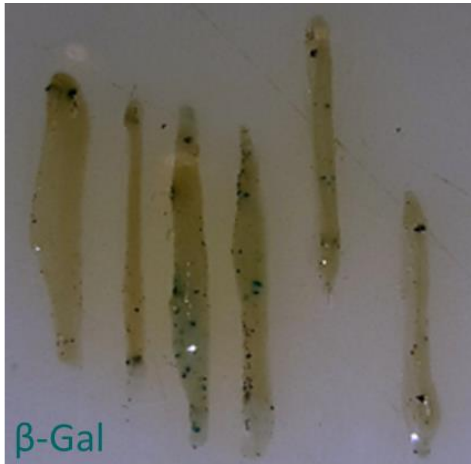


Figure 6.5: Sporadic iNOS is driven from Tet-On iNOS overexpression mice.

LacZ coloration was developed in Tet-On iNOS mice, yet LacZ was only seen in rare units and in those it is expressed in the pit cell region. No parietal cell-specific expression was observed (not shown).

6.3 Discussion

NO expression is known to affect proliferation and other cellular processes in many physiological systems. Its solubility and short half-life, along with the highly controlled expression of iNOS allowing for dynamic NO concentration changes, make NO a prime candidate signal for how injured PCs might alert the rest of the gastric unit to damage and the need for increased proliferation. Experimental data support that NO may be active in such a role, as iNOS is seen in some PCs following injury and full-body NO increases raised gastric proliferation. Yet many complicating factors are seen for each experiment. While iNOS is seen

in some PCs following injury, it often stains extremely lightly, only staining as highly expressed in rare individual cells. SNAP shows a relatively weak effects compared to the full range of proliferation seen following injury, yet, it must be remembered that these blunt systemic drugs lack the intricate intra-glandular gradients that would be expected from a local signaler such as NO. Inhibiting iNOS activity via AG with D3 or 24h TAM had no noticeable effect on proliferation. Also, sGC expression was seen in chief cells and neck cells, two populations of cells known to proliferate following PC injury, however, sGC staining remained consistent even in sGC-floxed mice, so no conclusions could be drawn from these experiments. Likewise, our ‘Tet-On’ system to drive iNOS expression specifically in PCs following doxycycline injection could not be verified, as the LacZ reporter that should be driven alongside iNOS expression only appeared in rare clusters of cells.

Thus, while NO still holds promise as an agent used by injured cells to initiate proliferation of their surrounding cells, our available tools were insufficient to fully test whether this is the case in the stomach following PC injury.

6.4 Methods and Materials

Animals and Injections

All experiments involving animals were performed following protocols approved by the Washington University School of Medicine Animal Studies Committee. Mice were maintained in a specified pathogen-free barrier facility under a 12-hour light cycle. Wild type *C57BL/6* mice were purchased from Jackson Laboratories (Bar Harbor, ME). Littermate controls were housed together when possible. To induce SPEM, tamoxifen (5 mg/20 g body weight; Toronto Research

Chemicals, Inc, Toronto, Canada) was injected intraperitoneally daily for 3 days. Tamoxifen was dissolved in 10% ethanol and 90% sunflower oil (Sigma), following the procedure outlined in (Saenz et al., 2016). S-nitroso-N-acetyl penicillamine (SNAP, Sigma) was dissolved in 0.9% saline and normally injected three times daily with 3 mg /kg mouse mass. Aminoguanidine (Sigma) was also dissolved 0.9% saline and injected at 400mg/kg.

Immunofluorescence

Mice were given an intraperitoneal injection containing 5-bromo-2'-deoxyuridine (BrdU, 120 mg/kg) and 5-fluoro-2'-deoxyuridine (12 mg/kg) in sterile water 90 min before sacrifice. Following sacrifice, stomachs were immediately excised and flushed with PBS, then pinned out and fixed in freshly prepared methacarn (60% methanol, 30% chloroform, 10% glacial acetic acid) for 20 minutes or fixed overnight in cold formalin (3.4% formaldehyde in phosphate buffered saline; Sigma Aldrich, MO). Tissues were arranged in 3% agar in a tissue cassette, underwent routine paraffin processing, and 5µm sections were cut and mounted on glass slides. Sections underwent a standard deparaffinization and rehydration protocol, were blocked in 1% BSA, 0.3% Triton-X100 in PBS, left with primary antibodies overnight, washed then and incubated for one hour with secondary antibodies, washed, washed, then mounted using ProLong Gold antifade reagent with DAPI (Invitrogen, CA).

Primary Antibodies used in this study: rabbit anti-human gastric intrinsic factor (gift of Dr. David Alpers, Washington University), goat anti-BrdU (gift of Dr. Jeff Gordon, Washington University), goat anti-VEGFb (1:100, Santa Cruz), rabbit anti-iNOS (Abcam), rabbit anti-sGC (Sigma) or 1 g/ml fluorescently labeled GSII lectin (Alexafluor488, 594, Molecular Probes).

Secondary Antibodies included AlexaFluor (488, 594 or 647) conjugated donkey anti-goat, anti-rabbit, or anti-mouse (Molecular Probes).

Immunofluorescence quantification

All timepoints were quantified with at least three mice, with representatives from both genders. Stomachs were fluorescently stained with bisbenzimidazole and either anti-BrdU or anti-VEGFb markers along with the neck cell marker GSII lectin and zymogenic cell marker anti-GIF. Images were captured as TIFF files from a Zeiss Axiovert 200 microscope with AxioCam MRM camera and with Apotome optical sectioning filter. Each stomach had at least 5 images taken containing 10+ well-oriented gastric units each. Units were counted using the neck staining, and total quantifications of proliferating cells (BrdU+) or PCs (VEGFb+) were averaged over total unit numbers per mouse.

Tet-On system

TetO-iNOS-lacZ mice (Mungrue et al., 2002) were crossed with a constitutively active PC-specific Cre driver line (*ATP4b-Cre*) and a ROSA26-LSL-rtTA.IRES.EGFP line. To activate the rtTA, mice were injected intraperitoneally with Doxycycline hyclate (10 mg/mL solution in 0.9% saline injected at 10uL/g mouse mass, Sigma) daily for three days.

For LacZ staining, we followed a modified version of the protocol used in (Stange et al., 2013b). Freshly harvested stomachs were fixed in 4% PFA for 1 hour at 4 °C then washed in a solution containing 100 mM sodium phosphate, 2 mM MgCl₂, 0.1% sodium deoxycholate, and 0.02% Triton x-100. Stomachs were then stained overnight in a solution containing 1 mg/mL X-gal, 5

mM potassium ferricyanide, and 5mM potassium hexacyanoferrate. The following day, the stomachs were washed then post-fixed overnight in 4% PFA before being processed into blocks as usual.

Chapter 7: Neck cells undergo many of the defined steps of Paligenosis when re-entering the cell cycle following injury

7.1 Introduction

Recent work from our lab has highlighted that long-lived, mature cells between organs follow a conserved pathway to revert to a regenerative state, which we have termed paligenosis (Willet et al., 2018b). The pathway was defined in gastric chief cells and pancreatic acinar cells, and corresponding data was shown in numerous other organs. As chief cells and acinar cells are both terminally differentiated secretory cells, it is unproven whether paligenosis occurs in less mature, non-secretory, or even intermediate cells.

Neck cells are triangular cells found interspersed between parietal cells in the neck of the gastric unit. Classical papers using ³H-Thymidine pulse chase experiments indicate that neck cells are a short-lived intermediate population between the stem cell and the chief cell population at the base of the gastric unit with a turnover time of 9-16 days (Hattori and Fujita, 1976a; Karam and Leblond, 1993c). The idea that neck cells transdifferentiate into chief cells is further supported by the presence of transitional cells found between the neck and chief cell regions co-expressing neck and chief cell markers (Suzuki et al., 1983; Ramsey et al., 2007). Some have argued that neck cells should be regarded as an independent population since they appear to secrete protective proteins, and it would be unique throughout the GI tract to have a functional population mature into a separate functional population (Hanby et al., 1999), however, the

prevailing agreement in the field is that neck cells largely act as the bridge between stem cells and chief cells (Goldenring et al., 2011a).

While the contribution of neck cells in tamoxifen-mediated spasmodic polypeptide-expressing metaplasia (SPEM) has been largely overlooked due to the large changes undergone by the parietal cell and chief cell populations, our recent work with HKiDTR mice highlight that neck cells re-enter the cell cycle following parietal cell injury (Burclaff and Mills, 2018a). Neck cells are normally non-proliferative, with around 0.33 neck cells per unit taking up BrdU in a 90 min pulse (Burclaff et al., 2017), raising the question of how neck cells re-enter the cell cycle when the parietal cells are injured. Do neck cells follow the same paligenosis pathway as more mature secretory cells, or are they able to re-enter the cell cycle in a different manner due to their smaller size and simpler structure? Our lab's tamoxifen (TAM) and targeted diphtheria toxin (DT) models should allow us to test this.

7.2 Results

As recently published by our lab, mature cells need to undergo key regulatory changes to properly re-enter the cell cycle following injury (Willet et al., 2018b). Chief and acinar cells both have active Mtorc1 at homeostasis, as detected via phosphor-S6 immunostaining. This is quickly shut off following injury yet needs to return before the cells proliferate. Autophagy and lysosomal activity must also occur to reduce the levels of rough ER, secretory vesicles, and mitochondria in the complex secretory cells. Finally, metaplastic genes are seen to express in both cell types, including Sox9 and CD44v. All of these processes can be tested with specific attention paid to the neck cells following injury from TAM or targeted DT.

We first tested whether metaplastic genes express in neck cells following injury. Unlike chief and acinar cells, neck cells express high Sox9 at homeostasis, and this was not seen to change

following injury (Figure 7.1). However, other metaplastic genes such as CD44v and clusterin quickly express in neck cells following PC injury, as already shown in (Burclaff et al., 2017), consistent with the paligenosis pathway.

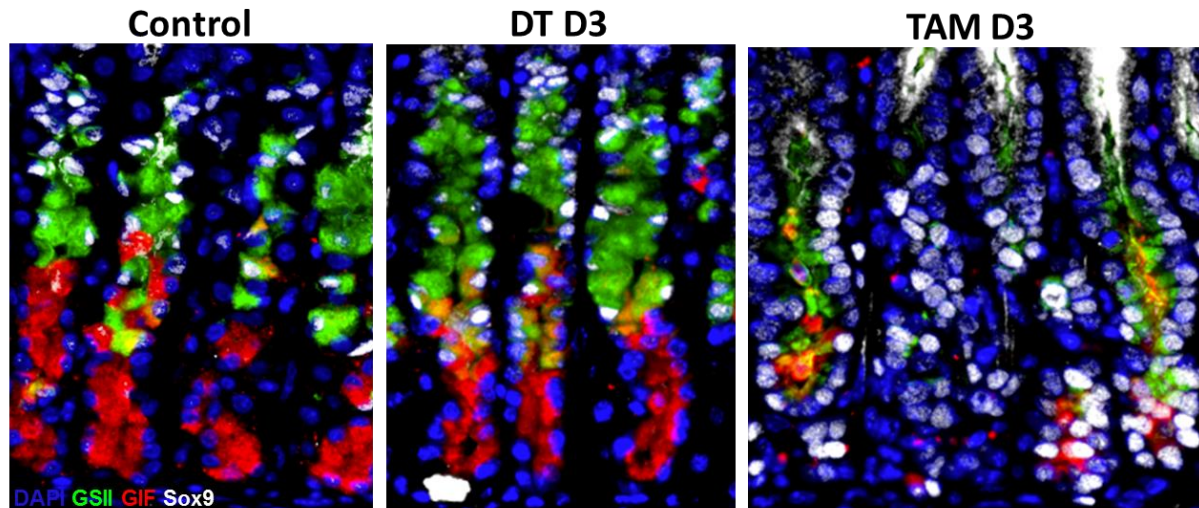


Figure 7.1: Sox9 expression in healthy and injured stomachs.

Immunofluorescence staining for Sox9 in healthy stomachs and stomachs of mice treated with DT or TAM for 3 days (red: GIF, green: GSII, white: SOX9). SOX9 expression in GSII⁺ appears consistent regardless of damage status.

We next examined mTorc1 activity using immunofluorescence staining for its downstream target pS6. Unlike chief and acinar cells, neck cells are not normally pS6⁺, so the initial deactivating step could not occur. However, mTorc1 was seen to activate throughout the neck regions by 24h TAM or DT, indicating that neck cells use mTorc1 activity in their proliferative response to injury similar to chief cells (Figure 7.2A) Intriguingly, nearly all neck cells are pS6⁺ following DT even in units where the PCs have not yet died, raising questions about how they recognize that damage is occurring, but that is outside the scope of this project. To test whether this mTorc1 activity is necessary for neck cell proliferation, we treated mice with rapamycin before

and alongside TAM or DT. When cell type-specific proliferation was quantified at D3 TAM or DT following rapamycin treatment, neck cell-specific proliferation was significantly decreased for both (Figure 7.2B,C). This indicates that neck cells have an mTorc1-activation checkpoint before they can properly proliferate, consistent with the paligenosis pathway.

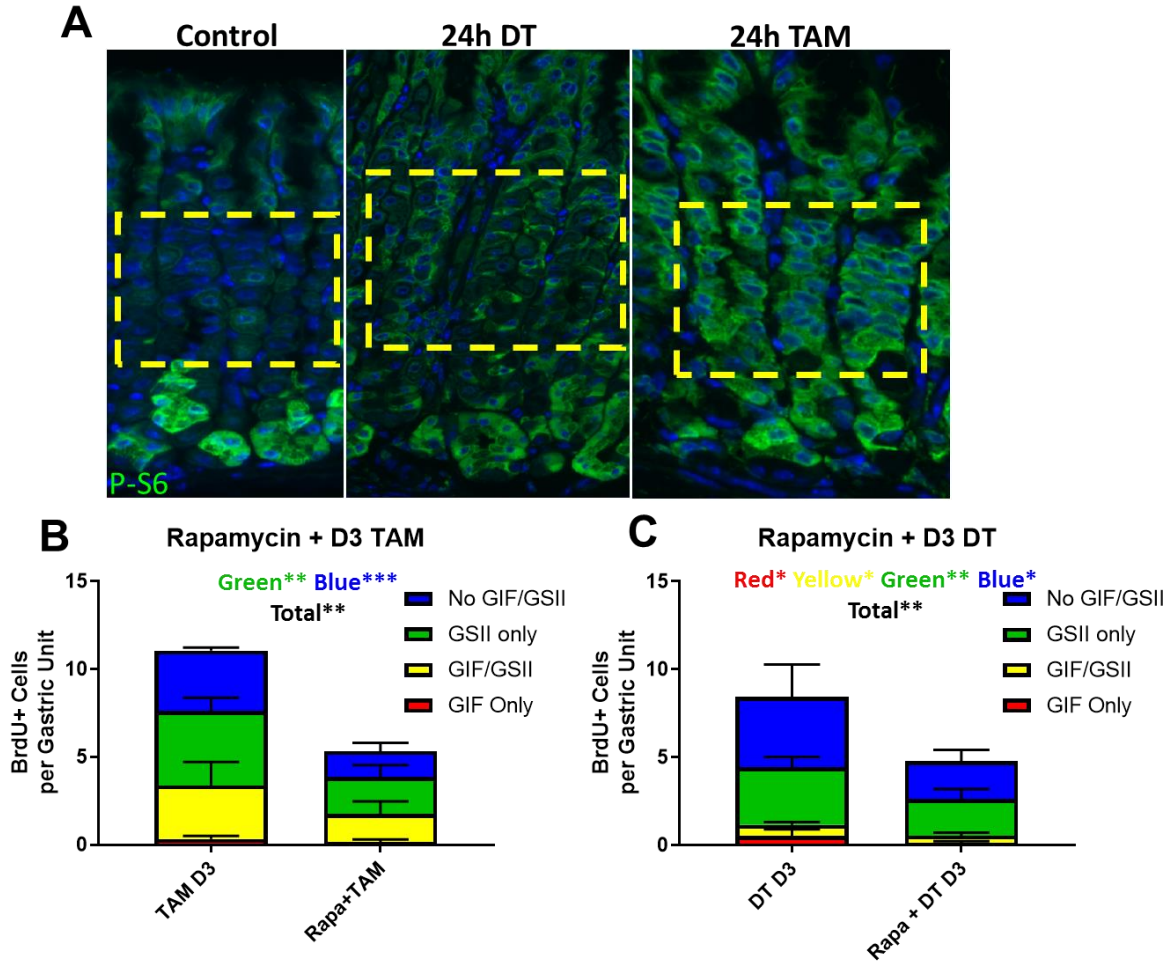


Figure 7.2: Neck cells have dynamic mTorc1 activity following injury.

A) Immunofluorescence for pS6 (green) in a healthy mouse stomach or 24h after injection with TAM or DT to HKiDTR mice. **B,C)** Quantification of proliferating cells by population following three daily injections of TAM or DT (Red = chief cells, yellow = SPEM cells, green = neck cells, blue = no differentiation markers expressed).

We next looked at autophagy and lysosomal activity in neck cells following injury. Neck cells would be expected to have less need for these processes, as they are already much smaller and less complex than chief cells, yet the question remains whether they necessitate any level of downscaling to successfully re-enter the cell cycle. Neck cells are closely latticed between parietal cells which are constitutively high for autophagy and lysosomy proteins, making analyzing neck cell autophagy by immunofluorescence difficult. We instead used transmission electron microscopy (tEM) to count autophagic events happening in individual neck and chief cells following TAM and DT. Autophagy is easy to identify in tEM images, determined as a double membrane surrounding contents separated from the rest of the cytoplasm (Figure 7.3A). A low level of autophagic events were seen in both cell types at homeostasis. These increased in both cell types 24h following TAM or DT, with a greater change seen in chief cells, as expected (Figure 7.3B). This indicates that increased autophagy does occur in neck cells following injury. To test whether this autophagy was necessary for proper re-entry into the cell cycle, we analyzed the proliferative response to TAM in lysosomal-defective *Gnptab*^{-/-} mice. The main phenotype of these mice is gland dropout following TAM, yet to probe neck cell-specific effects we had to quantify proliferation in the remaining full units. With that selection bias, the total decrease in proliferation was less than expected, yet neck cell-specific proliferation was still significantly decreased (Figure 7.3C). To avoid the gland dropout, we tried inhibiting lysosomal function by injecting Lys05, which is published to de-acidify lysosomes with 10x the efficiency of hydroxychloroquine (McAfee et al., 2012). We injected Lys05 before and throughout TAM, and extremely varied phenotypes were seen, ranging from full proliferative SPEM to SPEM lacking proliferation to regions with no SPEM and very few proliferating cells (Figure 7.3D). Due to the variance, we did not quantify neck cell-specific proliferation, but the stomachs lacking SPEM or

proper proliferation reinforce the need for lysosomal activity for the proper regenerative response to occur across gastric cell types. So while we were ultimately unable to directly prove that neck cells need lysosomal activity to proliferate, data from several experiments indicate that they have increased autophagy and that neck cells with inhibited lysosomes proliferate less following injury, consistent with paligenosis in chief cells.

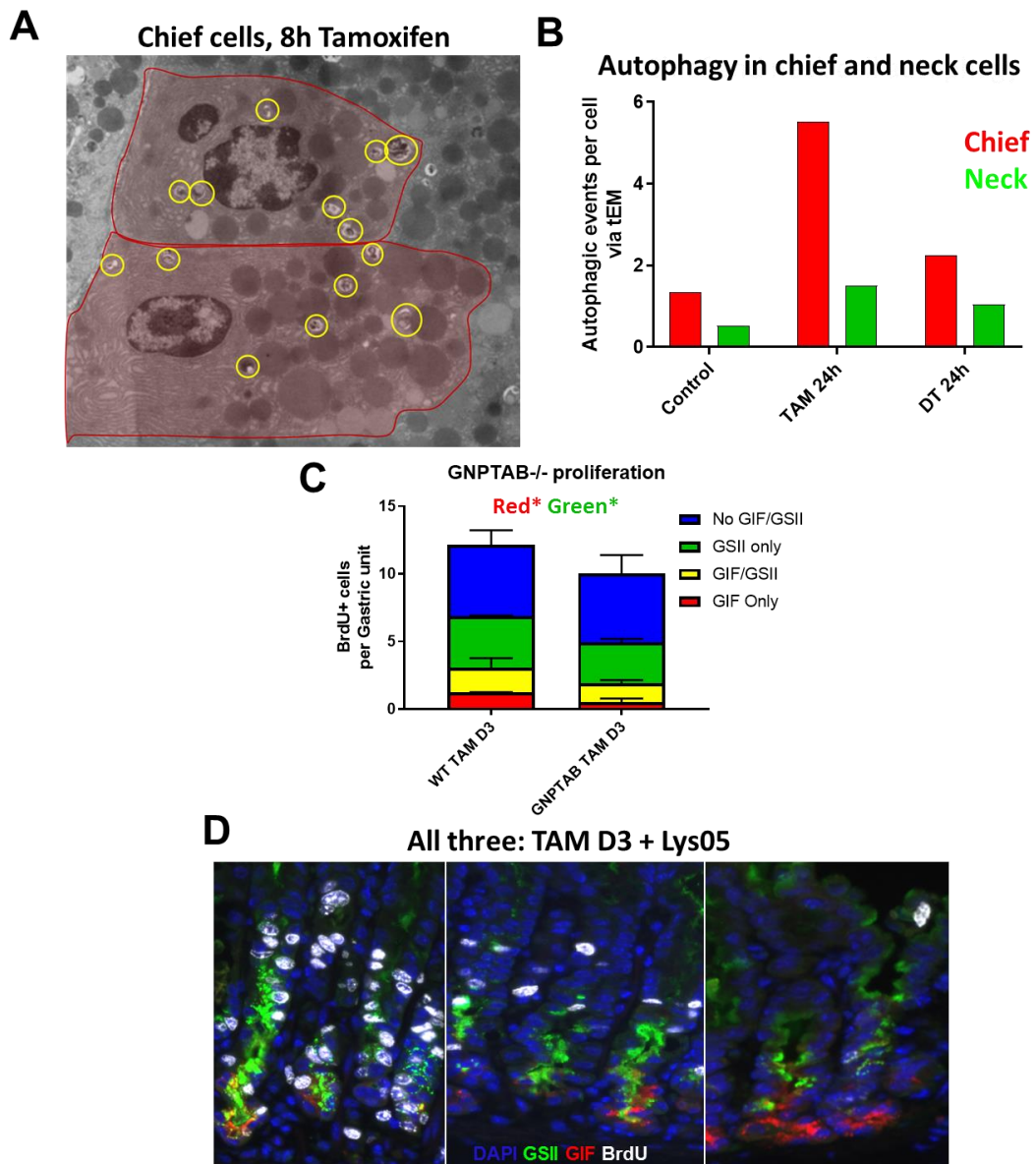


Figure 7.3: Neck cells activate autophagy following injury.

A) Example transmission electron microcopy image of two chief cells 8h following TAM. Chief cells are outlined in red. Autophagic events are circled in yellow. **B)** Quantification of autophagic events per cell in neck cells and chief cells in healthy stomachs or stomachs 24h following TAM or DT injections. **C)** Quantification of proliferating cells by population following three daily injections of TAM either alone or with Lys05 injected one day prior and alongside the TAM (Red = chief cells, yellow = SPEM cells, green = neck cells, blue = no differentiation markers expressed). * denotes significance for the population indicated $P < 0.05$. **D)** Immunofluorescence images of stomachs following injections with Lys05 and TAM (red: GIF, green: GSII, white: BrdU). All mice were treated identically, yet phenotypes ranged from proliferative SPEM (left) to non-proliferative SPEM (middle) to no proliferation or SPEM (right).

Unpublished data from our lab implicate another gene, *Ifrd1*, in the pathogenic response in chief and acinar cells, with *Ifrd1*^{-/-} mice unable to properly proliferate following gastric or pancreatic injury (Mark Lewis, unpublished). We bred *Ifrd1*^{-/-} mice with HKiDTR mice to test whether the knockout has any effect on neck cell proliferation. Across four knockout or control mice, proliferation was unchanged following DT treatment (Figure 7.4).

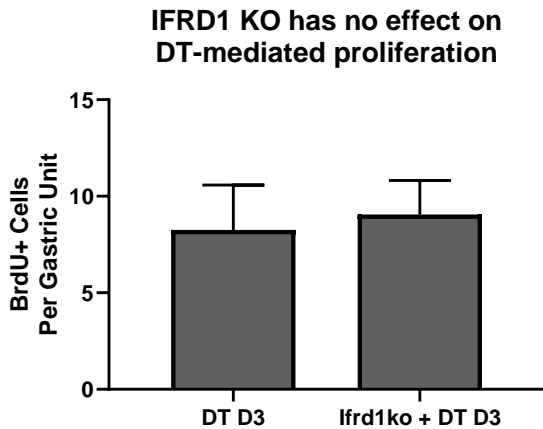


Figure 7.4: IFRD1 status has no effect on neck cell proliferation following injury.

Quantification of proliferating cells per unit at D3 DT showed no difference in proliferative capacity between HKiDTR or HKiDTR;*Ifrd1*^{flox/flox} mice.

7.3 Discussion

Paligenosis presents a useful paradigm for studying how non-proliferative cells re-enter the cell cycle following injury. This may advance our knowledge of acute injury responses, chronic inflammatory or metaplastic conditions, and possibly even cancer initiation (Burclaff and Mills, 2018b; Burclaff and Mills, 2018a). Our understanding of paligenosis is still nascent, and more phases and necessary proteins in the mechanism are currently being fleshed out by our group. However, as the mechanistic knowledge increases, it will also be important to say which cell types can and do undergo this important process. Will any non-proliferative cell that becomes regenerative following injury undergo the conserved changes? Will it depend on maturation state, cell age, or some cadre of genes being expressed by the cell at homeostasis? Here, we tried to answer some of these questions by looking at the regenerative response of gastric neck cells, which are smaller, shorter-lived, and less complex than chief cells.

Neck cells were found to undergo very similar changes as chief cells following injury, though often to a lesser extent. While neck cells express novel genes such as CD44v and Clusterin before proliferating, Sox9, one of the main metaplastic genes used to describe paligenosis, is already expressed by neck cells, possibly indicating that they may naturally be in a more metaplastic or closer to a regenerative state. Likewise, mTorc1 activation is necessary for proper neck cell proliferation, yet there is no mTorc1 originally active in the cells, so neck cells undergo less initial changes than chief cells. Finally, autophagy appears to occur and be necessary for proper proliferation in neck cells, yet neck cells were seen to increase their autophagic events per cells by a much smaller amount than chief cells.

While the three main changes defined in the introductory paligenosis paper may occur in neck cells, they lack other characteristics of the cell types shown to undergo paligenosis. For example,

they have no noticeable change in Sox9 and they do not need to lose mTorc1 activity in Phase 1. *Ifrd1* depletion also has no effect following DT, while it decreases basal proliferation following TAM. As future work in our lab and others should continue to define further steps and proteins involved in paligenosis, each newly defined aspect should be tested in neck cells or other intermediate and non-secretory cells to help solidify which cell types can undergo the full response.

7.4 Methods and Materials

Animals and Injections

All experiments involving animals were performed following protocols approved by the Washington University School of Medicine Animal Studies Committee. Mice were maintained in a specified pathogen-free barrier facility under a 12-hour light cycle. Wild type *C57BL/6* mice were purchased from Jackson Laboratories (Bar Harbor, ME). Littermate controls were housed together when possible. HKiDTR mice were bred from ROSA26^{iDTR/iDTR} mice purchased from Jackson Laboratories bred to ATP4b-Cre mice from our in house stock. Data for GNPTAB^{-/-} mice were taken directly from counts done for previously published experiments (Willet et al., 2018b).

To ablate PCs, diphtheria toxin (225ng/mouse in 0.9% sodium chloride saline; Sigma) was injected intraperitoneally every day for up to 16 days. To induce SPEM, tamoxifen (5 mg/20 g body weight; Toronto Research Chemicals, Inc, Toronto, Canada) was injected intraperitoneally daily for 3 days. Tamoxifen was dissolved in 10% ethanol and 90% sunflower oil (Sigma), following the procedure outlined in (Saenz et al., 2016). mTorc1 activity was inhibited with daily

injections of rapamycin beginning one day before TAM or DT (Sigma). Rapamycin was prepared by dissolving 30mg/mL in 100% ethanol then suspended the ethanol solution 1:50 in 0.25% Tween20, 0.25% PEG in 1xPBS, and 100 μ L/20g mouse mass was injected. Lysosomal activity was inhibited by injecting 40 or 60mg/kg mouse mass Lys06 daily beginning one day before TAM or DT (dissolved in PBS, Selleck Chemicals).

Immunofluorescence

Mice were given an intraperitoneal injection of 5-bromo-2'-deoxyuridine (BrdU, 120 mg/kg) and 5-fluoro-2'-deoxyuridine (12 mg/kg) in sterile water 90 min before sacrifice. Following sacrifice, stomachs were immediately excised and flushed with PBS, then inflated and fixed overnight in cold formalin (3.4% formaldehyde in phosphate buffered saline; Sigma). Tissues were arranged in 3% agar in a tissue cassette, underwent routine paraffin processing, and 5 μ m sections were cut and mounted on glass slides. Sections underwent a standard deparaffinization and rehydration protocol, were blocked in 1% BSA, 0.3% Triton-X100 in PBS, left with primary antibodies overnight, washed then and incubated for one hour with secondary antibodies, washed, washed, then mounted using ProLong Gold antifade reagent with DAPI (Invitrogen, CA).

Primary Antibodies used in this study: rabbit or goat anti-gastric intrinsic factor (gift of Dr. David Alpers, Washington University), goat anti-BrdU (gift of Dr. Jeff Gordon, Washington University), rabbit anti-Sox9 (Millipore), goat anti-clusterin (Santa Cruz), mouse anti-CD44v (CosmoBio), rabbit anti-pS6 (Cell Signaling), goat anti-cathepsin D (Santa Cruz), and 1 g/ml fluorescently labeled GSII lectin (Alexafluor488, 594, Molecular Probes). Secondary Antibodies

included AlexaFluor (488, 594 or 647) conjugated donkey anti-goat, anti-mouse, or anti-rabbit (Molecular Probes).

Tissue preparation and imaging for electron microscopy was done as previously described (Ramsey et al., 2007).

Immunofluorescence quantification

Proliferation counts were quantified from at least three mice for each condition. Stomachs were fluorescently stained with DAPI and anti-BrdU along with the neck cell marker GSII lectin and ZC marker anti-GIF. Images were captured as TIFF files from a Zeiss Axiovert 200 microscope with AxioCam MRM camera and with Apotome optical sectioning filter. Each stomach had at least 5 images taken and only well-oriented gastric units were counted. BrdU⁺ cell types were identified as ZC (red, GIF⁺/GSII⁻), transitional/SPEM cells (yellow, GIF⁺/GSII⁺), neck cells (green, GIF⁻/GSII⁺), or non-secretory cells (blue, GIF⁻/GSII⁻). Total counts were averaged over total unit numbers per mouse.

Chapter 8: Conclusions and Future Directions

8.1 Overall summary

Surprisingly little is known about the cellular populations of the stomach compared to other well-studied organisms. Since the stomach field lacks genetic drivers to mark most cell types in the adult stomach, much of our knowledge of the lifespans and interactions of gastric cells comes from simple pulse-chase experiments using ^3H -thymidine or by analyzing fixed tissues with immunostaining or in electron microscopy. This evidence has led the field to believe that all cells in the stomach arise from the isthmal stem cells, with neck cells transitioning to chief cells after around two weeks of migrating to the unit base, yet no direct proof of this has been shown.

Gastric cancer is the third most deadly form of cancer worldwide (Ferlay et al., 2015), yet little is known about the earliest steps of tumor progression. Pelayo Correa, a trailblazer in modeling gastric carcinogenesis, described a pathway to gastric cancer beginning with irritants causing superficial gastritis followed by atrophic gastritis, or chronic loss of parietal cells and mature chief cells, which then leads to intestinal metaplasia and eventually dysplasia and carcinoma (Correa, 1988). Thus, atrophic gastritis is an important step that should be well understood for the prevention and early treatment of gastric tumorigenesis. In the decades following Pelayo's work, the pathological condition of atrophic gastritis has been histologically described as Spasmolytic Polypeptide-Expressing Metaplasia (Schmidt et al., 1999), and it has become understood that the loss of mature chief cells is likely a result of their dedifferentiation into the metaplastic cells themselves (Nam et al., 2010). Furthermore, atrophic gastritis/SPEM has been shown to increase risk of cancer in patients (Kakinoki et al., 2009). Yet with these advances in

our understanding of the significance of SPEM, little is known about how it is initiated. Many papers have postulated that the loss of parietal cells causes the metaplastic changes to occur, as parietal cells are lost before all physiological forms of SPEM, but this has never been specifically tested. In the present work, we undertook multiple strategies to investigate what causes chief cells to dedifferentiate following injury, determine lifespan and fate dynamics for neck cells and chief cells at homeostasis and following injury, and test mechanisms involved in the re-entry of chief and neck cells to the cell cycle following injury.

In Chapter 2, we set out to identify signals from dying parietal cells which initiate the metaplastic response by developing a new model for selectively ablating parietal cells through apoptosis using an inducible diphtheria toxin receptor. As parietal cell death has long been linked to the chief cell changes, we expected this model to cause the normal SPEM response, similar to our high dose tamoxifen model, but in a more defined system allowing for easier analysis of damage signals. Instead, we found that targeted apoptosis of parietal cells caused increased proliferation through the neck of the gastric unit, but no proliferation or metaplasia in the chief cells (Burclaff et al., 2017). We further show that metaplasia can still be initiated when parietal cells are killed via DT and then the mice are co-injected with TAM or DMP-777. This work presents interesting hints about the dynamics of the gastric epithelial populations, as chief cells and parietal cells no longer appear as interconnected in their fates as previously believed. It also suggests that neck cells and chief cells may be more independent than previously understood, as necks can be called to proliferate following injury despite the absence of a chief cell response. During my time in lab, papers were published questioning the veracity and specificity of the *Mist1* promoter to track chief cell fate (Hayakawa et al., 2015; Kinoshita et al., 2018b). As *Mist1* lineage tracing accounts for the bulk of the published data proving that chief cells give rise to

SPEM cells (Nam et al., 2010), we developed a novel BrdU pulse-chase strategy to track the fate of long-lived cells in the stomach, as discussed in Chapter 3. Normal continuous pulsing with BrdU marks >10% of chief cells even after 8 weeks, so we pulsed BrdU throughout three days of TAM injections, allowing us to mark nearly all epithelial cells once the stomachs recovered from the TAM injury. BrdU is quickly diluted from proliferative populations, allowing us to track long-lived label-retaining cells over months of chasing. The results were surprising, with two thirds of chief cells retaining label even at 9 months chase, showing that they do not die and get replaced from neck cells in their published life-span of half a year. This indicates that the chief cell population is either extremely long-lived or that it maintains itself through rare duplication events. We tested whether all necks give rise to chief cells, as Karam also indicated (Karam and Leblond, 1993c), by pulsing BrdU into the necks for two weeks without injury, then chasing to see whether the label-retaining neck cells transitioned into chief cells. By 4 and 8 weeks of chase, neck cell labeling drastically decreased while chief cell staining stayed largely consistent, indicating that the majority of neck cells must have some ultimate fate other than becoming a chief cell and strengthening the idea that the chief cells are a self-maintaining population. We next tracked label-retaining chief cells upon injury with TAM or *Helicobacter pylori*, and the label-retention in chronic and acute metaplastic cells indicate that SPEM arises from chief cells in both insults. Finally, we tracked label retaining SPEM through recovery and found that these cells can redifferentiate into chief cells, supporting the Cyclical Hit Model, which posits that tumors can arise from long-lived non-stem cells which can cycle between dedifferentiating and redifferentiating in rounds of injury, accumulating and storing mutations along the way until one traps it in a proliferative, neoplastic state.

We further tested the independence of gastric chief cells by testing whether they can develop in the absence of mature parietal cells. Many papers have shown that chief cells do not develop correctly when parietal cells are ablated via *Atp4b-Cre*-driven viruses or toxins, yet these systems add high amounts of the expressed toxic substance to the gastric unit, and most wait until adulthood to test whether the chief cells are present. Our HKiDTR mice allowed us to test whether chief cells depend on parietal cells in much quicker and less toxic experiments. We injected with TAM for three days then DT for two weeks and showed that the metaplastic bases could redifferentiate into chief cells even with parietal cells continuously ablated. To test whether chief cells could develop in pups with no parietal cells present, we injected HKiDTR mice with DT from P5-P21, yet we again found that chief cells could develop normally with no parietal cells present. Further work will need to be done to ascertain why our model behaves differently than previous models. Possible explanations include that a lower level of toxin is introduced, that pre-parietal cells present already at P5 may be sufficient to provide necessary signals, or that ablating parietal cells for more than a couple weeks allows for outside pathogens to infect the stomach, causing a secondary metaplastic effect. Regardless, our experiments indicate for the first time that chief cells do not rely on parietal cells to develop or to maintain their maturation state.

Overall, the work in this dissertation has questioned multiple long-held notions in gastric epithelial cell dynamics. The new HKiDTR mice allow us to show that parietal cell loss is not sufficient to cause chief cell dedifferentiation, and that parietal cells are not even necessary for chief cells to recover from injury or develop in young pups. Our novel strategy for pulse-chasing BrdU throughout TAM injury also indicates that the relationship between neck cells and chief cells needs to be examined further, neck cells do not appear to become chief cells. The BrdU

evidence supports a model wherein chief cells in the adult stomach are a wholly self-maintaining population, both at homeostasis and following acute or chronic injury. These experiments may lay the groundwork for an entirely new understanding of the stomach, with the cell fates less interconnected than previously believed, and the possibility that not every cell type is actually replenished from a multipotent isthmal stem cell.

8.2 Future directions

1. Do cellular dedifferentiation, inflammation, and metaplasia increase cancer risk?

As discussed in Chapter 5, the carcinogen N- methyl-N-nitrosourea (MNU) can be used to drive tumorigenesis within the mouse stomach (Yamamoto et al., 2002). Tumor formation appears to be increased with rounds of metaplasia and inflammation caused by HD-TAM in pilot experiments, yet more work needs to be done to show this with statistical significance. The model has already been expanded to help with other projects in the lab. We have a paper under review investigating *Ddit4*, a gene we found to be necessary for cells to properly respond to tamoxifen-induced damage. A key figure in this paper is subjecting *Ddit4* knockout mice to the MNU system, and we found that the knockout mice formed more and larger tumors than wild type mice (Miao, et al. Under review). We have multiple other projects being run looking at further genes involved in the stomach's response to injury, and MNU-tumorigenesis experiments will help advance the significance of these as well.

We believe that the dedifferentiation of long-lived chief cells elicited by HD-TAM allows for increased accumulation and retention of tumor-causing mutations, as illustrated in the Cyclical Hit Model in Chapter 1 (Burclaff and Mills, 2018b; Burclaff and Mills, 2018a). We now have the tools to test this theory in our lab. HD-TAM causes increased proliferation from the gastric stem/progenitor cells, neck cells, and chief cells, while injections of diphtheria toxin (DT) to

HKiDTR mice increases proliferation in the isthmus and through the neck, but no metaplastic or proliferative effects are seen in the long-lived chief cells (Burclaff et al., 2017). Using these models side-by-side within an MNU timecourse will allow us to track whether cycles of chief cell dedifferentiation and redifferentiation increases tumorigenesis over rounds of injury and increased stem/progenitor cell proliferation alone.

We prepared for testing this theory by engineering a mouse line with the human diphtheria toxin receptor (DTR) gene driven directly by the ATP4b (HK) promotor (HKDTR) instead of relying on a promotor-cre allele and an inducible LSL-DTR allele (HKiDTR). We made this transgenic mouse in the FVB/N mouse background, since previous literature indicates that mouse strain has a large effect on sensitivity to MNU, and FVB mice were shown to have high tumor formation with a low mortality rate over the MNU timecourse (Yamamoto et al., 2002).

We prepared DNA for transgenic induction by synthesizing each gene portion separately (Genescript) then ligating them together within a pGIT3G plasmid (gift of Dr Blair Madison, Washington University). The construct included two copies of the cHSIV promotor in tandem followed by the nucleotides -1035 to +25 of the mouse *Atp4b* gene, the portion often used to drive parietal cell-specific gene expression (Zhao et al., 2010). A Kozak sequence (gcc)GCCACCATGG immediately followed the promotor, then the DTR gene itself followed (genbank #M93012 bp 56-682 (626 bp) from mRNA). To finish the construct, we added a gG-IVS2 intron and the SV40 late PolA sequence. The full construct is modeled in Figure 8.1

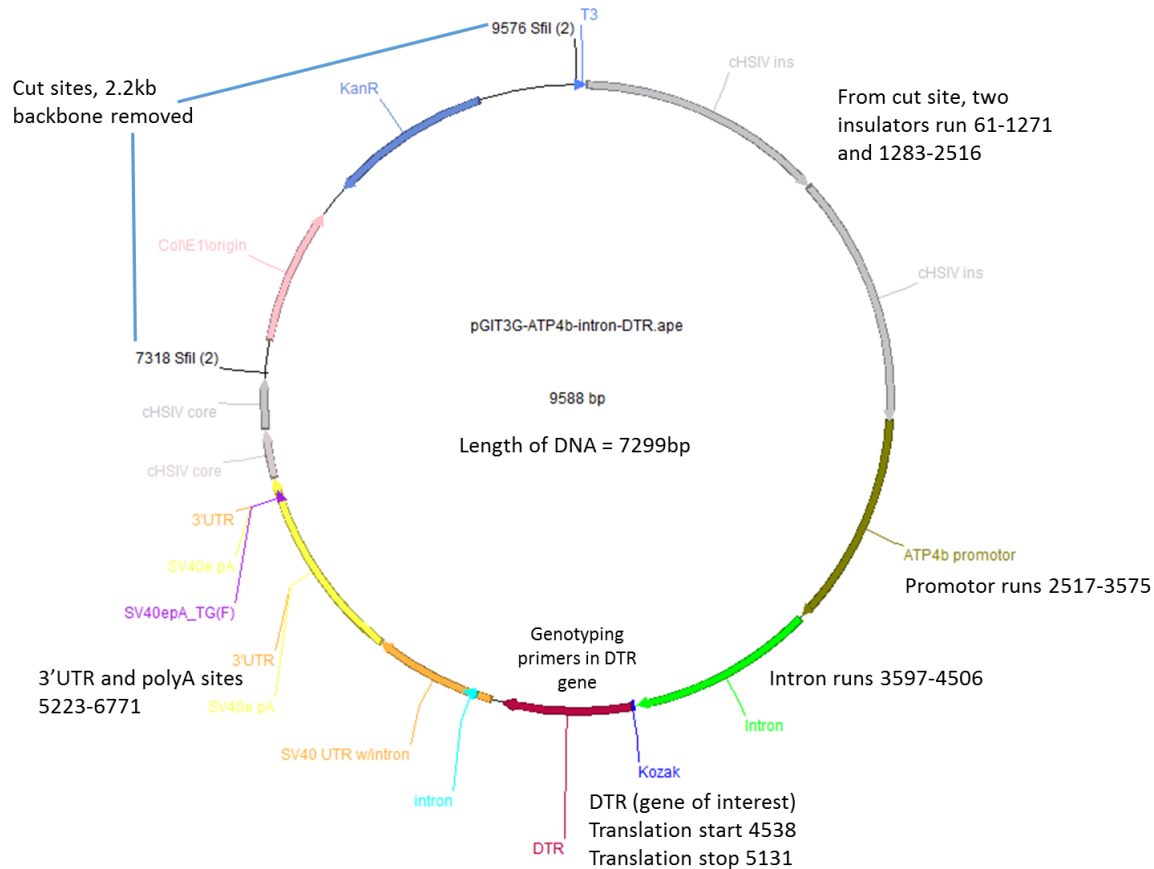


Figure 8.1: Transgenic construct for HKDTR mouse engineering.

A pGIT3G-ATP4b-intron-DTR plasmid was constructed by combining individual gene segments for insulators, the *Atp4b* promotor, the human diphtheria toxin receptor, an intron, and an SV40 polyA site.

We digested the full construct with SfiI, removing the 2.2kb backbone from the 7.3kb vector, separated the DNA bands with a long electrophoresis run, then extracted using a GeneJET Gel Extraction Kit (Thermo Fisher). Purified DNA was sent to the Washington University Mouse Genetics Core to be injected into the pronuclei of fertilized FVB/N oocytes. We received 16 founders from the core, as genotyped using DTR primers (DTR For: CTGGACCTTTTGAGAGTCACTTTATCCTCC, DTR Rev:

CTCTCCTATGGTACCTAAACATGAGAAGCC). Founders were paired with wild type FVB/N mice (Jackson Laboratories) to breed.

We next tested whether P1 progeny from each founder line developed a healthy stomach and properly caused PC ablation upon DT injection. Lines found to cause irregular development of the stomach were discontinued (Figure 8.2A), leaving only founder lines which developed and responded to DT properly (Figure 8.2B-D)

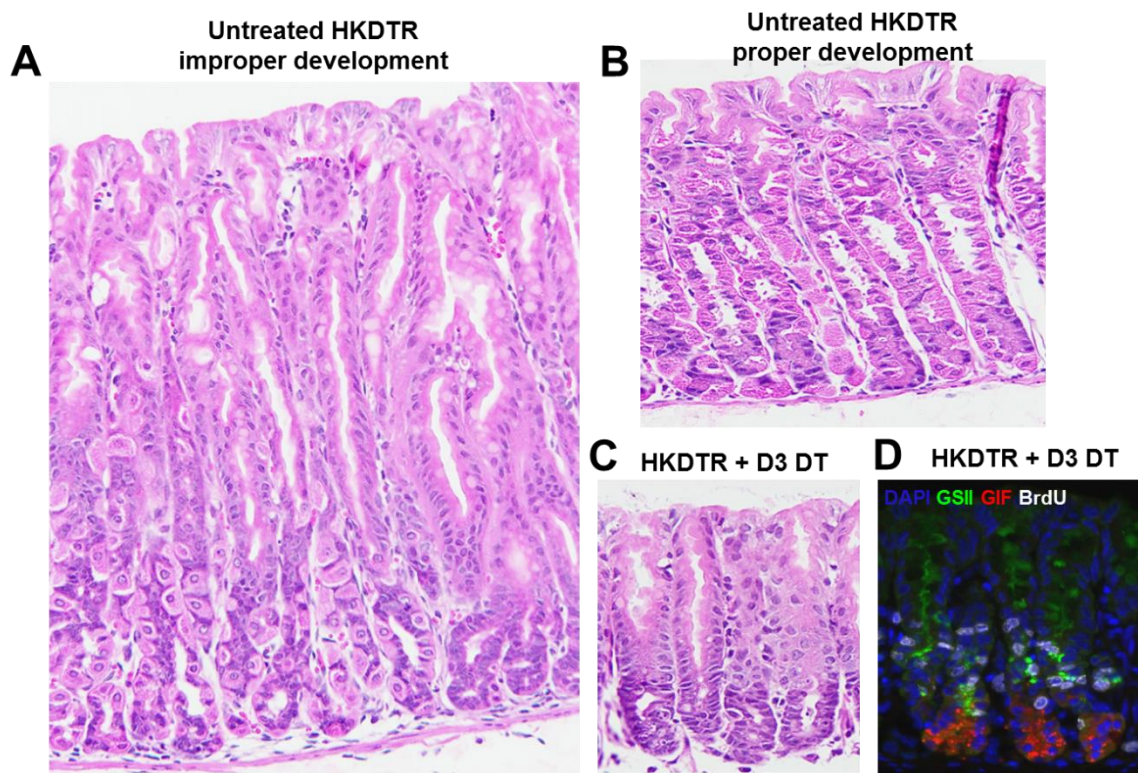


Figure 8.2: Checking for proper HKDTR mouse development.

A) Some HKDTR founder lines failed to develop correctly, forming few and small parietal cells and some corpus units appearing more antral-like. **B)** HKDTR lines with proper corpus gastric unit development were selected for. **C)** HKDTR lines show good parietal cell loss upon DT injection. **D)** HKDTR mice with D3 DT show proliferation through the neck but not in the base, consistent with previously reported HKiDTR phenotypes.

Future work will breed large numbers of mice expressing the HKDTR allele and run MNU carcinogenesis trials similar to those detailed in Chapter 5. All trials will use the 10 week protocol for administering 240ppm MNU in drinking water every other week. Trials will test the effect of rounds of DT, TAM, or VEH (2 days injected every three weeks) either during or following the 10 weeks of MNU. PET/CT scanning and stomach histology will be used to test time to tumorigenesis emphasizing tumor number, size, and position. We hypothesize that MNU+TAM mice should develop more gastric corpus tumors quicker than MNU+DT, with both developing significantly more than MNU+VEH treated mice.

2. Do dying parietal cell secrete metaplasia-inducing signals?

While HKiDTR mice efficiently kill parietal cells upon DT injection without initiating SPEM, they do not prove that dying parietal cells cannot secrete signals sufficient to drive chief cell dedifferentiation. DT is known to kill its targeted cells purely through apoptosis, while agents such as TAM and DMP-777 are believed to kill some cells through necrosis or other more immunogenic methods. These differences in death mechanism may account for differences seen in the chief cell response to DT vs TAM. To test this, *Atp4b-Cre;iDTR;mTmG* mice can be used to FACS sort parietal cells away from other gastric populations, as in (Willet et al., 2018b). Parietal cell can be cultured ex vivo for multiple days, as described in (Gliddon et al., 2008). This protocol was successfully completed in previous work in our lab, but a yeast infection prevented useful data from being obtained (data not shown). When parietal cells are cultured at high concentrations, TAM, DT, DMP-777, or VEH will be added to kill the parietal cell in each drug-dependent way. Media from each well will then be collected and gavaged into the stomachs

of untreated mice. Mice gavaged with media from DT or vehicle treated parietal cells would be expected not to have any gastric effects, while those from TAM or DMP-777 may experience chief cell dedifferentiation if dying parietal cells secrete metaplasia-inducing signals.

If metaplasia is found to occur following gavage with media from DMP-777 or TAM-treated parietal cells, each media can be probed using ELISA for levels of candidate proteins such as known cytokines and interleukins. Mass spectrometry can also be used to discover new candidate proteins in an unbiased manner. Newly implicated proteins can be studied further in vivo, with simple experiments tracking their expression at homeostasis or in injury, testing their necessity for SPEM through knock-out experiments from the *Atp4b*-Cre promotor, and testing whether they are sufficient to induce SPEM through knock-in experiments, possibly using the *Mist1*-CreERT2 promotor to inducibly express them directly to the base of the gastric unit.

Closing Remarks

The experiments proposed above will complement the other work completed in this dissertation to significantly advance our knowledge of plasticity and gastric cell dynamics. As shown in Chapter 3, it is becoming increasingly clear that mature cells can undergo multiple rounds of dedifferentiation and redifferentiation, a trait that will likely be conserved in other tissues such as the pancreas as well. This experimental data shows that the rounds of plasticity needed for the Cyclical Hit Model of Tumorigenesis (Mills and Sansom, 2015; Burclaff and Mills, 2018b; Burclaff and Mills, 2018a; Saenz and Mills, 2018a) to be feasible can occur in vivo. I test that the rounds of plasticity can occur in vivo in Chapter 3, so undertaking the MNU + TAM or DT timelines proposed here will finally directly test whether the chief cell plasticity increases tumor

formation over increased proliferation alone. This will be important information for the stomach as well as every other organ with long-lived cells shown to have the ability to re-enter the cell cycle.

The second experiment proposed above will show whether chief cells are completely independent of parietal cells. Chapters 2 and 4 show that the presence of parietal cells is not necessary for chief cells to maintain their mature state, re-differentiate following injury, or develop in young pups. A recent publication even shows that SPEM can occur before parietal cells are lost (Busada et al., 2019). The future work outlined above will allow us to demonstrate whether signals from parietal cells dying through necrosis or other non-apoptotic forms of death are sufficient for triggering chief cell dedifferentiation and the full regenerative SPEM response. This will inform the field whether our long-held belief that the fates of chief cells and parietal cells are closely intertwined is valid or if both populations maintain themselves independently of the other and just happen to respond to similar injury stimuli on similar timescales.

Appendix 1: Modeling murine gastric metaplasia through tamoxifen-induced acute parietal cell loss

The following chapter was published in *Gastrointestinal Physiology and Diseases*

Saenz, Jose B., Joseph Burclaff, and Jason C. Mills. "Modeling murine gastric metaplasia through tamoxifen-induced acute parietal cell loss." In *Gastrointestinal Physiology and Diseases*, pp. 329-339. Humana Press, New York, NY, 2016.

A1.1 Summary

Parietal cell loss represents the initial step in the sequential progression toward gastric adenocarcinoma. In the setting of chronic inflammation, the expansion of the mucosal response to parietal cell loss characterizes a crucial transition en route to gastric dysplasia. Here, we detail methods for using the selective estrogen receptor modulator tamoxifen as a novel tool to rapidly and reversibly induce parietal cell loss in mice in order to study the mechanisms that underlie these pre-neoplastic events.

A1.2 Introduction

Gastric adenocarcinoma remains one of the leading causes of cancer-related deaths worldwide (1). The sequence of events leading to the development of gastric dysplasia and neoplasia begins with the loss of acid-secreting parietal cells, a process known as oxyntic atrophy, followed by the expansion of pre-neoplastic changes in the setting of chronic inflammation (2). The early mucosal response to oxyntic atrophy includes reorganization of the gastric unit, characterized initially by an increased proliferation of gastric progenitor cells and the reprogramming of post-mitotic chief cells at the base of the gastric gland into a proliferating population of metaplastic cells (3). Overall, the pattern of gastric unit reorganization that characterizes the response to oxyntic atrophy is known as spasmolytic polypeptide-expressing metaplasia (SPEM), as the metaplastic chief cells express spasmolytic polypeptide (also known as trefoil factor family 2; TFF2). SPEM can either be a transient alteration in the gastric landscape, followed by repair and restoration of normal architecture, or it can represent a crucial pre-neoplastic event en route to gastric dysplasia in the setting of chronic inflammation. The study of the mechanisms underlying the development and evolution of SPEM has been accelerated by recently developed tools (4-6) that rapidly induce SPEM in animal models of

gastric dysplasia. Here, we describe the discovery and use of the selective estrogen receptor modulator, tamoxifen, as a model for studying SPEM.

In addition to its widespread therapeutic use as hormonal therapy, tamoxifen has recently found a role in conditional gene targeting in the mouse (7). Notably, the development of a ligand-dependent Cre-ER recombinase, in which the Cre enzyme is fused to a mutated hormone-binding domain of the estrogen receptor, has allowed for the use of tamoxifen to modulate gene expression in a spatiotemporal fashion (8). As a result, tamoxifen now serves as a tool for regulating tissue-specific Cre activity.

However, the use of tamoxifen for induction of the Cre-ER recombinase led to a serendipitous discovery in the mouse stomach that has broadened its role beyond the Cre-ER system and implicated tamoxifen as a unique agent for studying the early events following oxyntic atrophy (9, 10). Serial intra-peritoneal injections of various strains of wild-type mice with tamoxifen induced apoptosis in the vast majority of parietal cells, metaplastic changes in the chief cells at the bases of the gastric glands, and an increased proliferation of gastric progenitor cells, changes characteristic of and consistent with SPEM. This effect is reproducible (11), estrogen-independent, and reversible, with a normalization of gastric histology within weeks of tamoxifen discontinuation (10). The tamoxifen administration protocol described below therefore offers a unique method for reproducing oxyntic atrophy and dissecting early pre-neoplastic events leading to gastric dysplasia.

A1.3 Materials

Preparation of tamoxifen stock

1. Tamoxifen (see Note 1).

2. Sterile sunflower seed oil (see Note 2).
3. Ethanol (200 proof).
4. Sonic dismembrator with microtip (2 mm).
5. Eppendorf tubes (1.5 mL).
6. Benchtop vortex machine.
7. Pipettor.
8. Protective headphones.

Mouse injection

1. Insulin syringe with needle (0.5 mL, 27 gauge x 0.5 inch).
2. Balance.
3. Alcohol wipes.

A1.4 Methods

Carry out all procedures at room temperature unless otherwise specified.

The following protocol corresponds to a tamoxifen solution dissolved in 10% ethanol and 90% sunflower seed oil (see Note 3).

Preparation of tamoxifen stock

1. Weigh mice (see Note 4).

2. Weigh out 25 mg of dry tamoxifen and place it in a 1.5 mL Eppendorf tube (see Note 5).
3. Slowly add 100 μ L of 100% ethanol, trying to keep the tamoxifen at the bottom of the tube. Do not shake, mix, or pipet.
4. Measure 900 μ L of sterile sunflower seed oil in a separate 1.5 mL Eppendorf tube.
5. Sonicate the tamoxifen/ethanol mixture in the Eppendorf tube at 40% amplitude in 20-second pulses until the tamoxifen is completely dissolved (see Note 6).
6. Immediately combine the tamoxifen/ethanol mixture with the sunflower seed oil. Cap and vortex the solution to ensure adequate mixing (see Note 7).
7. The tamoxifen mixture can be stored at 4°C for up to three days or at -20°C indefinitely (see Note 8). Allow the mixture to warm to room temperature prior to injection.

Tamoxifen treatment

1. Using the insulin syringe needle, measure out the appropriate amount of the tamoxifen mixture so as to inject 5 mg tamoxifen for every 20 g mouse body weight (see Note 9).
2. Sanitize the injection site by wiping the mouse abdomen with an alcohol wipe. Intra-peritoneally inject the vehicle (10% ethanol/90% sunflower seed oil) or tamoxifen mixture (see Note 10).
3. Repeat the injection for three consecutive days using the same tamoxifen stock, stored at 4°C.

4. Mouse stomachs can be harvested at any time following the first injection or thereafter, and tissue can be processed accordingly (see Note 11, Figures A1.1 and A1.2).

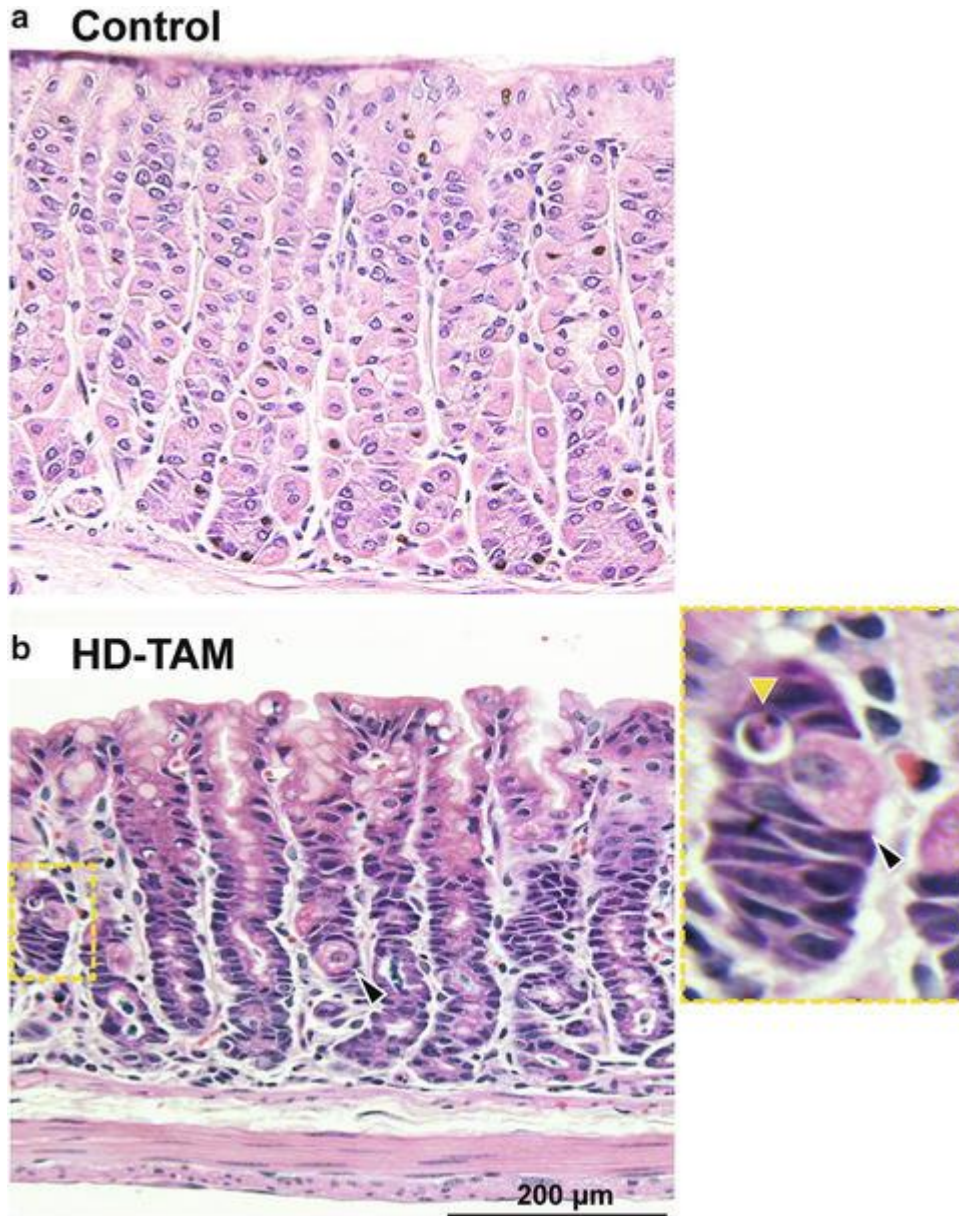
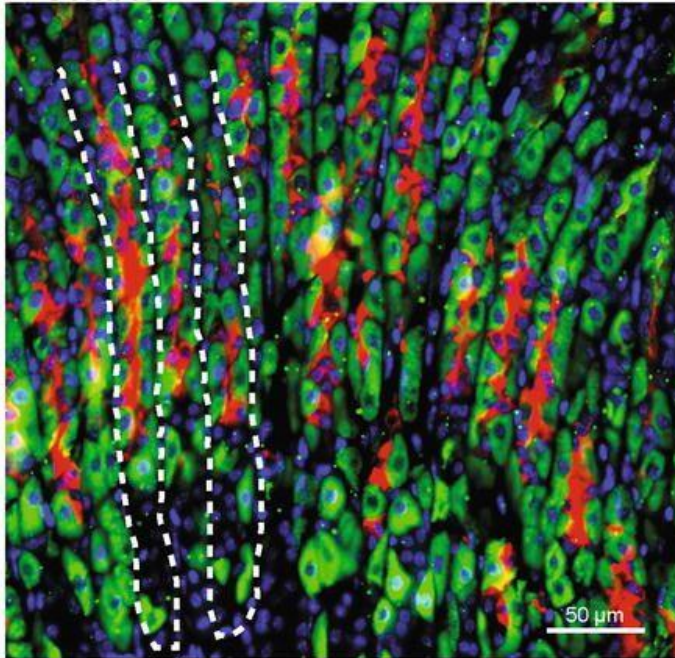


Figure A1.1: Tamoxifen treatment results in acute parietal cell loss.

Representative hematoxylin and eosin stain of gastric corpus from wild-type C57BL/6 mice after intra-peritoneal injection with 3 days of either vehicle (a; Control) or 5 mg/20 g body weight tamoxifen (b; HD-TAM). Note the relative decrease in parietal cells (*black arrowhead*) compared to the vehicle-treated mouse. An apoptotic body (*yellow arrowhead*) adjacent to a dying parietal cell is highlighted (*inset*)

a Control



b HD-TAM

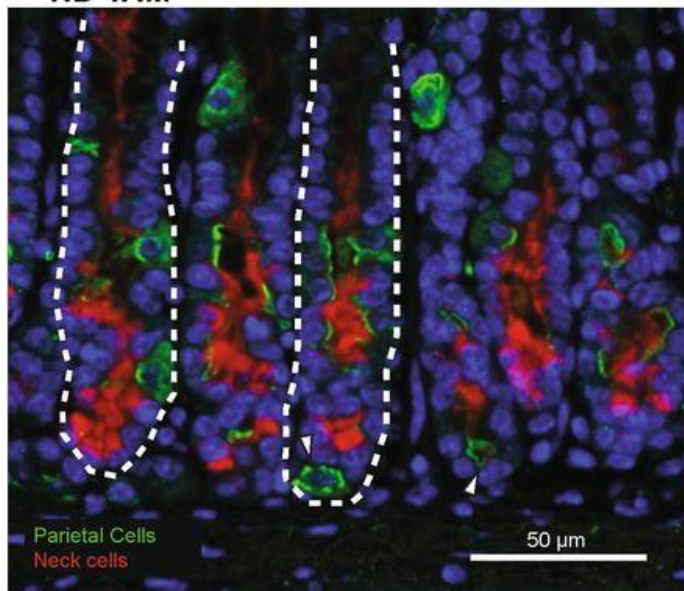


Figure A1.2 Tamoxifen treatment causes acute parietal cell loss and alters the GSII expression pattern in gastric units.

(a) Representative immunostain of the gastric corpus of a mouse intra-peritoneally injected with vehicle alone (Control) for 3 days demonstrates normal-appearing gastric units, highlighted by abundant parietal cells (stained with H^+/K^+ ATPase; *green*) and neck cells

(stained with GSII; *red*). Nuclei are stained with Hoescht (*blue*), and representative gastric units are highlighted by *dashed lines*. (b) A representative immunostain of the gastric corpus from a mouse intra-peritoneally injected with 5 mg/20 g body weight tamoxifen for 3 days (HD-TAM) shows an acute loss of parietal cells, as demonstrated by the relative paucity of VEGFb-staining cells (*green*). Fragments of parietal cells are highlighted by the *white arrowheads*. In addition, note the shift in GSII expression (*red*) toward the bases of glands in tamoxifen-treated mice compared to the vehicle-treated controls. Nuclei are stained with Hoescht (*blue*), and representative gastric units are highlighted by *dashed lines*

A1.5 Notes

1. The source of tamoxifen has no appreciable effect on the ability to induce parietal cell loss. Tamoxifen stocks from three separate commercial suppliers, Sigma (St. Louis, MO), Cayman Chemical Company (Ann Arbor, MI), and Toronto Research Company (Toronto, Canada), have demonstrated similar efficacy (10). In addition, parietal cell toxicity is specific to tamoxifen and not a general toxic effect of selective estrogen receptor modulators, as treatment with raloxifene, a member of the estrogen receptor modulator family with pro- and anti-estrogenic effects, had no appreciable toxicity at a comparable dose (10).
2. To sterilize the sunflower seed oil, heat an appropriate amount in an Erlenmeyer flask on a hot plate to 85-90°C for 15-20 minutes. Do not boil. Allow the flask to cool and store 40-mL aliquots at room temperature. Alternatively, the sunflower seed oil can be autoclaved prior to use.
3. The free base form of tamoxifen and one of its commonly used active metabolites, 4-hydroxytamoxifen (see Note 12), are largely insoluble in water. The original formulation for intra-peritoneal injection was found to be soluble in 60% ethanol (12), and its solubility has since been optimized in a sunflower seed oil/ethanol mixture (see Note 13). Tamoxifen citrate, an oral formulation that has been developed for administering tamoxifen to mice via chow (13; see Note

10), is soluble in water at 0.3 mg/L at 20°C. Tamoxifen free base powder should be stored at -20°C in the dark.

4. Our experience has shown that three different wild-type mouse strains (C57BL/6, BALB/c, and FVB/N; all purchased from the Jackson Laboratory) have similar gastric mucosal responses to tamoxifen treatment (10). In our limited experience with the strain, BALB/c mice are particularly sensitive to tamoxifen treatment, with mice commonly dying of unknown causes during treatment. Mice are typically used at 6-8 weeks of age, but SPEM is effectively induced in mice as old as 6 months of age. The effects on older mice are less obvious, potentially due to increased body fat causing changes in tamoxifen metabolism and distribution.

5. An injection dose of 5 mg/20 g mouse weight over 3 days results in a dramatic phenotype, with >90% loss of parietal cells, a significant increase in gastric progenitor cells, and morphologic changes in the chief cells at the bases of glands in the gastric corpus, histologic changes consistent with the induction of SPEM (10, Figures A1.1B and A1.2B). However, we have previously shown that tamoxifen injections at lower doses (≤ 1 mg/20 g body weight) can be used for efficient, inducible Cre-mediated recombination in the context of the Cre-ERT/loxP system, without the development of SPEM (9). It is thus possible to obtain specific recombination of floxed alleles in tamoxifen-inducible Cre lines in a dose-dependent manner while avoiding the stomach-altering effects seen at higher tamoxifen doses. Interestingly, though this has not been formally tested, SPEM induction by tamoxifen seems to have an all-or-none response, where no detectable damage can be seen at ≤ 1 mg/20 g mouse body weight, but ≥ 3 mg/20 g mouse body weight causes near complete SPEM, without an intermediate phenotype.

6. Make sure to wear protective headphones when using the sonicator.

7. Vortex the solution for at least 20 seconds. Allow the solution to sit at room temperature for several minutes. Proper mixing is crucial, and the mixture should be homogeneous. If it looks cloudy or layered, discard the mixture and start over.
8. No appreciable decline in the ability of tamoxifen to induce SPEM has been seen for tamoxifen mixtures stored at 4°C over the duration of injections. Similarly, the tamoxifen stock can be stored at -20° until further use. Our lab, however, makes a fresh tamoxifen stock prior to each treatment regimen and uses this stock for the duration of the treatment.
9. Given the viscosity of the tamoxifen mixture, aspiration into the syringe can take 10-15 seconds.
10. Various tamoxifen formulations and numerous modes of tamoxifen administration have been reported. We focus here on intra-peritoneal administration, which we use most commonly, though we also observe SPEM induction with oral gavage. It is worth noting that other methods, in addition to oral gavage (14), for inducing Cre recombinase activity via tamoxifen have been used, including via drinking water (15), chow (13, 16), and subcutaneous implantation (17). In that respect, we can only attest that oral gavage and intra-peritoneal administration of tamoxifen cause SPEM and have not tested the effects of other modes of tamoxifen administration.
11. The effects of tamoxifen on the mouse stomach can be seen within 12-24 hours of the first intra-peritoneal injection (10). Our laboratory nomenclature designates the first day of tamoxifen injection as day 0 (D0), with the last day of injection corresponding to day 2 (D2). A recent report found that a single intra-peritoneal injection at 4 mg/25 g mouse body weight induced a 57% loss of parietal cells in the gastric corpus (11). In our experience, the peak effect (i.e., maximal parietal cell loss, see Figures A1.1B and A1.2B) is seen at one day following the

third tamoxifen injection (D3). We have also achieved $\geq 90\%$ loss of parietal cells at D3 even after a single injection of tamoxifen at 5 mg/20 g mouse body weight. The single-injection protocol, however, shows more variability between mice than the 3-day injection protocol. A recovery of the gastric epithelium and a return to normal histology are seen within 14-21 days (10). Like previously described pharmacologic induction of SPEM (see Note 14), the effects of tamoxifen on the mouse stomach are transient. Many studies using tamoxifen-inducible Cre lines wait at least 2 weeks prior to assessing recombination, by which point parietal cells have largely recovered. This may explain how tamoxifen-induced parietal cell loss is often missed by investigators using tamoxifen to induce gene recombination in the stomach.

12. Tamoxifen is a prodrug that is hepatically metabolized to produce two predominant active metabolites, 4-hydroxytamoxifen and N-desmethyl-4-hydroxytamoxifen (18). Multiple studies have used 4-hydroxytamoxifen for induction of the Cre-ERT2 system. It is worth noting that 4-hydroxytamoxifen has shown higher affinity for the estrogen receptor than tamoxifen in vitro (19) and a greater inhibitory effect on proliferation of normal human breast cells as well as breast cancer cell lines in culture (20-22). Differential effects between tamoxifen and 4-hydroxytamoxifen have also been reported in apoptosis of human mammary epithelial cells (23) and uterine gene expression in rats (24). In our limited experience, intra-peritoneally administered 4-hydroxytamoxifen, at commonly used doses for Cre recombinase induction, induces less SPEM in mice compared to similar doses of tamoxifen.

13. It has been speculated that the observed effects of intra-peritoneal tamoxifen administration could be unrelated to the tamoxifen itself and rather an effect of the ethanol solvent on parietal cells. Though the effect of ethanol on parietal cell membranes and H^+/K^+ ATPase function has been reported (25), our experience has shown that intra-peritoneal injection

of mice with ethanol does not induce substantial parietal cell loss. On the other hand, excluding ethanol as a solvent results in poor solubility of tamoxifen. Oral gavage or intra-peritoneal injection of the resulting suspension, rather than solution, might cause suboptimal absorption and less substantial and/or consistent SPEM induction. Differences in solubilization methods may also explain why some investigators using tamoxifen for Cre recombinase induction may not have observed SPEM in their control mice.

14. Previous methods for inducing oxyntic atrophy and SPEM have been described, varying in their mechanism of action, onset of effect, and degree of inflammation (see Table 1). Chronic infection of mice with *Helicobacter felis* (26) or of Mongolian gerbils with *Helicobacter pylori* (27) results in the emergence of SPEM within months of infection. In contrast to these chronic infectious models, pharmacologic induction of SPEM has provided a more rapid and reversible means for achieving the same result. The neutrophil elastase inhibitor DMP-777 has been shown to cause a rapid loss of parietal cells in rats and mice within 3-4 days of daily dosing (4, 5). Treatment with this parietal cell-specific apical membrane protonophore leads to the emergence of SPEM within 7-10 days, in the absence of inflammation. Like tamoxifen (10), the effects on parietal cell loss can be mitigated by pretreatment with omeprazole. More recently, a related variant of DMP-777, known as L-635, was found to produce a more rapid onset of SPEM in mice within 3 days of treatment (6). The mechanism of action of L-635 is similar to that of DMP-777, though, unlike DMP-777, the onset of SPEM is accompanied by an exuberant inflammatory response.

A1.6 References

1. Ferlay, J., Soerjomataram, I., Dikshit, R., *et al.* (2015) Cancer incidence and mortality worldwide: sources, methods, and major patterns in GLOBOCAN 2012. *Int J Cancer* 136(5), E359-86.

2. Ernst, P.B., Peura, D.A., Crowe, S.E. (2006) The translation of *Helicobacter pylori* basic research to patient care. *Gastroenterology* 130(1), 188-206.
3. Goldenring, J.R., Nam, K.T., Mills, J.C. (2011) The origin of pre-neoplastic metaplasia in the stomach: chief cells emerge from the Mist. *Exp Cell Res* 317(19), 2759-64.
4. Goldenring, J.R., Ray, G.S., Coffey, R.J., *et al.* (2000) Reversible drug-induced oxyntic atrophy in rats. *Gastroenterology* 118(6), 1080-93.
5. Nomura, S., Yamaguchi, H., Ogawa, M., *et al.* (2005) Alterations in gastric mucosal lineages induced by acute oxyntic atrophy in wild-type and gastrin-deficient mice. *Am J Gastrointest Liver Physiol* 288(2), G362-75.
6. Nam, K.T., Lee, H.J., Sousa, J.F., *et al.* (2010) Mature chief cells are cryptic progenitors for metaplasia in the stomach. *Gastroenterology* 139(6), 2028-2037.
7. Saunders, T.L. (2011) Inducible transgenic mouse models. *Methods Mol Biol* 693, 103-115.
8. Hayashi, S., McMahon, A.P. (2002) Efficient recombination in diverse tissues by a tamoxifen-inducible form of Cre: a tool for temporally regulated gene activation/inactivation in the mouse. *Dev Biol* 244, 305-318.
9. Huh, W.J., Mysorekar, I.U., and Mills, J.C. (2010) Inducible activation of Cre recombinase in adult mice causes gastric epithelial atrophy, metaplasia, and regenerative changes in the absence of “floxed” alleles. *Am J Physiol Gastrointest Liver Physiol* 299(2), G368-80.
10. Huh, W.J., Khurana, S.S., Geahlen, J.H., *et al.* (2012) Tamoxifen induces rapid, reversible atrophy, and metaplasia in the mouse stomach. *Gastroenterology* 142(1), 21-24.
11. Sigal, M., Rothenberg, M.E., Logan, C.Y., *et al.* (2015) *Helicobacter pylori* activates and expands Lgr5+ stem cells through direct colonization of the gastric glands. *Gastroenterology* (in press) S0016-5085(15).
12. Sohal, D., Nghiem, M., Crackower, M.A., *et al.* (2001) Temporally regulated and tissue-specific gene manipulations in the adult and embryonic heart using a tamoxifen-inducible Cre protein. *Circ Res* 89(10), 20-25.
13. Casanova, E., Fehsenfeld, S., Lemberger, T., *et al.* (2002) ER-based double iCre fusion protein allows partial recombination in forebrain. *Genesis* 34(3), 208-14.
14. Park, E.J., Sun, X., Nichol, P., *et al.* (2008) System for tamoxifen-inducible expression of Cre-recombinase from the *Foxa2* locus in mice. *Dev Dyn* 237(2), 447-53.
15. Jones, M.E., Kondo, M., and Zhuang, Y. (2009) A tamoxifen inducible knock-in allele for investigation of E2A function. *BMC Dev Biol* 9, 51.
16. Kiermayer, C., Conrad, M., Schneider, M., *et al.* (2007) Optimization of spatiotemporal gene inactivation in mouse heart by oral application of tamoxifen citrate. *Genesis* 45(1), 11-16.
17. Sheh, A., Ge, Z., Parry, N.M., *et al.* (2011) 17 β -estradiol and tamoxifen prevent gastric cancer by modulating leukocyte recruitment and oncogenic pathways in *Helicobacter pylori*-infected INS-GAS male mice. *Cancer Prev Res (Phila)* 4(9), 1426-35.
18. Poon, G.K., Walter, B., Lonning, P.E., *et al.* (1995) Identification of tamoxifen metabolites in human HepG2 cell line, human liver homogenate, and patients on long-term therapy for breast cancer. *Drug Metab Dispos* 23(3), 377-82.
19. Robertson, D.W., Katzenellenbogen, J.A., Hayes, J.R., and Katzenellenbogen, B.S. (1982) Antiestrogen basicity – activity relationships: a comparison of the estrogen

- receptor binding and antiuterotrophic potencies of several analogues of (Z)-1,2-diphenyl-1-[4-[2-(dimethylamino)ethoxy]phenyl]-1-butene (tamoxifen, Nolvadex) having altered basicity. *J Med Chem* 25(2), 167-71.
20. Malet, C., Gompel, A., Spritzer, P., *et al.* (1988) Tamoxifen and hydroxytamoxifen isomers versus estradiol effects on normal human breast cells in culture. *Cancer Res* 48, 7193-9.
 21. Coezy, E., Borgna, J.L., and Rochefort, H. (1982) Tamoxifen and metabolites in MCF7 cells: correlation between binding to estrogen receptor and inhibition of cell growth. *Cancer Res* 42(1), 317-23.
 22. Vignon, F., Bouton, M.M., and Rochefort, H. (1987) Antiestrogens inhibit the mitogenic effect of growth factors on breast cancer cells in the total absence of estrogens. *Biochem Biophys Res Commun* 146(3), 1502-8.
 23. Dietze, E.C., Caldwell, L.E., Grupin, S.L., *et al.* (2001) Tamoxifen but not 4-hydroxytamoxifen initiates apoptosis in p53(-) normal human mammary epithelial cells by inducing mitochondrial depolarization. *J Biol Chem* 276(7), 5384-94.
 24. Reed, C.A., Berndtson, A.K., and Nephew, K.P. (2005) Dose-dependent effects of 4-hydroxytamoxifen, the active metabolite of tamoxifen, on estrogen receptor-alpha expression in the rat uterus. *Anticancer Drugs* 16(5), 559-67.
 25. Mazzeo, A.R., Nandi, J., and Levine R.A. (1988) Effects of ethanol on parietal cell membrane phospholipids and proton pump function. *Am J Physiol* 254, G57-64.
 26. Wang, T.C., Goldenring, J.R., Dangler, C., *et al.* (1998) Mice lacking secretory phospholipase A2 show altered apoptosis and differentiation with *Helicobacter felis* infection. *Gastroenterology* 114(4), 675-89.
 27. Yoshizawa, N., Takenaka, Y., Yamaguchi, H., *et al.* (2007) Emergence of spasmodic polypeptide-expressing metaplasia in Mongolian gerbils infected with *Helicobacter pylori*. *Lab Invest* 87(12), 1265-76.

**Appendix 2: Unintended targeting of Dmp1-
Cre reveals a critical role for Bmpr1a
signaling in the gastrointestinal mesenchyme
of adult mice**

The following chapter was published in Bone Research

Lim, Joohyun, Joseph Burclaff, Guangxu He, Jason C. Mills, and Fanxin Long. "Unintended targeting of Dmp1-Cre reveals a critical role for Bmpr1a signaling in the gastrointestinal mesenchyme of adult mice." Bone research 5 (2017): 16049.

A2.1 Abstract

Cre/loxP technology has been widely used to study cell type-specific functions of genes. Proper interpretation of such data critically depends on a clear understanding of the tissue specificity of Cre expression. The *Dmp1-Cre* mouse, expressing Cre from a 14-kb DNA fragment of the mouse *Dmp1* gene, has become a common tool for studying gene function in osteocytes, but the presumed cell specificity is yet to be fully established. By using the *Ai9* reporter line that expresses a red fluorescent protein upon Cre recombination, we find that in 2-month-old mice, *Dmp1-Cre* targets not only osteocytes within the bone matrix but also osteoblasts on the bone surface and preosteoblasts at the metaphyseal chondro-osseous junction. In the bone marrow, Cre activity is evident in certain stromal cells adjacent to the blood vessels, but not in adipocytes. Outside the skeleton, *Dmp1-Cre* marks not only the skeletal muscle fibers, certain cells in the cerebellum and the hindbrain but also gastric and intestinal mesenchymal cells that express *Pdgfra*. Confirming the utility of *Dmp1-Cre* in the gastrointestinal mesenchyme, deletion of *Bmpr1a* with *Dmp1-Cre* causes numerous large polyps along the gastrointestinal tract, consistent with prior work involving inhibition of BMP signaling. Thus, caution needs to be exercised when using *Dmp1-Cre* because it targets not only the osteoblast lineage at an earlier stage than previously appreciated, but also a number of non-skeletal cell types.

A2.2 Introduction

Dentin matrix protein 1 (DMP1) is an extracellular phosphorylated glycoprotein belonging to the SIBLING (small integrin-binding ligand N-linked glycoprotein) family of proteins.¹ Originally discovered in the dentin matrix, DMP1 is also highly expressed in other mineralized tissues including bone and cartilage.^{2,3,4} Functional studies have demonstrated important functions of DMP1 in regulating not only biomineralization but also phosphate homeostasis in both mice and

humans.^{5,6,7,8} Expression of DMP1 has also been detected in a variety of non-mineralizing tissues in the mouse, these including brain, liver, muscle, kidney, and pancreas, but its function there is not known.⁹

Cre/loxP technology enables gene deletion in specific cell types and thus allows for interrogation of gene function in a cell type-specific manner. Conditional deletion in specific lineages depends on the unique expression pattern of the Cre recombinase. The Dmp1-Cre transgenic mouse line was generated to express Cre from a 14-kb promoter fragment (-9 624 to +4 439) of the mouse Dmp1 gene.¹⁰ The promoter encompassed a 9 624-bp promoter, the 95-bp exon 1, the 4 326-bp intron I plus the 17-bp initial noncoding sequence of exon II. The initial characterization of the mouse line with the Rosa26R mouse (expressing β -galactosidase upon Cre recombination) identified strong Cre activity in osteocytes and odontoblasts but not osteoblasts.¹⁰ However, detection of β -galactosidase expression relied on an enzymatic reaction in vitro known to be susceptible to tissue preparation and reaction conditions. In fact, a more recent analysis of Dmp1-Cre with a reporter mouse expressing a fluorescent protein revealed Cre activity in additional cell types besides osteocytes, most notably skeletal muscle and osteoblasts.¹¹ The study also implicated cells within the bone marrow and those in the brain, but did not provide a detailed description. Thus, a systematic survey of tissues targeted by Dmp1-Cre in the mouse is warranted.

Much work has been done to decipher the contribution of BMP signaling to gastrointestinal development and maintenance, but the specific role of BMP reception by mesenchymal tissue remains unclear. In the stomach, Mx1-Cre-mediated Bmpr1a deletion resulted in polyp formation at the esophageal and antral transition zones.¹² Similarly, Bmpr1a removal by the ubiquitous inducible CAGGCreER driver cause dantral polyps and antral-pyloric hyperplasia.¹³

Conversely, overexpression of the secreted BMP antagonist Noggin in parietal cells and intestinal villi caused gastric cysts and intestinal polyps, respectively.^{14,15} However, when BMP signaling was selectively disrupted in the intestinal epithelium through deletion of *Bmpr1a*, no polyps formed despite increased proliferation and altered morphology within the epithelium.¹⁶ On the other hand, stromal deletion of *Bmpr2* with *nestin-Cre* led to colorectal epithelial overgrowth and polyp formation, but the interpretation there was complicated by the fact that *nestin-Cre* targets multiple lineages including the epithelium.¹⁷ Overall, BMP signaling within the mesenchymal compartment likely contributes to normal gastrointestinal development and maintenance, but this notion warrants further investigation.

Here we assess the cell types targeted by *Dmp1-Cre* in 2-month-old mice by monitoring the expression of a red fluorescent protein (dtTomato) from the *Ai9* reporter allele. Consistent with previous findings, *Dmp1-Cre* targets not only osteocytes but also osteoblasts and preosteoblasts, along with a subset of bone marrow stromal cells, as well as the skeletal muscle and certain brain cells. Unexpectedly, *Dmp1-Cre* selectively targets gastrointestinal mesenchymal cells with high efficiency. Deletion of *Bmpr1a* with *Dmp1-Cre* results in polyposis throughout the stomach and intestines, demonstrating a critical role of mesenchymal BMP signaling in maintaining a normal gastrointestinal tract.

A2.3 Materials and Methods

Mouse strains

Dmp1-Cre, *Ai9*, and *Bmpr1af/f* mouselines are as previously described.^{10,18,19} *Ai9* mice were purchased from the Jackson Laboratory (Bar Harbor, ME, USA); *Dmp1-Cre* and *Bmpr1af/f* mice were generously provided by Dr Jian Q Feng (Baylor College of Dentistry) and Dr Yuji Mishina (University of Michigan), respectively. Littermate mice with the genotype of *Dmp1-Cre*;

Bmpr1af/f (CKO) or Bmpr1af/f (control) were generated by breeding the two genotypes as previously produced.²⁰ The mice were in a mixed genetic background between C57BL6 and 129 strains. Both males and females were analyzed with similar results. All mouse procedures used in this study were approved by the Animal Studies Committee at Washington University.

Cryostat sections

Two-month-old mice were perfused with 4% paraformaldehyde (PFA) as described previously.²¹ After perfusion, tibias were dissected and fixed in 4% PFA at 4 °C overnight. The fixed tibias were decalcified in 14% EDTA (pH 7.4) for 3 days, incubated in 30% sucrose at 4 °C overnight and then snap-frozen in optimal cutting temperature (OCT) embedding medium. Frozen sections were cut at 8 µm thickness with a cryostat equipped with CryoJane (Leica, Buffalo Grove, IL, USA). The sections were kept at -20 °C until analyses.

Immunofluorescence staining

For detection of Pdgfra, perilipin, or endomucin, immunostaining was performed on cryostat sections using mouse polyclonal Pdgfra antibody (1:100; R&D Systems), or rabbit monoclonal perilipin antibody (1:100; Cell Signaling Technology, Danvers, MA, USA), or rat monoclonal endomucin antibody (1:100, Santa Cruz, Biotechnology, Dallas, TX, USA). The secondary antibodies are as follows: Alexa Fluor 488 goat anti-mouse IgG (for Pdgfa); Alexa Fluor 488 goat anti-rabbit IgG (for perilipin), and Alexa Fluor 488 goat anti-rat IgG (for endomucin) (all at 1:500, Life Technologies, Grand Island, NY, USA). Sections were mounted with

VECTASHIELD Mounting Medium containing DAPI (Vector Laboratories, Burlingame, CA, USA). Images were acquired with a Nikon confocal microscope (Melville, NY, USA).

Analyses of the gastrointestinal tract

For proliferation assays, mice were injected intraperitoneally with 5-bromo-2'-deoxyuridine (BrdU, 120 mg·kg⁻¹) and 5-fluoro-2'-deoxyuridine (12 mg·kg⁻¹) in sterile water 90 min before killing. Following killing, stomachs were immediately excised and flushed with phosphate-buffered saline then inflated with freshly prepared formalin (10% formaldehyde, Sigma, St. Louis, MO, USA) in phosphate-buffered saline and the pylorus clamped with a hemostat. Inflated stomachs and segments of the small and large intestines were allowed to fix overnight in 10% formalin then transferred to 70% ethanol. Tissues were arranged in 3% agar in a tissue cassette, underwent routine paraffin processing, and 5 µm sections were cut and mounted on glass slides. For immunohistochemistry, sections underwent a standard deparaffinization and rehydration protocol then were blocked with 5% horse serum for 1 h before staining for BrdU using Goat anti-BrdU (1:20 000, gift of Dr Jeff Gordon, Washington University) and biotinylated horse anti-goat (1:200, Vector Laboratories) antibodies. Images were acquired using a Nanozoomer Slide Scanner (Hamamatsu, Japan, model 2.0-HT).

A2.4 Results

Dmp1-Cre targets osteoblast-lineage cells, skeletal muscle, and bone marrow perivascular cells

To characterize the targeting specificity of Dmp1-Cre, we generated Dmp1-Cre; Ai9 mice (one copy each of Dmp1-Cre and Ai9) and analyzed tdTomato expression on sections of the limbs at 2 months of age. As expected, limb sections from the control Ai9 mice did not exhibit any red

fluorescence (Figure A2.1a-f), but those from Dmp1-Cre; Ai9 mice showed strong signals both in the long bone and in the adjacent skeletal muscle (Figure A2.1a'-f'). Targeting of the skeletal muscle was not previously reported, but was detected here in all muscle fibers (Figure A2.1f'). Within the long bone, Dmp1-Cre marked not only osteocytes but also osteoblasts in both cortical and cancellous bone (Figure A2.1b' and c'). In addition, the chondro-osseous junction immediately below the growth plate, an area enriched in preosteoblasts, expressed a strong signal even though the growth plate was negative (Figure A2.1d'). Red fluorescence was also detected in certain cells within the bone marrow, although generally at a lower intensity than those other cell types described above (Figure A2.1e'). Co-immunostaining experiments revealed that the red fluorescence-positive marrow cells were perivascular as they showed close proximity to the endothelium-expressing endomucin (Figure A2.2). On the other hand, perilipin staining showed that the bone marrow adipocytes were not targeted by Dmp1-Cre and generally did not show a close association with the targeted cells (Figure A2.3). Thus, in addition to osteocytes, Dmp1-Cre targets early-stage osteoblast-lineage cells, bone marrow perivascular cells as well as the skeletal muscle.

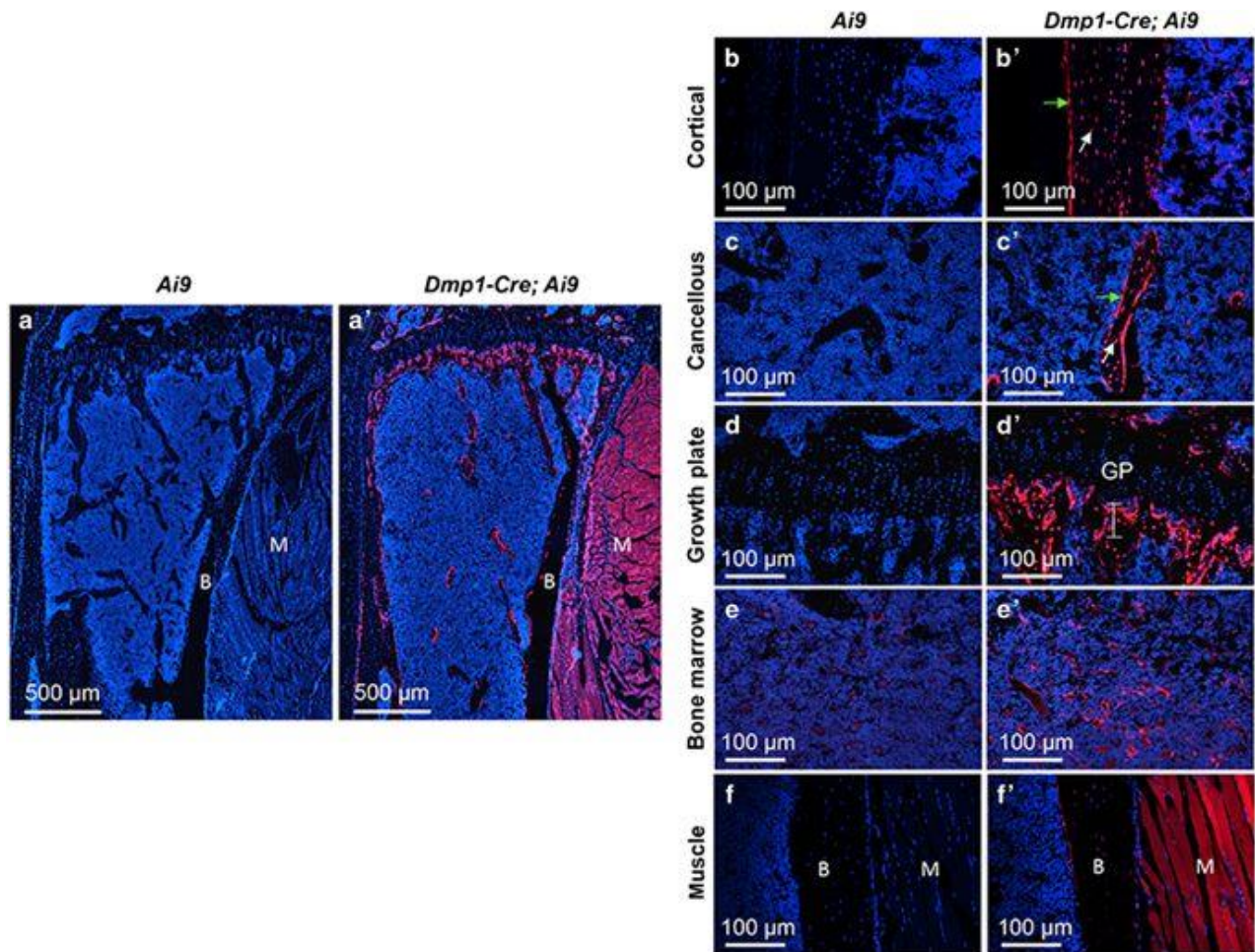


Figure A2.1: *Dmp1-Cre* targets osteoblast lineage cells, skeletal muscle, and bone marrow cells in 2-month-old mice.

(a,a') Confocal microscopy images of direct fluorescence from tdTomato on longitudinal sections of the proximal tibia. (b–f') Images at a higher magnification for different areas of bone as indicated. B, bone; M, skeletal muscle; GP, growth plate. Green arrow, osteoblast; white arrow, osteocyte. Line in (d') denotes chondro-osseous junction.

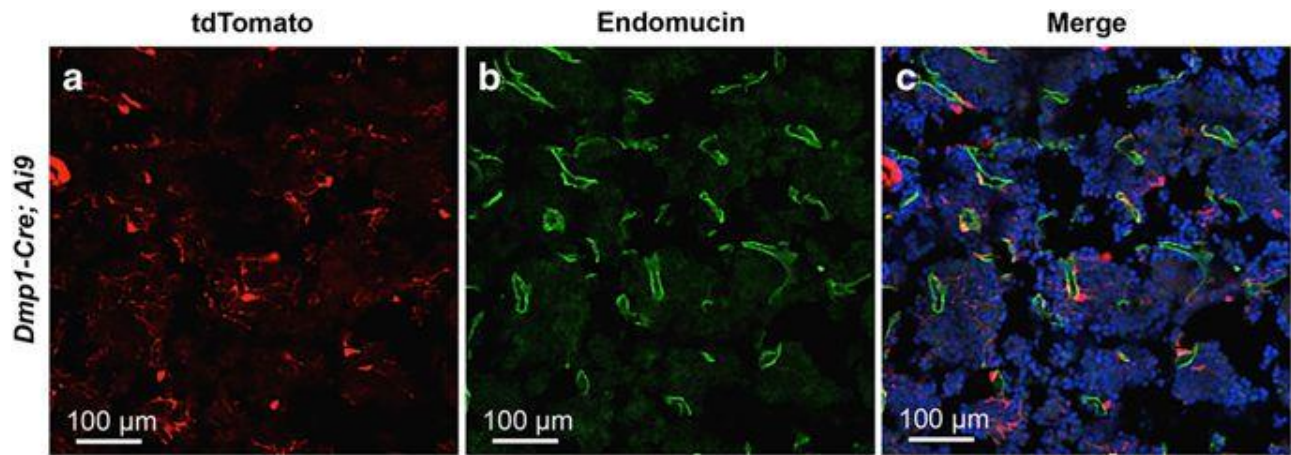


Figure A2.2: Dmp1-Cre targets bone marrow cells near blood vessels.

Immunostaining against endomucin and direct fluorescence of tdTomato on sections of the tibial bone marrow from 2-month-old Dmp1-Cre; Ai9 mice. (a) tdTomato; (b) endomucin; (c) merged image.

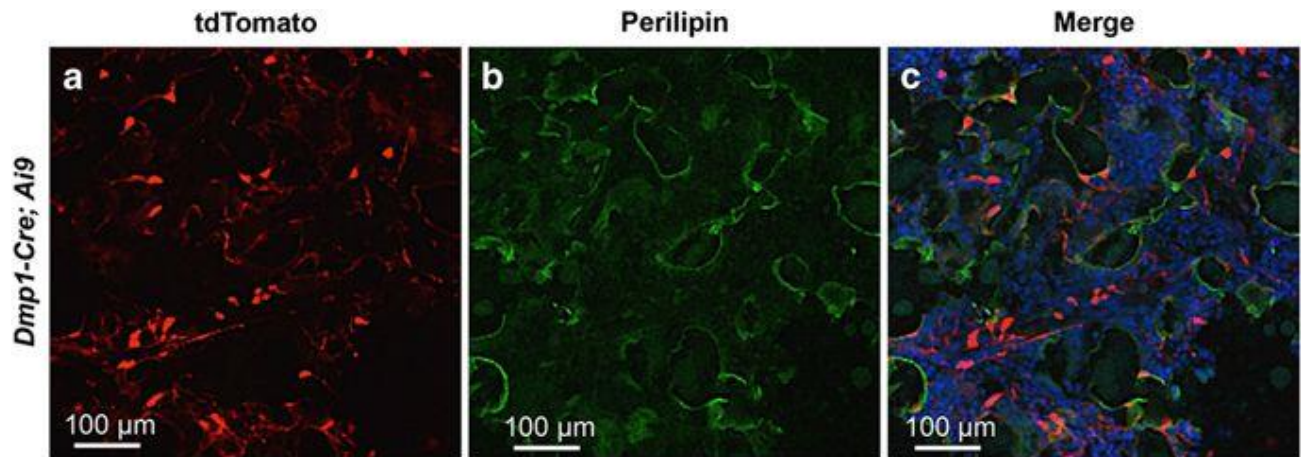


Figure A2.3: Dmp1-Cre does not target bone marrow adipocytes.

Immunostaining against perilipin and direct fluorescence of tdTomato on sections of the tibial bone marrow from 2-month-old Dmp1-Cre; Ai9 mice. (a) tdTomato; (b) perilipin; (c) merged image.

Dmp1-Cre targets brain cells as well as gastrointestinal mesenchymal cells

We next examined other tissues of the Dmp1-Cre; Ai9 mouse for potential targeting by Dmp1-Cre. No red fluorescence was detected in the liver, the spleen, or the gonadal fat depot. Coronal sections of the head through the parietal bone revealed a small number of red cells throughout the cerebellum and the hindbrain (Figure A2.4). The positive cells were present in both the molecular and granular layers of the cerebellum but did not present a specific distribution pattern; their identity was not pursued in the present study. In the stomach and the small intestine, Dmp1-Cre targeted many cells within the lamina propria of the mucosa (Figure A2.5). Co-immunostaining experiments identified the targeted intestinal cells as mesenchymal cells expressing Pdgfra (Figure A2.6). Interestingly, although Pdgfra-positive cells were also present in the muscle wall, Dmp1-Cre targeted nearly exclusively those within the lamina propria of the mucosa. Thus, Dmp1-Cre may be a useful tool for studying gene function in the mesenchyme of the gut mucosa.

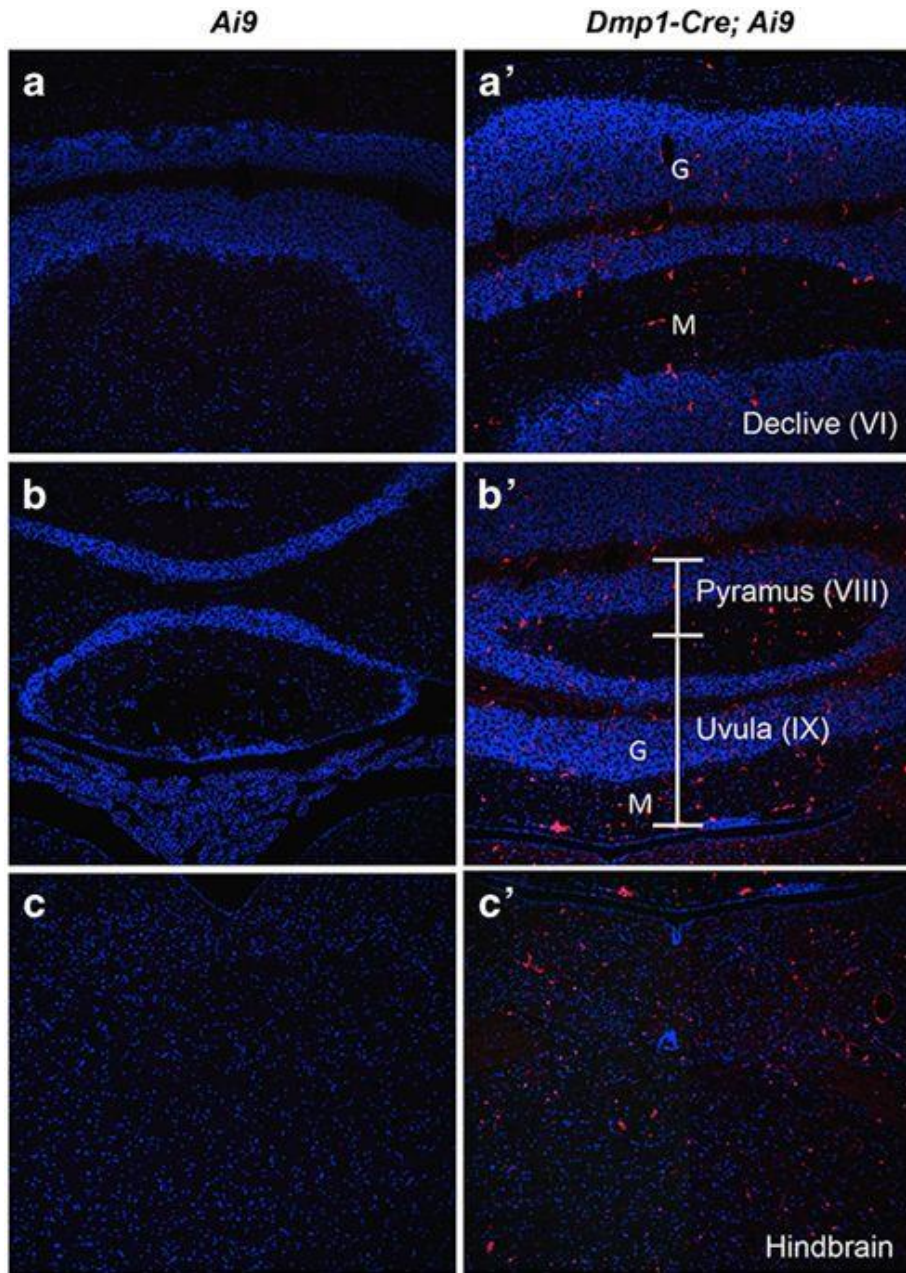


Figure A2.4: *Dmp1-Cre* targets cells in the cerebellum and the hindbrain.

Direct fluorescence of tdTomato on coronal sections of the cerebellum (a-b') and the hindbrain (c,c'). G, representative granular layer; M, representative molecular layer. Brain anatomy based on Allen Mouse Brain Atlas.

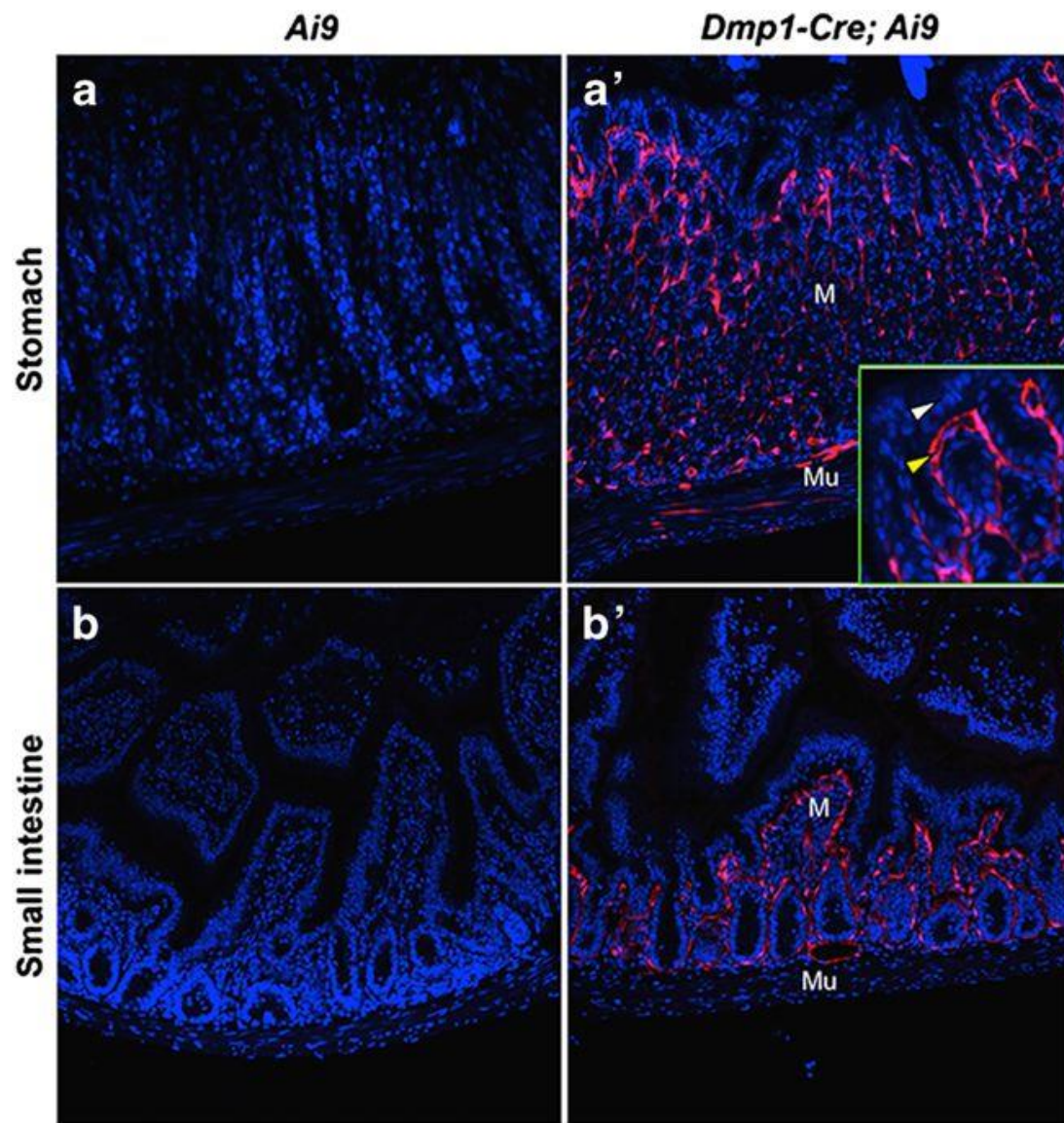


Figure A2.5: Dmp1-Cre targets lamina propria of the stomach and the small intestine.

Direct fluorescence of tdTomato on cross-sections of the stomach (a,a') and the small intestine (b,b'). M, mucosa; Mu, muscle wall. Inset in (a') shows higher magnification of a mucosa area, denoting epithelium (white arrowhead) versus mesenchyme (yellow arrowhead).

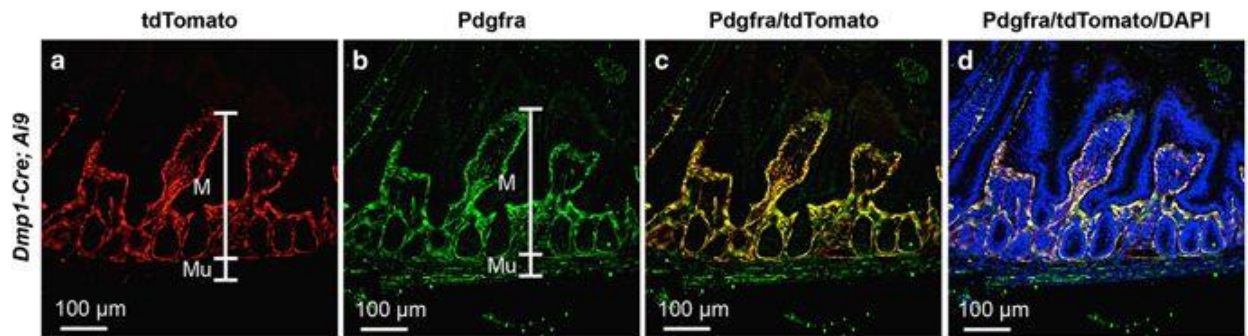


Figure A2.6: Dmp1-Cre targets Pdgfra-positive mesenchymal cells in the small intestine.

Immunostaining against Pdgfra and direct fluorescence of tdTomato on cross-sections of the small intestine. M, mucosa; Mu, muscle wall; (a) tdTomato; (b) Pdgfra; (c) merge of tdTomato and Pdgfra; (d) merge of tdTomato, Pdgfra and DNA staining by DAPI.

Deletion of *Bmpr1a* in gastrointestinal mesenchyme results in polyposis

BMP signaling has been shown to have critical roles in development and maintenance of the gastrointestinal tract, but the significance of BMP signaling within the mesenchyme has not been demonstrated. The highly efficient targeting of the gastrointestinal mesenchyme by Dmp1-Cre prompted us to analyze the gut of mice with the genotype of Dmp1-Cre; *Bmpr1af/f* (CKO). The CKO mice presented a notably higher incidence of rectal prolapse than the control littermates after 3 months of age, indicating abnormalities of the gastrointestinal tract. Histological analyses of the stomach at 5 months of age revealed that the CKO mice developed large polyps in the gastric antrum (Figure A2.7b and b'), whereas the *Bmpr1af/f* littermate exhibited no abnormality as expected (Figure A2.7a and a'). These polyps contain both epithelial and mesenchymal cells, with largely unremarkable morphology but occasional foci with mild nuclear crowding and hyperplasia (Figure A2.7b'). In the corpus, the CKO mice exhibited a mild pit/foveolar cell hyperplasia with expansion of surface cells relative to glandular invaginations (Figure A2.7d'). Examination of the intestine revealed large polyps in the CKO mice, typically with 20+ polyps in

the small intestine and 50+ in the large intestine, some as large as 2 mm in diameter. The polyps appeared largely hamartomatous, composed of a mixture of unremarkable epithelial, mesenchymal, and immune cells (Figure A2.8). Some polyps in the small intestine also contained foci harboring highly proliferative epithelium (Figure A2.8b', bracket). Surveying of the CKO mice at different ages revealed that the gastrointestinal phenotype was fully penetrant by 33 days of age (n=4) but not at 14 days. Thus, *Bmpr1a* signaling in the mesenchyme is critical for maintaining the integrity of the gastrointestinal tract in postnatal mice.

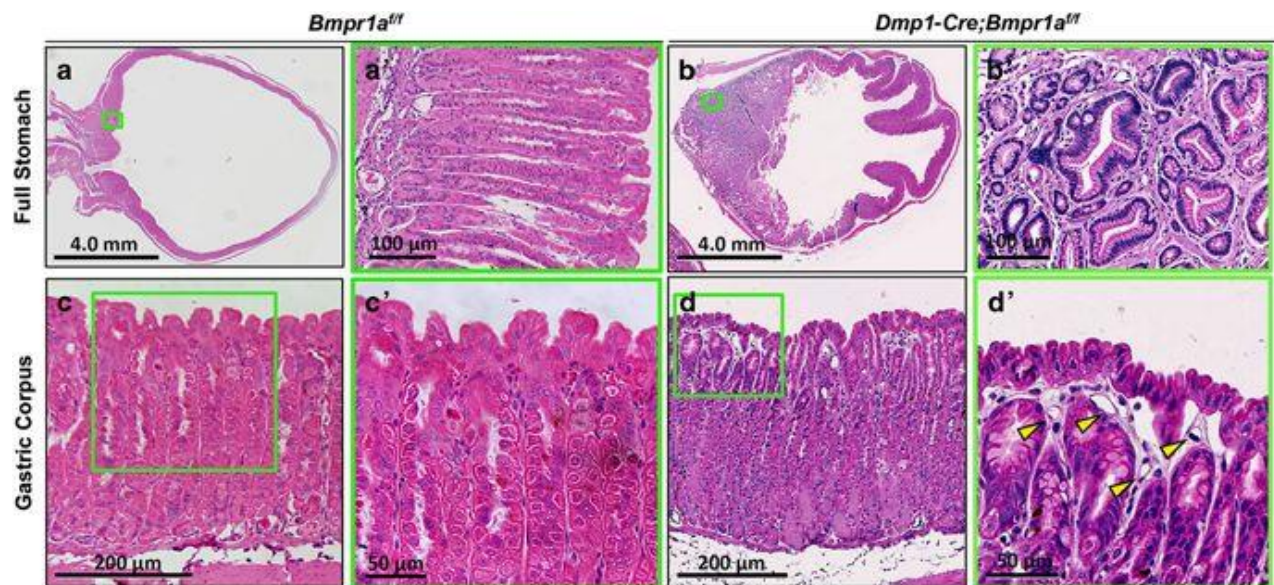


Figure A2.7: *Dmp1-Cre Bmpr1a^{fl/f}* mice develop gastric hyperplasia and polyps.

(a,b) H&E staining of sections through the entire stomach of control (*Bmpr1a^{fl/f}*) (a) versus CKO (*Dmp1-Cre; Bmpr1a^{fl/f}*) (b) littermate mice at 5 weeks of age. (a',b') Boxed areas in a and b, respectively, shown at higher magnification. (c,d) Gastric units in the gastric corpus of control (c) versus CKO (d) littermate mice. (c',d') Boxed areas in (c,d) shown at higher magnification. (d'), long stretches of surface pit cells with no opening into gastric units. Yellow arrowheads denote increased prominence of capillaries. H&E, hematoxylin and eosin.

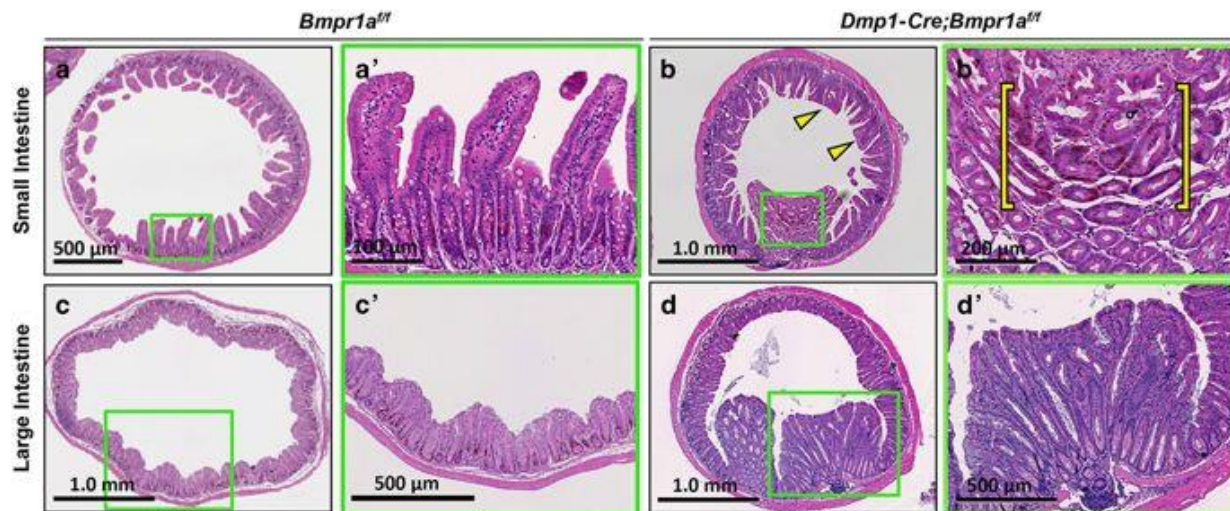


Figure A2.8: Dmp1-Cre Bmpr1af/f mice develop intestinal polyps.

(a–d) H&E staining of cross-sections through small (a,b) or large intestines (c,d) of control (Bmpr1af/f) (a,c) or CKO (Dmp1-Cre; Bmpr1af/f) (b,d) littermate mice. Yellow arrowheads in b denote fusing and blunting of villi. (a'–d') Higher-magnification images of boxed areas in (a–d), respectively, showing a polyp in small (b') or large (d') intestine. Yellow bracket in (b') denotes a pocket of proliferating epithelial cells stained brown for BrdU labeling. H&E, hematoxylin and eosin.

A2.5 Discussion

The current study has three principal findings. First, Dmp1-Cre targets the osteoblast lineage starting at the preosteoblast stage, considerably earlier than previously believed. This result confirms our previous observation by using the mT/mG reporter mouse.²⁰ Second, Dmp1-Cre also targets several non-skeletal tissues, including the skeletal muscle as previously noted, and the mesenchyme of the gastrointestinal mucosa as demonstrated here for the first time.²¹ Finally, by exploiting the unintended targeting in the gut, the study clarifies that deletion of the Bmpr1a receptor only in the mesenchyme of the gastrointestinal tract without affecting the epithelium is sufficient to cause hamartomatous polyps. Overall, Dmp1-Cre joins Osx-Cre as another example

for a bone-targeting Cre line to possess additional activities.²² The study further underscores the importance of assessing unintended recombination activities of many Cre strains.²³

Although both *Osx*-Cre and *Dmp1*-Cre target preosteoblasts, osteoblasts, and osteocytes, they show important differences in other aspects. Although *Osx*-Cre marks a majority of the bone marrow stroma, *Dmp1*-Cre targets a relatively small number of cells in the bone marrow.^{22,24} The *Dmp1*-targeted cells are near the blood vessels and appear to be stromal cells in nature. Others have recently shown that most of the *Dmp1*-targeted cells in the marrow represent a subset of the *Cxcl12*-abundant reticular cells.²⁵ The two Cre lines also show differences in the gastrointestinal tissues. Although *Osx*-Cre marks the epithelium of the mucosa in a mosaic fashion, *Dmp1*-Cre labels all of the *Pdgfra*-positive mesenchymal cells within the lamina propria. Distinct from *Osx*-Cre, *Dmp1*-Cre also targets all skeletal muscle fibers, as well as certain cells in the cerebellum and the hindbrain, likely reflecting the endogenous DMP1 expression in those tissues as previously reported.⁹ Similarly, *Dmp1*-Cre activity in the stomach and the intestines is consistent with endogenous *Dmp1* expression, as documented by the Human Protein Atlas (<http://www.proteinatlas.org/>). Thus, identification of a regulatory sequence truly specific to osteocytes would require further dissection of the *Dmp1* promoter. Among the other organs expressing DMP1, we did not detect Cre activity in the liver but did not examine the kidney or the pancreas.⁹ It should be noted that the efficiency of Cre recombination might vary between *Ai9* and the floxed gene of interest. The actual deletion efficiency of the targeted gene ought to be determined in a gene-specific manner. Nonetheless, we have presented a clear example that *Dmp1*-Cre can be used effectively to delete *Bmpr1a* in the gastrointestinal mesenchyme. Thus, the relevance of the other targeted cell types besides osteocytes should be considered when *Dmp1*-Cre is used in genetic studies.

BMP signaling has critical roles in normal development and maintenance of the gastrointestinal system. Loss of function mutations in *Bmpr1a* is a major cause for juvenile polyposis in patients.²⁶ Here we show that deletion of *Bmpr1a* with *Dmp1-Cre* in the mouse results in the formation of numerous polyps throughout the intestine; the phenotype is reminiscent of those caused by overexpression of *noggin* from the villin promoter.¹⁴ This similarity, together with the lack of polyposis when *Bmpr1a* was deleted in the epithelium, argues that the effect seen from the villin-driven *Noggin* may largely stem from the inhibition of BMP signaling in the mesenchyme instead of the epithelium as originally believed.¹⁶ Overall, the study provides evidence that BMP signaling within the mesenchyme by itself is critical for proper gastrointestinal maintenance.

A2.6 References

1. Fisher LW, Fedarko NS. Six genes expressed in bones and teeth encode the current members of the SIBLING family of proteins. *Connect Tissue Res* 2003; 44:33–40.
2. D'Souza RN, Cavender A, Sunavala G et al. Gene expression patterns of murine dentin matrix protein 1 (*Dmp1*) and dentin sialophosphoprotein (*DSPP*) suggest distinct developmental functions in vivo. *J Bone Miner Res* 1997; 12: 2040–2049.
3. Feng JQ, Zhang J, Dallas SL et al. Dentin matrix protein 1, a target molecule for *Cbfa1* in bone, is a unique bone marker gene. *J Bone Miner Res* 2002; 17: 1822–1831.
4. George A, Sabsay B, Simonian PA et al. Characterization of a novel dentin matrix acidic phosphoprotein. Implications for induction of biomineralization. *J Biol Chem* 1993; 268: 12624–12630.
5. Feng JQ, Ward LM, Liu S et al. Loss of *DMP1* causes rickets and osteomalacia and identifies a role for osteocytes in mineral metabolism. *Nat Genet* 2006; 38: 1310–1315.
6. Lorenz-Depiereux B, Bastepe M, Benet-Pages A et al. *DMP1* mutations in autosomal recessive hypophosphatemia implicate a bone matrix protein in the regulation of phosphate homeostasis. *Nat Genet* 2006; 38:1248–1250.

7. Velten M, Lin S, Liu Y et al. The in vivo role of DMP-1 and serum phosphate on bone mineral composition. *Bone* 2015; 81: 602–613.
8. Ye L, MacDougall M, Zhang S et al. Deletion of dentin matrix protein-1 leads to a partial failure of maturation of predentin into dentin, hypo- mineralization, and expanded cavities of pulp and root canal during postnatal tooth development. *J Biol Chem* 2004; 279: 19141–19148.
9. Terasawa M, Shimokawa R, Terashima T et al. Expression of dentin matrix protein 1 (DMP1) in nonmineralized tissues. *J Bone Miner Metab* 2004; 22: 430–438.
10. Lu Y, Xie Y, Zhang S et al. DMP1-targeted Cre expression in odontoblasts and osteocytes. *J Dent Res* 2007; 86: 320–325.
11. Kalajzic I, Matthews BG, Torreggiani E et al. In vitro and in vivo approaches to study osteocyte biology. *Bone* 2013; 54: 296–306.
12. Bleuming SA, He XC, Kodach LL et al. Bone morphogenetic protein signaling suppresses tumorigenesis at gastric epithelial transition zones in mice. *Cancer Res* 2007; 67: 8149–8155.
13. Huh WJ, Mysorekar IU, Mills JC. Inducible activation of Cre recombinase in adult mice causes gastric epithelial atrophy, metaplasia, and regenerative changes in the absence of "floxed" alleles. *Am J Physiol Gastrointest Liver Physiol* 2010; 299: G368–G380.
14. Haramis AP, Begthel H, van den Born M et al. De novo crypt formation and juvenile polyposis on BMP inhibition in mouse intestine. *Science* 2004; 303: 1684–1686.
15. Shinohara M, Mao M, Keeley TM et al. Bone morphogenetic protein signaling regulates gastric epithelial cell development and proliferation in mice. *Gastroenterology* 2010; 139: 2050–2060 e2052.
16. Auclair BA, Benoit YD, Rivard N et al. Bone morphogenetic protein signaling is essential for terminal differentiation of the intestinal secretory cell lineage. *Gastroenterology* 2007; 133: 887–896.
17. Beppu H, Mwiszerwa ON, Beppu Y et al. Stromal inactivation of BMPRII leads to colorectal epithelial overgrowth and polyp formation. *Oncogene* 2008; 27: 1063–1070.
18. Madisen L, Zwingman TA, Sunkin SM et al. A robust and high-throughput Cre reporting and characterization system for the whole mouse brain. *Nat Neurosci* 2010; 13: 133–140.
19. Mishina Y, Hanks MC, Miura S et al. Generation of Bmpr/Alk3 conditional knockout mice. *Genesis* 2002; 32:69–72.
20. Lim J, Shi Y, Karner CM et al. Dual function of Bmpr1a signaling in restricting preosteoblast proliferation and stimulating osteoblast activity in mouse. *Development* 2016; 143: 339–347.

21. Chen J, Long F. beta-catenin promotes bone formation and suppresses bone resorption in postnatal growing mice. *J Bone Miner Res* 2013; 28: 1160–1169.
22. Chen J, Shi Y, Regan J et al. *Osx-Cre* targets multiple cell types besides osteoblast lineage in postnatal mice. *PloS One* 2014; 9: e85161.
23. Heffner CS, Herbert Pratt C, Babiuk RP et al. Supporting conditional mouse mutagenesis with a comprehensive cre characterization resource. *Nat Commun* 2012; 3: 1218.
24. Liu Y, Strecker S, Wang L et al. *Osterix-cre* labeled progenitor cells contribute to the formation and maintenance of the bone marrow stroma. *PloS One* 2013; 8: e71318.
25. Zhang J, Link DC. Targeting of mesenchymal stromal cells by Cre-recombinase transgenes commonly used to target osteoblast lineage cells. *J Bone Miner Res* 2016; 31: 2001–2007.
26. Howe JR, Bair JL, Sayed MG et al. Germline mutations of the gene encoding bone morphogenetic protein receptor 1A in juvenile polyposis. *Nat Genet* 2001; 28: 184–187.

**Appendix 3: Metaplastic cells in the stomach
arise, independently of stem cells, via
dedifferentiation or transdifferentiation of
chief cells**

The following chapter was published in Gastroenterology

Radyk, Megan D., Joseph Burclaff, Spencer G. Willet, and Jason C. Mills. "Metaplastic cells in the stomach arise, independently of stem cells, via dedifferentiation or transdifferentiation of chief cells." *Gastroenterology* 154, no. 4 (2018): 839-843.

A3.1 Abstract

Spasmolytic polypeptide-expressing metaplasia (SPEM) develops in patients with chronic atrophic gastritis due to infection with *Helicobacter pylori*; it might be a precursor to intestinal metaplasia and gastric adenocarcinoma. Lineage tracing experiments of the gastric corpus in mice have not established whether SPEM derives from proliferating stem cells or differentiated, post-mitotic zymogenic chief cells in the gland base. We investigated whether differentiated cells can give rise to SPEM using a non-genetic approach in mice. Mice were given intraperitoneal injections of 5-fluorouracil, which blocked gastric cell proliferation, plus tamoxifen to induce SPEM. Based on analyses of molecular and histological markers, we found SPEM developed even in the absence of cell proliferation. SPEM therefore did not arise from stem cells. In histologic analyses of gastric resection specimens from 10 patients with adenocarcinoma, we found normal zymogenic chief cells that were transitioning into SPEM cells only in gland bases, rather than the proliferative stem cell zone. Our findings indicate that SPEM can arise by direct reprogramming of existing cells—mainly of chief cells.

A3.2 Stem Cell Independent Gastric Metaplasia

Spasmolytic Polypeptide-Expressing Metaplasia (SPEM) arises in the setting of chronic atrophic gastritis (CAG) in humans infected with *Helicobacter pylori* and may be a precursor to intestinal metaplasia and gastric adenocarcinoma (Schmidt et al., 1999; Petersen et al., 2017b). CAG is characterized by chronic inflammation, parietal cell death, and metaplastic expansion of cells coexpressing spasmolytic polypeptide (TFF2) and zymogenic chief cell (ZC) markers. Genetic lineage tracing studies have not definitively identified the cell-of-origin for SPEM cells. Tracing from *Mist1*^{CreERT2}-expressing cells indicated ZCs at the gland base gave rise to SPEM (Nam et al., 2010; Stange et al., 2013b; Leushacke et al., 2017; Matsuo et al., 2017; Choi et al., 2018). Another report disputed this because occasional cells in the upper, isthmal stem cell region of the

gland also expressed *Mist1^{CreERT2}*, indicating SPEM might be derived isthmally (Hayakawa et al., 2015). We use a new approach to determine if differentiated cells can give rise to SPEM.

For an isthmal stem cell to generate a gland full of SPEM cells, its progeny must proliferate to reach the gland base. We inhibited proliferation with the anti-mitotic drug 5-Fluorouracil (5FU) and found one 150mg/kg (Stange et al., 2013b) intraperitoneal injection of 5FU was sufficient to block proliferation for 24h with return to near-normal levels by 48h (Figure A3.1A,B).

Long-term 5FU is toxic beyond 4-5 days, thus we used a SPEM induction method shown by multiple labs to cause maximal, synchronous SPEM within three days: high dose tamoxifen (HDT) (Huh et al., 2012b; Saenz et al., 2016). Our selected 5FU+HDT regimen caused no mouse mortality, but blocked nearly all proliferation at the peak SPEM stage: <0.5 in 5FU+HDT vs. >8 cells/unit in HDT alone (Figure A3.1C).

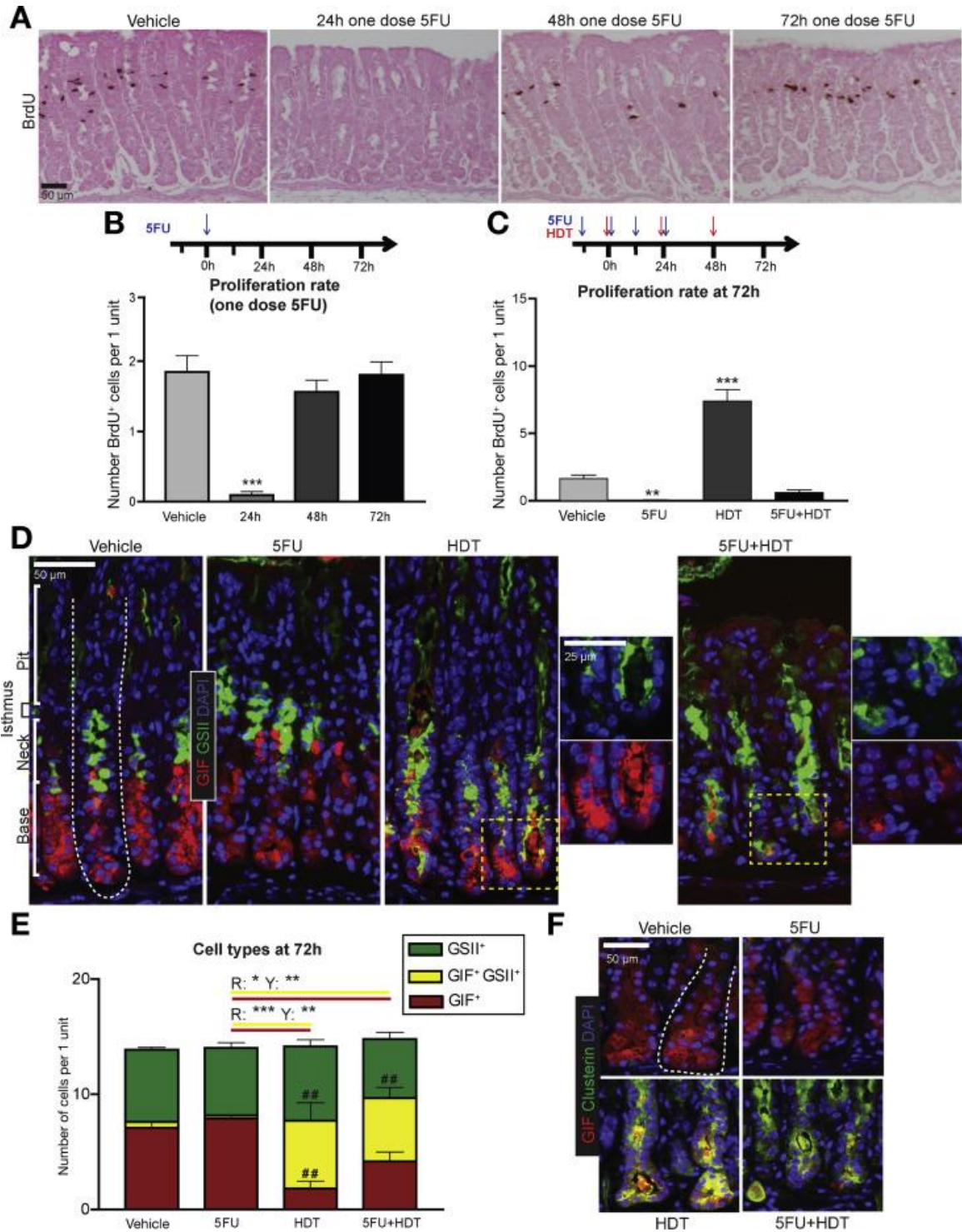


Figure A3.1: SPeM can occur without proliferation.

A) IHC staining for BrdU after one dose of 5FU (150mg/kg; intraperitoneal injection). Eosin Y counterstain. B) Experimental timeline and proliferation quantification. C) 5FU+HDT experimental timeline and proliferation quantification. D) Immunofluorescence of stomachs after

72h vehicle, 5FU, HDT, or 5FU+HDT treatment (red, GIF; green, GSII; blue, DAPI). Dotted line: gastric unit. E) Cell populations quantified, # indicates significance compared to vehicle, * indicates significance between treatment groups. R is significance between red columns, Y between yellow columns. F) Immunofluorescence of stomachs (red, GIF; green, Clusterin; blue, DAPI). * $p \leq 0.05$, ** $p \leq 0.01$ *** $p \leq 0.001$, variance analyzed with ANOVA/Tukey ($N \geq 3$ mice/group)

We monitored SPEM by immunofluorescence for the ZC marker, gastric intrinsic factor (GIF; red), and a lectin (GSII; green), which co-labels with TFF2. In control mice, GIF was located in ZCs at the gland base, separated from the GSII⁺ mucous neck cells in the middle of the gland. Consistent with previous reports (Huh et al., 2012b; Saenz et al., 2016), HDT caused SPEM, defined by pathognomonic GSII⁺GIF⁺ co-staining at the gland base (Figure A3.1D), yet few SPEM cells appeared at 24h (Figure A3.2). 5FU alone, or with HDT, did not significantly alter outcomes at any timepoint. At 72h, similar numbers of SPEM cells formed in HDT and HDT+5FU: 6.0 ± 1.5 SPEM cells in HDT, 5.6 ± 1.0 in HDT+5FU (Figure A3.1D,E). Additionally, 5FU vs. HDT+5FU mice displayed a similar magnitude of GIF⁺ cell loss and GIF⁺GSII⁺ SPEM cell increase ($\Delta -3.7 \pm 1.3$ GIF⁺ cells/unit, $\Delta +5.2 \pm 0.8$ GIF⁺GSII⁺ cells/unit), while GSII⁺ neck cells decreased only slightly ($\Delta G: -0.76 \pm 0.75$), implicating ZCs as the principal source for SPEM cells when proliferation is blocked.

Equivalent SPEM was confirmed in HDT±5FU mice by qRT-PCR for SPEM-associated transcripts *Mist1*, *Gif*, *He4*, and *Clusterin* (Engevik et al., 2016) (Figure A3.3) and immunofluorescence for Clusterin (Figure A3.1F).

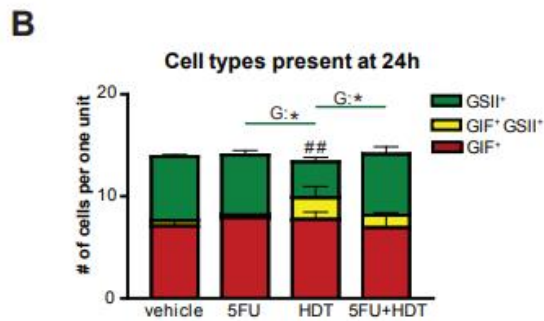
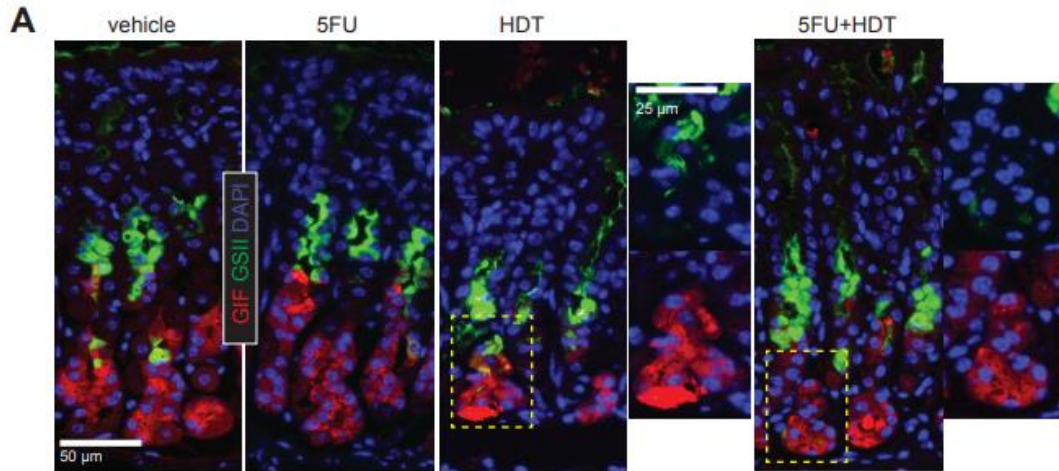


Figure A3.2: No SPEM occurs 24h after HDT treatment.

A) Immunofluorescence of stomachs after 24h of vehicle, 5FU, HDT, or 5FU+HDT treatment (red, GIF; green, GSII; blue, DAPI). B) Quantification of cell populations, # indicates significance of treatment compared to vehicle, * indicates significance between specified treatment groups. G is significance between green columns. * $p \leq 0.05$, variance analyzed with ANOVA/Tukey ($N \geq 3$ mice/group)

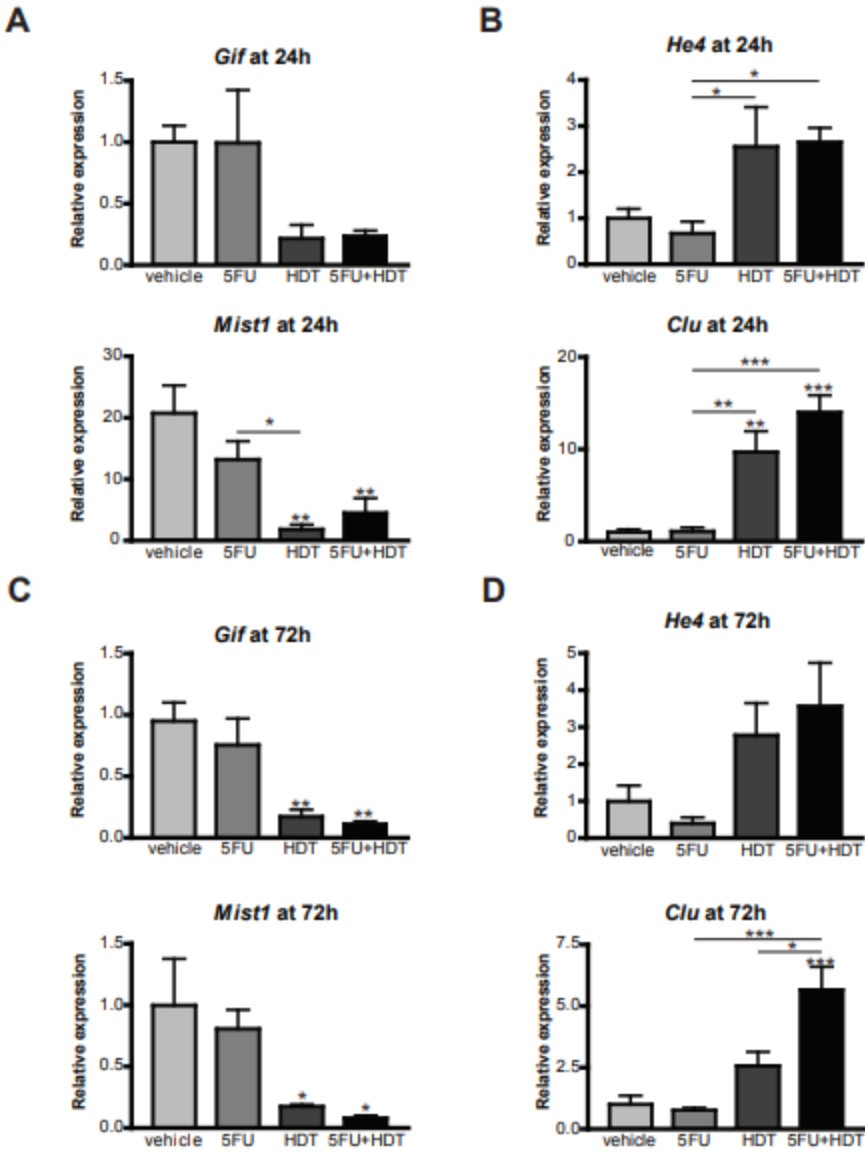


Figure A3.3: qRT-PCR for SPEM-associated genes.

A) Transcripts of zymogenic cell markers analyzed from RNA isolated from the whole gastric corpus of mice treated with vehicle, 5FU, HDT, or 5FU+HDT for 24 hours. B) Same RNA described from A analyzed for markers known to increase in SPEM. C) Transcripts of zymogenic cell markers analyzed from RNA isolated from the whole gastric corpus of mice treated with vehicle, 5FU, HDT, or 5FU+HDT for 72 hours. D) Same RNA described from C analyzed for markers known to increase in SPEM. * $p \leq 0.05$ ** $p \leq 0.01$ *** $p \leq 0.001$, variance analyzed with ANOVA/Tukey ($N \geq 3$ mice/group)

We examined the differentiation pattern and location of occasional cells escaping the 5FU blockade at 72h. Proliferating cells in control mice lacked neck/ZC markers, indicating proliferation primarily in isthmal stem cells (Figure A3.4A,B). HDT mice harbored proliferating isthmal, neck, SPEM, and occasional BrdU⁺ ZCs (Figure A3.4A,B). The 5FU+HDT regimen was designed such that cells escaping 5FU blockade at 72h would be in their first cell cycle, as gastric epithelial cells average one division per day (Potten, 1998). As expected, <1 cell/unit was BrdU⁺ at 72h 5FU+HDT, and units with >1 BrdU⁺ cell were exceedingly rare (Figure A3.4A). Proliferating cells could not be found prior to 72h (Figure 3.5). Proliferating cells at 72h expressed neck, SPEM, or ZC markers (Figure A3.4B). Interestingly, the largest cohort did not label with GSII or GIF. We suspect these cells are parietal cell progenitors based on cells, at 96h following HDT, expressing BrdU and beginning to show the characteristic, thick apical staining of parietal cell marker, ezrin (Lo et al., 2017) (Figure A3.6). Figure A3.4C plots zones in which proliferating cells emerged from isthmus to base, excluding upper pit/foveolar cells (Figure A3.7). In control mice, almost all proliferation was in the isthmus. In HDT and 5FU+HDT, proliferating cells appeared throughout the gland. Thus, multiple lines of evidence presented here indicate, in addition to isthmal stem cells, multiple cell types throughout the gland exhibit plasticity and can proliferate in response to damage.

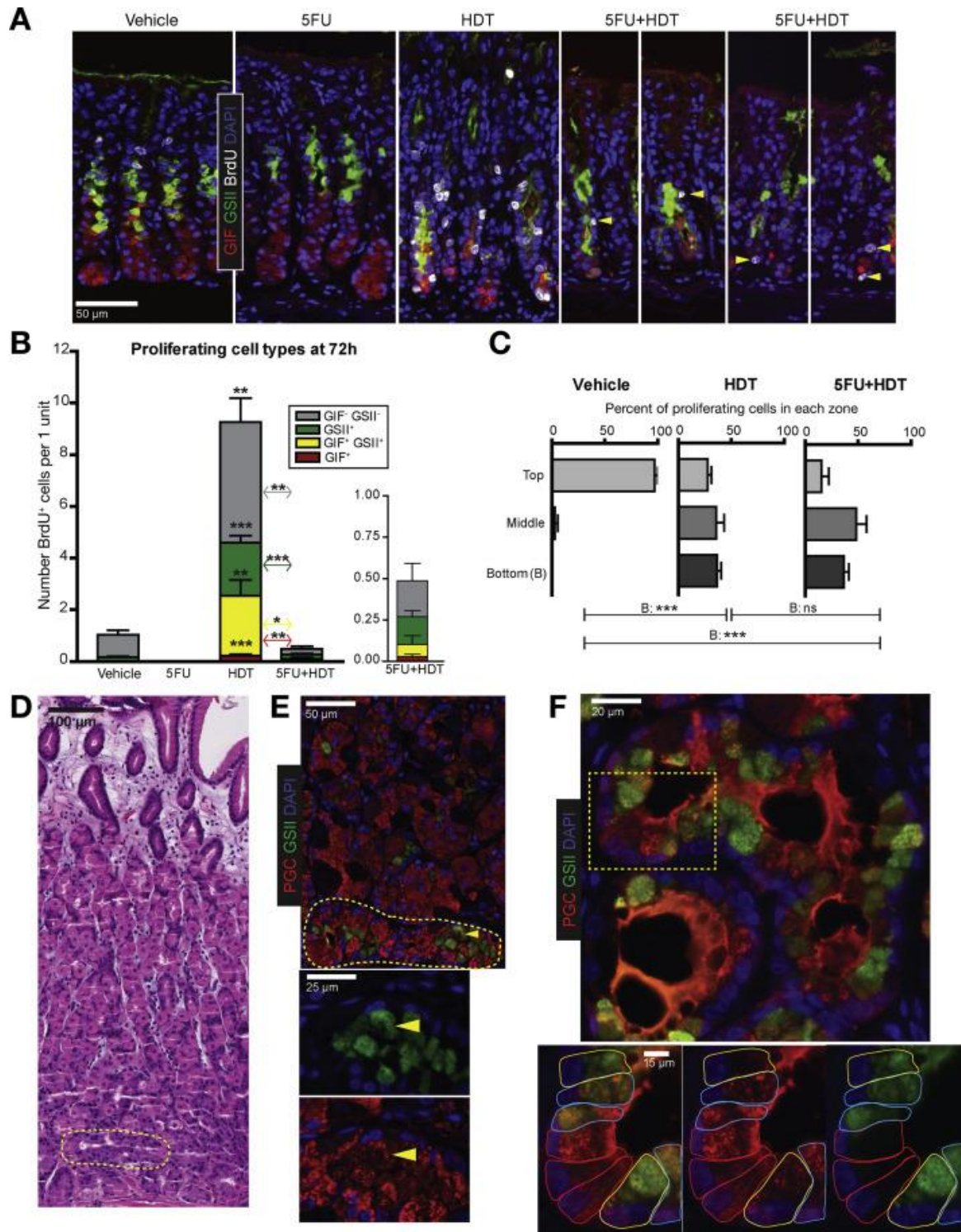


Figure A3.4: Metaplastic cells arise below the isthmus

A) Immunofluorescence of stomachs after 72h vehicle, 5FU, HDT, or 5FU+HDT (green, GSII; red, GIF; white, BrdU; blue, DAPI; arrowheads, rare BrdU⁺ cells in 5FU+HDT). B) Proliferating

cell populations quantified. C) Location of BrdU⁺ cells below the bottom-most AAA⁺ pit cell. D) Hematoxylin & eosin of early human SPEM (yellow circle) E) Immunofluorescence on serial section from 2D (red, PGC; green, GSII; blue, DAPI; arrowhead: SPEM cell). Yellow circle is SPEM area. F) Human SPEM within gland base showing transitional ZC→SPEM forms. Dotted box indicates area shown at higher magnification. Cells outlined in colors according to cell type (red, normal ZCs; blue, hybrid SPEM; yellow, full SPEM). *p≤0.05 **p≤0.01 ***p≤0.001, variance analyzed with ANOVA/Tukey (N ≥ 3 mice/group)

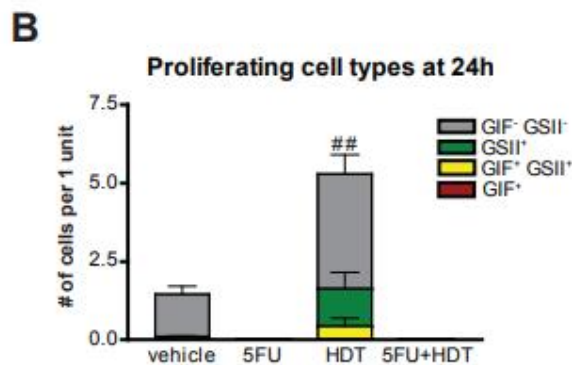
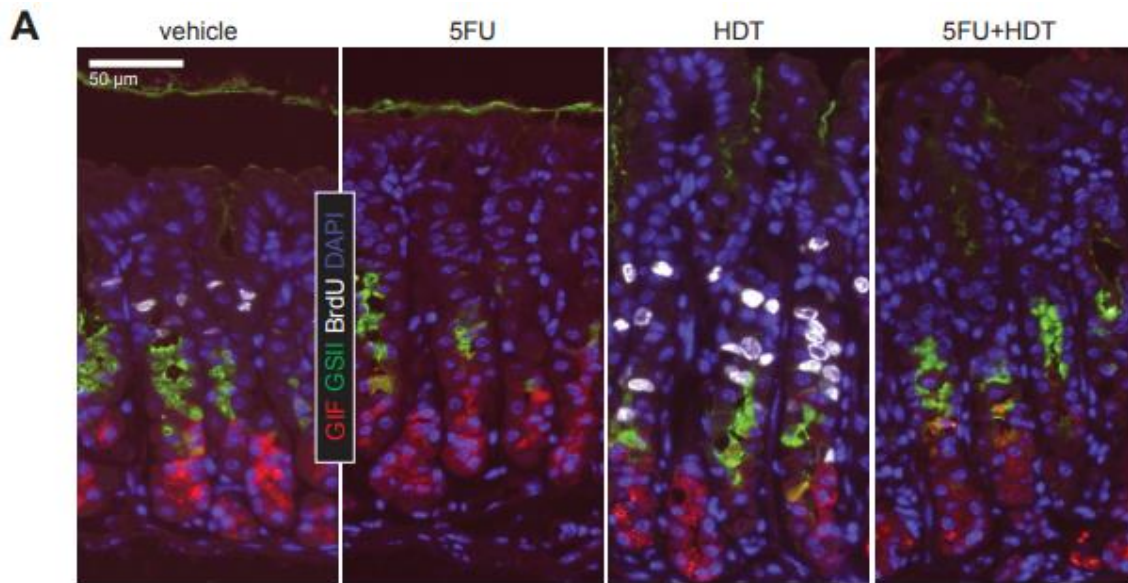


Figure A3.5: Proliferation is sufficiently blocked over the course of injury in 5FU+HDT mice.

A) Immunofluorescence of stomachs after 24h of vehicle, 5FU, HDT, or 5FU+HDT (green, GSII; red, GIF; white, BrdU; blue, DAPI). B) Quantification of proliferating cell populations. ## p≤0.01, variance analyzed with ANOVA/Tukey (N ≥ 3 mice/group)

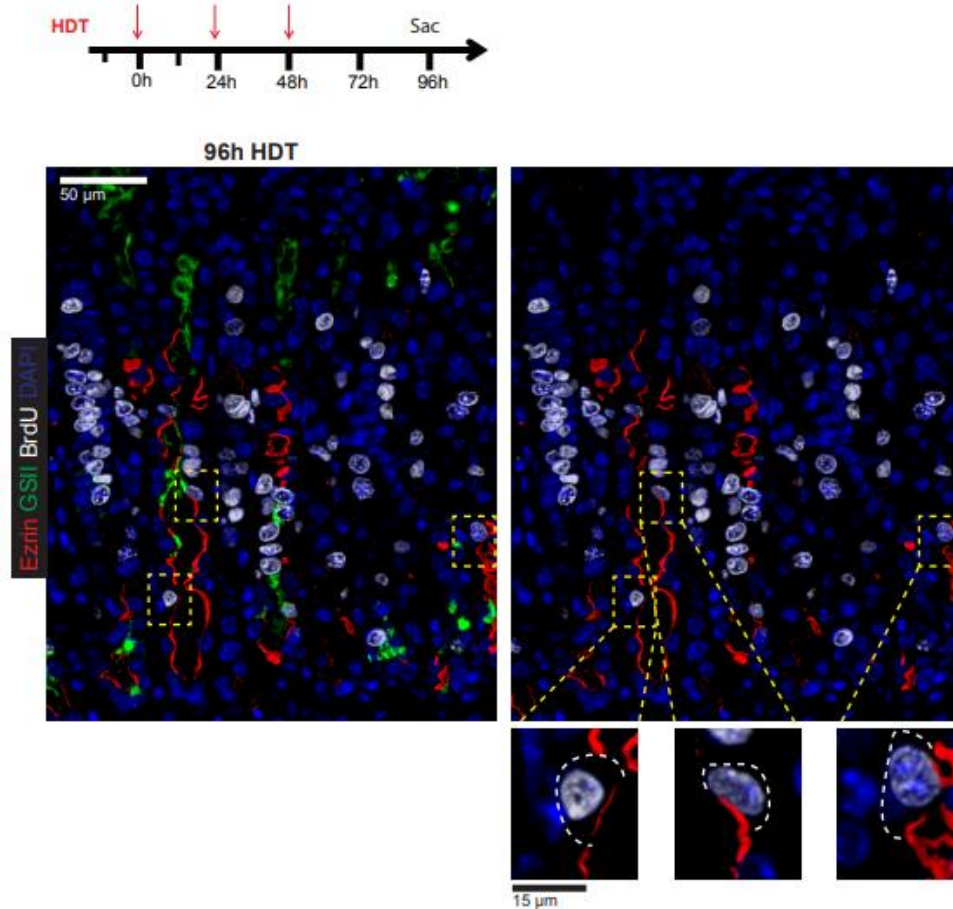


Figure A3.6: Proliferating pre-parietal cells begin to appear 96h after HDT treatment.

Timeline of treatment scheme. Immunofluorescence of stomachs after 96h of vehicle, 5FU, HDT, or 5FU+HDT (green, GSII; red, ezrin; white, BrdU; blue, DAPI). Yellow boxes indicate BrdU⁺ ezrin⁺ cells with basolateral surfaces of each cell outlined in dashed white line.

We stained for proliferative SPEM with CD44v (CD44v9 in humans) (Engevik et al., 2016). HDT and 5FU+HDT mice exhibited CD44v staining at the gland base (Supplementary Figure 5B) and increased expression of proliferation-associated markers *Check2* and *Ccnb2* by qRT-PCR, indicating basally-located cells are poised to divide in 5FU+HDT stomachs (Figure A3.7).

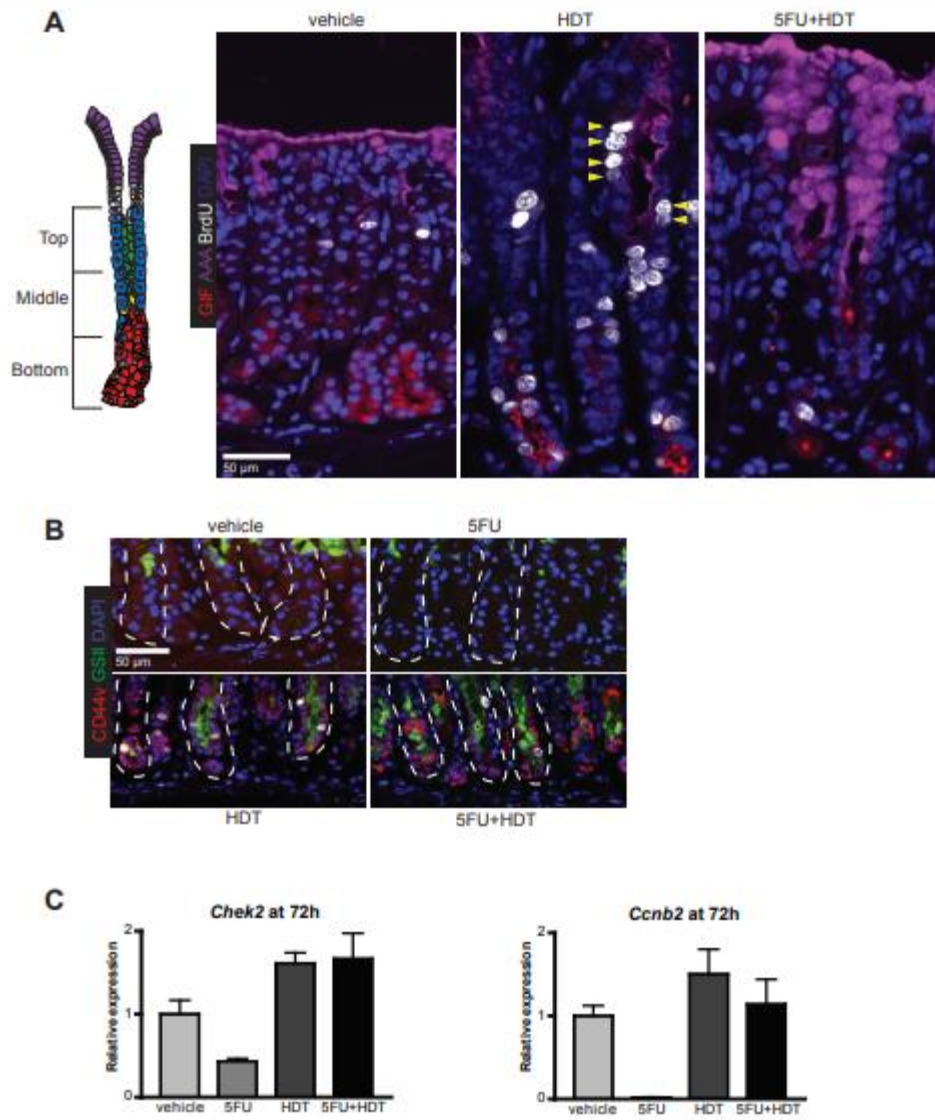


Figure A3.7: Proliferation after SPEM induction.

A) Immunofluorescence of stomachs after 72h of vehicle, HDT, or 5FU+HDT treatment (red, GIF; purple, AAA (*Anguilla anguilla* lectin); white, BrdU; blue, DAPI). Yellow arrowheads indicate cells that were not counted in quantification because they are in the pit zone and, thus, above the bottom-most AAA⁺ cell. B) Immunofluorescence of stomachs treated with vehicle, 5FU, HDT, or 5FU+HDT for 72h (red, CD44v; green, GSII; blue, DAPI). Dotted line: outlined unit bases. C) Transcripts of proliferative markers analyzed from RNA isolated from the whole gastric corpus of mice treated with vehicle, 5FU, HDT, or 5FU+HDT for 72 hours.

Our data suggest stem cells are responsible for pit- and neck cell-localized proliferation following HDT; however, SPEM itself is largely derived from ZCs, supporting previous work suggesting two foci of proliferation in the stomach (Burclaff et al., 2017). Our mouse experiments reflect ZC to SPEM transitions observed in humans previously extensively characterized from a large dataset of adenocarcinoma and gastritis biopsy and resection specimens (Lennerz et al., 2010). Figures A3.4D-F and A3.8 depict representative stomach glands from 10 additional patients with gastric adenocarcinoma. We again observe hybrid cells (cells with features of mature ZCs and SPEM cells) occurred predominantly in the base. Specifically, we see apparent transition among a variety of cell phenotypes from mature ZCs (expressing PGC in large apical granules) to cells expressing abundant PGC with scant GSII (likely indicating early SPEM change) to phenotypically complete SPEM conversion (scant PGC with abundant GSII) (Figure A3.4F). A stem cell-origin of SPEM in humans would mean cell fate changes to SPEM cells should occur at the isthmus, and SPEM cells would have to expand downward and replace mature ZCs to populate the base. Thus, the interpretation that SPEM originates exclusively from the isthmus would be inconsistent with the presence of cells transitioning to SPEM consistently found in the base.

Differentiated cells are long-lived and may accumulate mutations that become unmasked upon cell cycle re-entry after injury. For example, *Kras* mutations in ZCs or pancreatic acinar cells can fuel tumorigenic transformation (Leushacke et al., 2017). Therefore, our current work, highlighting how differentiated cells are called back into the cell cycle in an acute injury model, should interest those studying tumorigenesis and/or regeneration.

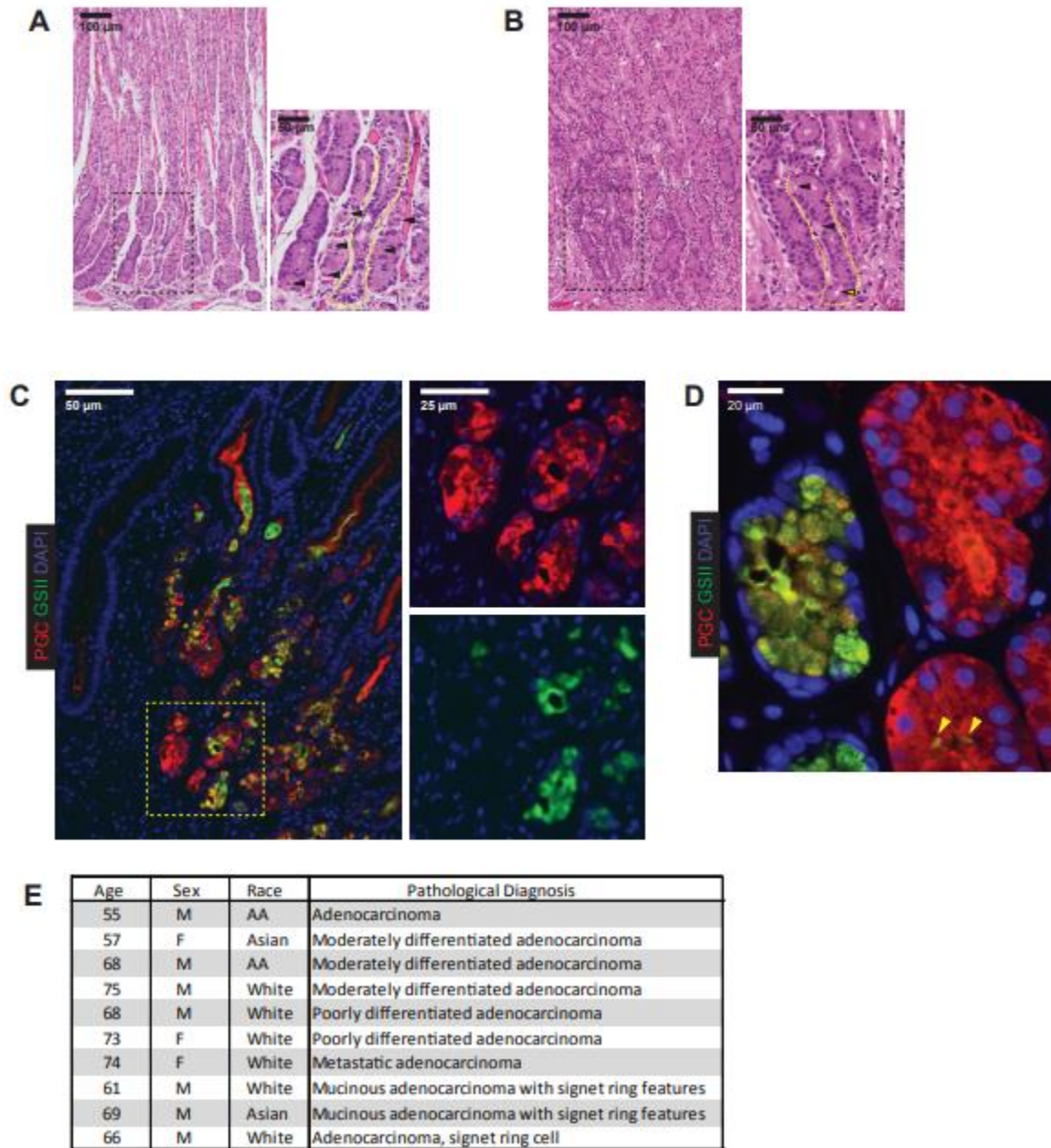


Figure A3.8: Human SPEM in gastric cancer patients

A) H&E of human corpus glands with early atrophic gastritis exhibiting focal gland bases transitioning to SPEM. Arrows refer to parietal cells in healthy glands. SPEM gland outlined in yellow has a wide lumen and lacks parietal cells. B) Same as panel A but a different patient with more active gastritis. Early SPEM gland outlined in yellow shows opening of lumen at gland base (yellow arrow) and contains degenerating parietal cells (black arrows). C) Immunofluorescence of human SPEM (red, PGC; green, GSII; blue, DAPI). Note many hybrid forms in gland bases ranging from cells with only red PGC (mature, normal ZCs) to those

showing mature SPEM (prominent green GSII, scant red PGC). D) Immunofluorescence of the base of yet another patient's corpus. A mature SPEM gland is located next to a normal gland with mature ZCs. A third gland shows hybrid forms wherein ZCs express focal, apical GSII (yellow arrowheads). E) Table detailing the demographic aspects and pathological diagnoses of the 10 patients analyzed in this manuscript.

A3.3 Methods and Materials

Animals and Injections

All experiments involving animals were performed according to protocols approved by the Washington University School of Medicine Animal Studies Committee. Mice were maintained in a specified pathogen-free barrier facility under a 12-hour light cycle. Wild-type C57BL/6 mice were purchased from Jackson Laboratories (Bar Harbor, ME). All mice used in experiments were females 6–8 weeks old. To induce SPEM, tamoxifen (250 mg/kg body weight; Toronto Research Chemicals, Inc, Toronto, Canada) was administered daily for 3 days by intraperitoneal injection. Tamoxifen was dissolved in a vehicle of 10% ethanol and 90% sunflower oil (Sigma, St Louis, MO) as described previously (Petersen et al., 2017b). To block proliferation, 5-FU (150 mg/kg body weight; Sigma F6627) was given by intraperitoneal injection twice daily for 2 days. 5-FU was dissolved in a solution containing 10% dimethyl sulfoxide and 0.9% sodium chloride. All mice were given an intraperitoneal injection containing BrdU (120 mg/kg) and 5-fluoro-2'deoxyuridine (12 mg/kg) 90 minutes before sacrifice.

Patient Samples

Human gastric tissue was obtained with approval from the Institutional Review Board of Washington University School of Medicine. The database of metaplastic samples showing

hybrid SPEM forms has been described previously (Schmidt et al., 1999; Nam et al., 2010; Stange et al., 2013b).

Immunofluorescence and Immunohistochemistry

Stomachs were excised immediately, flushed with phosphate-buffered saline (PBS) via the duodenal stub and then inflated with freshly prepared 4% paraformaldehyde. The stub was clamped by hemostat, and the stomach suspended in fixative in a 50-mL conical for 8–12 hours, followed by 3 rinses in 70% EtOH, arrangement in 2% agar in a tissue cassette, and routine paraffin processing. Sections (5 μm) were cut, deparaffinized, and rehydrated with graded xylenes, alcohols, and water, then antigen-retrieved in sodium citrate buffer (2.94 g sodium citrate, 500 μL Tween 20, pH 6.0) using a pressure cooker. Slides were blocked in 5% normal goat serum, 0.2% Triton-X 100, in PBS. Slides were incubated overnight at 4°C in primary antibodies, then rinsed in PBS, incubated 1 hour at room temperature in secondary antibodies and/or fluorescently labeled lectin (Alexa Fluor 647 made by directly conjugating E-Y Laboratories [San Mateo, CA] lectin to Molecular Probes [Eugene, OR] Alexa Fluor 647), rinsed in PBS, mounted in ProLong Gold Antifade Mountant with 4',6-diamidino-2-phenylindole (Molecular Probes). For immunohistochemistry, steps were identical except the following. An extra quenching step was performed for 15 minutes in a methanol solution containing 1.5% H₂O₂ after antigen retrieval. Substrate reaction and detection was performed using ImmPACT VIP Peroxidase (horseradish peroxidase) Substrate Kit (Vector Laboratories, Burlingame, CA) as detailed per the manufacturer's protocol and slides were mounted in Permount Mounting Medium.

Imaging

Fluorescence microscopy was performed using a Zeiss Axiovert 200 microscope with an Axiocam MRM camera and Apotome II instrument for grid-based optical sectioning. Post-imaging adjustments, including contrast, fluorescent channel overlay, and pseudo-coloring, were performed with Axiovision and Adobe Photoshop CS6. Histology of stomach and immunohistochemistry were imaged using an Olympus BX51 light microscope and Olympus SZX12 dissecting microscope w/12 MPixel Olympus DP70 camera. Images were analyzed and post-imaging adjustments were performed with Adobe Photoshop CS6.

Antibodies

Primary antibodies used in this study were as follows: fluorescently conjugated *Anguilla anguilla* lectin (Alexa Fluor 647; 1:1000; EY Laboratories), goat anti-BrdU (1:20,000; a gift from Dr Jeff Gordon, Washington University, St Louis, MO), rat anti-CD44 v10-e16, ortholog of human v9 (1:200; Cosmo Bio, Tokyo, Japan), goat anti-Clusterin (1:100; Santa Cruz Biotechnology, Santa Cruz, CA), mouse anti-ezrin (1:250; Santa Cruz Biotechnology), fluorescently conjugated GSII lectin (Alexa Fluor 647; 1:1,000; Invitrogen, Carlsbad, CA), rabbit anti-human gastric intrinsic factor (1:10,000; a gift from Dr David Alpers, Washington University, St Louis, MO), and sheep anti-PGC (1:10,000; Abcam, Cambridge, MA). Secondary antibodies included Alexa Fluor 488, 594, or 647-conjugated donkey anti-goat, anti-rabbit, or anti-mouse (1:500; Molecular Probes).

Immunofluorescence and Immunohistochemistry Quantification

For counts from units expressing neck, chief, and proliferative markers all time points were quantified with at least 3 mice as previously described by Burclaff et al, 2017 (Burclaff et al., 2017). Stomach corpus slides were stained for BrdU, the neck cell marker GSII, and zymogenic cell marker GIF. Images were captured as TIFF files from a Zeiss Axiovert 200 microscope with an Axiocam MRM camera with an Apotome optical sectioning filter (Carl Zeiss, Jena, Germany). Each stomach had at least 5 randomly distributed 20× images taken, which contained 10 or more well-oriented gastric units. Units were counted using the neck staining, and total quantifications of proliferating cells (BrdU) were averaged over the total unit numbers per mouse. For total proliferation counts from immunohistochemistry at least 3 mice per treatment group were quantified. Stomach corpus slides were stained with an antibody for BrdU. Whole slides were scanned using a NanoZoomer 2.0 HT microscope and analyzed with NanoZoomer Digital Pathology software (Hamamatsu; Hamamatsu City, Japan). At least 40 corpus units were analyzed and counted per stomach. Proliferation rate for each mouse was an average of all units counted.

Quantitative Real-Time Reverse Transcription Polymerase Chain Reaction

RNA was isolated using RNeasy (Qiagen, Valencia, CA) per the manufacturer's protocol. The quality of the mRNA was verified with a BioTek (Winooski, VT) Take3 spectrophotometer and electrophoresis on a 2% agarose gel. RNA was treated with DNase I (Invitrogen), and 1 µg RNA was reverse-transcribed with SuperScript III (Invitrogen) following the manufacturer's protocol. Measurements of complementary DNA abundance were performed by real-time quantitative

reverse transcription polymerase chain reaction using either a Stratagene (La Jolla, CA) MX3000P detection system or a Bio-Rad (Hercules, CA) CFX Connect system. Power SYBR Green master mix (Thermo Scientific, Waltham, MA) fluorescence was used to quantify the relative amplicon amounts of each gene (normalizing gene was TATA box binding protein). Primer design and sequence are in Figure A3.9.

Gene	Sequence
<i>Clusterin</i> Forward	CCAGCCTTTCTTTGAGATGA
<i>Clusterin</i> Reverse	CTCCTGGCACTTTTCACACT
<i>Gif</i> Forward	GAAAAGTGGATCTGTGCTACTTGCT
<i>Gif</i> Reverse	AGACAATAAGGCCCCAGGATG
<i>He4</i> Forward	TGCCTGCCTGTCGCCTCTG
<i>He4</i> Reverse	TGTCCGCACAGTCCTTGCCA
<i>Mist1</i> Forward	GAGCGAGAGAGGCAGCGGATG
<i>Mist1</i> Reverse	AGTAAGTATGGTGGCGGTCAG
<i>Tbp</i> Forward	CAAACCCAGAATTGTTCTCCTT
<i>Tbp</i> Reverse	ATGTGGTCTTCCTGAATCCCT

Figure A3.9: Primers used for quantitative RT-PCR

Graphing and Statistics

All graphs and statistics were completed in GraphPad Prism (GraphPad, La Jolla, CA) using 1-way analysis of variance with the Tukey post-hoc multiple comparison test to determine significance. Sample sizes were determined based on statistical significance and practicality. $P \leq 0.05$ was considered significant.

Appendix 4: Regenerative proliferation of differentiated cells by mTORC1-dependent paligenosis

The following chapter was published in The EMBO Journal

Willet, Spencer G., Mark A. Lewis, Zhi-Feng Miao, Dengqun Liu, Megan D. Radyk, Rebecca L. Cunningham, Joseph Burclaff et al. "Regenerative proliferation of differentiated cells by mTORC1-dependent paligenosis." The EMBO journal (2018): e98311.

A4.1 Abstract

In 1900, Adami speculated that a sequence of context-independent energetic and structural changes governed the reversion of differentiated cells to a proliferative, regenerative state. Accordingly, we show here that differentiated cells in diverse organs become proliferative via a shared program. Metaplasia-inducing injury caused both gastric chief and pancreatic acinar cells to decrease mTORC1 activity and massively upregulate lysosomes/autophagosomes; then increase damage associated metaplastic genes such as Sox9; and finally reactivate mTORC1 and re-enter the cell cycle. Blocking mTORC1 permitted autophagy and metaplastic gene induction but blocked cell cycle re-entry at S-phase. In kidney and liver regeneration and in human gastric metaplasia, mTORC1 also correlated with proliferation. In lysosome-defective *Gnptab*^{-/-} mice, both metaplasia-associated gene expression changes and mTORC1-mediated proliferation were deficient in pancreas and stomach. Our findings indicate differentiated cells become proliferative using a sequential program with intervening checkpoints: (i) differentiated cell structure degradation; (ii) metaplasia- or progenitor-associated gene induction; (iii) cell cycle re-entry. We propose this program, which we term “paligenosis”, is a fundamental process, like apoptosis, available to differentiated cells to fuel regeneration following injury.

A4.2 Introduction

In 1900, George Adami wrote about the relationship between mitotic and differentiated cells, stating that he expected mitotic cells would generally devote energy toward replication and differentiated cells toward performing physiological functions (Adami, 1900). He also observed that upon injury, differentiated cells had the capacity to revert to a more primitive state, becoming mitotic again to promote tissue repair. Adami's observations on such cellular plasticity

have largely been forgotten, as the focus in the 20th century was nearly exclusively on the unidirectional differentiation of stem cells into functional, “post-mitotic” cells.

However, over the past decade or two, numerous examples have emerged to support plasticity in differentiated cells. First, it became clear that normal, somatic cells could be reprogrammed to pluripotency (Takahashi & Yamanaka, 2006). Furthermore, in tissues, injury can induce a repair process that recruits largely post-mitotic, differentiated cells back into the cell cycle in most, if not all, organs and species, for example, glia (Boerboom et al, 2017; Mindos et al, 2017); lung (Logan & Desai, 2015); heart in mammals (Wang et al, 2017) and fish (Karra et al, 2015); in multiple gastrointestinal tract organs (Mills & Sansom, 2015). Each such example to date has been studied essentially in isolation within the context of a particular type of injury and a single organ; however, because the process is so widespread, we have postulated that it may be governed by a shared, evolutionarily conserved molecular and cellular program that is independent of tissue and species (Mills & Sansom, 2015).

It has long been known that the response of both the corpus of the stomach and the digestive-enzyme-secreting (exocrine) pancreas to certain types of injury involves phenotypical changes in cell differentiation and tissue architecture, known as metaplasia. In the acute setting, the metaplastic response appears to be a tissue repair mechanism and can be temporary, with full restoration of normal tissue architecture (Nomura et al, 2005; Huh et al, 2012). Chronically, however, ongoing damage and long-term metaplasia are associated with and may fuel the majority of gastric and pancreatic adenocarcinomas (Mills & Sansom, 2015; Giroux & Rustgi,

2017; Storz, 2017). In both organs, the cells of origin for the metaplastic, proliferating epithelial cells are thought to be differentiated secretory cells (zymogenic chief cells in the stomach and acinar cells in the pancreas) that reprogram to re-enter the cell cycle (Mills & Sansom, 2015; Murtaugh & Keefe, 2015; Mills & Goldenring, 2017; Radyk & Mills, 2017).

Here, we report that differentiated cells in both pancreas and stomach exhibit high levels of mTORC1 activity during homeostasis. Proliferation-inducing injury caused rapid mTORC1 loss and a dramatic induction of autodegradative machinery (lysosomes and autophagy). As the functional and structural components were recycled, cells changed gene expression patterns (e.g., inducing the metaplastic marker Sox9); thereafter, they reactivated mTORC1 and re-entered the cell cycle. Such changes in mTORC1 activity were corroborated in tissues from human patients. Also, established models of injury to differentiated cells in mouse liver (Espeillac et al, 2011) and kidney (Chang-Panesso & Humphreys, 2017) correlate mTORC1 activity with the recruited proliferating cells. Blocking mTORC1 with rapamycin in murine pancreas and stomach impaired only cell cycle re-entry but not earlier cellular changes. Differentiated cells in autophagy-defective *Gnptab*^{-/-} mice were blocked from both SOX9 expression and cell cycle re-entry phases, consistent with the upstream autodegradative phase being necessary for downstream mTORC1-mediated S-phase entry.

Our results in the context of numerous previous reports on cellular reprogramming lead us now to propose that recruiting differentiated cells into a regenerative phenotype occurs via stepwise metabolic and molecular phases that constitute a conserved, fundamental, cellular program, akin

to mitosis or apoptosis. This cellular program occurs during cell fate changes of various types (e.g., reversion, dedifferentiation, transdifferentiation, reprogramming). The lack of a standard term for the actual cellular process itself impedes finding shared features that transcend cell types, tissues, and model systems. We propose a new, unifying term: “paligenosis” from the Greek: pali/n/m (meaning backward or recurrence) + genea (born of, producing) + osis (an action or process).

A4.3 Diverse organs show similar changes in metabolic activity during acute injury

To induce injury in the stomach, we employed a high-dose tamoxifen (“HD-Tam”) injury model that has been used by us and others (Huh et al, 2012; Burkitt et al, 2017; Lee et al, 2017; Leushacke et al, 2017). HD-Tam causes loss of nearly all acid-secreting parietal cells in the body of the stomach (Figures A4.1) and induces mature, differentiated digestive-enzyme-secreting chief cells at the base of the unit to give rise to a proliferating cell population (Radyk et al, 2017). These former chief cells maintain low-level expression of some mature chief cell markers and induce expression of wound repair-associated genes like mucins and TFF2 (aka spasmolytic polypeptide). The pattern of parietal cell loss and abundant, proliferative cells co-expressing TFF2 and chief cell markers has been called spasmolytic polypeptide-expressing metaplasia (SPEM) or pseudopyloric metaplasia (Schmidt et al, 1999). Maximal parietal cell loss and proliferation stemming from chief cells occurs at 3 days after the first dose of tamoxifen (Schematized in Figure A4.2). By 7 days, parietal cells have returned, and the entire stomach regenerates to pre-treatment cell censuses within 14–21 days (Huh et al, 2012). HD-Tam is a rapid, synchronous method to model, in a manner that lends itself to molecular analyses, the

mechanisms of stomach repair that also occurs in human stomachs infected with the bacterium *Helicobacter pylori*.

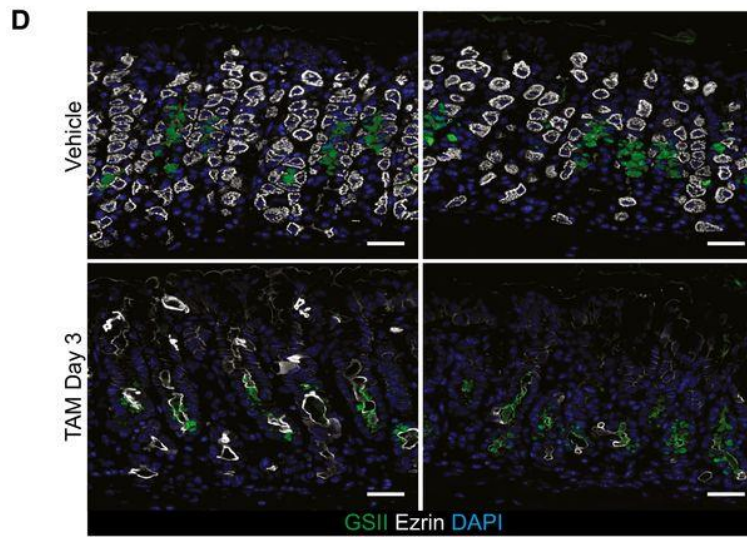
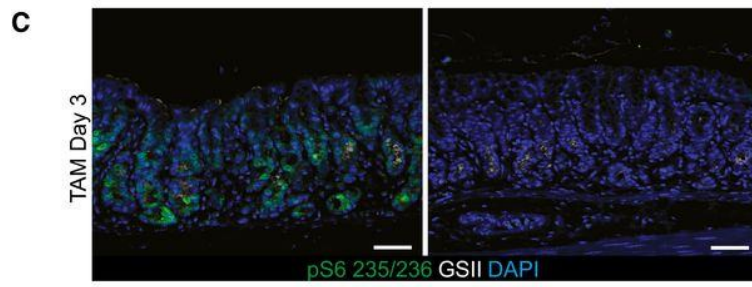
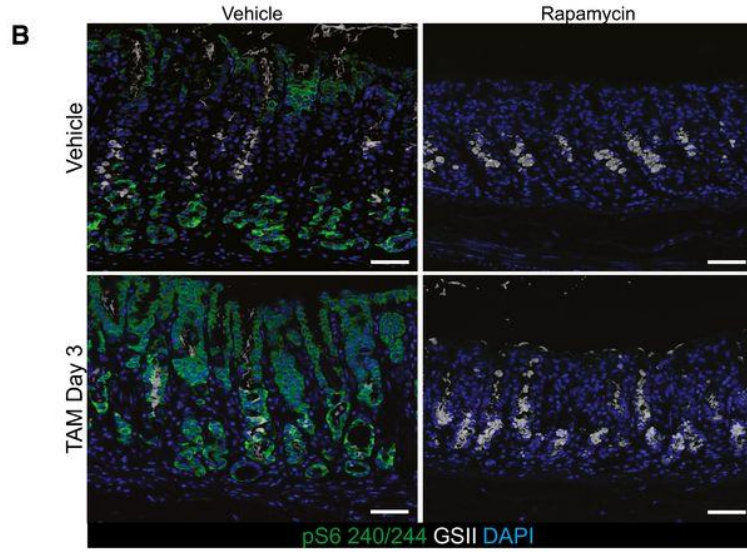
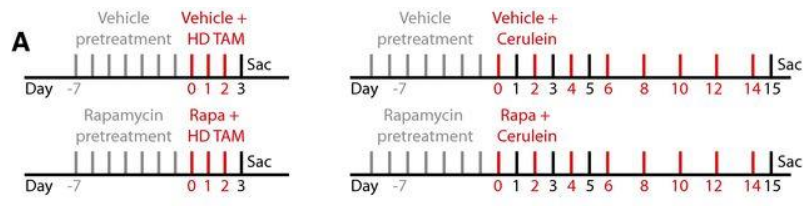


Figure A4.1: pS6 is an accurate proxy for rapamycin-sensitive mTORC1 activity and shows that loss of mTORC1 does not affect parietal cell death or induction of metaplastic gene expression in reprogramming chief cells.

A) Injection schemes for injury experiments with rapamycin in stomach (left) and pancreas (right). **B)** Representative epifluorescence images of the distribution of pS6 in the normal and injured stomach \pm rapamycin treatment. pS6 is restricted to the chief cell zone (base) and pit zone of the normal corpus unit. At peak (HD-Tam day 3) SPEM stages, it is located at high level throughout the unit. Upon rapamycin treatment, all pS6 staining is lost throughout the normal and injured corpus unit. The characteristic induction of GSII staining in reprogramming chief cells at the base of gastric units (indicating SPEM) occurs at least as markedly in the presence of rapamycin, indicating mTORC1 is not required for metaplastic gene induction. Green, pS6; white, GSII; blue, DAPI. Scale bars: 50 μ m. **C)** At peak metaplasia stages, pS6 235/6 is upregulated in the stomach epithelium and rapamycin treatment at this stage abolishes all staining. Scale bars: 50 μ m. **D)** Representative epifluorescence images of the loss parietal cells (marked by ezrin) upon injury and rapamycin treatment. Treatment with HD-Tam caused the loss of the vast majority of parietal cells throughout the corpus. Rapamycin does not rescue that injury. Green, GSII; white, ezrin; blue, DAPI. Scale bars: 50 μ m.

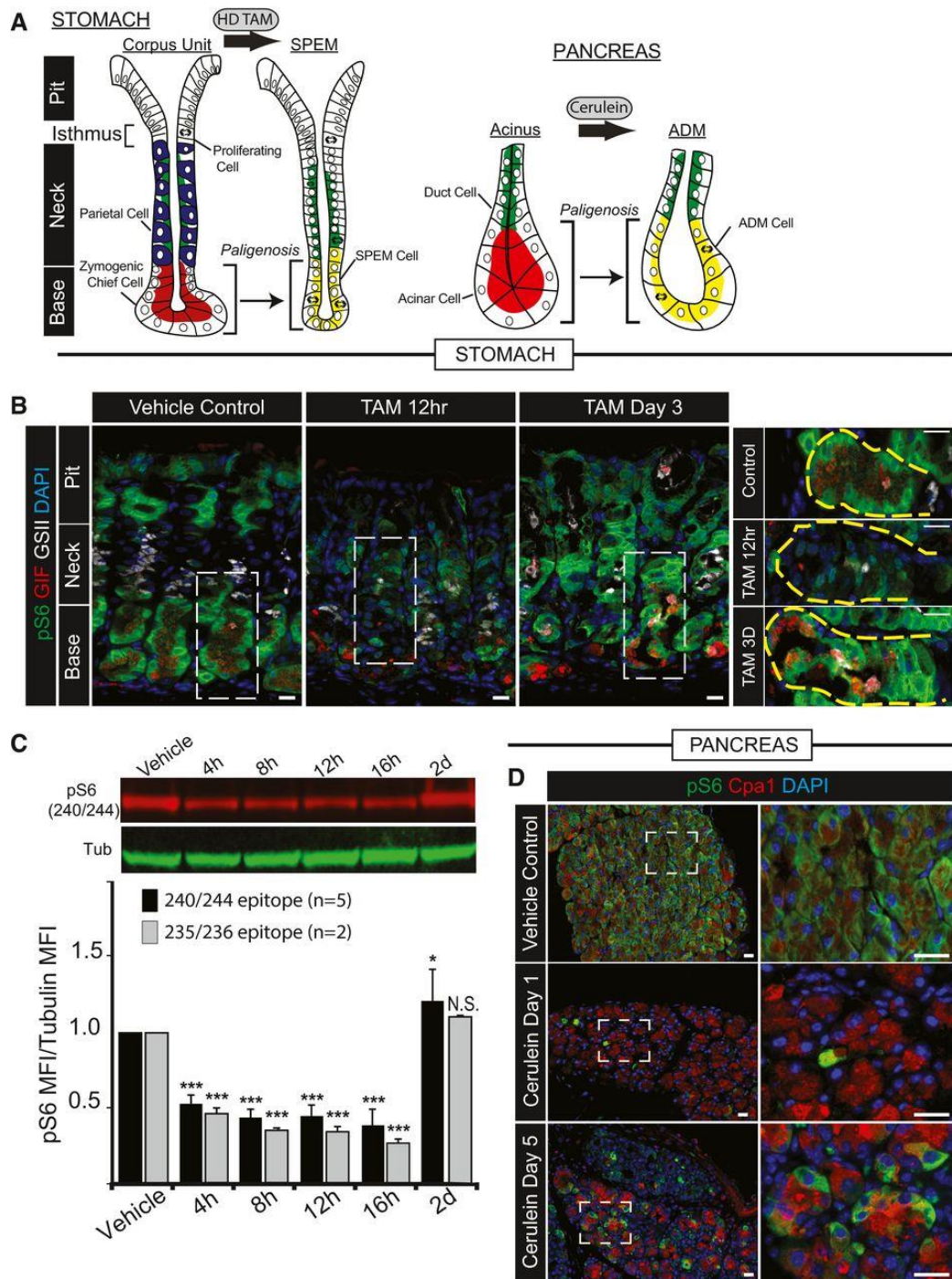


Figure A4.2: mTORC1 activity undergoes dramatic changes during stomach and pancreas metaplastic injury response.

A,B Digestive-enzyme-secreting (zymogenic) mature cell populations in the stomach (A) and pancreas (B) are recruited back into the cell cycle to fuel metaplasia in response to large-scale injury. Digestive enzyme expression (red) decreases, and markers of mucous neck cells (green,

stomach) or duct cells (green, pancreas) increase in metaplastic, proliferating cells (red + green = yellow). Stomach is further characterized by loss of acid-secreting parietal cells (blue). (B) Representative epifluorescence images of mouse gastric corpus glands during homeostasis, early after injury (HD-Tam 12 h) and at maximal metaplastic response (HD-Tam Day 3), stained for mTORC1 activity using a downstream target, pS6 as a proxy. Green, pS6; red, GIF (gastric intrinsic factor, a chief cell marker); white, GSII (a mucous neck cell marker); blue, DAPI. Right—higher magnification images of boxed areas on left focus exclusively on the base of the unit where the digestive-enzyme-secreting cells are reprogramming. Yellow dashed area outlines the base of a single gastric unit. Scale bar, 20 μm ; boxed area pull out, 10 μm . C) Western blot of pS6 (red) and β -tubulin control (green) from whole corpus protein extracts at various injury time points; pS6 (240/244 or 235/6) vs. tubulin fluorescent intensity from replicate blots quantified below (error bars = standard deviation). * $P < 0.05$, *** $P < 0.001$. Statistical analysis with both antibodies was done using ANOVA with a post hoc Dunnett's test. D) Representative epifluorescence images of pS6 staining of pancreas during homeostasis, acute injury (cerulein 12 h), and maximal injury (cerulein day 5). Green, pS6; red, amylase; blue, DAPI. Boxed areas on left depicted at higher magnification on right. Scale bar, 20 μm ; boxed area pull out, 10 μm .

To induce injury in pancreas, we used a well-described rapid method involving daily injection of the secretagogue cerulein. Cerulein injections cause large-scale damage to the digestive-enzyme-secreting acinar cells of the exocrine pancreas (Adler et al, 1985; Niederau et al, 1985; Saluja et al, 1985). To repair the damage, acinar cells re-enter the cell cycle, forming duct-like structures called ADM (acinar-to-ductal metaplasia; schematic in Figure A4.2). In our protocol, ADM peaks 5 days after commencement of cerulein. Thereafter, there is continued damage if cerulein administration is maintained, but the pancreas gradually adapts to the injury over 2 weeks. Similar to HD-Tam injury in the stomach, cerulein injury models a metaplastic process that can also be a precursor for pancreatic ductal adenocarcinoma.

To determine whether the reversion from the differentiated to the replicative state involves conserved shifts in cellular energy use, we examined metabolic activity in both tissues using phosphorylated ribosomal S6 protein (pS6). The principal mediator of S6 phosphorylation is the

S6 kinase enzyme via the cellular metabolism hub mTOR complex 1 (mTORC1). To confirm that S6 phosphorylation depends on mTORC1 activity, we treated mice with rapamycin, a specific inhibitor of the mTORC1-mediated S6 kinase activity. We used an antibody against residues 240/244 of S6, because those sites are phosphorylated principally by pS6 kinase 1, whereas the 235/236 phosphorylation sites can have input from other signaling pathways. For example, 235/236 can be phosphorylated by p90 ribosomal S6 kinases that can be activated via ERK signaling (Roux et al, 2007). Figure A4.1 shows that rapamycin, which is a specific inhibitor of mTORC1-mediated S6 Kinase activity, abolished pS6 240/44 staining, which was normally abundant in gastric pit cells nearer the stomach lumen and in gastric chief cells. Rapamycin also blocked S6 phosphorylation efficiently during the HD-Tam protocol (Figure A4.1). Antibodies against 235/236 also showed strong phosphorylation at peak metaplasia as well as a similar abrogation of staining in the presence of rapamycin (Figure A4.1). As anti-240/244 antibodies have stronger signal in our experiments and are more specific for mTORC1-mediated phosphorylation, we will use anti-240/244 pS6 as a surrogate for mTORC1 activity for the remainder of the manuscript unless otherwise mentioned.

HD-Tam or cerulein caused dramatic changes in pS6 expression. In stomach, pS6 was largely lost by 12 h. By 3 days, when SPEM is maximal in this system, the entire gastric unit expressed abundant pS6 (Figure A4.2B). Molecular and cellular changes in the stomach following HD-Tam are sufficiently synchronous across the whole stomach that quantitative, molecular approaches can be used (Huh et al, 2012). Quantitatively, phosphorylation status of both pS6 240/244 and 235/236 in the corpus of the stomach was decreased by nearly half within the first 4 h and

returned to at or above baseline by 48 h (Figure A4.2C). In pancreas, despite a slower and less synchronous time course, the same pattern of mTORC1 activity could be observed by immunofluorescence. pS6 was abundant in acinar cells at baseline, was nearly undetectable by 24 h, and recovered in many cells by day 5, when ADM is maximal (Figure A4.2D).

Thus, both tissues, when recruiting proliferative cells for repair, undergo a well-defined pattern of changes in mTORC1 activity. During homeostasis, the organs are replete with differentiated secretory cells that are not dividing but are energetically active in synthesizing protein using their elaborate secretory apparatus (Mills & Taghert, 2012; Lo et al, 2017). When replicating cells must be recruited from those differentiated cells, the cells shut off mTORC1 temporarily, then re-induce it at the time of maximal regenerative proliferation.

To further assess whether the upregulation of pS6 is a common feature during the recruitment of differentiated cells to regenerate damaged tissue, we examined liver (two-thirds partial hepatectomy) and kidney (tunicamycin-induced acute injury) for changes in S6 phosphorylation. Both injury models have previously been shown to involve recruitment of differentiated cells back into the cell cycle (Newberry et al, 2008). In kidney, as expected, tubules in the cortex and outer medulla are damaged as evinced by vacuolation (Figure A4.3). Non-damaged tubules show increased BrdU as cells re-enter the cell cycle (Figure A4.3). The proliferative tubules show marked increase in pS6. Similarly, the well-known recruitment of hepatocytes into the cell cycle 48 h following partial hepatectomy is also accompanied by increased S6 phosphorylation (Figure A4.3).

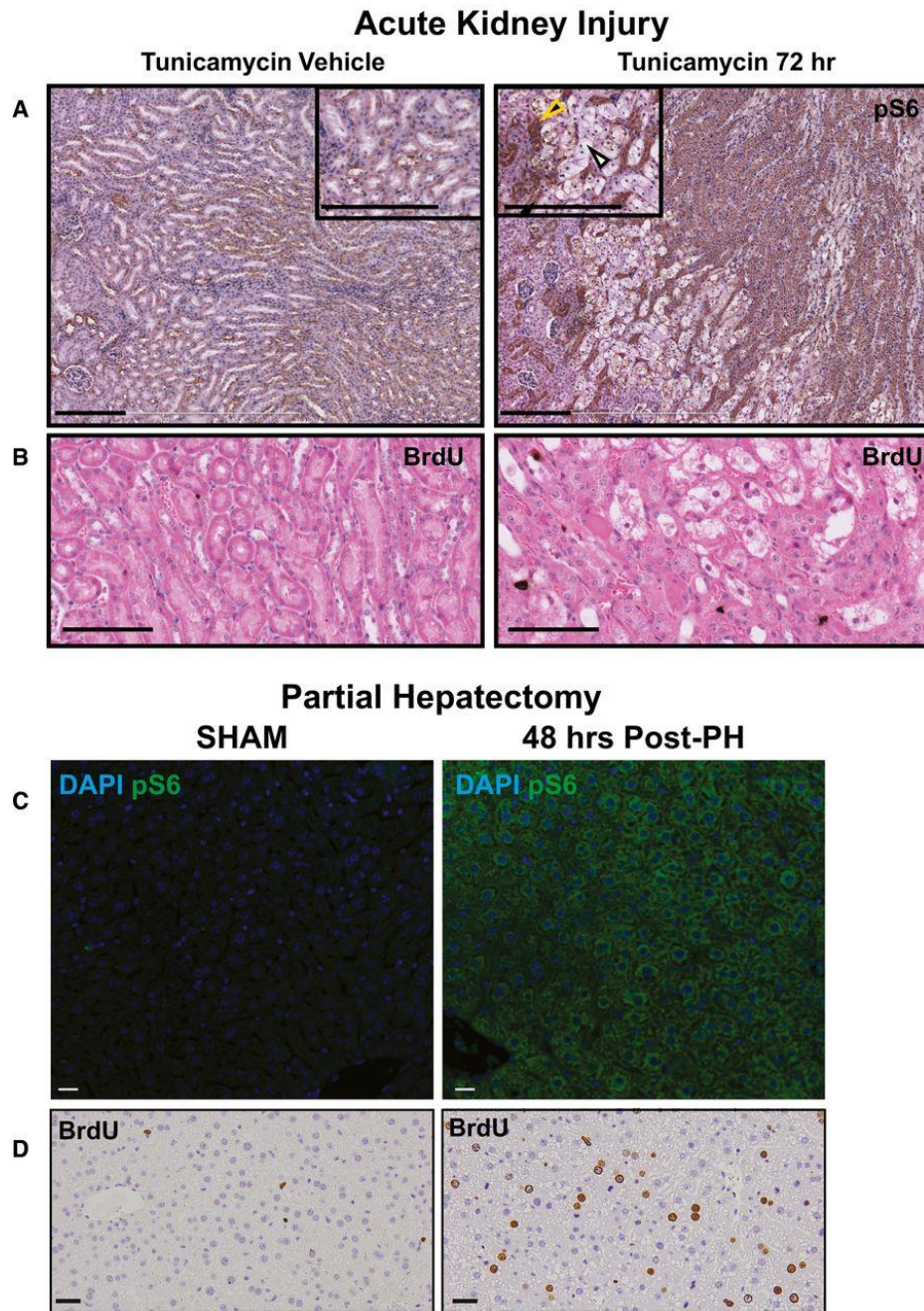


Figure A4.3: Acute kidney injury and partial hepatectomy both cause upregulation of mTORC1 activity during proliferative phases.

A) Upon injury with tunicamycin, tubule cells in the kidney are damaged (white arrowhead) and surviving tubule cells (yellow arrowhead) upregulate pS6. Scale bars: 100 μ m. **B)** Upregulation of the pS6 is associated with increased proliferation in this injury model as seen by BrdU+ nuclei. Scale bars: 100 μ m. **C)** Two-thirds partial hepatectomy causes a pronounced upregulation of pS6 in the remaining hepatocyte mass. Scale bars: 20 μ m. **D)** The pS6+ hepatocytes are highly proliferative at this stage. Scale bars: 20 μ m.

A4.4 mTORC1 is required for injury-induced proliferation

During SPEM and ADM, expression of genes encoding secretory cargo (like digestive enzymes) is scaled down, whereas wound repair and progenitor-associated genes are scaled up (Capoccia et al, 2013). Many such scaled up genes (e.g., Cd44 and Sox9) are increased in both pancreas and stomach during the recruitment of differentiated cells back into the cell cycle. To determine whether blocking mTORC1 affected response to injury, we subjected mice to HD-Tam or cerulein and examined the effects of blocking mTORC1 with rapamycin (Figure A4.4). Figures A4.1 and A4.4 show that parietal cell death occurred in HD-Tam even without mTORC1 activity. The gastric units also remodeled as expected with chief cells assuming the ductular morphology, characteristic of SPEM (Figure A4.4).

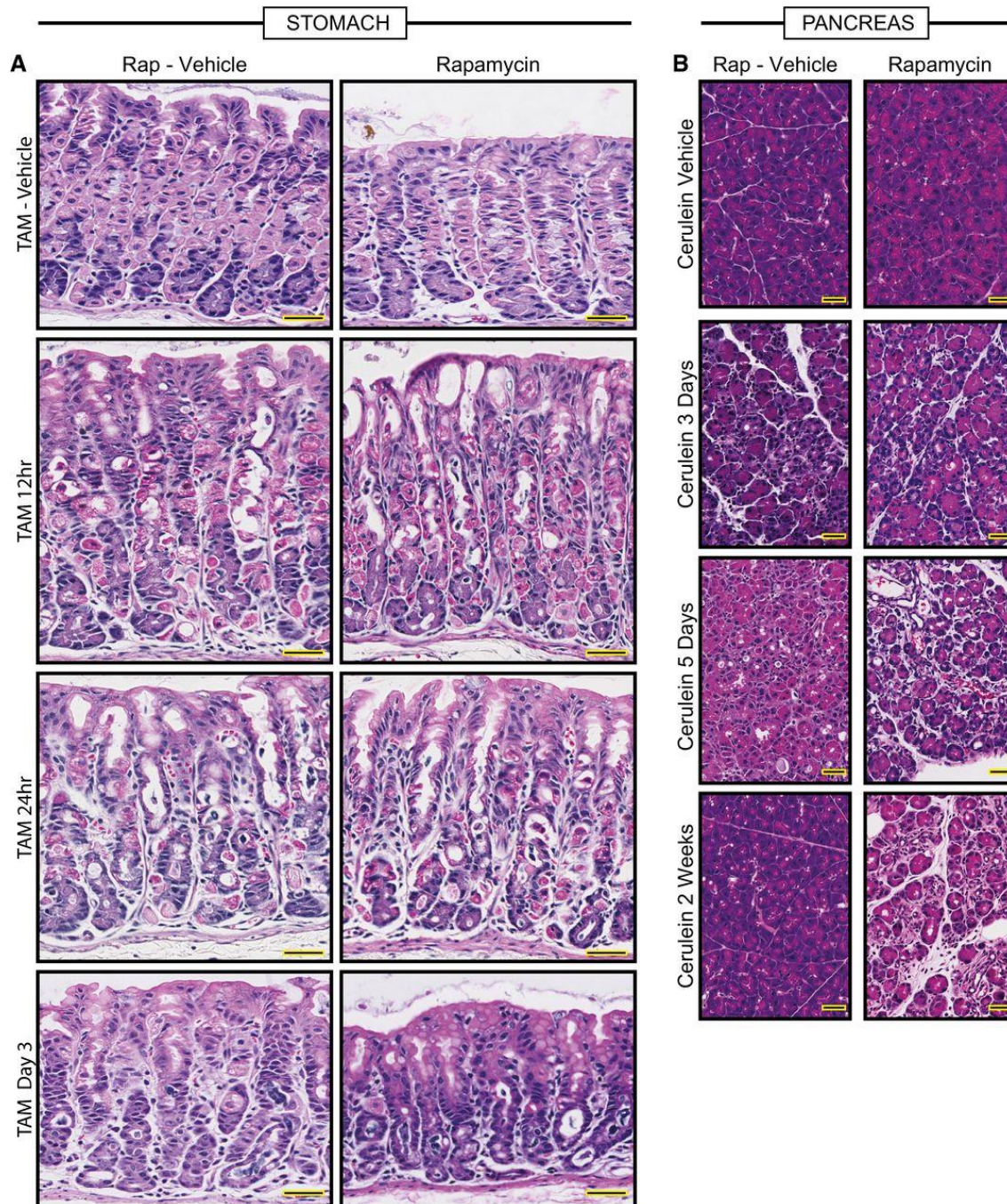


Figure A4.4: Histological changes in the injured stomach and pancreas with and without rapamycin treatment.

A) Representative hematoxylin and eosin counterstained images of HD-TAM stomach tissue \pm rapamycin. Treatment with tamoxifen causes acute loss of parietal cells (large eosinophilic cells) by 12–24 h post-injury. By 3 days, chief cells have reprogrammed into SPEM cells. The general pattern of loss of parietal cells and conversion of chief cells to metaplastic cells is not affected by rapamycin (right panels). Scale bars, 50 μ m. **B)** Representative hematoxylin and eosin counterstained images of pancreas tissue injured with cerulein at various stages

±rapamycin. Cerulein injury causes mosaic, asynchronous conversion of acinar cells into proliferative, acinar-ductal metaplastic cells with maximal features of the process at day 5 in our protocol. By 2 weeks, the pancreas has compensated for the continuous injury and recovers a relatively normal morphology. Dual treatment with rapamycin and cerulein does not rescue the metaplastic response by day 5 and impedes normal tissue compensation by 2 weeks injury, with most of the tissue continuing to show abundant metaplastic forms. Scale bars, 50 μ m.

We next examined the effects of rapamycin on induced proliferation. We noted that in control experiments, without HD-Tam, proliferation of the cells in the isthmus (the narrow zone between pit and upper neck, Figure A4.2), where there is active mitosis in homeostasis, was not affected markedly by rapamycin (Figures A4.5A and C). However, rapamycin decreased the injury-induced proliferation by nearly half ($P < 0.001$; Figure A4.5C). The lack of proliferation did not affect SPEM induction, as defined by cells co-stained with GSII and the chief cell marker, GIF (Figure A4.5A and B). Indeed, the SPEM marker SOX9 was induced in reprogramming chief cells to levels at least as high as those observed in HD-Tam without rapamycin (Figure A4.6). That cells expressing molecular features of metaplasia can arise in the absence of proliferation is consistent with multiple previous reports showing that chief cells can give rise directly to SPEM cells without contribution from the isthmal stem cell (Nam et al, 2010; Radyk et al, 2017).

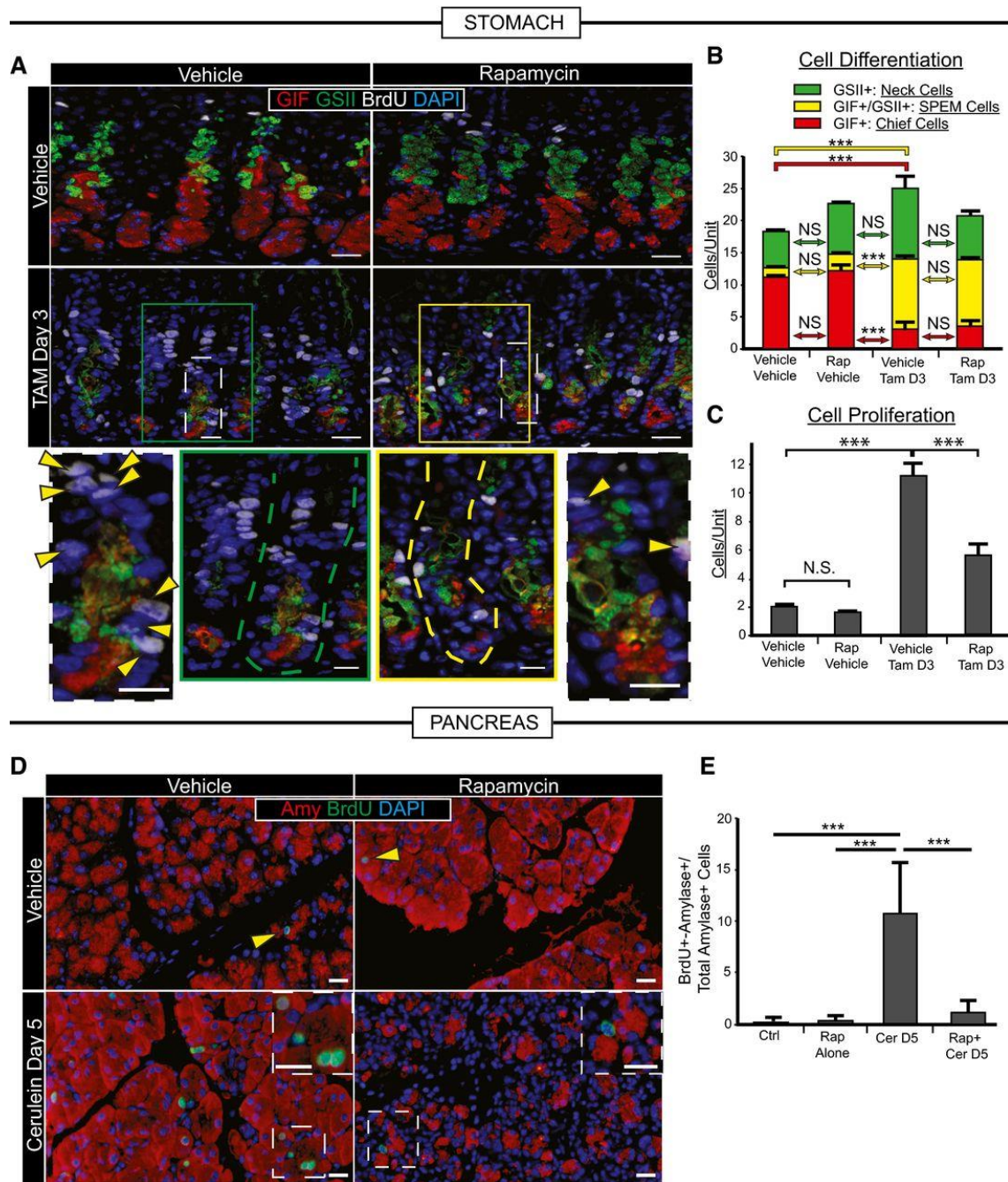


Figure A4.5: Recruitment of proliferating cells during stomach and pancreas metaplastic injury depends on mTORC1.

A) Representative immunofluorescence images of stomach tissue \pm metaplastic injury \pm rapamycin treatment. Green, neck cells (GSII); red, chief cells (GIF); white, proliferating cells (BrdU); blue, nuclei (DAPI). Scale bars 20 μ m; 10 μ m for bottom images. Bottom—boxed areas from top pictures are shown at higher magnification with individual bases of gastric units (where reprogramming occurs) outlined by dashed lines and proliferating cells by arrowheads. **B**) Cells of each differentiation type, following scheme in Figure A4.2, are quantified by scoring

immunofluorescence images from multiple experiments. Metaplastic injury induces a massive accumulation of yellow (SPEM) cells and loss of red (Chief) cells (compare vehicle–vehicle with vehicle-Tam, D3) that is not significantly affected by rapamycin treatment (compare vehicle-Tam D3 with Rap-Tam D3). **C**) Proliferative cells are quantified as for panel (B). Injury induces massive proliferation (compare vehicle–vehicle with vehicle-Tam D3) significantly inhibited by rapamycin (compare vehicle-Tam D3 with Rap-Tam D3). **D**) Top panel arrowheads indicate rare proliferative acinar cells during homeostasis with or without rapamycin treatment. Cerulein induces proliferation of acinar cells recruited into the cell cycle that is inhibited by rapamycin. Boxed areas are magnified in insets. Note multiple BrdU⁺ cells (green) staining with amylase (red) a digestive enzyme, indicating acinar cell origin. BrdU⁺ cells following rapamycin + cerulein treatment are often not co-stained with amylase. Blue, DAPI (nuclei). Scale bars 20 μm ; 10 μm for insets. **E**) Quantification of multiple experiments with mice treated as in panel (D).

Data information: *** $P < 0.001$; N.S. = not statistically significant; data displayed as mean \pm SEM from 3 independent experiments with quantification from up to 13 low-power fields, from each of 4–5 total mice; significance determined by ANOVA with Tukey's post hoc test.

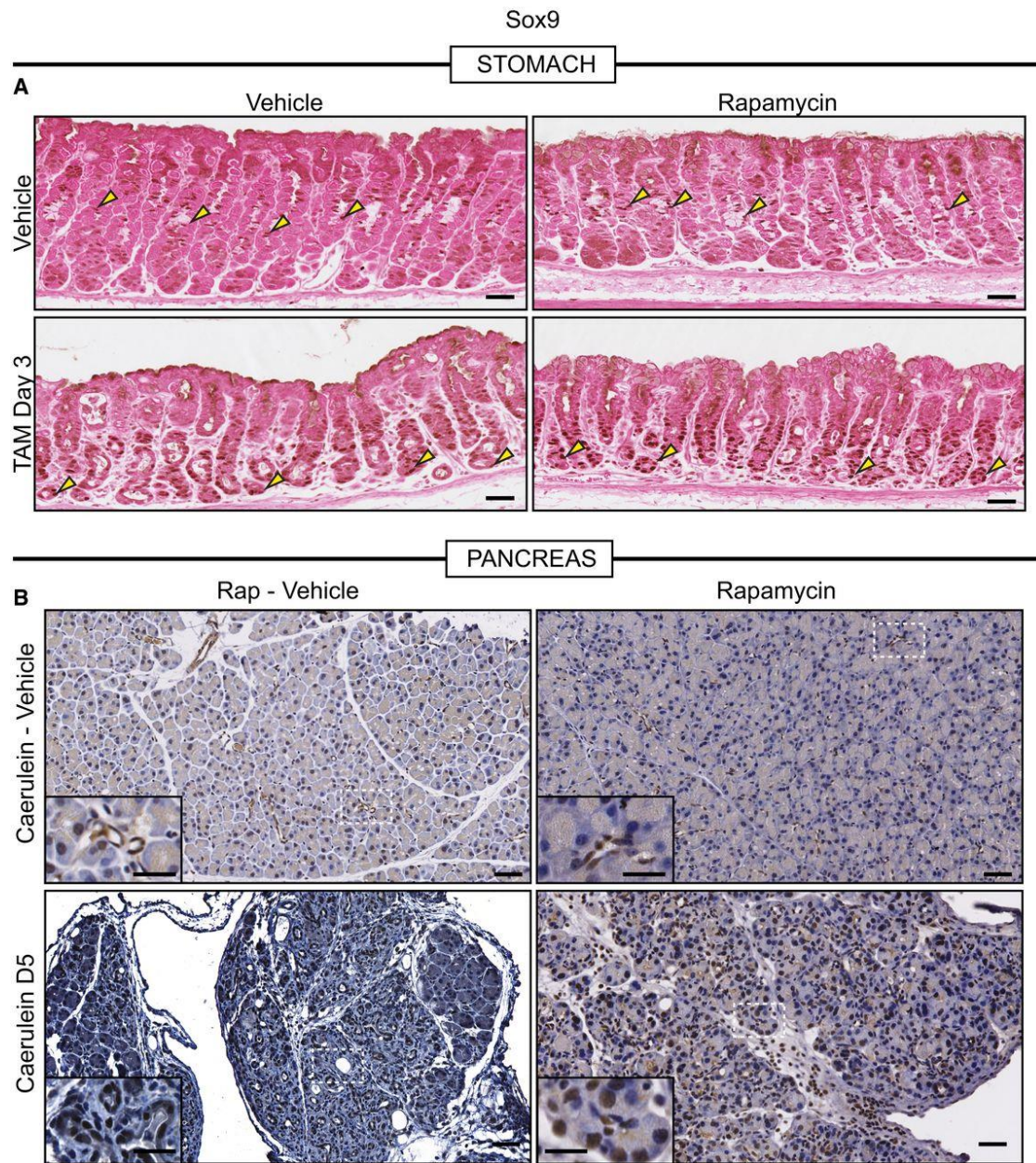


Figure A4.6: mTORC1 is not required for increased SOX9 during metaplasia.

A) Representative eosin counterstained IHC images of normal or metaplastic gastric tissue stained for SOX9. SOX9, in control tissue, stains the isthmal and mucous neck cells, which are proliferative progenitors (yellow arrowheads), of the corpus units and is generally excluded from the base of units. Upon injury with HD-TAM, SOX9 expression is induced in the base of units (yellow arrowheads). Treatment with rapamycin does not alter either the normal or metaplasia distribution of SOX9 (yellow arrowheads). Scale bars, 50 μ m. **B)** Representative hematoxylin counterstained IHC images of normal or metaplastic pancreatic tissue stained for SOX9. SOX9 expression in normal pancreatic tissue is restricted to the duct (see inset in top left panel which is

a high magnification view of the boxed area). At peak metaplasia stages, SOX9 becomes expressed in dedifferentiating acinar cells (see bottom left inset). Treatment with rapamycin in normal (see top right inset) or injured (see bottom right inset) does not alter SOX9 expression. Scale bars 50 μm ; inset 25 μm .

Rapamycin had equivalent effects on the pancreas. Metaplastic induction of SOX9 was not affected (Figure A4.6); however, cell proliferation was even more substantially blocked than in the stomach (Figure A4.5D and E). This may be because the pancreas is entirely dependent on reprogramming acinar cells as a source for proliferation, whereas the stomach also has a constitutive stem cell that continues to proliferate even in the presence of rapamycin (Figure A4.2). Continued HD-Tam injections kill mice, so we cannot study adaptation of stomachs; however, we have maintained cerulein injections for up to 2 weeks by which point wild-type pancreas usually adapts to the injury. Thus, we used the pancreas to determine whether mTORC1-dependent proliferation was required for pancreatic repair. Figure A4.4 shows that 2-week cerulein with mTORC1 blocked led to tissue loss relative to cerulein treatment alone.

A4.5 Changes in mTORC1 also characterize human metaplasia

To determine whether mTORC1 activity is modulated in human disease states, we first examined a database of stomach tissues from human patients exhibiting metaplastic response to *H. pylori* infection, previously compiled at Washington University (Lennerz et al, 2010; Radyk et al, 2017). A representative region from this dataset is shown in Figure 3A. As in mice, morphologically normal chief cells showed high pS6. In regions of SPEM, pS6 abundance varied. In lesions that had histological features of cells undergoing acute conversion to SPEM (what we have previously termed “hybrid SPEM” (Lennerz et al, 2010; Radyk et al, 2017) based on examination of a large dataset of SPEM lesions), pS6 levels were high (Figure 3A). In regions

where basal cells showed more uniform metaplasia (“established SPEM”), pS6 levels were lower. In humans, SPEM is thought to be either transient and rapidly resolve (as in the mouse HD-Tam model) or chronic and persist for decades, involving large patches of the stomach (Peterson, 2002). In the chronic case, SPEM is equivalent to the lesion pathologists call chronic atrophic gastritis (Rugge et al, 2008). In addition, SPEM is thought to progress to (or predate) another, proliferative, pre-cancerous lesion, intestinal metaplasia (Yoshizawa et al, 2007; Correa & Piazzuelo, 2012; Spechler et al, 2017) and to increase risk for progression to a cytologically atypical lesion, dysplasia, as well as to cancer itself.

To further clarify the link between mTORC1 activity and metaplastic changes in humans, we analyzed pS6 levels in gastric tissue microarrays (Figure A4.7) comprising tissue cores representing the following histological phenotypes: normal mucosa, SPEM, IM, dysplasia, and gastric adenocarcinoma. pS6 showed consistent, mid-level expression in nearly all normal mucosal samples, in agreement with our smaller sample showing expression of pS6 in normal chief cells and with our mouse data (Figure A4.8B). Both cancer and dysplastic lesions showed higher average pS6 expression, though there was also more variability in that over a third of such lesions showed much stronger expression than normal tissue, while about a third showed lower expression (Figure A4.8B). On average, intestinal metaplasia pS6 levels were close to those of normal mucosa (Figures A4.8B and A4.9). SPEM lesions showed a clear biphasic pattern with the majority like the “established SPEM” with low-to-no detectable pS6 (cf. Figures A4.8A and A4.9) but with some SPEM lesions having much stronger pS6 (Figures A4.8 and A4.9).

Total Sample Number	772
Normal Mucosa	100
SPEM	162
IM	163
Dysplasia	23
Cancer	324
Age Range	25-84
Average Age	64
Gender	
Male	448
Female	324

Figure A4.7: Patient Demographics.

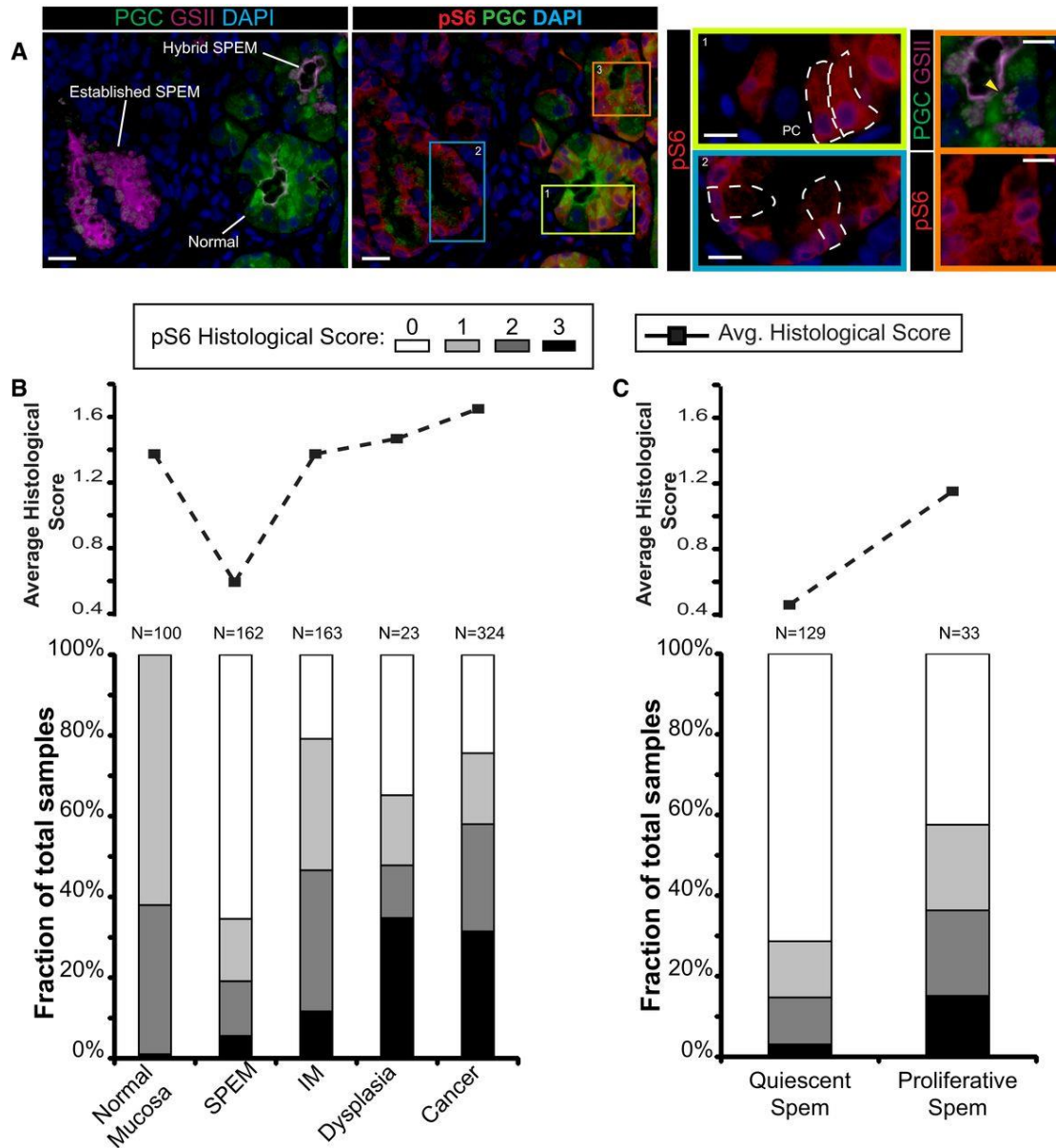


Figure A4.8: mTORC1 activity correlates with stages of metaplasia during human gastric tumorigenesis.

A) Immunofluorescent images of human gastric tissue from a patient with intestinal-type gastric adenocarcinoma elsewhere. In this non-carcinoma containing region of the gastric corpus, various states of metaplasia can be observed that reflect mouse injury models. Extensive previous work (Lennerz et al, 2010) of a dataset of such resection specimens and of biopsies showing SPEM in a non-cancer setting has indicated likely stages of progression of SPEM from essentially normal wherein large, pyramidal-columnar cells at the base express only chief cell markers like pepsinogen C (PGC, green) to “hybrid SPEM” (yellow arrowhead, inset) where smaller, cuboidal columnar cells label with varying degrees of PGC and the neck/SPEM cell marker GSII (purple) to “established SPEM” characterized by cells that label extensively with

GSII and have scant PGC; established SPEM cells are mucus-stuffed, with peripheral, basal, flattened nuclei (blue, DAPI). Higher magnification of each cellular phenotype is shown by color-coded box on right. As parietal cells are lost in SPEM, the remnant one in the yellow boxed area (labeled “PC”) is consistent with the normal chief cell phenotype (representative individual cells outlined by white dashed lines). Note that there is consistently high expression of pS6 (red) throughout the cytoplasm of such normal chief cells but that this pS6 varies in the hybrid SPEM lesion and is largely scaled down in the established SPEM region (note pS6 only around the nuclei of these cells). Scale bar, 20 μm ; pullouts 10 μm . **B**) Analysis of a human gastric tissue microarray with normal, metaplastic, and cancer tissue all represented from patients with resections for gastric cancer. Serial tissues sections of the array were stained by immunohistochemistry with pS6 or Ki67, counterstained with hematoxylin, and visually graded by blinded observers, supervised by a human pathologist, for staining intensity (from score 0 meaning undetectable to 3 most intense). Top—average histological score is plotted for each phenotype. Bottom—the relative fraction of tissue cores with each score is plotted (total scores of each type provided at the top of each column). **C**) Given the biphasic nature of the SPEM histological score and given that established SPEM, as observed in panel (A), shows decreased pS6, we separated all the SPEM lesions into Ki-67+ (“proliferative”) and Ki-67- (“quiescent”) and replotted as for panel (B).

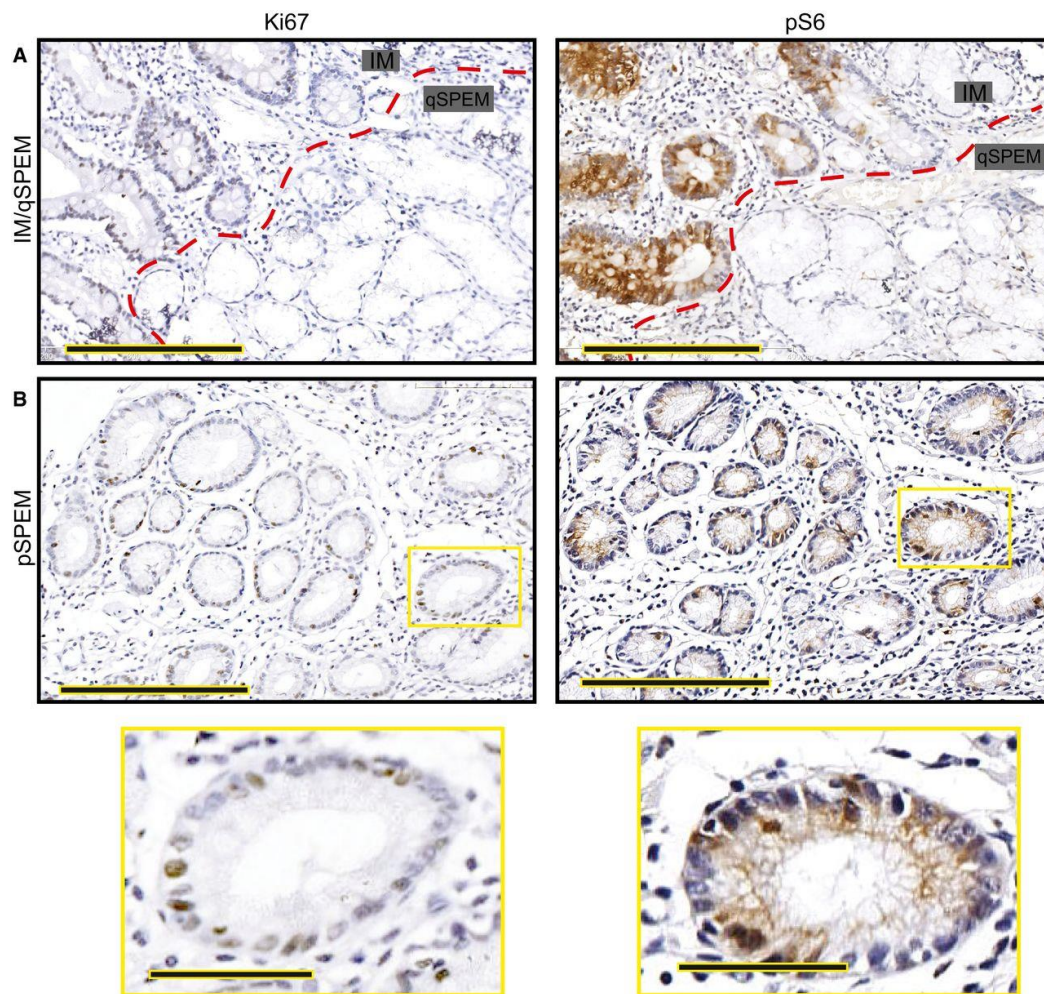


Figure A4.9: Representative IHC images from human tissue microarray.

A) Intestinal metaplasia (“IM” indicating the glands to upper left of red dashed line) is generally proliferative as evinced by frequent Ki-67+ cells (left) and is strongly pS6 positive. Most SPEM has a quiescent phenotype (glands labeled on “qSPEM” side of panels) characterized by cells with abundant mucus, flattened basal nuclei, and a lack of both Ki-67 and pS6 staining Scale bar, 200 μ m. **B)** Rare SPEM lesions show cells with cuboidal columnar morphology. These lesions show Ki-67 positivity usually associated with pS6 positivity. Boxed regions are shown at higher magnification below. Scale bar, 200 μ m; pullout, 50 μ m.

SPEM lesions with lower pS6 activity tended to express abundant mucin as well as epitope for the SPEM-identifying lectin GSII (Figure A4.9A); nuclei tended to be flat and eccentric (Figure A4.9). pS6-expressing SPEM cells were more cuboidal columnar, resembling the SPEM cells in the acute, proliferative mouse SPEM that resolves in a few days after HD-Tam. We hypothesized that SPEM with increased pS6 represented metaplastic cells that are actively proliferating (like D3 HD-Tam in mice) to repair an injury, whereas the decreased pS6 lesions of established SPEM may be mitotically quiescent. Hence, we divided the SPEM lesions into mitotically active (“proliferative SPEM”) and inactive (“quiescent SPEM”) based on Ki-67 staining of the same tissue core on another microtome section (Figure A4.9) and then correlated those phenotypes to the previously scored pS6 expression for that lesion. Proliferative SPEM was far more likely to be associated with pS6 expression, whereas quiescent SPEM was largely negative for pS6 (Figure A4.8C, $P < 0.001$ by χ^2). Thus, pS6 is low-moderate in normal, physiologically active mucosa and high in most lesions that have increased proliferation (proliferative SPEM, IM, dysplasia, cancer). We conclude that metabolic activity correlates with differentiation state and recruitment into the cell cycle in humans as well as mice.

A4.6 Loss of mTORC1 inhibits cell cycle progression at S-phase

Because gastric chief cells respond to injury more synchronously than pancreatic acinar cells, we are able to perform molecular analyses based on changes of gene expression. We used this approach to determine specifically where the block in cell cycle re-entry occurs when mTORC1 activity is inhibited. We analyzed Affymetrix GeneChips of whole gastric corpora \pm HD-Tam (3D) \pm rapamycin by Gene Set Enrichment Analysis (GSEA) with a combination of both a publicly available and custom gene sets. In a control experiment to validate our approach, we dissociated gastric epithelial cells from *Atp4b-Cre; ROSA26mTmG* mouse stomachs and used flow cytometry to isolate parietal cells (GFP+) from other epithelial cells (Tomato+). Expression of isolated, amplified RNA applied to GeneChips was analyzed by Partek Genomics Suite, and the 94 genes whose expression was enriched \geq eightfold in parietal cells vs. other epithelial cells was computed. As expected, GSEA showed that these PC-enriched genes were highly preferentially expressed in control stomachs vs. HD-Tam stomachs; the addition of rapamycin did not affect this pattern (Figure A4.10). Thus, global gene expression profiling with GSEA can detect the loss of parietal cells that epitomizes HD-Tam-induced metaplasia and also shows that parietal cell loss is independent of mTORC1, consistent with the histological data. In another control experiment, we performed GSEA of a published gene set of mature chief cell enriched genes (Capoccia et al, 2013) and contrasted HD-Tam vs. HD-Tam + rapamycin. There was no substantial effect of rapamycin, suggesting that the change in chief cell gene expression induced by injury is also not substantially affected by loss of mTORC1 (Figure A4.10).

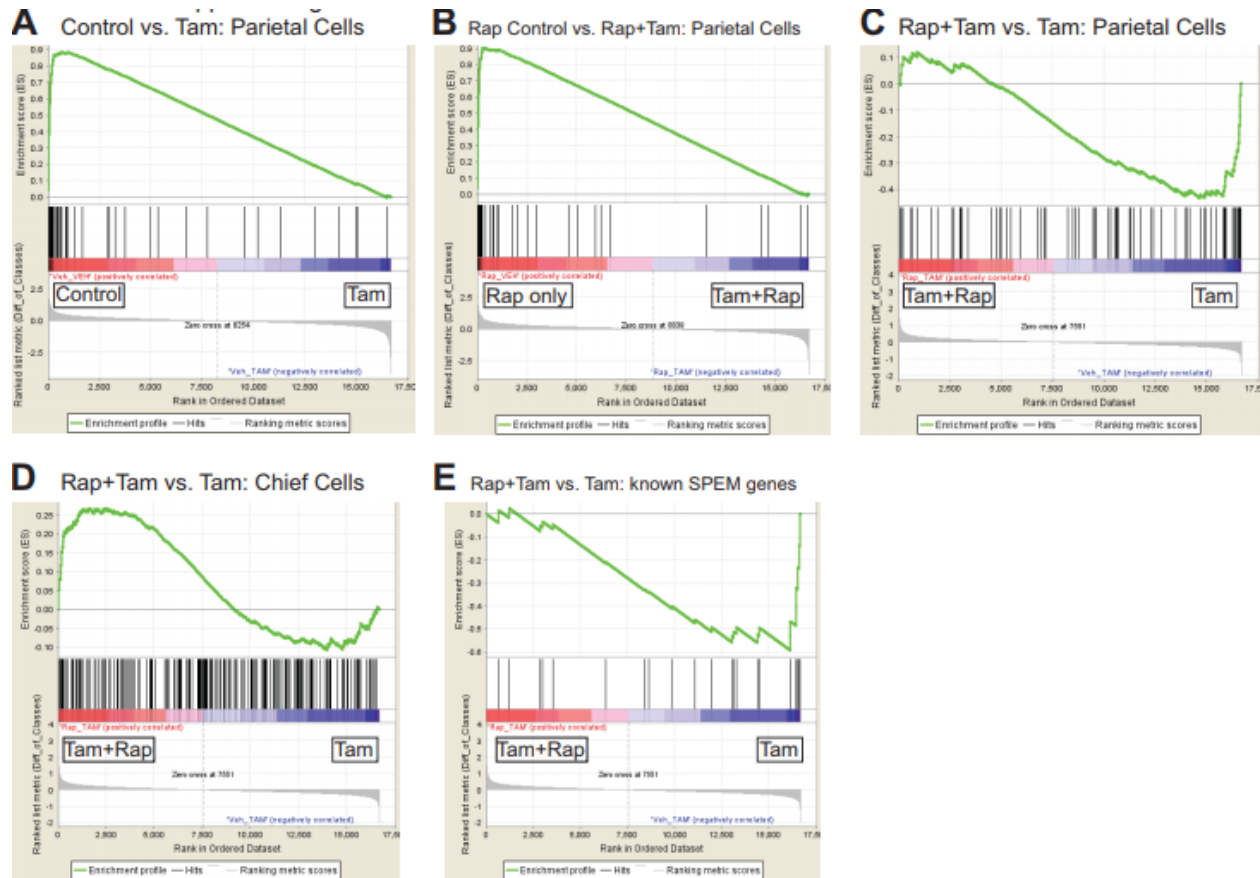


Figure A4.10: Gene Set Enrichment Analyses for Rapamycin + Tamoxifen experiments.

On the other hand, although many transcripts from a previously published gene set of SPEM-associated genes (Nozaki et al, 2008) did not show particular changes when rapamycin was administered in HD-Tam, there was a cluster of genes enriched only when mTORC1 levels were normal (Figure A4.10). Injury that causes metaplasia induces both wound-healing-associated genes (e.g., Clu, Sox9, CD44v) and proliferation-associated genes. Given that rapamycin blocks proliferation specifically in our histological analysis, we next examined the effects of rapamycin on the cell cycle using GSEA. Figure A4.11A shows that, indeed, rapamycin induces a marked de-enrichment of cell cycle gene expression in HD-Tam. The block appears specifically at the S-phase and beyond, as gene sets for G1-S, S, G2, and

G2-M showed that G1-S genes were relatively similarly distributed regardless of mTORC1 activity, whereas genes expressed during the later stages in the cell cycle were skewed toward the HD-Tam alone condition (Figure A4.11B–E). We used a slightly different approach to further investigate the interaction of mTORC1 with cell cycle stage by first determining the top 20 genes skewed most toward the HD-Tam (vs. vehicle-treated controls) in each cell cycle stage gene set. We then determined the average increased expression of those genes in both HD-Tam and HD-Tam + rapamycin vs. vehicle controls. Figure 4.11F shows that rapamycin decreased expression of the 20 top G1/S-phase HD-Tam-enriched genes by only $16 \pm 3\%$, whereas gene expression at other cell cycle stages was inhibited substantially more. Expression of G2/M-phase genes was decreased by $49 \pm 3\%$ with rapamycin treatment ($P < 0.001$, HD-Tam vs. HD-Tam + rapamycin in G2-M genes; $P < 0.05$ for G2-M vs. G1-S).

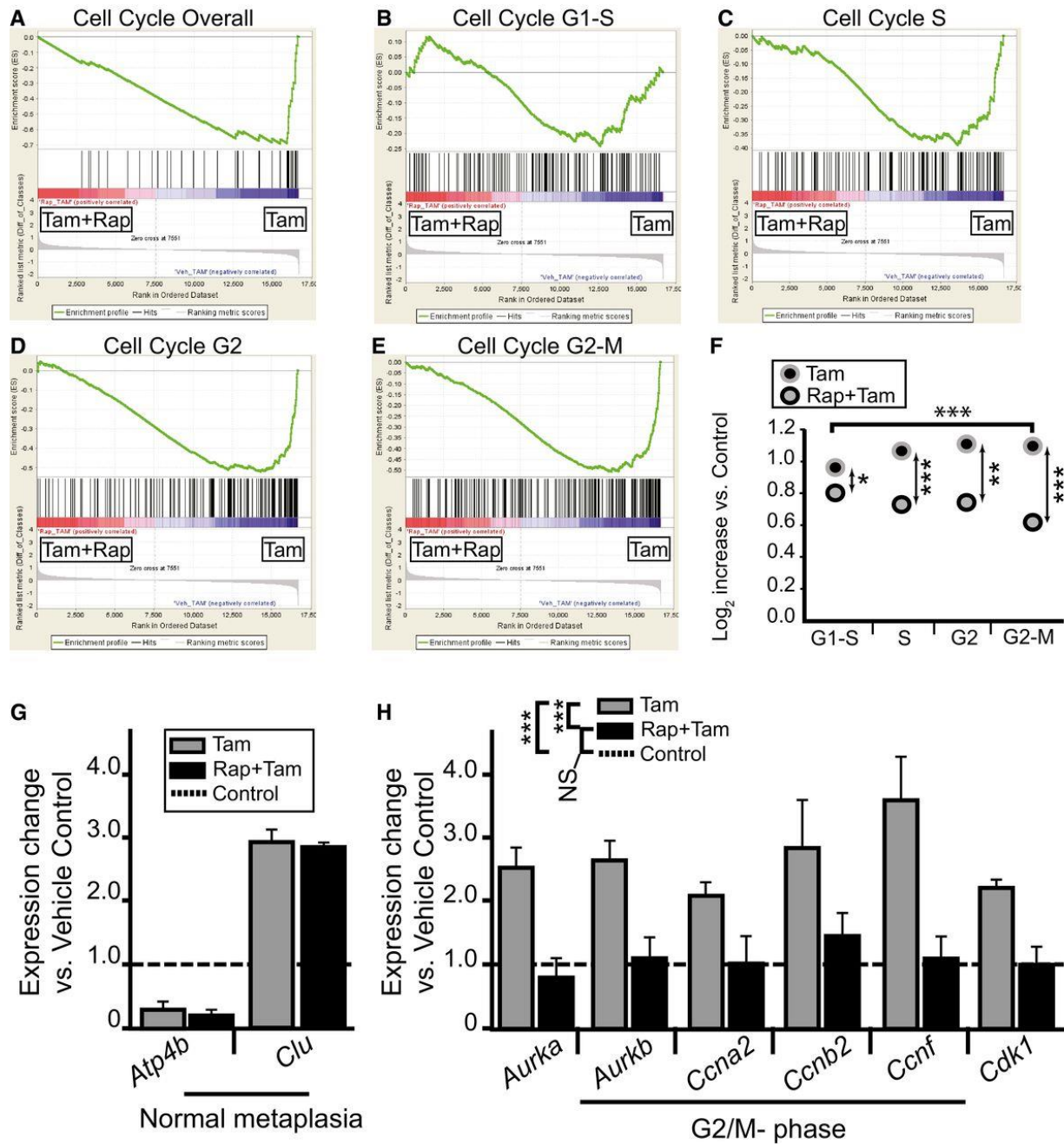


Figure A4.11: mTORC1 activity is required predominately for progression through S-, G2-, and M-phases during metaplastic induction of proliferation.

A–E) Microarrays of stomach corpora at D3 ± HD-Tam ± rapamycin were analyzed using GSEA “Difference of Classes” function comparing rapamycin + HD-Tam (“Tam+Rap”) vs. rapamycin vehicle + HD-Tam (“Tam”). Whitfield Gene Sets specific for either overall cell cycle genes or specific phases of cell cycle are depicted. Note that rapamycin correlates with decreased cell cycle gene expression that is largely due to decreased S-G2 phase gene expression. F) The dot

plots are of the actual average expression levels (in rapamycin + HD-Tam and HD-Tam alone Genechips) of the top 20 genes enriched in various Whitfield Gene Sets GSEA comparisons of HD-Tam vs. vehicle controls (both without rapamycin). Expression levels of HD-Tam and HD-Tam + rapamycin for all genes were normalized to expression level in vehicle control Genechip to facilitate plotting and expressed as Log₂ such that 1 = 2-fold enriched vs. control. Note that average expression of G1-phase genes is only somewhat reduced by rapamycin (by t-test of Tam vs. Rap-Tam, *P < 0.05, **P < 0.01; ***P < 0.001), whereas later phases of the cell cycle are substantially reduced (decrease in G2/M-phase relative to G1-phase by ANOVA with Dunnett's post hoc test is ***P < 0.001). **G, H** qRT-PCR of select transcripts. Control genes known to be increased or decreased in SPEM (G) and genes associated with specifically with G2-M cell cycle phase (H). Expression was normalized to housekeeping gene Tbp, then vehicle control samples for each gene were set at 1, and HD-Tam and HD-Tam + rapamycin expression was normalized to the control sample (statistics for the entire set of cell cycle genes among the different treatments are shown in legend, ***P < 0.001 by ANOVA with Tukey's post hoc test; data represented as mean ± SEM of the means from 3 replicates from a total of 3 independent experiments).

To independently validate the GeneChip findings, we performed qRT-PCR that showed that the expected decreases in a parietal cell (Atp4b) transcript and increase in a non-cell-cycle SPEM transcript (Clu) were not affected by rapamycin (Figure A4.11G). Also matching the GeneChip results, the G1 transcript, Ccnd1, was increased similarly regardless of mTORC1 status. As expected, a G2/M-phase transcript cohort was uniformly increased in HD-Tam but not in HD-Tam + rapamycin (Figure A4.11H). Thus, molecular analysis indicates that inhibition of mTORC1 activity does not substantially affect chief cell G1-phase entry from the quiescent, G₀ state but slows S, G₂, and M-phase progression. BrdU uptake and incorporation into DNA occurs during S-phase; thus, the block in BrdU seen histologically corroborates the molecular data suggesting that mTORC1 is required for G₁ to S transition.

A4.7 Autodegradative machinery is massively upregulated early following injury

We so far have observed that mTORC1 activity is rapidly extinguished within hours of inducing injury. Later, as cells re-enter the cell cycle, mTORC1 is rekindled. Blocking re-emergence of mTORC1 activity inhibits induced proliferation in both stomach and pancreas. In pancreas, where repair is entirely dependent on reprogramming, loss of mTORC1 activity blocks tissue regeneration. We hypothesized that the scaling down of mature cell architecture to “retool” a cell for more efficient proliferation would likely involve activation of lysosomes and autophagic machinery. The autodegradation of cellular structure could then liberate key macromolecules (nucleotides, amino acids, lipids) that would both stimulate mTORC1 reactivation and provide building blocks for replication. Figure A4.12 shows that there is a massive increase of lysosomes (by luminal marker Cathepsin D, Figure A4.12A) and autophagosomal puncta (by LC3-GFP, Figure A4.12C) early following injury in gastric chief cells. Figure 5B quantifies a large spike in lysosomes, as a percentage of their PGC+ (pepsinogen C; chief cell marker) cell area, by 12–24 h of HD-Tam that begins to resolve by later stages, when many cells have re-entered the cell cycle. Increased lysosomes, autophagosomes, and autolysosomes can also be seen at the ultrastructure level (Figures A4.12D and E) on transmission electron microscopy (tEM). tEM analysis shows that rER, mitochondria, and secretory granules are all targeted for recycling during these early stages. The pancreas also shows an equivalent time course of changes in autodegradative machinery, with a spike in lysosome and autophagic puncta 8–24 h following cerulein, followed by decreasing, but still elevated levels, at D3 and near baseline levels at the time of maximal proliferation and pS6 activity (D5: Figures A4.12F, A4.13).

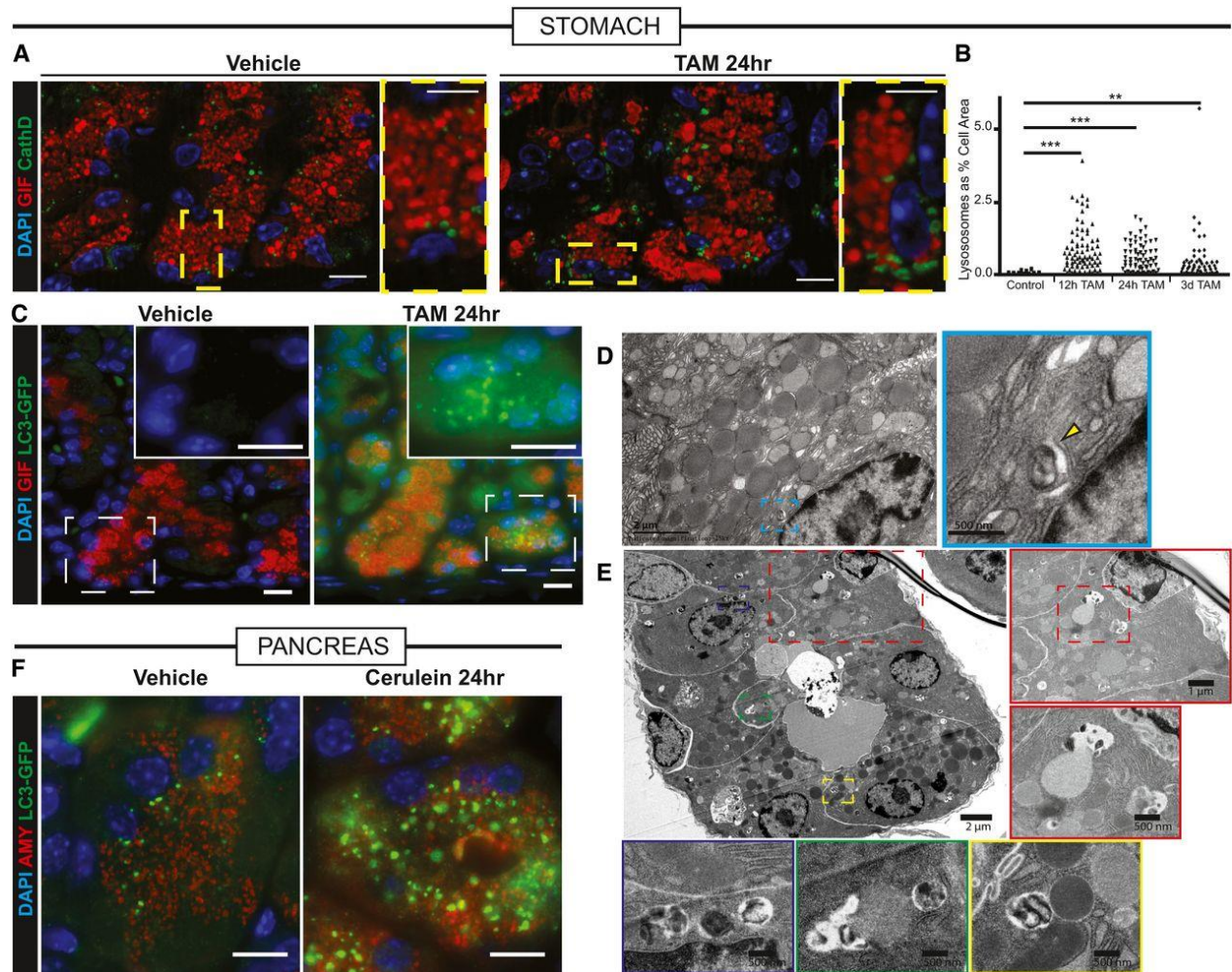


Figure A4.12: Lysosomal and autophagic pathways are upregulated acutely following stomach and pancreas injury.

A) Injured zymogenic cells upregulate Cathepsin D+ puncta (green) 24 h follow HD tamoxifen. Red, chief cells (GIF); blue, nuclei (DAPI). Boxed areas are shown at higher magnification at right of each panel. Scale bars 20 μm ; 10 μm for pullouts. **B)** Quantification of Cathepsin D+ area in chief cells at various stages following injury. $**P < 0.01$; $***P < 0.001$ by ANOVA with Dunnett's post hoc test. Each datapoint is an individual counted cell. **C)** LC3 puncta (detected by GFP fluorescence in Lc3-gfp mice) shows increased autophagosomal puncta paralleling Cathepsin D+ results. Green, LC3-GFP; red, GIF; blue, DAPI. Boxed areas are shown at higher magnification and differing fluorescence channels in insets. Scale bars 20 μm . **D)** Transmission electron micrographs of a normal zymogenic cell. Yellow arrowhead indicates a rare lysosome seen during homeostatic conditions. **E)** Transmission electron micrographs of corpus units 24 h follow tamoxifen injury. Various selected pullouts highlight double membrane-bound structures attacking cytosolic components in reprogramming chief cells. **F)** Acinar cells in pancreas have increased LC3-GFP+ puncta following acute injury with cerulein. Green, LC3-GFP; red, GIF; blue, DAPI. Scale bar 20 μm .

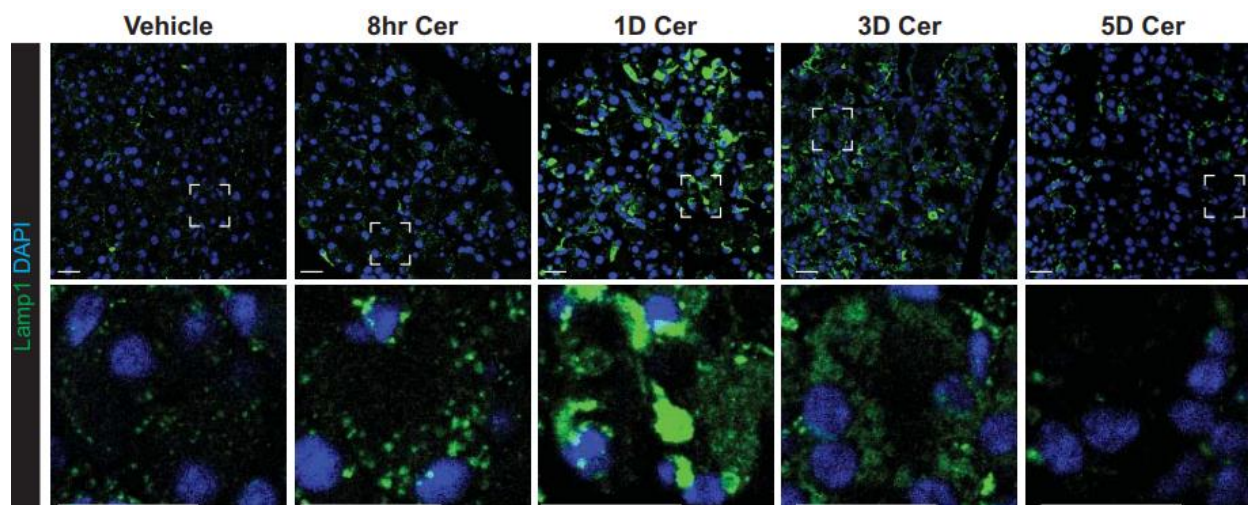


Figure A4.13: Lysosomal activity is raised in the pancreas in early injury.

A4.8 Autodegradative machinery is required for normal progression to later stages

We next sought to address whether autodegradative machinery activation is both upstream of and required for metaplasia formation and proliferation. To do this, we used mice defective in lysosomal hydrolase trafficking that have been shown previously to have defects in autodegradative function specifically in exocrine secretory cells like chief and acinar cells (Boonen et al, 2011). *Gnptab*^{-/-} mice are deficient in an enzyme required for the addition of mannose-6-phosphate to lysosomal enzymes to ensure their proper trafficking. We treated *Gnptab*^{-/-} and littermate controls (*Gnptab*^{-/+} and *Gnptab*^{+/+}) with HD-Tam or cerulein. HD-Tam treatment in *Gnptab*^{-/-} mice caused the expected loss of parietal cells; however, chief cell reprogramming was dramatically compromised (Figure A4.14). Most units did not show loss of large chief cells with eccentric nuclei at all (red arrowhead, Figure A4.14), suggesting reprogramming did not occur, whereas some gastric units showed complete loss of the base zone where chief cells normally reside (green arrowhead, Figure A4.14), indicating chief cells were aberrantly lost instead of reprogrammed. Rarer gastric units seemed to complete the

reprogramming (yellow arrowhead, Figure A4.14). In pancreas, we detected almost no ADM in *Gnptab*^{-/-} mice (Figure A4.14) by D5. Rather, cells remained in an aberrant acinar morphology with considerable loss of eosinophilic cytoplasm but no decrease in size. By 2 weeks, whereas wild-type controls had largely adapted to the cerulein injury, in *Gnptab*^{-/-} mice, the exocrine pancreas comprised only scattered ducts and SOX9⁻ acinar cells, still organized in typical lobules. Cytologically, these remnant cells were characterized by generous pale cytoplasm ranging from foamy to hyaline and lacking nearly all distinguishing features.

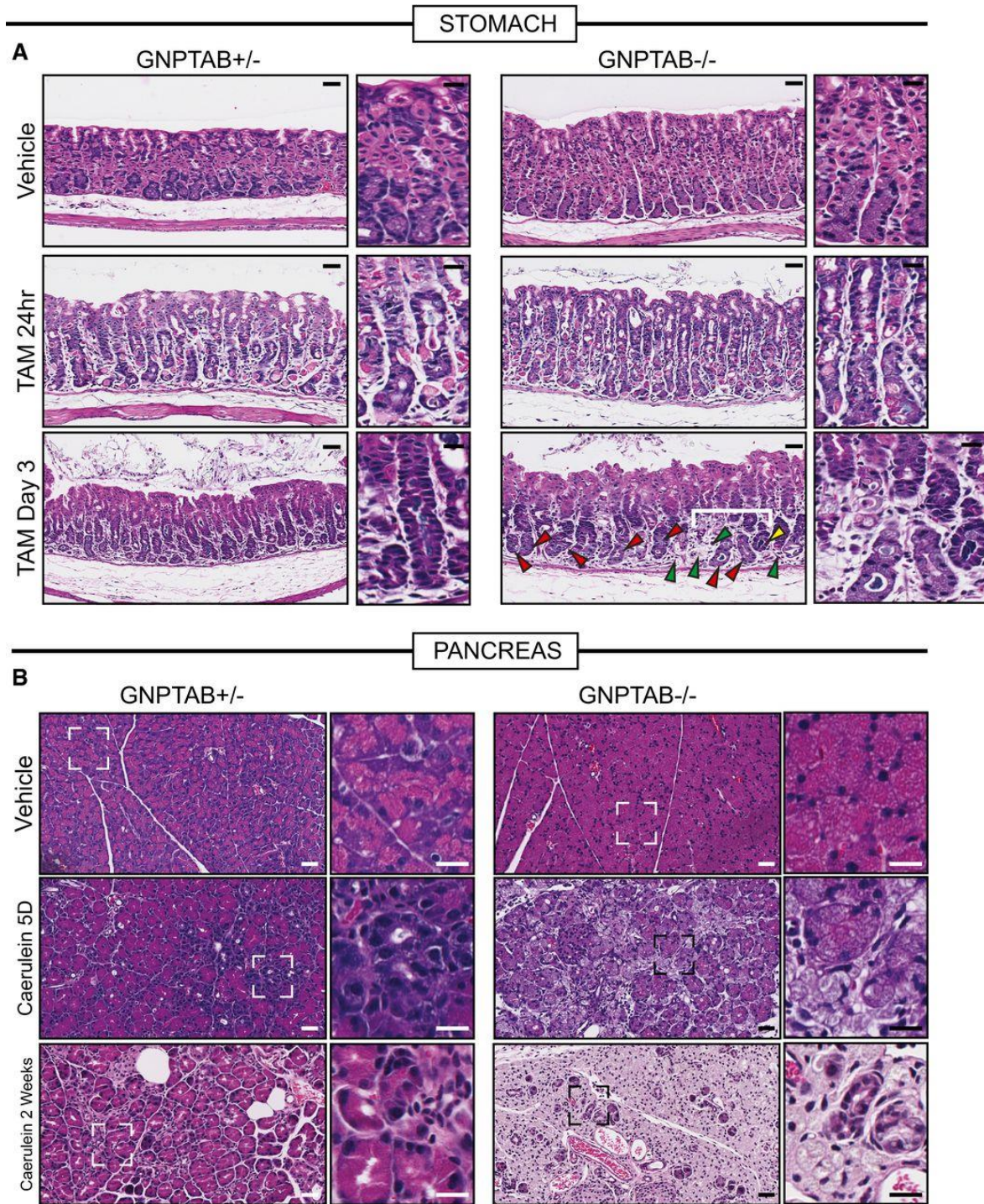


Figure A4.14: Histological appearance of *Gnptab*^{-/-} stomach and pancreas tissue at injury time point.

A) Representative hematoxylin and eosin counterstained images of *Gnptab*^{+/-} and *Gnptab*^{-/-} stomach tissue. *Gnptab*^{-/-} chief cell cytoplasm has a hypertrophic, frothy appearance compared to control zymogenic cells. Loss of parietal cells (fried-egg appearing eosinophilic cells)

following HD-Tam is not affected by loss of GNPTAB; however, the base zones in *Gnptab*^{-/-} mice at day 3 HD-Tam are usually resistant to dedifferentiation (red arrowheads) with large, frothy chief cells remaining largely non-reprogrammed. Another, less common phenotype is that all chief cells are lost such that most of the base of the unit disappears (green arrowheads). Rare units partially undergo morphological metaplastic changes, though usually those are also associated with loss of basal cells (yellow arrowheads). Higher magnification views are to right of each panel, with white bracket delineating particular region of interest in *Gnptab*^{-/-} stomach. Scale bar 50 μ m; pullout, 25 μ m. **B)** Representative hematoxylin and eosin counterstained images of *Gnptab*^{+/+} and *Gnptab*^{-/-} pancreas. Similar to the stomach zymogenic cells, pancreatic acinar cells also have a hypertrophic, frothy appearance. Whereas control samples treated with cerulein show diffuse, asynchronous acinar-to-ductal metaplasia, *Gnptab*^{-/-} mice have acinar cells that simply become less eosinophilic and foamy over time without undergoing ADM. By 2 weeks, wild-type pancreas has largely adapted to cerulein, whereas *Gnptab*^{-/-} pancreas parenchyma comprises only lobules of excessively pale (hyaline), frothy acinar cells and scattered reactive ducts. Scale bar 50 μ m; pullout, 25 μ m.

We next examined the molecular phenotype of the block in *Gnptab*^{-/-} mice. In control stomachs in response to injury, reprogramming cells in the base showed the expected abundant increase in metaplastic genes like Sox9 (Figure A4.15A) and the epitope for GSII (Figure A4.15C).

Proliferation in the base of the unit, where chief cells were reprogramming, was nearly equivalent to the rate of proliferation in the normal stem cell zone in the neck (Figure A4.15B and D). The bases of gastric units in *Gnptab*^{-/-} mice were markedly compromised in both metaplastic changes and proliferation (Figure A4.15A–D). In *Gnptab*^{-/-} mice, chief cells in the base remained both BrdU⁻ and SOX9-negative (Figure A4.15E and F). They also failed to reactivate mTORC1, as pS6 in these mice was largely not detectable in the base (Figure A4.16).

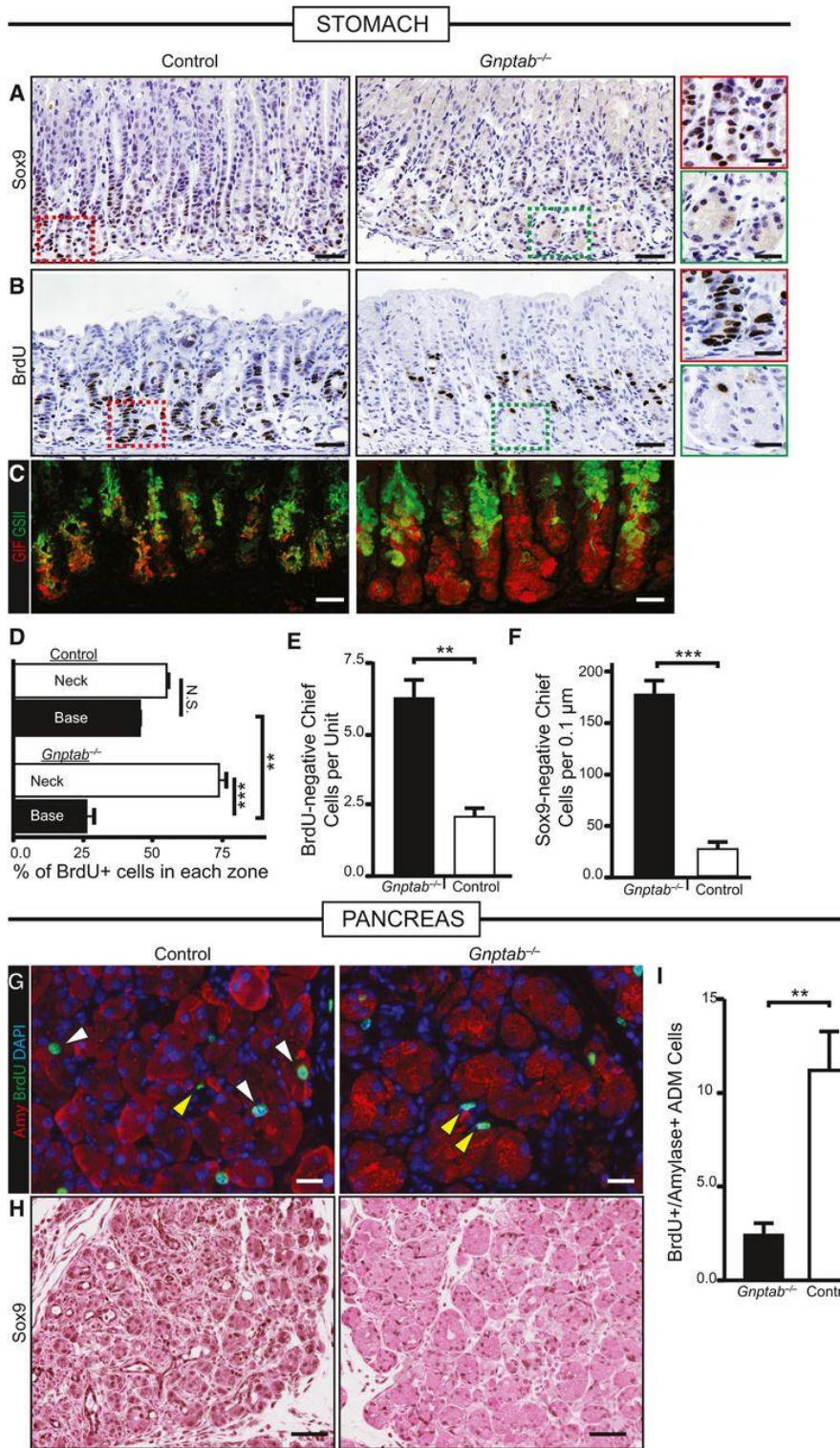


Figure A4.15: Lysosomal function is required for metaplasia-associated gene expression and increased proliferation.

A) Immunohistochemical analysis of SOX9 expression at peak SPEM stages following gastric injury. In control and Gnptab^{-/+} mice, SOX9 becomes expressed in reprogramming chief cells in the bases of the corpus at SPEM stages, but not in Gnptab^{-/-} mice. Color-coded boxes shown at higher magnification shown at right for panels (A and B). Scale bar, 50 μ m; 25 μ m pullout. **B)** S-phase, cell cycle marker BrdU is incorporated throughout the gastric corpus unit at peak SPEM stages in control WT or Gnptab^{-/+} mice. In Gnptab^{-/-} mice, the gastric unit bases, where proliferation is recruited from chief cells, show a marked relative deficit in BrdU⁺ cells. Scale bar, 50 μ m; 25 μ m pullout. **C)** Immunofluorescence analysis of injured gastric tissue from Gnptab^{-/-} and control mice. GIF/GSII co-expression is the hallmark of SPEM. In control mice, the vast majority of corpus unit bases are converted to GIF/GSII co-expression state. In Gnptab^{-/-} mice, bases are resistant to conversion and remain as GIF single positive cells. Red, GIF; green, GSII. Scale bar, 20 μ m. **D)** Quantification of randomly sampled 20 \times fields stained with BrdU. Distribution of BrdU in neck region vs. base region (note total = 100%) is plotted. Note control mice have equivalent amounts of BrdU-labeled cells in the neck and base (~50% in each), whereas Gnptab^{-/-} mice BrdU-labeled cells substantially shifted away from the paligenotic base of units and into the isthmal-neck region, where the constitutive stem cell is active. **E)** Quantification of randomly sampled 20 \times fields stained with BrdU in control and Gnptab^{-/-} mice. Gnptab^{-/-} mice have significantly more BrdU-negative base cells compared to control animals. **F)** Quantification of control and Gnptab^{-/-} corpus units stained for SOX9 scored for the amount of SOX9-negative chief cells per unit at peak SPEM stages. Gnptab^{-/-} mice have significantly more SOX9-negative bases compared to control animals. **G)** Representative immunofluorescence images of injured control and Gnptab^{-/-} pancreatic tissue at cerulein 5 days. Red, amylase; green, BrdU; blue, DAPI. White arrows show proliferating, amylase+ acinar-derived cells (note these are not seen in Gnptab^{-/-} mice). Yellow arrowheads show proliferating stromal cells that are not affected by loss of GNPTAB. Scale bar, 20 μ m. **H)** Representative immunohistochemistry of SOX9 stained control and Gnptab^{-/-} pancreatic tissue at cerulein 5 days. Gnptab^{-/-} tissue has reduced metaplastic phenotype and reduced expression of SOX9. Scale bar, 50 μ m. **I)** Quantification of amylase⁺BrdU⁺ cells of control and Gnptab^{-/-} tissue in randomly sampled 20 \times fields at 5 days of cerulein injury.

Data information: **P < 0.01; ***P < 0.001 by t-test with unequal variance; data represented as mean \pm SEM of the means from 10 low-power fields each from 3 independent experiments.

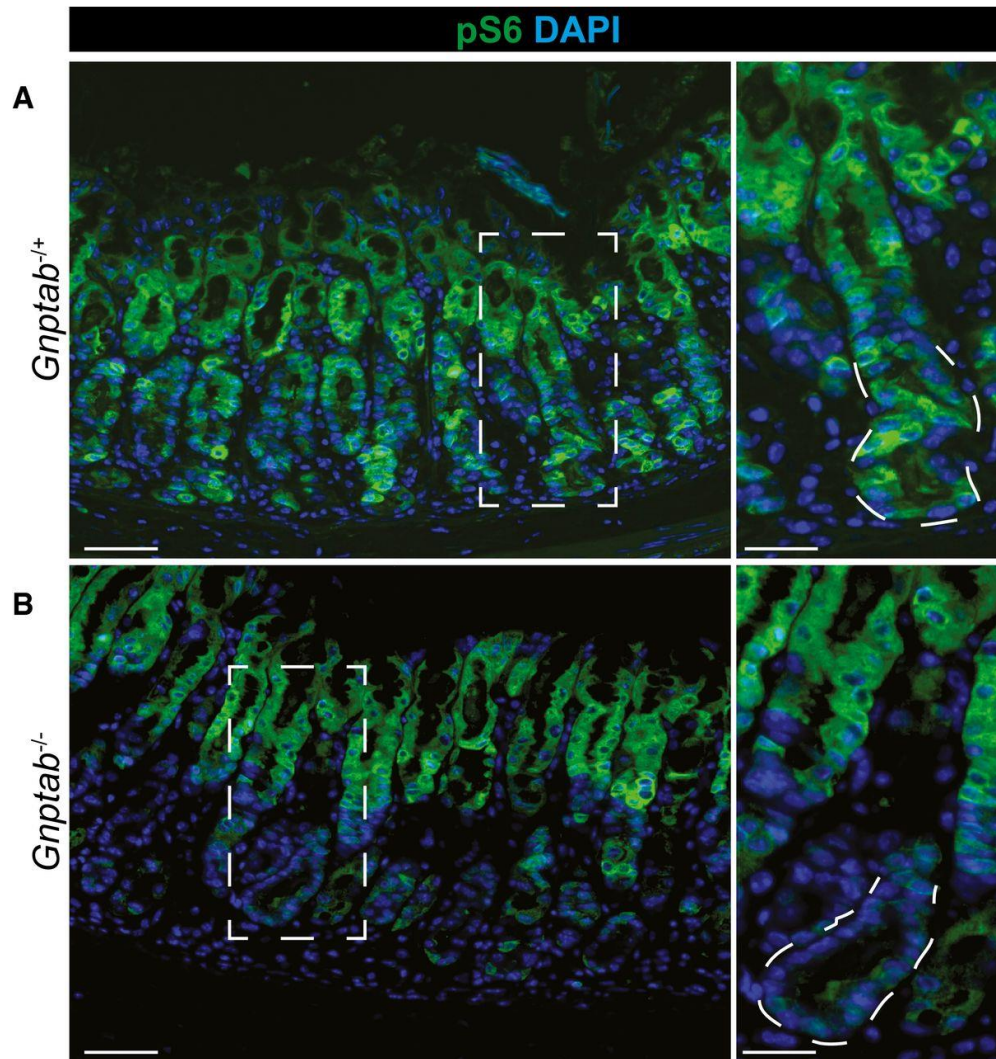


Figure A4.16: Lysosomal activity is required to re-activate mTORC1 following HD tamoxifen injury.

A) At peak metaplasia stages in *Gnptab*^{+/+} tissue, pS6 is re-expressed throughout the stomach epithelium, including intense staining within the pit and metaplastic base. Scale bars: 50 μm ; pullout, 25 μm . **B)** In *Gnptab*^{-/-} tissue, pS6 is not reactivated in the base, indicating lysosomal activity is required for mTORC1 re-activation at later stages following injury. Boxed regions are shown at higher magnification at right with a representative base (in which pS6 remains inactive without lysosomal activity) outlined by dotted line. Lysosomal activity appears dispensable for pit cells (at top of gastric unit) mTORC1 activity. Scale bars: 50 μm ; pullout, 25 μm .

In the pancreas, there was a similar defect in both BrdU (Figure A4.15G and I) and Sox9 (Figure A4.15H). The remnant acinar cells that remained in *Gnptab*^{-/-} mice following 2 weeks of cerulein treatment expressed E-cadherin and low levels of amylase but were not positive for other mature acinar nuclear markers like GATA4 or metaplasia markers like CK8/18 (Figure 4.17).

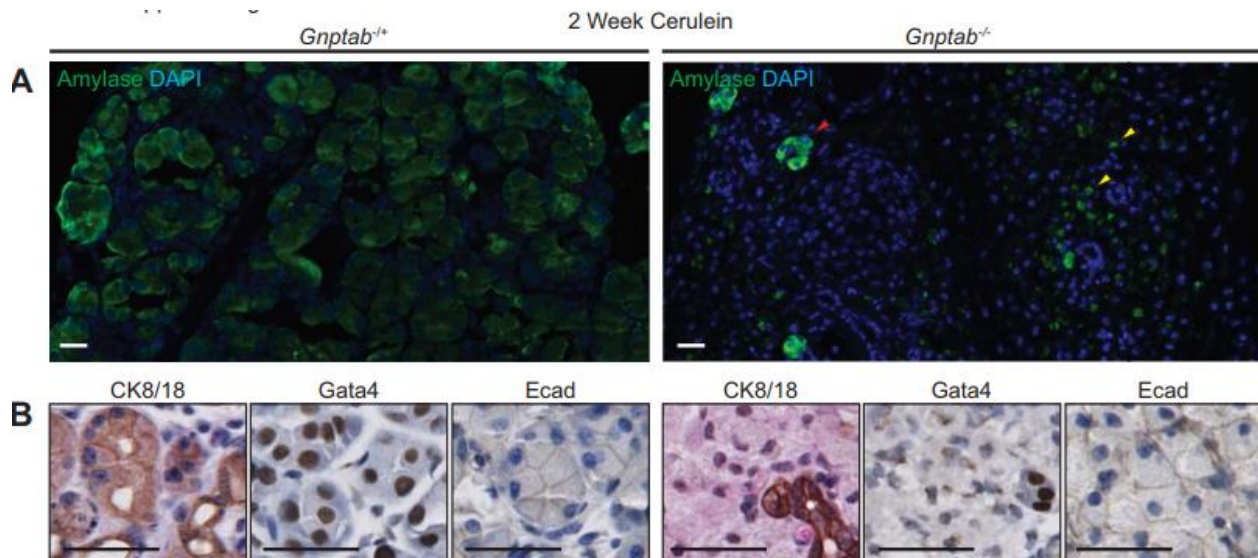


Figure A4.17: *Gnptab*^{-/-} acinar cells maintain mature markers following injury.

Finally, to determine whether the dropout of gastric bases was due to increased cell death in the absence of lysosomal hydrolase activity, we examined tissue for cleaved caspase 3. In wild-type mice (either with or without rapamycin), we did not detect substantial apoptotic death of the chief cells, consistent with our previous observations that death in HD-Tam is essentially confined to parietal cells (Huh et al, 2012; Radyk et al, 2017; Figure A4.1). In *Gnptab*^{-/-} mice, however, we frequently observed multiple cells in some bases of gastric units that were undergoing apoptosis (Figure 4.18). Thus, in stomach, aberrant autodegradative function leads either to stalling of the chief cell reprogramming process or cell death. In pancreas, we observed

a pattern of scattered apoptosis of acinar cells in wild-type mice \pm rapamycin following cerulein treatment. Loss of GNPTAB did not seem to affect this basal rate of death, which is consistent with the survival of many acinar cell remnants out to 2 weeks, as discussed above.

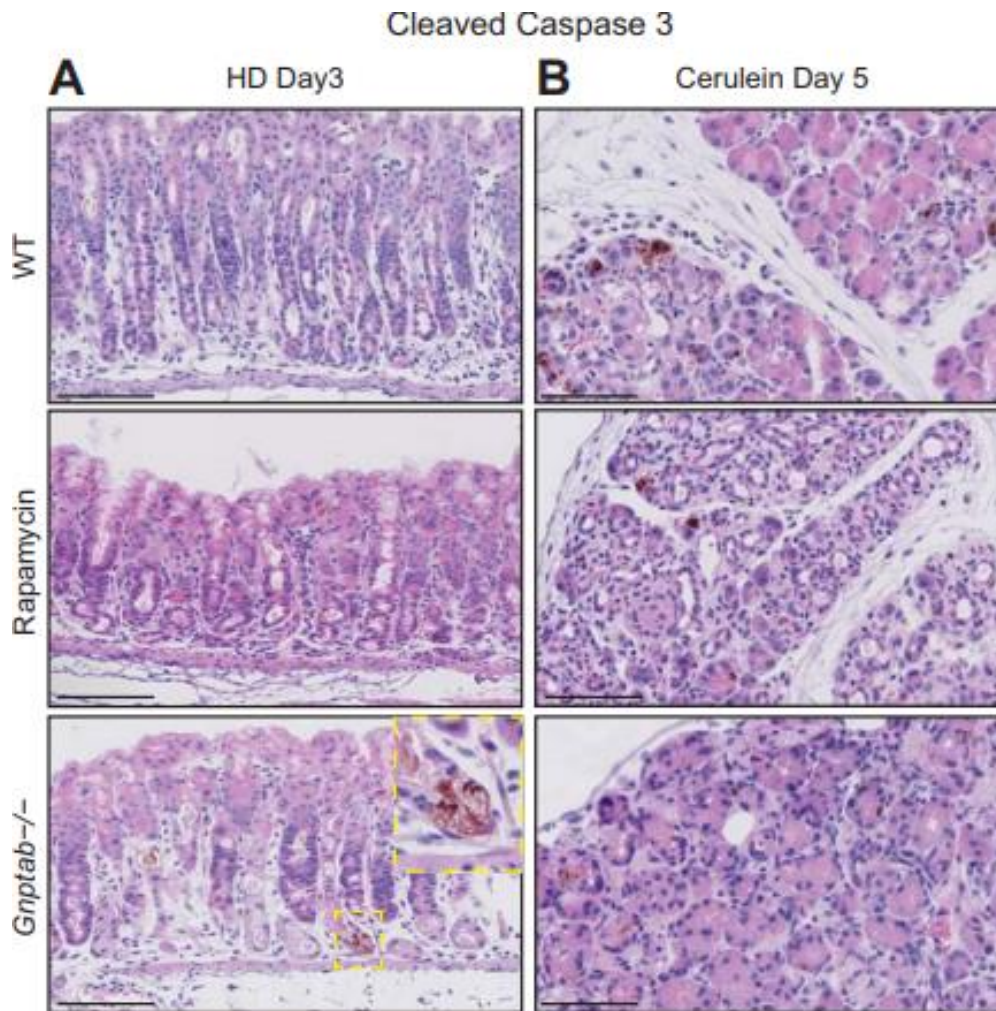


Figure A4.18: Loss of GNPTAB increases apoptosis of chief cells following injury.

A4.9 Discussion

There has been a recent burgeoning of examples of cellular plasticity in tissue in response to injury, not to mention a growing, already large literature on in vitro systems for reprogramming cells back to progenitors. The instances of such plasticity span numerous species and nearly all

tissues. Despite the breadth of examples of cellular reprogramming, studies focusing on the specific molecular mechanisms responsible for the process are still relatively scant. This is particularly true in studies of cells in tissue, likely because investigators have focused more on the outcome of cellular reprogramming—regeneration or tumorigenesis—than on the stepwise mechanisms differentiated cells use to contribute to those outcomes. Here, we have speculated that there could be a shared cellular program that governs the many diverse examples of differentiated cells changing their fate to facilitate repair. There have been many terms that either focus on the outcome of the program or are overly broad: “dedifferentiation”, “transdifferentiation”, “reversion”, “reprogramming”. We now propose “paligenosis” as a specific term describing the cellular process differentiated cells use to re-acquire regenerative capacity. We highlight that paligenosis may be a conserved cellular process with shared molecular and cellular regulation akin to other basic cellular processes like mitosis and apoptosis.

To support our assertion that there may be a shared program for recruiting differentiated cells, we have analyzed the cellular and molecular changes that occur during injury-induced reprogramming in two distinct organs. Upon injury, both the stomach and pancreas have the capacity to repair tissue damage through the recruitment of fully differentiated cells into a less differentiated, proliferative state to replenish cell numbers. This pattern of change in cell phenotype is known to pathologists as metaplasia. We find that the cellular and molecular changes that characterize cells undergoing such metaplastic injury response in either stomach or pancreas are remarkably similar. Specifically, we found that acutely following injury, autodegradative pathways increase alongside a decrease in mTORC1 activity (Figure A4.19). As the injury progresses, we observed the induction of genes that are known to occur during

metaplasia followed by the rise of mTORC1 activity and increased proliferation (Figure A4.19). A similar pattern of changes in mTORC1 activity relative to metaplasia and the differentiated vs. proliferative phenotype was observed in human patients. We found that mTORC1 activity was specifically required for progression through S-phase. Previous literature has also shown that mTORC1 activity is critical for S-phase progression of cancer cells following DNA damage, as mTORC1 is needed to generate pyrimidines in a nutrient-poor environment (Robitaille et al, 2013; Silvera et al, 2017; Zhou et al, 2017). mTORC1 activation is also needed for yeast to pass through G1 into S-phase as they emerge from quiescence (Dhawan & Laxman, 2015; Moreno-Torres et al, 2015). Using an animal model of lysosomal dysfunction, we uncovered that normal lysosomal function after injury is required for cell phenotype and gene expression changes associated with metaplasia. In pancreas, where constitutive stem cells are not available for regeneration, loss of either autodegradative function or mTORC1 activity compromised eventual organ repair.

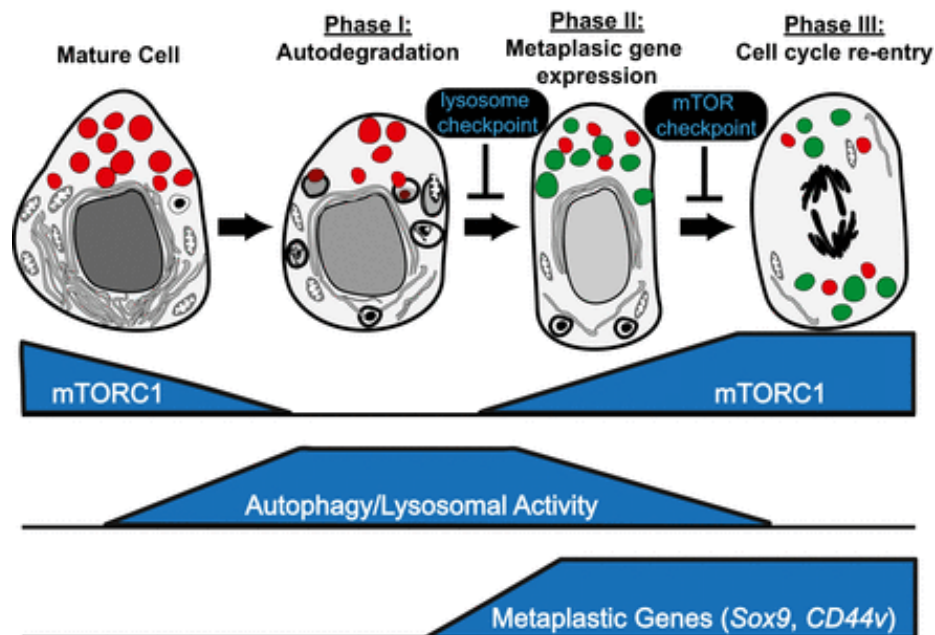


Figure A4.19: Schematic model of shared program: paligenesis.

Data presented in the paper suggest that differentiated cells revert to a regenerative/proliferative state via a program involving stepwise progression through three stages. Progression can be blocked at intervening checkpoints. The potential context-independent nature of this sequence of structural-energetic changes suggests that it is available to differentiated cells in multiple organs and species. We have termed this general program of differentiated cells acquiring regenerative potential “paligenosis”.

Recent advances in the understanding of how mTORC1 is controlled have described a role for the lysosome as an activator of the pathway through the release of nutrients like key amino acids (Zoncu et al, 2011). Thus, our current working model is that due to injury-induced stress, autodegradative pathways are upregulated, and flux increases. The activation of autodegradative pathways appears to act in parallel with loss of the mature gene regulatory network, as forcing expression of key mature-cell-promoting transcription factors like MIST1 (BHLHA15) impairs the injury/repair process (Direnzo et al, 2012; Lo et al, 2017). MIST1 controls a cassette of genes that help direct a cell's energy toward secretion and away from lysosomal activation and autophagy (Mills & Taghert, 2012). We reason, as did Adami over a century ago, that to convert from the differentiated state (structurally complex, energetically active) to the replicative state (structurally simple, energetically active), cellular energy use must be repurposed as an autodegradative program is activated to convert differentiated cell structure into building blocks for replication. The release of nutrients through the lysosome is sensed in cells during the autodegradative phase, resulting in reactivation of mTORC1, which, once the cell has reached sufficient energy levels, subsequently facilitates cell cycle progression and growth to replace cells lost during the injury.

Pancreatic adenocarcinoma and—to a lesser extent—gastric adenocarcinoma are commonly driven by oncogenic mutations in Kras. In mouse models in both the pancreas (Hingorani et al, 2005) and stomach (Choi et al, 2016), KrasG12D mutations, in concert with tissue inflammation,

promote changes in gene expression and cell phenotypes resembling injury-induced metaplasia. In the pancreas, genetically disabling autophagy in the context of K-Ras mutations prevents K-Ras from driving high-grade lesions (Rosenfeldt et al, 2013). Furthermore, cells unable to phosphorylate S6 in the context of activating K-Ras mutations also exhibit less pancreatic cancer progression (Khalailah et al, 2013). A similar critical role for mTORC1 downstream of another key driver oncogene pathway, Wnt activation mediated by APC mutation, has been described in intestinal carcinogenesis (Morran et al, 2014). Thus, tumorigenesis in diverse tissues may also involve modulating lysosomal activity and mTORC1, similar to what we observe in our injury models here. Other pathways downstream of K-Ras, such as PI3K/Rac1 signaling (Heid et al, 2011; Wu et al, 2014), also play similar roles in injury-induced metaplasia.

If there truly is a shared cellular program, paligenosis, underlying the process of recruiting mature cells to become regenerative cells, we would expect the general features we have described here in stomach and pancreas to be recapitulated in many other tissues and species. Obviously, it will be important to conduct new studies in other systems to begin to support that assertion; however, we can at this point re-examine the extant literature to determine whether roles for lysosomes/autophagy and/or mTORC1 in the process of cellular reprogramming to a regenerative state have previously been described. One such previous study, using a different injury protocol, with the endpoint to determine the role of mTORC1 and autophagy in severity of pancreatitis, similarly showed a pattern of early autodegradation followed by mTORC1 activation (Hu et al, 2015). The authors also found that rapamycin worsened severity of pancreatitis. In liver, it has long been known that the earliest phase of hepatocyte response to partial hepatectomy is massive activation of autophagy/lysosomes (Becker & Lane, 1965). mTORC1 is required for the later stages of the process, when proliferation is maximal, consistent

with observations we make in the current manuscript (Jiang et al, 2001; Nelsen et al, 2003; Buitrago-Molina et al, 2009; Espeillac et al, 2011). In kidney, the reprogramming process involves mTORC1 (Kato et al, 2012), and we show here that mTORC1 activity is increased specifically in the tubular cells, which are the cell population called back into the cell cycle to regenerate damaged tissue. To our knowledge, lysosomes/autophagy has not been examined in regenerating kidney. In mature glial cells that dedifferentiate following axonal injury, activation of autophagy/lysosomes is a well-established early event (Jessen & Mirsky, 2016). To our knowledge, mTORC1 activity has not been examined in the process. Furthermore, in tissue culture cellular reprogramming models to generate induced pluripotent stem cells, there is an emerging literature that an early autophagy phase is followed eventually by mTORC1 activation. Inhibition of either autophagy or prolonged inhibition of mTORC1 reduces reprogramming efficiency (He et al, 2012; Wang et al, 2013; Wu et al, 2015). Hence, the stages and checkpoints appear to be the same as the ones we examine in the current manuscript.

Thus, there are numerous reports indicating that the pattern we show here systematically of autodegradation first, then mTORC1 activation may be universal. Moreover, teleologically, it makes sense that a mature cell would first recycle cellular components required for physiological function to use them as substrates for subsequent synthesis of components needed for proliferation. In organs like the vertebrate pancreas or liver, where there are no constitutively active stem cells, repair would likely depend in large part on paligenosis. In tissues with constitutive stem cells, like stomach and intestines, the tissues would have the choice of regenerating with either constitutive stem cells or paligenotic cells, depending potentially on type, extent, and location of injury.

Not all differentiated cells are likely to be able to undergo paligenosis. In the stomach, for example, we have never observed this phenomenon in mature parietal cells (Huh et al, 2012; Mills & Sansom, 2015). Cells that are constitutively undifferentiated and replicative like those of the isthmus of the stomach or LGR5+ crypt-base columnar cells should not need any stage of paligenosis (Figure A4.19). They may acquire the building block nucleotides and amino acids from the blood and/or extracellular environment, given that, by definition, their lack of differentiation means they contain limited non-nuclear components to recycle. Other cells, such as mucous neck cells in the stomach or +4 cells in the intestine (van Es et al, 2012; Roth et al, 2012; Buczacki et al, 2013), may be able to respond to injury but are less well differentiated and thus may be able to skip the autodegradative phase and go directly to the activating mTORC1 and cell division phase of paligenosis.

Paligenosis may be beneficial for its potential to provide lifelong tissue repair in adult organs, but this capacity also seems inherently tied to increased risk for tumorigenesis. Chronic injury of the type that repetitively induces paligenotic/metaplastic events has long been known to increase risk for acquisition of mutations and progression to neoplasm. We have proposed that the reason that risk increases with age is that cycles of paligenosis and subsequent redifferentiation allow accumulation of mutations that may be stored in long-lived, differentiated cells. Eventually, a critical mutation may be unmasked during paligenosis, and a clone of cells that is unable to redifferentiate arises. We have termed this the “cyclical hit” model of tumorigenesis (Mills & Sansom, 2015; Saenz & Mills, 2018).

There are numerous questions that our current study prompts. What molecular events underlie the competence to pass through each stage of paligenosis? What is the relationship between

paligenosis and chronic injury, and what causes the increased risk for cancer? Why are some cells able to undergo paligenosis, whereas others are not? We expect that the framework of sequential phases of paligenosis that we introduce here, along with the potential checkpoints that serve as molecular barriers between each stage of the process, can serve as a starting point for future questions.

A4.10 Materials and Methods

Animal studies and reagents

All experiments using animals followed protocols were approved by the Washington University School of Medicine Animal Studies Committee. WT C57BL/6 mice were purchased from Jackson Laboratories (Bar Harbor, ME). Tg(Atp4b-cre)1Jig/JcmiJ (Atp4b-Cre) (Syder et al, 2004), Gt(ROSA)26Sortm4(ACTB-tdTomato,-EGFP)Luo/J (ROSA26mtmg) (Muzumdar et al, 2007), Gnptab (Gelfman et al, 2007), and LC3-GFP (Mizushima et al, 2004) mice were previously described. Gnptab mice were a kind gift from Dr. Stuart Kornfeld of Washington University. Tamoxifen (5 mg/20 g body weight; Toronto Research Chemicals) was injected intraperitoneally (IP) daily for 2–3 days to induce maximal gastric injury (Huh et al, 2012; Saenz et al, 2016). Tamoxifen was prepared by first dispersing in 100% ethanol by sonication and then emulsifying in sunflower oil (Sigma-Aldrich) 9:1 (oil:ethanol). Pancreatitis was induced by 6 hourly IP injections of 50 µg/kg (in 0.9% saline) cerulein (Sigma-Aldrich) given every other day for up to 2 weeks. Mice were sacrificed 24 h after the final cerulein injection. Rapamycin (60 µg/20 g body weight; LC Laboratories) was injected IP in 0.25% Tween-20, 0.25% polyethylene glycol in PBS for 3–7 days prior to starting and throughout injury time course. Tunicamycin

(Carlisle et al, 2014) and two-thirds partial hepatectomy (Blanc et al, 2010) injuries were performed as previously described. Mice were given an IP injection containing 5-bromo-2'-deoxyuridine (BrdU; 120 mg/kg) and 5-fluoro-2'-deoxyuridine (12 mg/kg) in sterile water 90 min before sacrifice for all BrdU labeling experiments.

For parietal cell isolation, stomachs were harvested and washed several times with PBS. The forestomach and antrum were carefully removed and the remaining corpus minced with a razor blade. The tissue was mechanically dissociated using a 50 μ m Medicon (Beckman) for two 30-s pulses. Chunks of tissue were further dissociated by incubating in 10 ml HBSS with 5 mM EDTA and 1 mM DTT with vigorous shaking for 1 h at 37°C, and then, the solution was run through a 100- μ m filter. Single cells were allowed to rest at 37°C, while filtered chunks were incubated in 10 ml RPMI 1640 with 5% BSA (Sigma) and 1.5 mg/ml Dispase II (Stem Cell Technologies) with vigorous shaking for 1.5 h at 37°C and then filtered again. Dissociated cells were pelleted and washed with cold HBSS three times and then resuspended in PBS with 1% BSA and 5 mM EDTA. Cells were sorted into a parietal cell population (GFP) and all remaining cells (tdTomato) using a MoFlo FACS machine (Dako/Cytomation)

Imaging and tissue analysis

Mouse tissues were immediately excised and flushed with phosphate-buffered saline and fixed overnight in 4% paraformaldehyde in PBS. Tissues were washed, embedded in 3% agar, and then underwent routine paraffin processing. Sections prepared for immunofluorescence or immunohistochemistry underwent standard deparaffinization and rehydration protocols, were blocked in 5% normal serum, and left overnight with primary antibodies. Sections were washed in phosphate-buffered saline and incubated for 1 h with secondary antibodies and then washed

prior to mounting. For antibodies used in this study, see Appendix Table S2.

Immunofluorescence images were taken on a Zeiss Apotome or LSM710 confocal (Zeiss).

Bright field images were taken on a Nanozoomer (Hamamatsu) whole slide scanner or DP70 microscope (Olympus). Counting of stomach cell populations and proliferation was done as previously described (Burclaff et al, 2017), except for analysis of *Gnptab*^{-/-} mice. To account for frequent gland loss in the base of these mice, a different approach was taken. For chief cell quantification (SOX9⁺ and BrdU⁺), 10 random, 20× fields were chosen in three *Gnptab*^{-/-} and three control animals, and chief cells scored in slides from SOX9 or BrdU immunostained sections. For BrdU, distribution, the 10 fields were further subdivided into two rectangular regions: a basal one 100 μm perpendicular and 450 μm parallel to the muscularis mucosa and a region of the same size immediately adjacent and encompassing the neck of the gastric unit. All BrdU⁺ cells were scored and the proportion in each zone calculated. Quantification of proliferation in the pancreas was done by counting 10 randomly sampled whole 20× fields per condition. Cathepsin D⁺ area was calculated by generating a region of interest around PGC⁺ zymogenic cell cytoplasm and using particle counting analysis in ImageJ (NIH) to calculate Cathepsin D⁺ area relative to total cytoplasmic area. Tissue preparation and imaging for electron microscopy was done as previously described (Ramsey et al, 2007).

Human tissue studies

Human gastric pathological tissue specimens were obtained with approval by the Institutional Review Board of Washington University School of Medicine. Figure 3A is a representative image from a qualitative analysis of 44 separate curated gastric clinical samples that have been previously described (Lennerz et al, 2010; Radyk et al, 2017). The study of tissue microarray cases included in this paper was also approved by the China Medical University First Hospital

Institutional Review Board and Ethics Committee. This patient cohort was initially treated at the China First Medical University, and routine standard of care specimens was obtained from patients treated between 2005 and 2009. Tumor, metaplastic, and uninvolved normal tissue from each patient was formalin-fixed and paraffin-embedded. Staining was scored on the following scale: 0, no staining; 1, minimal staining; 2, moderate to strong staining in at least 20% of cells; 3, strong staining in at least 50% of cells. The scoring system was designed, and independently verified, by a human pathologist.

Bioinformatics, microarray, qRT-PCR, and statistical analyses

For qRT-PCR and microarray analyses of mouse stomach \pm rapamycin, two independent experiments were run and a total of two to three separate mice and corresponding microarrays were generated for each condition. All mice were harvested 3 days after first injection and treated as per protocol in (Figure A4.1). Conditions were Veh-Veh (rapamycin vehicle regimen + 3 days of tamoxifen vehicle), Veh-Tam (3 days of rapamycin vehicle regimen + 3 days of HD-Tam), Rap-Veh (rapamycin regimen, 3 days of tamoxifen vehicle); Rap-Tam (rapamycin regimen + 3 days of HD-Tam). RNA for microarray and qRT-PCR analysis was isolated as previously described (Lo et al, 2017). For microarray, samples were processed and hybridized to Affymetrix Mouse Gene 2.0 ST per the manufacturer's instructions by the Washington University Genome Technology Access Core (GTAC). GeneChips were analyzed with Partek Genomic Suite 6.6 (Partek, Inc.) analysis software using default settings (Lo et al, 2017). Mapping to Gene Symbols was done either via GSEA (Subramanian et al, 2005) or GenePattern software (Reich et al, 2006). GSEA was done using default 3.0 settings. GMX files were made using previously published microarray data in the case of laser-capture micro-dissected chief

cells (Capoccia et al, 2013), generated de novo or acquired from GSEA molecular signatures database. For the list of parietal cell-specific genes generated de novo for the current manuscript, flow cytometry was used to sort parietal cells and control cells into 500 μ l RNA protect reagent (Qiagen). RNA was isolated using the RNeasy Micro Kit (Qiagen) following the manufacturer's instructions. Mouse Gene 2.0 ST Array (Affymetrix) was used to analyze gene expression, and the gene set whose expression was enhanced at least eightfold (96 separate genes) in parietal cells vs. control was determined by Partek. For primers used in qRT-PCR, see Appendix Table S3. Statistics for cell counts and qRT-PCR were done by Student's t-test (in the case of pair-wise analysis of significance) or ANOVA (if multiple conditions were compared). For determining statistically significant differences among various conditions in ANOVA, the post hoc tests were either Tukey's (for multiple crosswise comparisons of means) or Dunnett's (for comparisons of multiple experimental samples to a single control). For the tissue microarray, a χ^2 analysis was performed.

Western blot

Approximately 100 mg mouse corpus stomach tissue was lysed in urea buffer (8 M urea, 1% SDS, 150 mM Tris-HCl, pH = 7.0) with 1 \times protease/phosphatase inhibitor cocktail (Thermo). Protein concentration was determined using the DC protein assay (Bio-Rad). Protein (30 μ g) was separated using a 10% SDS-PAGE gel and transferred to PVDF membranes (Millipore). Membranes were incubated overnight at 4°C with Rabbit polyclonal pS6 240/244 or 235/236 (1:1,000 diluted, CST) and Rabbit polyclonal beta-tubulin antibody (1:1,000 diluted, CST) and then incubated with infrared fluorescent dye-conjugated secondary antibodies (LI-COR Biosciences). Protein signal intensities were normalized against a tubulin loading control for

each sample. Fluorescent intensity values were determined and quantified on Western blots at non-saturating exposures using the ImageJ software. Statistical analysis with both antibodies was done using ANOVA with a post hoc Dunnett's test.

Data availability

All analyzed microarray data have been deposited in NCBI GEO under accession GSE103570.

A4.11 Author contributions

Study concept and design: SGW, MAL, JCM, GS, and DL. Data acquisition and analysis: SGW, MAL, Z-FM, JCM, RLC, MDR, GS, and H-YGL. Drafting of manuscript: SGW and JCM. Key manuscript revisions and figure preparation: SGW, JCM, MAL, JB, MDR, Z-FM, NOD, and VB. Histopathological interpretation: SGW, MAL, Z-FM, and JCM. Bioinformatics and statistics: JCM and Z-FM. Supplied crucial reagents and funding: JCM, Z-FM, Z-NW, and DL.

A4.12 References

- Adami JG (1900) On growth and overgrowth. In “Festschrift” in honor of Abraham Jacobi, MD, LL.D: to commemorate the seventieth anniversary of his birth, May sixth, 1900, Huber F, Sondern FE (eds), pp 422 – 432. New Rochelle, NY: Knickerbocker Press
- Adler G, Hahn C, Kern HF, Rao KN (1985) Cerulein-induced pancreatitis in rats: increased lysosomal enzyme activity and autophagocytosis. *Digestion* 32: 10 – 18
- Becker FF, Lane BP (1965) Regeneration of the mammalian liver. I. Auto- phagocytosis during dedifferentiation of the liver cell in preparation for cell division. *Am J Pathol* 47: 783 – 801
- Blanc V, Sessa KJ, Kennedy S, Luo J, Davidson NO (2010) Apobec-1 complementation factor modulates liver regeneration by post- transcriptional regulation of interleukin-6 mRNA stability. *J Biol Chem* 285: 19184 – 19192

Boerboom A, Reusch C, Pieltain A, Chariot A, Franzen R (2017) KIAA1199: a novel regulator of MEK/ERK-induced Schwann cell dedifferentiation. *Glia* 65: 1682 – 1696

Boonen M, van Meel E, Oorschot V, Klumperman J, Kornfeld S (2011) Vacuolization of mucopolipidosis type II mouse exocrine gland cells represents accumulation of autolysosomes. *Mol Biol Cell* 22: 1135 – 1147

Buczacki SJ, Zecchini HI, Nicholson AM, Russell R, Vermeulen L, Kemp R, Winton DJ (2013) Intestinal label-retaining cells are secretory precursors expressing Lgr5. *Nature* 495: 65 – 69

Buitrago-Molina LE, Pothiraju D, Lamle J, Marhenke S, Kossatz U, Breuhahn K, Manns MP, Malek N, Vogel A (2009) Rapamycin delays tumor development in murine livers by inhibiting proliferation of hepatocytes with DNA damage. *Hepatology* 50: 500 – 509

Burclaff J, Osaki LH, Liu D, Goldenring JR, Mills JC (2017) Targeted apoptosis of parietal cells is insufficient to induce metaplasia in stomach. *Gastroenterology* 152: 762 – 766 e7

Burkitt MD, Williams JM, Townsend T, Hough R, Pritchard DM (2017) Mice lacking NF-kappaB1 exhibit marked DNA damage responses and more severe gastric pathology in response to intraperitoneal tamoxifen administration. *Cell Death Dis* 8:e2939

Capoccia BJ, Jin RU, Kong YY, Peek RM Jr, Fassan M, Rugge M, Mills JC (2013) The ubiquitin ligase Mindbomb 1 coordinates gastrointestinal secretory cell maturation. *J Clin Invest* 123: 1475 – 1491

Carlisle RE, Brimble E, Werner KE, Cruz GL, Ask K, Ingram AJ, Dickhout JG (2014) 4-Phenylbutyrate inhibits tunicamycin-induced acute kidney injury via CHOP/GADD153 repression. *PLoS One* 9:e84663

Chang-Panesso M, Humphreys BD (2017) Cellular plasticity in kidney injury and repair. *Nat Rev Nephrol* 13: 39 – 46

Choi E, Hendley AM, Bailey JM, Leach SD, Goldenring JR (2016) Expression of activated ras in gastric chief cells of mice leads to the full spectrum of metaplastic lineage transitions. *Gastroenterology* 150: 918 – 930 e13

Correa P, Piazuelo MB (2012) The gastric precancerous cascade. *J Dig Dis* 13: 2 – 9

Dhawan J, Laxman S (2015) Decoding the stem cell quiescence cycle—lessons from yeast for regenerative biology. *J Cell Sci* 128: 4467 – 4474

Direnzo D, Hess DA, Damsz B, Hallett JE, Marshall B, Goswami C, Liu Y, Deering T, Macdonald RJ, Konieczny SF (2012) Induced Mist1 expression promotes remodeling of mouse pancreatic acinar cells. *Gastroenterology* 143: 469 – 480

van Es JH, Sato T, van de Wetering M, Lyubimova A, Yee Nee AN, Gregorieff A, Sasaki N, Zeinstra L, van den Born M, Korving J, Martens ACM, Barker N, van Oudenaarden A, Clevers H (2012) Dll1+ secretory progenitor cells revert to stem cells upon crypt damage. *Nat Cell Biol* 14: 1099 – 1104

Espeillac C, Mitchell C, Celton-Morizur S, Chauvin C, Koka V, Gillet C, Albrecht JH, Desdouets C, Pende M (2011) S6 kinase 1 is required for rapamycin-sensitive liver proliferation after mouse hepatectomy. *J Clin Invest* 121: 2821 – 2832

Gelfman CM, Vogel P, Issa TM, Turner CA, Lee WS, Kornfeld S, Rice DS (2007) Mice lacking alpha/beta subunits of GlcNAc-1-phosphotransferase exhibit growth retardation, retinal degeneration, and secretory cell lesions. *Invest Ophthalmol Vis Sci* 48: 5221 – 5228

Giroux V, Rustgi AK (2017) Metaplasia: tissue injury adaptation and a precursor to the dysplasia-cancer sequence. *Nat Rev Cancer* 17: 594 – 604

He J, Kang L, Wu T, Zhang J, Wang H, Gao H, Zhang Y, Huang B, Liu W, Kou Z, Zhang H, Gao S (2012) An elaborate regulation of Mammalian target of rapamycin activity is required for somatic cell reprogramming induced by defined transcription factors. *Stem Cells Dev* 21: 2630 – 2641

Heid I, Lubeseder-Martellato C, Sipos B, Mazur PK, Lesina M, Schmid RM, Siveke JT (2011) Early requirement of Rac1 in a mouse model of pancreatic cancer. *Gastroenterology* 141: 719 – 730, 730.e1–7

Hingorani SR, Wang L, Multani AS, Combs C, Deramaudt TB, Hruban RH, Rustgi AK, Chang S, Tuveson DA (2005) Trp53R172H and KrasG12D cooperate to promote chromosomal instability and widely metastatic pancreatic ductal adenocarcinoma in mice. *Cancer Cell* 7: 469 – 483

Hu YY, Zhou CH, Dou WH, Tang W, Hu CY, Hu DM, Feng H, Wang JZ, Qian MJ, Cheng GL, Wang SF (2015) Improved autophagic flux is correlated with mTOR activation in the later recovery stage of experimental acute pancreatitis. *Pancreatology* 15: 470 – 477

Huh WJ, Khurana SS, Geahlen JH, Kohli K, Waller RA, Mills JC (2012) Tamoxifen induces rapid, reversible atrophy, and metaplasia in mouse stomach. *Gastroenterology* 142: 21 – 24 e7

Jessen KR, Mirsky R (2016) The repair Schwann cell and its function in regenerating nerves. *J Physiol* 594: 3521 – 3531

Jiang YP, Ballou LM, Lin RZ (2001) Rapamycin-insensitive regulation of 4e-BP1 in regenerating rat liver. *J Biol Chem* 276: 10943 – 10951

Karra R, Knecht AK, Kikuchi K, Poss KD (2015) Myocardial NF-kappaB activation is essential for zebrafish heart regeneration. *Proc Natl Acad Sci USA* 112: 13255 – 13260

Kato H, Nakajima S, Saito Y, Takahashi S, Katoh R, Kitamura M (2012) mTORC1 serves ER stress-triggered apoptosis via selective activation of the IRE1-JNK pathway. *Cell Death Differ* 19: 310 – 320

Khalaileh A, Dreazen A, Khatib A, Apel R, Swisa A, Kidess-Bassir N, Maitra A, Meyuhas O, Dor Y, Zamir G (2013) Phosphorylation of ribosomal protein S6 attenuates DNA damage and tumor suppression during development of pancreatic cancer. *Cancer Res* 73: 1811 – 1820

Lee C, Lee H, Hwang SY, Moon CM (2017) Hong SN (2017) IL-10 plays a pivotal role in tamoxifen-induced spasmodic polypeptide-expressing metaplasia in gastric mucosa. *Gut Liv* 11: 789 – 797

Lennerz JK, Kim SH, Oates EL, Huh WJ, Doherty JM, Tian X, Bredemeyer AJ, Goldenring JR, Lauwers GY, Shin YK, Mills JC (2010) The transcription factor MIST1 is a novel human gastric chief cell marker whose expression is lost in metaplasia, dysplasia, and carcinoma. *Am J Pathol* 177: 1514 – 1533

Leushacke M, Tan SH, Wong A, Swathi Y, Hajamohideen A, Tan LT, Goh J, Wong E, Denil S, Murakami K, Barker N (2017) Lgr5-expressing chief cells drive epithelial regeneration and cancer in the oxyntic stomach. *Nat Cell Biol* 19: 774 – 786

Lo HG, Jin RU, Sibbel G, Liu D, Karki A, Joens MS, Madison BB, Zhang B, Blanc V, Fitzpatrick JA, Davidson NO, Konieczny SF, Mills JC (2017) A single transcription factor is sufficient to induce and maintain secretory cell architecture. *Genes Dev* 31: 154 – 171

Logan CY, Desai TJ (2015) Keeping it together: pulmonary alveoli are maintained by a hierarchy of cellular programs. *BioEssays* 37: 1028 – 1037

Mills JC, Taghert PH (2012) Scaling factors: transcription factors regulating subcellular domains. *BioEssays* 34: 10 – 16

Mills JC, Sansom OJ (2015) Reserve stem cells: differentiated cells reprogram to fuel repair, metaplasia, and neoplasia in the adult gastrointestinal tract. *Sci Signal* 8:re8

Mills JC, Goldenring JR (2017) Metaplasia in the stomach arises from gastric chief cells. *Cell Mol Gastroenterol Hepatol* 4: 85 – 88

Mindos T, Dun XP, North K, Doddrell RD, Schulz A, Edwards P, Russell J, Gray B, Roberts SL, Shivane A, Mortimer G, Pirie M, Zhang N, Pan D, Morrison H, Parkinson DB (2017) Merlin

controls the repair capacity of Schwann cells after injury by regulating Hippo/YAP activity. *J Cell Biol* 216: 495 – 510

Mizushima N, Yamamoto A, Matsui M, Yoshimori T, Ohsumi Y (2004) In vivo analysis of autophagy in response to nutrient starvation using transgenic mice expressing a fluorescent autophagosome marker. *Mol Biol Cell* 15: 1101–1111
Moreno-Torres M, Jaquenoud M, De Virgilio C (2015) TORC1 controls G1-S cell cycle transition in yeast via Mpk1 and the greatwall kinase pathway. *Nat Commun* 6: 8256

Morran DC, Wu J, Jamieson NB, Mrowinska A, Kalna G, Karim SA, Au AY, Scarlett CJ, Chang DK, Pajak MZ, Australian Pancreatic Cancer Genome I, Oien KA, McKay CJ, Carter CR, Gillen G, Champion S, Pimlott SL, Anderson KI, Evans TR, Grimmond SM et al (2014) Targeting mTOR dependency in pancreatic cancer. *Gut* 63: 1481 – 1489

Murtaugh LC, Keefe MD (2015) Regeneration and repair of the exocrine pancreas. *Annu Rev Physiol* 77: 229 – 249
Muzumdar MD, Tasic B, Miyamichi K, Li L, Luo L (2007) A global double- fluorescent Cre reporter mouse. *Genesis* 45: 593 – 605

Nam KT, Lee HJ, Sousa JF, Weis VG, O’Neal RL, Finke PE, Romero-Gallo J, Shi G, Mills JC, Peek RM Jr, Konieczny SF, Goldenring JR (2010) Mature chief cells are cryptic progenitors for metaplasia in the stomach. *Gastroenterology* 139: 2028 – 2037 e9

Nelsen CJ, Rickheim DG, Tucker MM, Hansen LK, Albrecht JH (2003) Evidence that cyclin D1 mediates both growth and proliferation downstream of TOR in hepatocytes. *J Biol Chem* 278: 3656 – 3663

Newberry EP, Kennedy SM, Xie Y, Luo J, Stanley SE, Semenkovich CF, Crooke RM, Graham MJ, Davidson NO (2008) Altered hepatic triglyceride content after partial hepatectomy without impaired liver regeneration in multiple murine genetic models. *Hepatology* 48: 1097 – 1105

Niederau C, Ferrell LD, Grendell JH (1985) Caerulein-induced acute necrotizing pancreatitis in mice: protective effects of proglumide, benzotript, and secretin. *Gastroenterology* 88: 1192 – 1204

Nomura S, Yamaguchi H, Ogawa M, Wang TC, Lee JR, Goldenring JR (2005) Alterations in gastric mucosal lineages induced by acute oxyntic atrophy in wild-type and gastrin-deficient mice. *Am J Physiol Gastrointest Liver Physiol* 288:G362 –G375

Nozaki K, Ogawa M, Williams JA, Lafleur BJ, Ng V, Drapkin RI, Mills JC, Konieczny SF, Nomura S, Goldenring JR (2008) A molecular signature of gastric metaplasia arising in response to acute parietal cell loss. *Gastroenterology* 134: 511 – 522

- Peterson WL (2002) Review article: *Helicobacter pylori* and gastric adenocarcinoma. *Aliment Pharmacol Ther* 16(Suppl 1): 40 – 46
- Radyk MD, Burclaff J, Willet SG, Mills JC (2017) Metaplastic cells in the stomach arise, independently of stem cells, via dedifferentiation or transdifferentiation of chief cells. *Gastroenterology* <https://doi.org/10.1053/j.gastro.2017.11.278>
- Radyk MD, Mills JC (2017) A chief source of cancer and repair in stomachs. *EMBO J* 36: 2318 – 2320
- Ramsey VG, Doherty JM, Chen CC, Stappenbeck TS, Konieczny SF, Mills JC (2007) The maturation of mucus-secreting gastric epithelial progenitors into digestive-enzyme secreting zymogenic cells requires *Mist1*. *Development* 134: 211 – 222
- Reich M, Liefeld T, Gould J, Lerner J, Tamayo P, Mesirov JP (2006) *GenePattern 2.0*. *Nat Genet* 38: 500 – 501
- Robitaille AM, Christen S, Shimobayashi M, Cornu M, Fava LL, Moes S, Prescianotto-Baschong C, Sauer U, Jenoe P, Hall MN (2013) Quantitative phosphoproteomics reveal mTORC1 activates de novo pyrimidine synthesis. *Science* 339: 1320 – 1323
- Rosenfeldt MT, O'Prey J, Morton JP, Nixon C, MacKay G, Mrowinska A, Au A, Rai TS, Zheng L, Ridgway R, Adams PD, Anderson KI, Gottlieb E, Sansom OJ, Ryan KM (2013) p53 status determines the role of autophagy in pancreatic tumour development. *Nature* 504: 296 – 300
- Roth S, Franken P, Sacchetti A, Kremer A, Anderson K, Sansom O, Fodde R (2012) Paneth cells in intestinal homeostasis and tissue injury. *PLoS One* 7: e38965
- Roux PP, Shahbazian D, Vu H, Holz MK, Cohen MS, Taunton J, Sonenberg N, Blenis J (2007) RAS/ERK signaling promotes site-specific ribosomal protein S6 phosphorylation via RSK and stimulates cap-dependent translation. *J Biol Chem* 282: 14056 – 14064
- Rugge M, Correa P, Di Mario F, El-Omar E, Fiocca R, Geboes K, Genta RM, Graham DY, Hattori T, Malfertheiner P, Nakajima S, Sipponen P, Sung J, Weinstein W, Vieth M (2008) OLGA staging for gastritis: a tutorial. *Dig Liver Dis* 40: 650 – 658
- Saenz JB, Burclaff J, Mills JC (2016) Modeling murine gastric metaplasia through tamoxifen-induced acute parietal cell loss. *Methods Mol Biol* 1422: 329 – 339
- Saenz JB, Mills JC (2018) Acid and the basis for cellular plasticity and reprogramming in gastric repair and cancer. *Nat Rev Gastroenterol Hepatol* [In Press]
- Saluja A, Saito I, Saluja M, Houlihan MJ, Powers RE, Meldolesi J, Steer M (1985) In vivo rat pancreatic acinar cell function during supramaximal stimulation with caerulein. *Am J Physiol* 249:G702 –G710

Schmidt PH, Lee JR, Joshi V, Playford RJ, Poulson R, Wright NA, Goldenring JR (1999) Identification of a metaplastic cell lineage associated with human gastric adenocarcinoma. *Lab Invest* 79: 639 – 646

Silvera D, Ernlund A, Arju R, Connolly E, Volta V, Wang J, Schneider RJ (2017) mTORC1 and -2 coordinate transcriptional and translational reprogramming in resistance to DNA damage and replicative stress in breast cancer cells. *Mol Cell Biol* 37:e00577 – 16

Spechler SJ, Merchant JL, Wang TC, Chandrasoma P, Fox JG, Genta RM, Goldenring JR, Hayakawa Y, Kuipers EJ, Lund PK, McKeon F, Mills JC, Odze RD, Peek RM Jr, Pham T, Que J, Rustgi AK, Shaheen NJ, Shivdasani RA, Souza RF et al (2017) A summary of the 2016 James W. Freston conference of the American gastroenterological association: intestinal metaplasia in the esophagus and stomach: origins, differences, similarities and significance. *Gastroenterology* 153:e6 – e13

Storz P (2017) Acinar cell plasticity and development of pancreatic ductal adenocarcinoma. *Nat Rev Gastroenterol Hepatol* 14: 296 – 304 Subramanian A, Tamayo P, Mootha VK, Mukherjee S, Ebert BL, Gillette MA, Paulovich A, Pomeroy SL, Golub TR, Lander ES, Mesirov JP (2005) Gene set enrichment analysis: a knowledge-based approach for interpreting genome-wide expression profiles. *Proc Natl Acad Sci USA* 102: 15545 – 15550

Syder AJ, Karam SM, Mills JC, Ippolito JE, Ansari HR, Farook V, Gordon JI (2004) A transgenic mouse model of metastatic carcinoma involving transdifferentiation of a gastric epithelial lineage progenitor to a neuroendocrine phenotype. *Proc Natl Acad Sci USA* 101: 4471 – 4476

Takahashi K, Yamanaka S (2006) Induction of pluripotent stem cells from mouse embryonic and adult fibroblast cultures by defined factors. *Cell* 126: 663 – 676

Wang S, Xia P, Ye B, Huang G, Liu J, Fan Z (2013) Transient activation of autophagy via Sox2-mediated suppression of mTOR is an important early step in reprogramming to pluripotency. *Cell Stem Cell* 13: 617 – 625

Wang WE, Li L, Xia X, Fu W, Liao Q, Lan C, Yang D, Chen H, Yue R, Zeng C, Zhou L, Zhou B, Duan DD, Chen X, Houser SR, Zeng C (2017) Dedifferentiation, proliferation, and redifferentiation of adult mammalian cardiomyocytes after ischemic injury. *Circulation* 136: 834 – 848

Wu CY, Carpenter ES, Takeuchi KK, Halbrook CJ, Peverley LV, Bien H, Hall JC, DelGiorno KE, Pal D, Song Y, Shi C, Lin RZ, Crawford HC (2014) PI3K regulation of RAC1 is required for KRAS-induced pancreatic tumorigenesis in mice. *Gastroenterology* 147: 1405 – 1416 e7

Wu Y, Li Y, Zhang H, Huang Y, Zhao P, Tang Y, Qiu X, Ying Y, Li W, Ni S, Zhang M, Liu L, Xu Y, Zhuang Q, Luo Z, Benda C, Song H, Liu B, Lai L, Liu X et al (2015) Autophagy and mTORC1 regulate the stochastic phase of somatic cell reprogramming. *Nat Cell Biol* 17: 715 – 725

Yoshizawa N, Takenaka Y, Yamaguchi H, Tetsuya T, Tanaka H, Tatematsu M, Nomura S, Goldenring JR, Kaminishi M (2007) Emergence of spasmodic polypeptide-expressing metaplasia in Mongolian gerbils infected with *Helicobacter pylori*. *Lab Invest* 87: 1265 – 1276

Zhou X, Liu W, Hu X, Dorrance A, Garzon R, Houghton PJ, Shen C (2017) Regulation of CHK1 by mTOR contributes to the evasion of DNA damage barrier of cancer cells. *Sci Rep* 7: 1535

Zoncu R, Bar-Peled L, Efeyan A, Wang S, Sancak Y, Sabatini DM (2011) mTORC1 senses lysosomal amino acids through an inside-out mechanism that requires the vacuolar H(+)-ATPase. *Science* 334: 678 – 683.

Works Cited

- Adami, J.** (1900). On Growth and Overgrowth. "Festschrift" in Honor of Abraham Jacobi, M.D., L.L.D.: To Commemorate the Seventieth Anniversary of His Birth. *Knickerbocker Press*, 422-432.
- Adams, J. F., Glen, A. I., Kennedy, E. H., Mackenzie, I. L., Morrow, J. M., Anderson, J. R., Gray, K. G. and Middleton, D. G.** (1964). The Histological and Secretory Changes in the Stomach in Patients with Autoimmunity to Gastric Parietal Cells. *Lancet* **1**, 401-403.
- Ahrlund-Richter, L. and Hendrix, M. J.** (2014). Oncofetal signaling as a target for cancer therapy. *Semin Cancer Biol* **29**, 1-2.
- Baker, A. M., Cereser, B., Melton, S., Fletcher, A. G., Rodriguez-Justo, M., Tadrous, P. J., Humphries, A., Elia, G., McDonald, S. A., Wright, N. A., et al.** (2014). Quantification of crypt and stem cell evolution in the normal and neoplastic human colon. *Cell Rep* **8**, 940-947.
- Barker, N., Huch, M., Kujala, P., van de Wetering, M., Snippert, H. J., van Es, J. H., Sato, T., Stange, D. E., Begthel, H., van den Born, M., et al.** (2010). Lgr5(+ve) stem cells drive self-renewal in the stomach and build long-lived gastric units in vitro. *Cell stem cell* **6**, 25-36.
- Bjerknes, M. and Cheng, H.** (2002). Multipotential stem cells in adult mouse gastric epithelium. *Am J Physiol Gastrointest Liver Physiol* **283**, G767-777.
- Bredemeyer, A. J., Geahlen, J. H., Weis, V. G., Huh, W. J., Zinselmeyer, B. H., Srivatsan, S., Miller, M. J., Shaw, A. S. and Mills, J. C.** (2009). The gastric epithelial progenitor cell niche and differentiation of the zymogenic (chief) cell lineage. *Dev Biol* **325**, 211-224.
- Buch, T., Heppner, F. L., Tertilt, C., Heinen, T. J., Kremer, M., Wunderlich, F. T., Jung, S. and Waisman, A.** (2005). A Cre-inducible diphtheria toxin receptor mediates cell lineage ablation after toxin administration. *Nat Methods* **2**, 419-426.
- Burclaff, J. and Mills, J. C.** (2018a). Plasticity of differentiated cells in wound repair and tumorigenesis, part I: stomach and pancreas. *Dis Model Mech* **11**.
- (2018b). Plasticity of differentiated cells in wound repair and tumorigenesis, part II: skin and intestine. *Dis Model Mech* **11**.
- Burclaff, J., Osaki, L. H., Liu, D., Goldenring, J. R. and Mills, J. C.** (2016). Targeted Apoptosis of Parietal Cells Is Insufficient to Induce Metaplasia in Stomach. *Gastroenterology*.
- (2017). Targeted Apoptosis of Parietal Cells Is Insufficient to Induce Metaplasia in Stomach. *Gastroenterology* **152**, 762-766 e767.
- Burke, A. J., Sullivan, F. J., Giles, F. J. and Glynn, S. A.** (2013). The yin and yang of nitric oxide in cancer progression. *Carcinogenesis* **34**, 503-512.
- Busada, J. T., Ramamoorthy, S., Cain, D. W., Xu, X., Cook, D. N. and Cidlowski, J. A.** (2019). Endogenous glucocorticoids prevent gastric metaplasia by suppressing spontaneous inflammation. *J Clin Invest*.

- Canfield, V., West, A. B., Goldenring, J. R. and Levenson, R.** (1996). Genetic ablation of parietal cells in transgenic mice: a new model for analyzing cell lineage relationships in the gastric mucosa. *Proc Natl Acad Sci U S A* **93**, 2431-2435.
- Capoccia, B. J., Jin, R. U., Kong, Y. Y., Peek, R. M., Jr., Fassan, M., Rugge, M. and Mills, J. C.** (2013). The ubiquitin ligase Mindbomb 1 coordinates gastrointestinal secretory cell maturation. *J Clin Invest* **123**, 1475-1491.
- Choi, E., Hendley, A. M., Bailey, J. M., Leach, S. D. and Goldenring, J. R.** (2016). Expression of Activated Ras in Gastric Chief Cells of Mice Leads to the Full Spectrum of Metaplastic Lineage Transitions. *Gastroenterology* **150**, 918-930 e913.
- Choi, E., Lantz, T. L., Vlachich, G., Keeley, T. M., Samuelson, L. C., Coffey, R. J., Goldenring, J. R. and Powell, A. E.** (2018). Lrig1+ gastric isthmal progenitor cells restore normal gastric lineage cells during damage recovery in adult mouse stomach. *Gut* **67**, 1595-1605.
- Corbett, J. A. and McDaniel, M. L.** (1996). Selective Inhibition of Inducible Nitric Oxide Synthase by Aminoguanidine. *Methods Enzymol* **268**, 398-408.
- Correa, P.** (1988). A human model of gastric carcinogenesis. *Cancer Res* **48**, 3554-3560.
- Ding, S., Eric Blue, R., Chen, Y., Scull, B., Kay Lund, P. and Morgan, D.** (2012). Molecular imaging of gastric neoplasia with near-infrared fluorescent activatable probes. *Mol Imaging* **11**, 507-515.
- Engevik, A. C., Feng, R., Choi, E., White, S., Bertaux-Skeirik, N., Li, J., Mahe, M. M., Aihara, E., Yang, L., DiPasquale, B., et al.** (2016). The Development of Spasmolytic Polypeptide/TFF2-Expressing Metaplasia (SPEM) During Gastric Repair Is Absent in the Aged Stomach. *Cell Mol Gastroenterol Hepatol* **2**, 605-624.
- Fearon, E. R. and Vogelstein, B.** (1990). A genetic model for colorectal tumorigenesis. *Cell* **61**, 759-767.
- Ferlay, J., Soerjomataram, I., Dikshit, R., Eser, S., Mathers, C., Rebelo, M., Parkin, D. M., Forman, D. and Bray, F.** (2015). Cancer incidence and mortality worldwide: sources, methods and major patterns in GLOBOCAN 2012. *Int J Cancer* **136**, E359-386.
- Franic, T. V., Judd, L. M., Robinson, D., Barrett, S. P., Scarff, K. L., Gleeson, P. A., Samuelson, L. C. and Van Driel, I. R.** (2001). Regulation of gastric epithelial cell development revealed in H(+)/K(+)-ATPase beta-subunit- and gastrin-deficient mice. *Am J Physiol Gastrointest Liver Physiol* **281**, G1502-1511.
- Friedmann-Morvinski, D. and Verma, I. M.** (2014). Dedifferentiation and reprogramming: origins of cancer stem cells. *EMBO Rep* **15**, 244-253.
- Giroux, V. and Rustgi, A. K.** (2017). Metaplasia: tissue injury adaptation and a precursor to the dysplasia-cancer sequence. *Nat Rev Cancer* **17**, 594-604.
- Gliddon, B. L., Nguyen, N. V., Gunn, P. A., Gleeson, P. A. and van Driel, I. R.** (2008). Isolation, culture and adenoviral transduction of parietal cells from mouse gastric mucosa. *Biomed Mater* **3**, 034117.
- Goldenring, J. R., Nam, K. T. and Mills, J. C.** (2011a). The origin of pre-neoplastic metaplasia in the stomach: chief cells emerge from the Mist. *Exp Cell Res* **317**, 2759-2764.
- Goldenring, J. R., Nam, K. T. and Mills, J. C.** (2011b). The origin of pre-neoplastic metaplasia in the stomach: chief cells emerge from the Mist. *Experimental cell research* **317**, 2759-2764.
- Goldenring, J. R., Nam, K. T., Wang, T. C., Mills, J. C. and Wright, N. A.** (2010). Spasmolytic polypeptide-expressing metaplasia and intestinal metaplasia: time for

- reevaluation of metaplasias and the origins of gastric cancer. *Gastroenterology* **138**, 2207-2210, 2210 e2201.
- Goldenring, J. R., Ray, G. S., Coffey, R. J., Meunier, P. C., Haley, P. J., Barnes, T. B. and Car, B. D.** (2000). Reversible drug-induced oxyntic atrophy in rats. *Gastroenterology* **118**, 1080-1093.
- Goldenring, J. R., Ray, G. S., Soroka, C. J., Smith, J., Modlin, I. M., Meise, K. S. and Coffey, R. J., Jr.** (1996). Overexpression of transforming growth factor-alpha alters differentiation of gastric cell lineages. *Dig Dis Sci* **41**, 773-784.
- Hanby, A. M., Poulosom, R., Playford, R. J. and Wright, N. A.** (1999). The mucous neck cell in the human gastric corpus: a distinctive, functional cell lineage. *J Pathol* **187**, 331-337.
- Hattori, T.** (1986). Development of adenocarcinomas in the stomach. *Cancer* **57**, 1528-1534.
- Hattori, T. and Fujita, S.** (1976a). Tritiated thymidine autoradiographic study of cell migration and renewal in the pyloric mucosa of golden hamsters. *Cell Tissue Res* **175**, 49-57.
- (1976b). Tritiated thymidine autoradiographic study on cellular migration in the gastric gland of the golden hamster. *Cell Tissue Res* **172**, 171-184.
- Hayakawa, Y., Ariyama, H., Stancikova, J., Sakitani, K., Asfaha, S., Renz, B. W., Dubeykovskaya, Z. A., Shibata, W., Wang, H., Westphalen, C. B., et al.** (2015). Mist1 Expressing Gastric Stem Cells Maintain the Normal and Neoplastic Gastric Epithelium and Are Supported by a Perivascular Stem Cell Niche. *Cancer Cell* **28**, 800-814.
- Hayakawa, Y., Fox, J. G. and Wang, T. C.** (2017). Isthmus Stem Cells Are the Origins of Metaplasia in the Gastric Corpus. *Cell Mol Gastroenterol Hepatol* **4**, 89-94.
- Hetrick, E. M. and Schoenfisch, M. H.** (2013). Analytical Chemistry of Nitric Oxide.
- Huh, W. J., Esen, E., Geahlen, J. H., Bredemeyer, A. J., Lee, A. H., Shi, G., Konieczny, S. F., Glimcher, L. H. and Mills, J. C.** (2010). XBP1 controls maturation of gastric zymogenic cells by induction of MIST1 and expansion of the rough endoplasmic reticulum. *Gastroenterology* **139**, 2038-2049.
- Huh, W. J., Khurana, S. S., Geahlen, J. H., Kohli, K., Waller, R. A. and Mills, J. C.** (2012a). Tamoxifen induces rapid, reversible atrophy, and metaplasia in mouse stomach. *Gastroenterology* **142**, 21-24.e27.
- Huh, W. J., Khurana, S. S., Geahlen, J. H., Kohli, K., Waller, R. A. and Mills, J. C.** (2012b). Tamoxifen induces rapid, reversible atrophy, and metaplasia in mouse stomach. *Gastroenterology* **142**, 21-24 e27.
- Jensen, J. N., Cameron, E., Garay, M. V., Starkey, T. W., Gianani, R. and Jensen, J.** (2005). Recapitulation of elements of embryonic development in adult mouse pancreatic regeneration. *Gastroenterology* **128**, 728-741.
- Jopling, C., Boue, S. and Izpisua Belmonte, J. C.** (2011). Dedifferentiation, transdifferentiation and reprogramming: three routes to regeneration. *Nat Rev Mol Cell Biol* **12**, 79-89.
- Kakinoki, R., Kushima, R., Matsubara, A., Saito, Y., Okabe, H., Fujiyama, Y. and Hattori, T.** (2009). Re-evaluation of histogenesis of gastric carcinomas: a comparative histopathological study between Helicobacter pylori-negative and H. pylori-positive cases. *Dig Dis Sci* **54**, 614-620.
- Karam, S. M.** (1993). Dynamics of epithelial cells in the corpus of the mouse stomach. IV. Bidirectional migration of parietal cells ending in their gradual degeneration and loss. *Anat Rec* **236**, 314-332.

- Karam, S. M. and Leblond, C. P.** (1993a). Dynamics of epithelial cells in the corpus of the mouse stomach. I. Identification of proliferative cell types and pinpointing of the stem cell. *Anat Rec* **236**, 259-279.
- (1993b). Dynamics of epithelial cells in the corpus of the mouse stomach. II. Outward migration of pit cells. *Anat Rec* **236**, 280-296.
- (1993c). Dynamics of epithelial cells in the corpus of the mouse stomach. III. Inward migration of neck cells followed by progressive transformation into zymogenic cells. *Anat Rec* **236**, 297-313.
- Kaufman, C. K., Mosimann, C., Fan, Z. P., Yang, S., Thomas, A. J., Ablain, J., Tan, J. L., Fogley, R. D., van Rooijen, E., Hagedorn, E. J., et al.** (2016). A zebrafish melanoma model reveals emergence of neural crest identity during melanoma initiation. *Science* **351**, aad2197.
- Keeley, T. M. and Samuelson, L. C.** (2010). Cytodifferentiation of the postnatal mouse stomach in normal and Huntingtin-interacting protein 1-related-deficient mice. *Am J Physiol Gastrointest Liver Physiol* **299**, G1241-1251.
- Kharitonov, V. G., Sharma, V. S., Magde, D. and Koesling, D.** (1997). Kinetics of nitric oxide dissociation from five- and six-coordinate nitrosyl hemes and heme proteins, including soluble guanylate cyclase. *Biochemistry* **36**, 6814-6818.
- Khurana, S. S., Riehl, T. E., Moore, B. D., Fassan, M., Rugge, M., Romero-Gallo, J., Noto, J., Peek, R. M., Jr., Stenson, W. F. and Mills, J. C.** (2013). The hyaluronic acid receptor CD44 coordinates normal and metaplastic gastric epithelial progenitor cell proliferation. *J Biol Chem* **288**, 16085-16097.
- Kinoshita, H., Hayakawa, Y., Niu, Z., Konishi, M., Hata, M., Tsuboi, M., Hayata, Y., Hikiba, Y., Ihara, S., Nakagawa, H., et al.** (2018a). Mature gastric chief cells are not required for the development of metaplasia. *Am J Physiol Gastrointest Liver Physiol*.
- (2018b). Mature gastric chief cells are not required for the development of metaplasia. *Am J Physiol Gastrointest Liver Physiol* **314**, G583-G596.
- Lennerz, J. K., Kim, S. H., Oates, E. L., Huh, W. J., Doherty, J. M., Tian, X., Bredemeyer, A. J., Goldenring, J. R., Lauwers, G. Y., Shin, Y. K., et al.** (2010). The transcription factor MIST1 is a novel human gastric chief cell marker whose expression is lost in metaplasia, dysplasia, and carcinoma. *Am J Pathol* **177**, 1514-1533.
- Leushacke, M., Tan, S. H., Wong, A., Swathi, Y., Hajamohideen, A., Tan, L. T., Goh, J., Wong, E., Denil, S., Murakami, K., et al.** (2017). Lgr5-expressing chief cells drive epithelial regeneration and cancer in the oxyntic stomach. *Nat Cell Biol* **19**, 774-786.
- Li, Q., Karam, S. M. and Gordon, J. I.** (1995). Simian virus 40 T antigen-induced amplification of pre-parietal cells in transgenic mice. Effects on other gastric epithelial cell lineages and evidence for a p53-independent apoptotic mechanism that operates in a committed progenitor. *J Biol Chem* **270**, 15777-15788.
- (1996). Diphtheria toxin-mediated ablation of parietal cells in the stomach of transgenic mice. *J Biol Chem* **271**, 3671-3676.
- Lo, H. G., Jin, R. U., Sibbel, G., Liu, D., Karki, A., Joens, M. S., Madison, B. B., Zhang, B., Blanc, V., Fitzpatrick, J. A., et al.** (2017). A single transcription factor is sufficient to induce and maintain secretory cell architecture. *Genes Dev* **31**, 154-171.
- Lopez-Garcia, C., Klein, A. M., Simons, B. D. and Winton, D. J.** (2010). Intestinal stem cell replacement follows a pattern of neutral drift. *Science* **330**, 822-825.

- Martinez-Ruiz, A., Cadenas, S. and Lamas, S.** (2011). Nitric oxide signaling: classical, less classical, and nonclassical mechanisms. *Free Radic Biol Med* **51**, 17-29.
- Matsuo, J., Kimura, S., Yamamura, A., Koh, C. P., Hossain, M. Z., Heng, D. L., Kohu, K., Voon, D. C., Hiai, H., Unno, M., et al.** (2017). Identification of Stem Cells in the Epithelium of the Stomach Corpus and Antrum of Mice. *Gastroenterology* **152**, 218-231 e214.
- McAfee, Q., Zhang, Z., Samanta, A., Levi, S. M., Ma, X. H., Piao, S., Lynch, J. P., Uehara, T., Sepulveda, A. R., Davis, L. E., et al.** (2012). Autophagy inhibitor Lys05 has single-agent antitumor activity and reproduces the phenotype of a genetic autophagy deficiency. *Proc Natl Acad Sci U S A* **109**, 8253-8258.
- Messal, H. A., Cremona, C. A., Lan, L. and Behrens, A.** (2018). Paligenosis: prepare to regenerate! *EMBO J* **37**.
- Mills, J. C., Andersson, N., Stappenbeck, T. S., Chen, C. C. and Gordon, J. I.** (2003). Molecular characterization of mouse gastric zymogenic cells. *J Biol Chem* **278**, 46138-46145.
- Mills, J. C. and Goldenring, J. R.** (2017). Metaplasia in the Stomach Arises From Gastric Chief Cells. *Cell Mol Gastroenterol Hepatol* **4**, 85-88.
- Mills, J. C. and Sansom, O. J.** (2015). Reserve stem cells: Differentiated cells reprogram to fuel repair, metaplasia, and neoplasia in the adult gastrointestinal tract. *Sci Signal* **8**, re8.
- Mills, J. C. and Shivdasani, R. A.** (2011). Gastric epithelial stem cells. *Gastroenterology* **140**, 412-424.
- Mills, J. C., Syder, A. J., Hong, C. V., Guruge, J. L., Raaij, F. and Gordon, J. I.** (2001). A molecular profile of the mouse gastric parietal cell with and without exposure to *Helicobacter pylori*. *Proc Natl Acad Sci U S A* **98**, 13687-13692.
- Mungrue, I. N., Gros, R., You, X., Pirani, A., Azad, A., Csont, T., Schulz, R., Butany, J., Stewart, D. J. and Husain, M.** (2002). Cardiomyocyte overexpression of iNOS in mice results in peroxynitrite generation, heart block, and sudden death. *J Clin Invest* **109**, 735-743.
- Muzumdar, M. D., Tasic, B., Miyamichi, K., Li, L. and Luo, L.** (2007). A global double-fluorescent Cre reporter mouse. *Genesis* **45**, 593-605.
- Nam, K. T., Lee, H. J., Mok, H., Romero-Gallo, J., Crowe, J. E., Jr., Peek, R. M., Jr. and Goldenring, J. R.** (2009). Amphiregulin-deficient mice develop spasmodic polypeptide expressing metaplasia and intestinal metaplasia. *Gastroenterology* **136**, 1288-1296.
- Nam, K. T., Lee, H. J., Sousa, J. F., Weis, V. G., O'Neal, R. L., Finke, P. E., Romero-Gallo, J., Shi, G., Mills, J. C., Peek, R. M., Jr., et al.** (2010). Mature chief cells are cryptic progenitors for metaplasia in the stomach. *Gastroenterology* **139**, 2028-2037 e2029.
- Nathan, C.** (1992). Nitric oxide as a secretory product of mammalian cells. *The FASEB Journal*, 3051-3064.
- Nitsche, H., Ramamoorthy, S., Sareban, M., Pausawasdi, N. and Todisco, A.** (2007). Functional role of bone morphogenetic protein-4 in isolated canine parietal cells. *Am J Physiol Gastrointest Liver Physiol* **293**, G607-614.
- Nomura, S., Baxter, T., Yamaguchi, H., Leys, C., Vartapetian, A. B., Fox, J. G., Lee, J. R., Wang, T. C. and Goldenring, J. R.** (2004). Spasmodic polypeptide expressing metaplasia to preneoplasia in *H. felis*-infected mice. *Gastroenterology* **127**, 582-594.

- Nomura, S., Yamaguchi, H., Ogawa, M., Wang, T. C., Lee, J. R. and Goldenring, J. R.** (2005). Alterations in gastric mucosal lineages induced by acute oxyntic atrophy in wild-type and gastrin-deficient mice. *Am J Physiol Gastrointest Liver Physiol* **288**, G362-375.
- Nozaki, K., Ogawa, M., Williams, J. A., Lafleur, B. J., Ng, V., Drapkin, R. I., Mills, J. C., Konieczny, S. F., Nomura, S. and Goldenring, J. R.** (2008). A molecular signature of gastric metaplasia arising in response to acute parietal cell loss. *Gastroenterology* **134**, 511-522.
- Osaki, L. H., Curi, M. A., Alvares, E. P. and Gama, P.** (2010). Early weaning accelerates the differentiation of mucous neck cells in rat gastric mucosa: possible role of TGF α /EGFR. *Differentiation* **79**, 48-56.
- Palmer, R. M., Ferrige, A. G. and Moncada, S.** (1987). Nitric oxide release accounts for the biological activity of endothelium-derived relaxing factor. *Nature* **327**, 524-526.
- Petersen, C. P., Meyer, A. R., De Salvo, C., Choi, E., Schlegel, C., Petersen, A., Engevik, A. C., Prasad, N., Levy, S. E., Peebles, R. S., et al.** (2017a). A signalling cascade of IL-33 to IL-13 regulates metaplasia in the mouse stomach. *Gut*.
- Petersen, C. P., Mills, J. C. and Goldenring, J. R.** (2017b). Murine Models of Gastric Corpus Preneoplasia. *Cell Mol Gastroenterol Hepatol* **3**, 11-26.
- Petersen, C. P., Weis, V. G., Nam, K. T., Sousa, J. F., Fingleton, B. and Goldenring, J. R.** (2014). Macrophages promote progression of spasmolytic polypeptide-expressing metaplasia after acute loss of parietal cells. *Gastroenterology* **146**, 1727-1738 e1728.
- Pheesse, T. J. and Sansom, O. J.** (2017). Lgr5 joins the club of gastric stem cell markers in the corpus. *Nat Cell Biol* **19**, 752-754.
- Potten, C. S.** (1998). Stem cells in gastrointestinal epithelium: numbers, characteristics and death. *Philos Trans R Soc Lond B Biol Sci* **353**, 821-830.
- Pyriochou, A. and Papapetropoulos, A.** (2005). Soluble guanylyl cyclase: more secrets revealed. *Cellular signalling* **17**, 407-413.
- Quante, M., Marrache, F., Goldenring, J. R. and Wang, T. C.** (2010). TFF2 mRNA transcript expression marks a gland progenitor cell of the gastric oxyntic mucosa. *Gastroenterology* **139**, 2018-2027 e2012.
- Radyk, M. D., Burclaff, J., Willet, S. G. and Mills, J. C.** (2018). Metaplastic Cells in the Stomach Arise, Independently of Stem Cells, via Dedifferentiation or Transdifferentiation of Chief Cells. *Gastroenterology* **154**, 839-843 e832.
- Radyk, M. D. and Mills, J. C.** (2017). A chief source of cancer and repair in stomachs. *EMBO J* **36**, 2318-2320.
- Ramsey, V. G., Doherty, J. M., Chen, C. C., Stappenbeck, T. S., Konieczny, S. F. and Mills, J. C.** (2007). The maturation of mucus-secreting gastric epithelial progenitors into digestive-enzyme secreting zymogenic cells requires Mist1. *Development* **134**, 211-222.
- Ritsma, L., Ellenbroek, S. I. J., Zomer, A., Snippert, H. J., de Sauvage, F. J., Simons, B. D., Clevers, H. and van Rheenen, J.** (2014). Intestinal crypt homeostasis revealed at single-stem-cell level by in vivo live imaging. *Nature* **507**, 362-365.
- Saenz, J. B., Burclaff, J. and Mills, J. C.** (2016). Modeling Murine Gastric Metaplasia Through Tamoxifen-Induced Acute Parietal Cell Loss. *Methods Mol Biol* **1422**, 329-339.
- Saenz, J. B. and Mills, J. C.** (2018a). Acid and the basis for cellular plasticity and reprogramming in gastric repair and cancer. *Nat Rev Gastroenterol Hepatol* **15**, 257-273.
- (2018b). Acid and the basis for cellular plasticity and reprogramming in gastric repair and cancer. *Nat Rev Gastroenterol Hepatol*.

- Saenz, J. B., Vargas, N. and Mills, J. C.** (2018). Tropism for Spasmolytic Polypeptide-Expressing Metaplasia Allows *Helicobacter pylori* to Expand Its Intra-gastric Niche. *Gastroenterology*.
- Saenz, J. B., Vargas, N. and Mills, J. C.** (In press.). *Helicobacter pylori*'s tropism for spasmolytic polypeptide-expressing metaplasia allows it to expand its intra-gastric niche. *Gastroenterology*.
- Schmidt, P. H., Lee, J. R., Joshi, V., Playford, R. J., Poulson, R., Wright, N. A. and Goldenring, J. R.** (1999). Identification of a metaplastic cell lineage associated with human gastric adenocarcinoma. *Lab Invest* **79**, 639-646.
- Sigal, M., Rothenberg, M. E., Logan, C. Y., Lee, J. Y., Honaker, R. W., Cooper, R. L., Passarelli, B., Camorlinga, M., Bouley, D. M., Alvarez, G., et al.** (2015). *Helicobacter pylori* Activates and Expands Lgr5(+) Stem Cells Through Direct Colonization of the Gastric Glands. *Gastroenterology* **148**, 1392-1404 e1321.
- Singh, R. J., Hogg, N., Joseph, J. and Kalyanaraman, B.** (1996). Mechanism of Nitric Oxide Release from S-Nitrosothiols. *Journal of Biological Chemistry* **271**, 18596-18603.
- Snippert, H. J., Schepers, A. G., van Es, J. H., Simons, B. D. and Clevers, H.** (2014). Biased competition between Lgr5 intestinal stem cells driven by oncogenic mutation induces clonal expansion. *EMBO Rep* **15**, 62-69.
- Snippert, H. J., van der Flier, L. G., Sato, T., van Es, J. H., van den Born, M., Kroon-Veenboer, C., Barker, N., Klein, A. M., van Rheenen, J., Simons, B. D., et al.** (2010). Intestinal crypt homeostasis results from neutral competition between symmetrically dividing Lgr5 stem cells. *Cell* **143**, 134-144.
- Song, I. Y. and Balmain, A.** (2015). Cellular reprogramming in skin cancer. *Semin Cancer Biol* **32**, 32-39.
- Spicer, Z., Miller, M. L., Andringa, A., Riddle, T. M., Duffy, J. J., Doetschman, T. and Shull, G. E.** (2000). Stomachs of mice lacking the gastric H,K-ATPase alpha -subunit have achlorhydria, abnormal parietal cells, and ciliated metaplasia. *J Biol Chem* **275**, 21555-21565.
- Stamler, J. S.** (1994). Redox signaling: nitrosylation and related target interactions of nitric oxide. *Cell* **78**, 931-936.
- Stange, D. E., Koo, B.-K., Huch, M., Sibbel, G., Basak, O., Lyubimova, A., Kujala, P., Bartfeld, S., Koster, J., Geahlen, J. H., et al.** (2013a). Differentiated Troy+ chief cells act as reserve stem cells to generate all lineages of the stomach epithelium. *Cell* **155**, 357-368.
- Stange, D. E., Koo, B. K., Huch, M., Sibbel, G., Basak, O., Lyubimova, A., Kujala, P., Bartfeld, S., Koster, J., Geahlen, J. H., et al.** (2013b). Differentiated Troy+ chief cells act as reserve stem cells to generate all lineages of the stomach epithelium. *Cell* **155**, 357-368.
- Suzuki, S., Tsuyama, S. and Murata, F.** (1983). Cells intermediate between mucous neck cells and chief cells in rat stomach. *Cell Tissue Res* **233**, 475-484.
- Syder, A. J., Karam, S. M., Mills, J. C., Ippolito, J. E., Ansari, H. R., Farook, V. and Gordon, J. I.** (2004). A transgenic mouse model of metastatic carcinoma involving transdifferentiation of a gastric epithelial lineage progenitor to a neuroendocrine phenotype. *Proc Natl Acad Sci U S A* **101**, 4471-4476.
- Takahashi, K. and Yamanaka, S.** (2006). Induction of pluripotent stem cells from mouse embryonic and adult fibroblast cultures by defined factors. *Cell* **126**, 663-676.

- Tata, P. R. and Rajagopal, J.** (2016). Cellular plasticity: 1712 to the present day. *Curr Opin Cell Biol* **43**, 46-54.
- Uriel, J.** (1979). Retrodifferentiation and the fetal patterns of gene expression in cancer. *Adv Cancer Res* **29**, 127-174.
- Visvader, J. E.** (2011). Cells of origin in cancer. *Nature* **469**, 314-322.
- Vogelstein, B. and Kinzler, K. W.** (1993). The multistep nature of cancer. *Trends Genet* **9**, 138-141.
- von Figura, G., Morris, J. P. t., Wright, C. V. and Hebrok, M.** (2014). Nr5a2 maintains acinar cell differentiation and constrains oncogenic Kras-mediated pancreatic neoplastic initiation. *Gut* **63**, 656-664.
- Wada, T., Ishimoto, T., Seishima, R., Tsuchihashi, K., Yoshikawa, M., Oshima, H., Oshima, M., Masuko, T., Wright, N. A., Furuhashi, S., et al.** (2013). Functional role of CD44v-xCT system in the development of spasmolytic polypeptide-expressing metaplasia. *Cancer Sci* **104**, 1323-1329.
- Watanabe, H., Fujii, I. and Terada, Y.** (1980). Induction of intestinal metaplasia in the rat gastric mucosa by local X-irradiation. *Pathol Res Pract* **170**, 104-114.
- Weis, V. G., Petersen, C. P., Weis, J. A., Meyer, A. R., Choi, E., Mills, J. C. and Goldenring, J. R.** (2017). Maturity and age influence chief cell ability to transdifferentiate into metaplasia. *Am J Physiol Gastrointest Liver Physiol* **312**, G67-G76.
- Weis, V. G., Sousa, J. F., LaFleur, B. J., Nam, K. T., Weis, J. A., Finke, P. E., Ameen, N. A., Fox, J. G. and Goldenring, J. R.** (2013). Heterogeneity in mouse spasmolytic polypeptide-expressing metaplasia lineages identifies markers of metaplastic progression. *Gut* **62**, 1270-1279.
- White, A. C. and Lowry, W. E.** (2015). Refining the role for adult stem cells as cancer cells of origin. *Trends Cell Biol* **25**, 11-20.
- Willet, S. G., Lewis, M. A., Miao, Z. F., Liu, D., Radyk, M. D., Cunningham, R. L., Burclaff, J., Sibbel, G., Lo, H. G., Blanc, V., et al.** (2018a). Regenerative proliferation of differentiated cells by mTORC1-dependent paligenesis. *EMBO J*.
- (2018b). Regenerative proliferation of differentiated cells by mTORC1-dependent paligenesis. *EMBO J* **37**.
- Willet, S. G. and Mills, J. C.** (2016). Stomach Organ and Cell Lineage Differentiation: from Embryogenesis to Adult Homeostasis. *Cell Mol Gastroenterol Hepatol* **2**, 546-559.
- Wright, N.** (2016). The Gastric Epithelium: Slow Starter in the Stem Cell/Lineage Specification Stakes? *Cell Mol Gastroenterol Hepatol* **2**, 538-539.
- Xiao, C., Ogle, S. A., Schumacher, M. A., Orr-Asman, M. A., Miller, M. L., Lertkowitz, N., Varro, A., Hollande, F. and Zavros, Y.** (2010). Loss of parietal cell expression of Sonic hedgehog induces hypergastrinemia and hyperproliferation of surface mucous cells. *Gastroenterology* **138**, 550-561, 561 e551-558.
- Yamachika, T., Nakanishi, H., Inada, K., Tsukamoto, T., Shimizu, N., Kobayashi, K., Fukushima, S. and Tatematsu, M.** (1998). N-methyl-N-nitrosourea concentration-dependent, rather than total intake-dependent, induction of adenocarcinomas in the glandular stomach of BALB/c mice. *Jpn J Cancer Res* **89**, 385-391.
- Yamamoto, M., Furihata, C., Ogiu, T., Tsukamoto, T., Inada, K., Hirano, K. and Tatematsu, M.** (2002). Independent variation in susceptibilities of six different mouse

strains to induction of pepsinogen-altered pyloric glands and gastric tumor intestinalization by N-methyl-N-nitrosourea. *Cancer Lett* **179**, 121-132.

- Yoshizawa, N., Takenaka, Y., Yamaguchi, H., Tetsuya, T., Tanaka, H., Tatematsu, M., Nomura, S., Goldenring, J. R. and Kaminishi, M.** (2007). Emergence of spasmolytic polypeptide-expressing metaplasia in Mongolian gerbils infected with *Helicobacter pylori*. *Laboratory investigation; a journal of technical methods and pathology* **87**, 1265-1276.
- Zhang, H., Morgan, D., Cecil, G., Burkholder, A., Ramocki, N., Scull, B. and Lund, P. K.** (2008). Biochromoendoscopy: molecular imaging with capsule endoscopy for detection of adenomas of the GI tract. *Gastrointest Endosc* **68**, 520-527.
- Zhao, Z., Hou, N., Sun, Y., Teng, Y. and Yang, X.** (2010). Atp4b promoter directs the expression of Cre recombinase in gastric parietal cells of transgenic mice. *J Genet Genomics* **37**, 647-652.

Curriculum Vitae

Joseph Burclaff

Department of Gastroenterology
Washington University School of Medicine in St Louis
Campus Box #8228
660 S Euclid Ave
St. Louis, MO 63110
joseph.burclaff@wustl.edu

EDUCATION

Doctor of Philosophy in Developmental, Regenerative, and Stem Cell Biology

Washington University in St Louis, MO. Division of Biology and Biomedical Sciences,
August 2013 – May 2019

Bachelor of Science Degree in Biochemistry and Molecular Biology

Marquette University, Milwaukee, WI. College of Arts and Sciences, 2013
Summa cum Laude, Dean's list 2009-2013, Phi Beta Kappa inductee

Wausau East High School

Class of 2009, Wausau, WI

Valedictorian (class size 329), National Honors Society, Eagle Scout

RESEARCH EXPERIENCE

Graduate Research at Washington University in St Louis, 2013-present

Lab of Dr. Jason C Mills M.D./Ph.D., Department of Gastroenterology

Determining mechanisms of gastric regeneration following parietal cell injury

Undergraduate Research Project in Biological Sciences at Marquette University 2011–2013

Lab of Dr. James T Anderson, Ph.D.

Characterizing the Mtr4 protein by analyzing the effects of point mutations in vivo and in vitro

AWARDS & FUNDING

Greg Sibbel Memorial Travel Award, 2018

DeNardo Research and Education Foundation, 2017-2019

\$100,000 initiative award for project and stipend funding

Philip and Sima Needleman Student Fellowship in Regenerative Medicine, 2016-2018

NIH T32 Training Grant Recipient, 2013-2016

Marquette University Department of Biology Academic Achievement Award, 2013

SCHOLARSHIP

Joseph Burclaff and Jason C Mills. "Plasticity of differentiated cells in wound-repair and tumorigenesis part II: skin and intestine." *Disease Models and Mechanisms* 11.8 (2018): dmm035071

Joseph Burclaff and Jason C. Mills. "Plasticity of differentiated cells in wound repair and tumorigenesis, part I: stomach and pancreas." *Disease Models & Mechanisms* 11.7 (2018): dmm033373.

Spencer G. Willet, Mark A. Lewis, Zhi-Feng Miao, Dengqun Liu, Megan D. Radyk, Rebecca L. Cunningham, **Joseph Burclaff**, Greg Sibbel, Hei-Yong G. Lo, Valerie Blanc, Nicholas O. Davidson, Zhen-Ning Wang, Jason C. Mills. "Regenerative proliferation of differentiated cells by mTORC1-dependent paligenesis." *The EMBO journal* (2018): e98311.

Radyk, Megan D, **Joseph Burclaff**, Spencer G Willett, Jason C Mills. "Metaplastic Cells in the Stomach Arise, Independently of Stem Cells, via Dedifferentiation or Transdifferentiation of Chief Cells." *Gastroenterology* (2018). * Mentioned on cover *F1000 recommended

Joseph Burclaff, Jason C. Mills. "Cell biology: Healthy skin rejects cancer." *Nature* 548(7667) (2017): 289-290.

Joseph Burclaff, Luciana Osaki, Dengqun Liu, James R Goldenring, and Jason C. Mills. "Targeted Apoptosis of Parietal Cells is Insufficient to Induce Metaplasia in Stomach." *Gastroenterology* 152.4 (2017): 762-766.

Joo Hyun Lim, **Joseph Burclaff**, Guangxu He, Jason C. Mills, and Fanxin Long. "Unintended targeting of Dmp1-Cre reveals a critical role for Bmpr1a signaling in the gastrointestinal mesenchyme of adult mice." *Bone Research* 5 (2017): 16049.

Saenz, Jose B., **Joseph Burclaff**, and Jason C. Mills. "Modeling Murine Gastric Metaplasia through Tamoxifen-Induced Acute Parietal Cell Loss." *Gastrointestinal Physiology and Diseases: Methods and Protocols* (2016): 329-339.

Li, Yan, **Joseph Burclaff**, and James T. Anderson. "Mutations in Mtr4 Structural Domains Reveal Their Important Role in Regulating tRNA i Met Turnover in *Saccharomyces cerevisiae* and Mtr4p Enzymatic Activities In Vitro." *PLoS one* 11.1 (2016): e0148090.

ORAL PRESENTATIONS

Mapping how mature cells re-enter the cell cycle

Selected speaker, Developmental Regenerative and Stem Cell Biology Recruiting Weekend, 2018

Defining levels of recruit-able stem cells

3rd Annual Regenerative Medicine Symposium, Washington University in St. Louis, 2017

Do cycles of dedifferentiation and metaplasia increase risk of tumorigenesis over proliferation alone?

Developmental, Regenerative, and Stem Cell Biology Program Retreat, 2017

Parietal cell atrophic death is insufficient to drive metaplasia in the stomach

Midwest Regenerative Medicine Meeting, Monticello, IL 2016

*Selected for short oral presentation *Poster presentation selected 2nd place out of 46

Investigating initiation requirements for metaplastic injury response in the stomach

2nd Annual Regenerative Medicine Symposium, Washington University in St. Louis, 2016

Parietal cell apoptosis is insufficient to initiate the gastric metaplastic response

Developmental, Regenerative, and Stem Cell Biology Program Retreat, 2016

Determining the role of nitric oxide signaling in gastric regeneration following parietal cell injury

FASEB Science Research Conference: Gastrointestinal Tract XVI: GI Homeostasis, the Microbiome and the Barrier, Development & Disease, Steamboat Springs, CO 2015

Nitric Oxide Regulates Metaplasia in Response to Helicobacter Pylori in Mice and Humans

International Congress of Mucosal Immunology, Berlin, Germany 2015

*Selected for oral presentation, presented by PI

POSTERS

Mature gastric chief cells act as recruitable stem cells in cycles of acute or chronic metaplasia

Keystone Symposia on Cellular Plasticity: Reprogramming, Regeneration, and Metaplasia Keystone, CO 2019

Mature gastric chief cells act as recruitable stem cells in cycles of acute or chronic metaplasia

Gordon Research Conference on Tissue Niches and Resident Stem Cells in Adult Epithelia Waterville Valley, NH 2018

Determining initiation requirements for dedifferentiation of zymogenic chief cells as recruited stem cells following gastric injury.

FASEB Science Research Conference: Gastrointestinal Tract XVII: Current Biology of the GI Tract, Mucosa, Microbiota, and Beyond, Steamboat Springs, CO 2017

*Poster Award with Travel Award

Determining requirements for recruitment of the quiescent gastric stem cell

Gordon Research Conference on Epithelial Differentiation and Keratinization, Lucca, Italy 2017

Investigating the initiation of gastric metaplastic regeneration following injury

Washington University in St Louis, Cellular Molecular Biology Mini-Symposium, 2016

*Poster Award

Determining the role of nitric oxide signaling in gastric regeneration following parietal cell injury

Developmental, Regenerative, and Stem Cell Biology Program retreat, 2014 + 2015

TEACHING EXPERIENCE

Mentored high school student for 8 week lab internship including a paper and presentation

Washington University in St Louis, Young Scientist Program, June-July 2017

Lab consulting and training

China Medical University, Shenyang, China.

Lab of Dr. Zhin-ning Wang, M.D., August-September 2016

Writing Course Instructor for high school students: Young Scientists Program Summer Focus

Washington University in St Louis, Summers 2015 and 2016

Teaching Assistant, Undergraduate Course: Collaborative Phage Bioinformatics

Washington University in St Louis, Spring Semester 2015

SERVICE

Tutoring Coordinator, Young Scientist Program, Washington University in St Louis, 2014-2016

Organized graduate student volunteers to tutor at Soldan International Studies High School

*Volunteer Choice award for Outstanding Tutor at YSP 25th Anniversary Gala, 2016

Organizer, Student Run Seminar for Developmental Biology and Molecular & Cellular Biology, 2014-2015

OTHER EXPERIENCE

Proofreader for biomedical labs at the China Medical University, Shenyang, China.

60+ publications, 2016-present